BEHAVIOR AND MODELLING OF RC BEAMS WITH AN FRP-STRENGTHENED WEB OPENING

XUEFEI NIE

PhD

The Hong Kong Polytechnic University

2018

The Hong Kong Polytechnic University

Department of Civil and Environmental Engineering

BEHAVIOR AND MODELLING OF RC BEAMS WITH AN FRP-STRENGTHENED WEB OPENING

XUEFEI NIE

A Thesis Submitted in Partial Fulfilment of the Requirements

for the Degree of Doctor of Philosophy

March 2018

CERTIFICATE OF ORIGINALITY

I hereby declare that this thesis is my own work and that, to the best of my knowledge and belief, it reproduces no material previously published or written, nor material that has been accepted for the award of any other degree or diploma, except where due acknowledgement has been made in the text.

__________ _________ (Signed)

_____________ Xuefei NIE __________ (Name of student)

ABASTRACT

The strong column-weak beam hierarchy has been widely accepted in the design of reinforced concrete (RC) frames for good seismic performance. In many existing RC frames designed according to previous codes, however, such a hierarchy was not enforced. To rectify this deficiency, a novel seismic retrofit method (the beam opening technique or the BO technique) based on the Beam-end Weakening in combination with FRP Strengthening (BWFS) concept is studied in this thesis for such frames. The BO technique, which involves the creation of an opening in the web of a T-section beam for a reduction in the flexural capacity of the beam and the use of local FRP strengthening to avoid shear failure of the weakened beam to ensure a ductile failure process, can also meet the functional requirement of accommodating passages for utility ducts/pipes. The study presented in this thesis is aimed at assessing the feasibility of the BO technique and providing an in-depth understanding of the behaviour of RC beams with a web opening through combined experimental, numerical and theoretical investigations.

An experimental study on full-scale RC T-section beams with a web opening was conducted, and the test results are presented in this thesis. A total of 14 full-scale RC beams were designed and tested under static loading to assess the effect of the BO technique on the behaviour of T-section RC beams. The test results show that the BO technique can effectively reduce the flexural capacity of a T-section beam, and the proposed FRP strengthening system to avoid shear failure ensures

a ductile response of the beam.

This thesis also presents finite element (FE) studies of RC beams with a web opening. Three alterative FE approaches with the explicit central difference method available in ABAQUS as the solution method are proposed, and their predictions are compared with results of tests on RC beams with a web opening collected from the published literature and conducted by the candidate to identify the most reliable approach. The FE results show that the selection of the FE approach should be based on the possible failure mode of the beam: the FE approach based on the concrete damaged plasticity model is recommended for beams with a flexural failure mode, while the FE approach based on the brittle cracking model with secant modulus of concrete is recommended for beams with a shear failure mode.

Finally, for ease of use in engineering practice, a strength model is proposed for predicting the strength of RC beams with a web opening. In addition, the moment (M)-rotation (Θ) relationship (M-Θ model) for the idealized plastic hinges at the two ends of the opening of RC beams with a web opening is established. The proposed M-Θ model is employed in the FE modelling of RC beams with a web opening using beam elements, and its accuracy is verified with test results.

LIST OF PUBLICATIONS

Refereed Journal Paper:

Nie, X.F., Zhang, S.S., Teng, J.G. and Chen, G.M. (2018). "Experimental study on RC T-section beams with an FRP-strengthened web opening", *Composite Structures*, (185), 273-285.

Conference Papers:

1. Teng, J.G., Zhang, S.S., Jing, D.H., Nie, X.F. and Chen, G.M. (2013). "Seismic retrofit of RC frames through beam-end weakening in conjunction with FRP strengthening", *Proceeding of Fourth Asia Pacific Conference on FRP Composites in Structures (APFIS 2013)*, 11-13 December 2013, Melbourne, Australia.
2. Nie, X.F., Zhang, S.S., Teng, J.G. and Chen, G.M. (2017). "Flexural weakening-shear strengthening (FWSS) technique for seismic retrofit: experimental study", *Proceeding of 6th Asia-Pacific Conference on FRP in Structures (APFIS 2017)*, 19-21 July 2017, Singapore.

AKNOWLEDGEMENTS

It is not easy to complete a Doctor of Philosophy (PhD) degree research programme. During the six years I have spent on my PhD programme, it is quite fortunate for me to have received a great deal of help and support from many people. I would like to express my sincere thanks to them upon the completion of this PhD thesis.

First of all, I wish to express my sincere gratitude to my supervisor, Professor Jin-Guang Teng, who is a distinguished scholar, for accepting me as one of his PhD students six years ago; for his continuous support to me during my PhD study; and for his patience, motivation and immense knowledge. His guidance helped me throughout my PhD study and the writing of this thesis. Moreover, the strict research training he has provided to me in the past six years will definitely benefit me in my academic career in the future.

My sincere thanks also go to my two co-supervisors, Prof. Guang-ming Chen from Guangdong University of Technology (GDUT) and Dr. Tao YU from the University of Wollongong. The FE model for FRP-strengthened RC beams proposed by Prof. Guang-ming Chen served as the foundation of the numerical studies presented in this PhD thesis. In addition, Dr. Shi-shun Zhang from the University of Wollongong provided much constructive advice on the work presented in my PhD thesis and a great deal of help with the revision of this PhD thesis. Their guidance and assistance helped me overcome many difficulties encountered by me during my PhD study.

I am also very grateful to many past and current members of Professor Teng's research group, who provided help to me in many different ways during my PhD study: Dr. Guan Lin, Dr. Bing Fu, Dr. Yi-nan Yang, Dr. Qiong-Guan Xiao, Dr. Bing Zhang, Dr. Jun-jie Zeng, Mr. Qing-kai Wang, Ms. Pang Xie and Dr. Jian-Guo Dai.

Thanks are also due to both The Hong Kong Polytechnic University and the Research Grants Council of the Hong Kong Special Administrative Region for providing me with the financial support. I would also like to thank The Hong Kong Polytechnic University for providing the research facilities.

I am also grateful for the technical support received at Guangdong University of Technology and The Hong Kong Polytechnic University. I am very grateful to the technical staff of the laboratories, especially, Mr. Zhen-xiong Wang, Mr. K.H. Wong, Mr. Y.H., Yiu and Mr. John Chan, for their valuable assistance and advice during the experimental work of my PhD study. I spent a substantial period of my PhD candidature at GDUT to complete the major part of my experimental work, and sincere thanks are due to Prof. Lijuan Li, Dean of the School of Civil and Transportation Engineering during my stay at GDUT, for making the laboratory facilities freely available for my experimental work.

Last but not the least, I wish to thank my family for their constant understanding, support and encouragement throughout the period of my PhD study.

CONTENTS

CHAPTER 4 FE MODELLING OF EXISTING TESTS ON RC BEAMS WITH AN FRP-STRENGTHENED WEB OPENING...... 145

LIST OF FIGURES

LIST OF TABLES

NOTATIONS

Notation	Meaning
A_b	Cross-sectional area of bottom chord
A_{bL}	Cross-sectional area of the left end of bottom chord after cracking
A_{bR}	Cross-sectional area of the right end of bottom chord after cracking
$\frac{A_e}{A_c}$	Effective confinement area ratio
A_g	Gross area of the column section with rounded corner
A_{sv}	Sum of cross-sectional areas of vertical legs of a stirrup at a certain cross-section of the chord
A_t	Cross-sectional area of top chord
A_{tL}	Cross-sectional area of the left end of top chord after cracking
A_{tR}	Cross-sectional area of the right end of top chord after cracking
b	Width of rectangular column
b_c	Width of beam
b_f	Width of FRP
C	Stiffness-proportional Rayleigh damping
d_t	Stiffness degradation variables of cracked concrete
$\dot{d}$	Velocity
D	The diameter of an equivalent column
D_a	The maximum aggregate size
E_f	Elastic modulus of FRP sheet
E_{frp}	Elastic modulus of FRP in the hoop direction
E_0	Elastic modulus of concrete
E_2	Slope of the straight second portion of the stress-strain model for FRP-confined concrete (Lam and Teng 2003)
f_c	Cylinder compressive strength of concrete

Notation	Meaning
$f_{cc}^{'}$	Compressive strength of confined concrete
$f_{co}^{'}$	Compressive strength of unconfined concrete
f_{cu}	Cube compressive strength of concrete
f_{fd}	Tensile strength of FRP sheet
f_l	Confining pressure in an equivalent circular column
f_t	Tensile strength of concrete
f_{yv}	Tensile strength of steel stirrups
F	Ultimate load of the beam
G_f	Interfacial fracture energy
G_F	Tensile fracture energy required to create a stress-free crack over a unit area
h	Depth of rectangular column
h_c	Crack band
h_f	Height of FRP sheet
h_s	Height of steel stirrup
h_0	Effective height of the chord
I_b	Second moment of area of bottom chord
I_{bL}	Second moment of area of the cross section at the left end of bottom chord after cracking
I_{bR}	Second moment of area of the cross section at the right end of bottom chord after cracking
I_t	Second moment of area of top chord
I_{tL}	Second moment of area of the cross section at the left end of top chord after cracking
I_{tR}	Second moment of area of the cross section at the right end of top chord after cracking
I_1	The first invariant of stresses
J_2	The second invariant of deviatoric stresses

Notation	Meaning
k_{s1}	Shape factor for strength enhancement
k_{s2}	Shape factor for strain enhancement
k_1	Confinement effectiveness coefficient
k_2	Strain enhancement coefficient
K	Stiffness matrix
K_f	Coefficient of FRP debonding
l	Length of web opening
l_{bL}	Length of cracking region at the left end of bottom chord
l_{bR}	Length of cracking region at the right end of bottom chord
l_{tL}	Length of cracking region at the left end of top chord
l_{tR}	Length of cracking region at the right end of top chord
L	Length of the clear span of the beam
L_L	Distance between the left end of the opening and the left support
L_{LS}	Length of the left span of the beam
L_R	Distance between the right end of the opening and the right support
M	Bending moment
M_{bL}	Bending moment at the left end of bottom chord
M_{bR}	Bending moment at the right end of bottom chord
M_{ch}	Flexural capacity of the critical chord under hogging bending
M_{cs}	Flexural capacity of the critical chord under sagging bending
M_L	Total moment at the left end of the opening
M_{Lcr}	Bending moment at left end of the opening at cracking of the beam
M_{Ly}	Bending moment at left end of the opening at the yielding of the beam
M_R	Total moment at the right end of the opening
M_{Rcr}	Bending moment at right end of the opening at cracking of the beam
M_{Ry}	Bending moment at right end of the opening at the yielding of the beam
M_{tL}	Bending moment at the left end of top chord

Notation	Meaning
M_{tR}	Bending moment at the right end of top chord
$\sum M_B$	Sum of the flexural capacities of the beams at a joint
$\sum M_C$	Sum of the flexural capacities of the columns at a joint
n	The exponent controlling the rate of shear degradation in the shear retention model
n_f	Layers of FRP sheet
N_b	Axial force in bottom chord
N_t	Axial force in top chord
R_c	Rounded corner radius
s	Slip
s_f	Clear distance between two adjacent FRP sheets
s_s	Distance between two adjacent stirrups
s^r	Rotational hourglass scaling factor
s^s	Displacement hourglass scaling factor
s^w	Out-of-plane displacement hourglass scaling factor
s_0	The slip when the bond stress reaches $\tau_{\max}$
t_f	Thickness of FRP sheet
T_1	The period of the fundamental vibration mode of the beam
u_b	Relative horizontal displacement between the two ends of bottom chord
u_{bc}	Relative horizontal displacement between the two ends of bottom chord after cracking
u_t	Relative horizontal displacement between the two ends of top chord
u_{tc}	Relative horizontal displacement between the two ends of top chord after cracking
v_b	Relative vertical displacement between the two ends of bottom chord
v_{bc}	Relative vertical displacement between the two ends of bottom chord after cracking
v_t	Relative vertical displacement between the two ends of top chord

Notation	Meaning
v_{tc}	Relative vertical displacement between the two ends of top chord after cracking
V	Reaction at the right support
V_b	Shear force in bottom chord
V_c	Shear capacity of the critical chord
V_{cc}	Shear contributions from concrete
V_{cf}	Shear contributions from FRP
V_{crbL}	Reaction force at the right support corresponding to the cracking of the left end of bottom opening
V_{crbR}	Reaction force at the right support corresponding to the cracking of the right end of bottom opening
V_{crtL}	Reaction force at the right support corresponding to the cracking of the left end of top opening
V_{crtR}	Reaction force at the right support corresponding to the cracking of the right end of top opening
V_{cs}	Shear contributions from steel stirrups
V_L	Reaction at the right support calculated from M_L
V_R	Reaction force at the right support calculated from M_R
V_t	Shear force in top chord
w_f	Width of FRP sheet
w_0	Crack opening displacement at the complete release of stress or fracture energy
w_t	Crack opening displacement
x	Height of compressive zone of the cross section
x_b	Distance between the centroids of the cross sections at the left end and right end of bottom chord after cracking
x_t	Distance between the centroids of the cross sections at the left end and right end of top chord after cracking
y_L	Deflection of left end of the opening

Notation	Meaning
y_O	Relative vertical displacement between the two ends of the opening
y_R	Deflection of right end of the opening
z	Distance between the midlines of the top and bottom chords
z_n	Distance between the centroids of the top and bottom chords
z_L	Distance between the centroids of the top and bottom chords at the left end of the opening after cracking
z_R	Distance between the centroids of the top and bottom chords at the right end of the opening after cracking
α	The coefficient representing the initial tangent modulus of concrete
β	Damping factor
β_s	Shear retention factor
β_{w}	Width ratio factor
γ	Inter story drift angle
ε	Compressive strain of concrete
ε_c	Axial strain of confined concrete
ε_{cr}	Concrete cracking strain
$\varepsilon_{cr,u}$	Concrete cracking strain at the complete release of stress or fracture energy
ε_{cu}	Ultimate axial strain of confined concrete
ε_{fd}	Maximum tensile strain of FRP
$\varepsilon_{fe,v}$	Effective strain of FRP sheet
ε_{frp}	FRP material ultimate tensile strain
$\varepsilon_{h,rup}$	Actual hoop rupture strain of FRP
ε_j	Nominal hoop rupture strain in the equivalent FRP-confined circular column
ε_p	The corresponding strain of σ_p
ε_t	The axial strain at the transition point of the stress-strain model for FRP-confined concrete
ε_{to}	The corresponding tensile strain of σ_{to}

Notation	Meaning
η_C	Column-to-beam flexural strength ratio
θ_b	Relative rotation between the two ends of bottom chord
θ_{bc}	Relative rotation between the two ends of bottom chord after cracking
θ_L	Rotation under the bending moment M_L
θ_{Lcr}	Rotation under the bending moment M_{Lcr}
θ_{Ly}	Rotation under the bending moment M_{Ly}
θ_O	Relative rotation between the two ends of the opening
θ_R	Rotation under the bending moment M_R
θ_{Rcr}	Rotation under the bending moment M_{Rcr}
θ_{Ry}	Rotation under the bending moment M_{Ry}
θ_t	Relative rotation between the two ends of top chord
θ_{tc}	Relative rotation between the two ends of top chord after cracking
λ_{Ef}	Characteristic value of shear strengthening
ρ_{sc}	Cross-sectional area ratio of the longitudinal steel reinforcement
σ	Compressive stress of concrete
σ_c	Axial stress of confined concrete
$\sigma_{f,vd}$	Effective tensile stress of FRP sheet
σ_j	The corresponding nominal hoop rupture stress of ε_{frp}
σ_p	The maximum compressive stress of concrete
σ_t	Tensile stress normal to the crack of concrete
σ_{to}	The maximum tensile stress of concrete
τ	Local shear bond stress between FRP and concrete
τ_b	Bond strength between FRP and concrete
$\tau_{\max}$	Local bond strength
τ^s	Local shear bond stress between steel bars and concrete
ϕ	Coefficient of FRP strengthening scheme

CHAPTER 1

INTRODUCTION

1.1 STRONG COLUMN-WEAK BEAM HIERARCHY IN SEISMIC DESIGN OF RC FRAME STRUCTURES

The enforcement of a strong column-weak beam hierarchy based on the capacity design philosophy is widely accepted as an effective way to realize the beam sway mechanism (i.e., with plastic hinges at beam ends) in a reinforced concrete (RC) frame structure when subjected to seismic loading. The beam-sway mechanism is preferred to the storey-sway mechanism (i.e., with plastic hinges at column ends) as the former generally leads to better seismic performance. For this reason, many current design codes specify a flexural strength ratio (ratio between the sum of the flexural capacities of the columns at a joint to that of the beams framing into the joint) greater than 1 (such as 1.2 or other values) to ensure flexural failure in the beams preceding that of columns. For example, the required flexural strength ratio is 1.2 in the current ACI Code (ACI 318 2014), 1.2 or 1.35 corresponding to different requirements of structural ductility in the current European code (Eurocode-8 2004), and a variable within the range of 1.1~1.7 in the current Chinese code (GB-50011 2010).

Despite the strength ratios specified in the current design codes as mentioned above, studies of failed structures after major earthquakes have shown that the beam-sway mechanism rarely occurred (ATC-40 1996) because most of the failed frames were designed according to codes (generally previous codes) which do not or do not adequately enforce the strong column-weak beam requirement. The above observation is particularly relevant to the recent magnitude (Ms) 8.0 Wenchuan earthquake in 2008 (Chinese Academy of Building Research 2008), where failure of cast-in-place RC frames commonly occurred at column ends (Fig. 1.1) (Ye et al. 2008; Gao and Ma 2009; Lin et al. 2009); the beam-sway mechanism was normally found only in frames with no floor slabs or with precast floor slabs (Fig. 1.2). The prevalence of column end failures has been attributed to one major deficiency in the previous version of the Chinese code (GB-50011 2008): the code did not include the contribution of the cast-in-place slab in tension to the flexural capacity of the beam in negative bending (Lin et al. 2009). Existing experimental studies on both exterior joints and interior joints with a slab (e.g. Ehsani and Wight 1985; Durrani and Wight 1987; Pantazopoulou and Moehle 1990; Zerbe and Durrani 1990; Guimaraes et al 1992; Siao 1994; LaFave and Wight 1999; Pantazopoulou and French 2001; Shin and LaFave 2004a, 2004b; and Canbolat and Wight 2008) have established conclusively that a cast-in-place slab in tension can contribute significantly to the negative flexural capacity of a beam. As a result, it can be expected that in many RC frames in the Chinese mainland, the beams are stronger than the columns at a joint. The latest Chinese seismic design code (GB-50011 2010), which came into force in December 2010, requires the consideration of the contribution of a cast-in-place slab to the beam flexural capacity in addition to the adoption of higher flexural strength ratios. Many existing RC buildings cannot meet these new requirements. In other countries or regions, similar threats induced by the violation of the strong column-weak beam hierarchy in the older existing buildings may also exist. For example, buildings designed in accordance with ACI 318 (1983) or older versions which did not consider the contribution of the cast-in-place slab in tension to the flexural capacity of the beam in negative bending are likely to violate this hierarchy.

To enforce the strong column-weak beam hierarchy in existing cast-in-place RC frames whose design does not satisfy this hierarchy, strengthening of columns might be an option. Common column retrofitting methods include concrete jacketing (e.g. Thermou et al. 2007), steel jacketing (e.g. Xiao and Wu 2003) and fiber-reinforced polymeric (FRP) jacketing (Teng et al. 2002). The former two methods may lead to increases in mass and/or stiffness and thus increases in seismic forces, while FRP jacketing has been widely used in recent years as a simple but effective method for column strengthening. However, the strength enhancement may be small, especially when FRP jacketing is applied for confining non-circular columns. And even when column strengthening is sufficient, the location of failure may simply shift from column ends to the foundation and/or beam-column joints, which are both difficult to retrofit. Therefore, column strengthening alone is often not enough to change the strength hierarchy.

1.2 PROPOSED SEISMIC RETROFIT TECHNIQUES

Against the above background, a novel seismic retrofit method for cast-in-place RC frames which violate the strong column-weak beam hierarchy is proposed by Prof. Teng to implement the strong column-weak beam hierarchy (Teng et al. 2013). This method is based on Beam-end Weakening in combination with FRP

Strengthening (referred to as the BWFS method hereafter for simplicity). Based on the concept of BWFS, the following three seismic retrofit techniques could be used to enforce the strong column-weak beam hierarchy where necessary and/or appropriate (Teng et al. 2013):

1) The first technique, referred to as the beam opening (BO) technique, involves the creation of an opening on the web in each end region of a T-section beam adjacent to the beam-column joint, as shown in Fig. 1.3. The internal longitudinal steel reinforcement should be kept intact during the weakening process. If the opening is large enough, the flexural capacity of the T-section beam in negative bending can be expected to reduce to a desired value. Local strengthening of regions adjacent to the opening (e.g. using FRP wraps and/or near-surface mounted FRP strips) is needed, particularly to ensure that the weakened beam still has an adequate shear resistance.

2) The second technique, referred to as the section reduction (SR) technique, involves the removal of concrete (and some of the longitudinal steel bars if necessary) from the bottom zone of the beam (i.e. the compression zone under negative bending) adjacent to the beam-column joint, as shown in Fig. 1.4. This method reduces the effective section height under negative bending and is expected to be highly effective in reducing the beam flexural capacity. The severing of some of the bottom longitudinal steel bars directly reduces the amount of longitudinal steel compression reinforcement under negative bending. Local strengthening of the region adjacent to the gap induced by material removal can also be implemented using FRP warps and/or near-

surface mounted FRP strips.

3) The third technique, referred to as the slab slit (SS) technique, involves the separation of the slab in the corner region from each supporting beam by cutting a slit (including the severing of the steel bars crossing the slit) between them, as shown in Fig. 1.5. In this method, the path of stress transfer from the beam to the slab near the beam-column joint is weakened so that the contribution of a cast-in-place slab to the beam flexural capacity in negative bending is substantially reduced or totally eliminated. Strengthening of the slab for its sagging moment capacity, as a result of the introduction of slits, can be easily achieved using FRP reinforcement if needed.

It should be noted that all the three techniques described above can be used in combination with column strengthening if necessary. While the BO method cannot be used together with the SR method, either of these two methods can be used in conjunction with the SS method to achieve a better weakening effect on the flexural capacity of the beam in negative bending.

To the best of the candidate's knowledge, the first two techniques are new and no research is available on their effectiveness and the relevant design methods. Only a few studies on the effectiveness of the SS technique have been conducted (Zhang et al. 2011; Wang et al. 2012; Zhang 2013). For these techniques to be used in practice, research is needed on the effects of each intervention technique on the beam flexural and shear capacities as well as the seismic response of such a weakened beam.

For the BO technique, it should be noted that creating web openings in RC beams is not a new thing. For the passage of utility ducts/pipes, such as electricity, heating, water supply systems as well as air conditioning, telephone, internet cables and sewage conduits, pre-formed rectangular or circular web openings in RC beams have been widely used in new structures (e.g. Kennedy and Abdalla 1992; Mansur 1998; Tan et al. 2001). With such web openings in the beam, extra storey heights for accommodating such ducts/pipes are not necessary anymore. This could help reduce the overall height of the building and thus decrease the loads on the load-carrying structural members and foundation, leading to a more cost-effective design of the building. In existing structures, if such ducts/pipes are needed and there are no pre-formed web openings in RC beams for such a purpose, cutting web openings in the beams is an appealing solution and has already been adopted in real projects (e.g. Mansur et al. 1999; Maaddawy and Sherif 2009; Maaddawy and Ariss 2012). This kind of web openings is usually located in the regions where the bending moment is small. If the web opening is moved to be located near the beam end, the two requirements can be met at the same time: one is to weaken the beam end to meet the strong column-weak beam hierarchy, and the other one is to meet the functional requirements such as electricity conduits, which will be very attractive.

For the SR technique, the removal of the compressive concrete (and some of the steel bars) is expected to reduce the section flexural capacity significantly; this reduction can be easily estimated by a conventional section analysis, but the accuracy of such an approach does need some verification.

For the SS technique, the method may appear to have a simple and clear effect on the seismic performance of the beam, but the real effect may be quite complicated. The introduction of slits modifies the stress transfer path from the beams to the slab: due to the presence of slits, the stress transfer path may now form around the slits and spread to a wider region of the slab. This effect needs to be understood and quantified in research. In addition, the slits modify the support condition of the slab, and leads to greater sagging moments in the slab under gravity loading. As a result, the sagging moment capacity of the slab may need to be enhanced with appropriate strengthening measures.

1.3 OBJECTIVES, SCOPE AND LAYOUT OF THIS THESIS

Of the three techniques mentioned in the preceding section, the flexural capacity reduction caused by the SR and the SS techniques can be estimated relatively easily, but the same is not true about the BO method. Moreover, as discussed above, the BO technique can also meet the functional requirement of accommodating utility ducts. The present PhD study, therefore, is mainly focused on the effect of the BO method on the flexural capacity of the beam, with the aims being to assess its feasibility and to develop corresponding strength models/design methods.

Although the existing studies motivated by the need to create one or more web openings in an existing structure for the passage of utility ducts have provided useful information on the behaviour of RC beams with such openings (referred to simply as "beams with a web opening" or "beams with an opening" for simplicity regardless of the number of openings as the openings are generally far apart and do not interact with each other), a rational and reliable method of predicting the load capacities of such RC beams, which is a prerequisite for the development of a strengthening method for such RC beams, is still lacking. So far, most existing experimental studies on the behaviour of RC beams with a web opening have been focused on rectangular beams, with only the study of Mansur et al. (1999) concerned with T-section beams with a circular opening being an exception, so more experimental studies need to be conducted to investigate effect of drilling a web opening on the behaviour of T-section beams.

While experimental studies are essential in understanding the structural behaviour of RC beams with a web opening, there are many aspects that cannot be easily exposed or well understood using experimental tests alone. In this context, the use of finite element (FE) models is a powerful and economical alternative to laboratory testing to obtain a better understanding of the structural behaviour of RC beam with a web opening, and reliable FE models can also be used in parametric studies to generate extensive data for developing strength models and design methods. However, so far most existing studies on the behaviour of RC beams with a web opening were experimentally based and only a very limited number of studies have been carried out on numerical simulation (Pimanmas 2010; Chin et al. 2012; Hawileh et al. 2012). These limited studies have not led to establish a reliable FE model for RC beams with a web opening.

Against the above background, the research presented in this thesis was aimed to provide an in-depth understanding of RC beams with an un-strengthened/FRP-strengthened web opening through combined experimental and numerical investigations, with the main objectives being:

1) To carry out systematic experimental tests to investigate the behavior of RC T-section beams with an un-strengthened/FRP-strengthened web opening and clarify the effect of web opening dimensions on the behavior of such RC beams;
2) To develop advanced finite element models, which can then be verified with the tests conducted by the candidate and those collected from open literature. The established FE models enable a better understanding of the behavior of RC beams with an un-strengthened/FRP-strengthened web opening;
3) To develop a strength model for RC beams with an un-strengthened/FRP-strengthened web opening to predict the flexural capacity of such beams; and
4) To establish a moment-rotation model for the web opening region. This moment-rotation model could be directly defined as a beam property in the modelling of structures using an existing structural analysis package (e.g., OpenSees) that can accommodate such moment-rotation models.

The experimental studies were conducted at either the Structural Engineering Research Laboratory of The Hong Kong Polytechnic University or the Civil Engineering Experimental Demonstration Center of Guangzhou University of Technology. Finite element modelling was carried out by employing the general-purpose FE program ABAQUS (2012). The contents of this thesis are summarized below.

Chapter 2 presents a comprehensive literature review of existing experimental, numerical and theoretical studies related to the present topic. It starts with a review of the strong column-weak beam design philosophy, including the relevant existing research and the implementation history of this philosophy in design provisions. Afterwards, for the proposed beam opening (BO) technique based on the concept of BWFS, a review of the existing experimental and numerical studies on RC beams with a web opening is given. From the review, it can be seen that the existing studies have not been sufficient to obtain a full understanding of the structural behaviour of RC beams with a web opening.

Chapter 3 proposes a 2-dimentional nonlinear FE model for the existing experimental studies which have been mainly focused on RC beams with an un-strengthened web opening, based on the work done by Chen et al. (2011) for the modelling of RC beams strengthened using externally bonded FRP reinforcement. The proposed FE model employs the dynamic analysis approach (i.e., the explicit central difference method available in ABAQUS) instead of the static analysis approach (e.g. Newton-Raphson method and the arc-length method) in order to overcome the severe numerical convergence difficulties commonly encountered in the modelling of cracked concrete using a static analysis approach. In the proposed FE model, plane stress elements are employed to simulate the RC beam. The modelling of concrete (especially the cracked concrete) and the bond behaviour between the concrete and the internal steel reinforcement as well as the determination of the dynamic parameters were carefully considered. The accuracy of the proposed FE model was verified with existing tests collected from the open literature.

Chapter 4 extends the FE model proposed in Chapter 3 to simulate RC beams with an FRP-strengthened web opening, in which debonding between FRP and concrete is a possible failure mode. The bond-slip model proposed by Lu et al. (2005) for externally bonded FRP strengthening systems was incorporated into the FE model to simulate the bond behavior between FRP and concrete. The accuracy of the extended FE model was verified with existing tests collected from the open literature.

Chapter 5 presents a systematic experimental study conducted by the candidate to fill the knowledge gaps of the existing studies. While the existing studies were mainly concerned with rectangular RC beams with a web opening, the present study was focused on T-section RC beams with a web opening. A total of 14 full-scale RC beams, including one rectangular beam and 13 T-section beams, were designed and tested under static loading to assess the effect of a beam opening on the behaviour of T-section RC beams. The studied parameters cover the dimensions of web opening and the effect of FRP strengthening (including CFRP wraps on the concrete web chord and CFRP U-jackets on the beam web). The experimental study not only proved the effectiveness of the proposed BO technique in weakening the flexural capacity of T-section beams and the effectiveness of the proposed FRP strengthening system in compensating for the shear capacity loss of the beam due to the existence of the web opening, but also provided detailed test data for the calibration and verification of the subsequent numerical and theoretical studies conducted by the candidate.

Chapter 6 presents an FE study on T-section RC beams with an un-strengthened or FRP-strengthened web opening. Due to the existence of a beam flange, the failure modes of T-section RC beams with a web opening are different from those observed in existing tests on rectangular RC beams with a web opening, and thus the FE models proposed in Chapters 3 and 4 may not be applicable anymore. The concrete damaged plasticity (DP) model and brittle cracking (BC) model available in ABAQUS (2012) were carefully examined by comparing FE predictions with test results. In addition, the confinement effect from the CFRP wrap on the web concrete chord was investigated by adopting the design-oriented stress-strain model for FRP-confined concrete in rectangular columns proposed by Lam and Teng (2003).

Chapter 7 presents a strength model for RC beams with a web opening. The proposed strength model is based on the strengths of the four plastic hinges formed at the ends of the two chords (the web and flange chords). The axial force-bending moment interaction diagrams of the cross-section at each end of the two chords are obtained first through section analysis. The strength of the beam is then obtained through a trial-and-error process by considering equilibrium of forces and moments in the beam and at the ends of the two chords, based on the assumption that the axial forces in the two chords have the same magnitude but different signs (i.e., one is in tension while the other in compression). The accuracy of the proposed strength model was verified with the tests conducted by the candidate.

Chapter 8 develops moment (M)-rotation (Θ) relationships for the two beam cross-sections at the two ends of the web opening, respectively, based on the findings from the tests conducted by the candidate and theoretical derivations on the basis of equilibrium and deformation compatibility. The proposed M-Θ relationships were then employed in a beam model established in OpenSees (OpenSees 2009) to simulate the behavior of RC beams with a web opening, which verified the accuracy of the proposed M-Θ relationships.

Chapter 9 presents a summary of conclusions from this PhD research project and elaborates on future research needs.

1.4 REFERENCES

ABAQUS (2012). *ABAQUS Analysis User's Manual (Version 6.12)*, Dassault Systems SIMULIA Corporation, Providence, Rhode Island, USA.

ACI 318 (1983). *Building Code Requirements for Structural Concrete and Commentary* (*ACI 318-83)*, ACI Committee 318, American Concrete Institute, Farmington Hills, MI.

ACI 318 (2014). *Building Code Requirements for Structural Concrete and Commentary* (*ACI 318-14)*, ACI Committee 318, American Concrete Institute, Farmington Hills, MI.

ATC-40 (1996). *Seismic Evaluation and Retrofit of Concrete Buildings*, Applied Technology Council, Redwood City, California.

Canbolat, B.B. and Wight, J.K. (2008). "Experimental investigation on seismic behavior of eccentric reinforced concrete beam-column-slab connections", *ACI Structural Journal*, 105(2), 154-162.

Chen, G.M., Teng, J.G. and Chen, J.F. (2011). "Finite element modeling of intermediate crack debonding in FRP-plated RC beams", *Journal of Composites for Construction*, ASCE, 15(3), 399-353.

Chin, S.C., Shafiq, N. and Nuruddin, M.F. (2012). "Strengthening of RC beams with large openings in shear by CFRP laminates: experiment and 2D nonlinear finite element analysis", *Research Journal of Applied Sciences, Engineering and Technology*, 4(9), 1172-1180.

Chinese Academy of Building Research (2008). *Photo Collection of 2008 Wenchuan Earthquake Damage to Buildings*, China Architectural & Building Press, Beijing, China (in Chinese).

Durrani, A.J. and Wight, J.K. (1987). "Earthquake resistance of reinforced concrete interior connections including a floor slab", *ACI Journal*, 84(5), 400-406.

Ehsani, M.R. and Wight, J.K. (1985). "Effect of transverse beams and slab on behavior of reinforced concrete beam to column connections", *ACI Journal*, 82(2), 188-195.

Eurocode 8 (2004). *Design of Structures for Earthquake Resistance – Part 1: General Rules, Seismic Actions and Rules for Buildings (EN 1998-1: 2004)*, CEN, Brussels.

Gao, Z.R. and Ma, Q.L. (2009). "Effect of cast-in-place slab on column-beam strength ratio in frame structure", *Shanxi Architecture*, 35(17), 1-3 (in Chinese).

GB-50011 (2001). *Code for Seismic Design of Buildings*, Architectural & Building Press, Beijing, China (in Chinese).

GB-50011 (2010). *Code for Seismic Design of Buildings*, Architectural & Building Press, Beijing, China (in Chinese).

Guimaraes, G.N., Kreger, M.E. and Jirsa, J.O. (1992). “Evaluation of joint-shear provisions for interior beam-column-slab connections using high-strength materials”, *ACI Structural Journal*, 89(1), 89-98.

Hawileh, R., El-Maaddawy, T., and Naser, M. (2012). “Nonlinear finite element modeling of concrete deep beams with openings strengthened with externally-bonded composites”, *Materials & Design* (DOI: 10.1016/j.matdes.2012.06.004, 378-387).

Kennedy, J.B. and Abdalla, H. (1992). “Static response of prestressed girders with openings”, *Journal of Structural Engineering*, ASCE, 118(2), 488-504.

LaFave, J.M. and Wight, J.K. (1999). “Reinforced concrete exterior wide beam-column-slab connections subjected to lateral earthquake loading”, *ACI Structural Journal*, 96(4), 577-587.

Lam, L. and Teng, J. G. (2003). "Design-oriented stress-strain model for FRP-confined concrete in rectangular columns", *Journal of Reinforced Plastics and Composites*, 22(13), 1149-1186.

Lin, X., Pan, P., Ye, L., Lu, X. and Zhao, S. (2009). “Analysis of the damage mechanism of a typical RC frame in Wenchuan earthquake”, *China Civil Engineering Journal*, 42(5), 13-20 (in Chinese).

Lu, X.Z., J.G. Teng, Ye, L.P. and Jiang, J.J. (2005). “Bond-slip models for FRP sheets /plates bonded to concrete”, *Engineering Structures*, 27(6), 920-937.

Maaddawy, T. and Sherif, S. (2009). “FRP composite for shear strengthening of reinforced concrete deep beams with openings”, *Composite Structures*, 89(1), 60-69.

Maaddawy, T. and El-Ariss, B. (2012). “Behavior of concrete beams with short shear span and web opening strengthened in shear with CFRP composites”, *Journal of Composites for Construction*, ASCE, 16(1), 47–59.

Mansur, M.A. (1998). “Effect of opening on the behaviour and strength of R/C beams in shear”, *Cement and Concrete Composites*, 20(6), 477-486.

Mansur, M.A., Tan K.H. and Wei, W. (1999). “Effects of creating an opening in existing beams”, *ACI Structural Journal*, 96(6), 899-906.

OpenSees (2009). *Open System for Earthquake Engineering Simulation*, Pacific Earthquake Engineering Research Center, University of California at Berkeley, http://opensees.berkeley.edu.

Pantazopoulou, S.J. and Moehle J.P. (1990). “Identification of effect of slabs on flexural behavior of beams”, *Journal of Engineering Mechanics*, ASCE, 116(1), 91-106.

Pantazopoulou, S.J. and French, C.W. (2001). “Slab participation in practical earthquake design of reinforced concrete frames”, *ACI Structural Journal*, 98(4), 479-489.

Pimanmas, A. (2010). “Strengthening R/C beams with opening by externally installed FRP rods: Behavior and analysis”, *Composite Structures*, 92(8), 1957-1976.

Shin, M. and LaFave, J.M. (2004a). “Seismic performance of reinforced concrete eccentric beam-column connections with floor slabs”, *ACI Structural Journal*, 101(3), 403-412.

Shin, M. and LaFave, J.M. (2004b). “Reinforced concrete edge beam-column-slab connections subjected to earthquake loading”, *Magazine of Concrete*

Research, 55(6), 273-291.

Siao, W.B. (1994). "Reinforced concrete column strength at beam/slab and column intersection", *ACI Structural Journal*, 91(1), 3-8.

Tan, K.H., Mansur, M.A., and Wei, W. (2001). "Design of reinforced concrete beams with circular openings", *ACI Structural Journal*, 98(3), 407-415.

Teng, J.G., Chen, J.F., Smith S.T. and Lam L. (2002). *FRP-Strengthened RC Structures*, John Wiley and Sons Ltd, UK, November, 245pp.

Teng, J.G., Zhang, S.S., Jing, D.H., Nie, X.F. and Chen, G.M. (2013). "Seismic retrofit of RC frames through beam-end weakening in conjunction with FRP strengthening", *Proceedings of the 4th Asia-Pacific Conference on FRP in Structures (APFIS 2013)*, 1-8.

Thermou, G.E., Pantazopoulou, S.J., Einashai, A.S. (2007). "Flexural behavior of brittle RC members rehabilitated with concrete jacketing", *Journal of Structural Engineering*, ASCE, 133(10), 1373-1384.

Wang, X.G., Shan, M.Y., Ge, N. and Shu, Y.P. (2012). "Finite element analysis of efficiency of slot-cutting around RC frame joint for 'strong column and weak beam'", *Journal of Earthquake Engineering and Engineering Vibration*, 32(1), 121-127 (in Chinese).

Xiao, Y. and Wu, H. (2003). "Retrofit of reinforced concrete columns using partially stiffened steel jackets", *Journal of Structural Engineering*, ASCE, 129(6), 725-732.

Ye, L.P., Qu, Z., Ma, Q.L., Lin, X.C, Lu, X.Z. and Pan, P. (2008). "Study on ensuring the strong column-weak beam mechanism for RC frames based on the damage analysis in the Wenchuan earthquake", *Building Structure*, 38(11), 52-67 (in Chinese).

Zerbe, H.E. and Durrani, A.J. (1990). “Seismic response of connections in two-bay reinforced concrete frame subassemblies with a floor slab”, *ACI Structural Journal*, 87(4), 406-415.

Zhang, J. (2013). *Research on Efficiency of Slot-cutting around Frame Joint for “Strong Column and Weak Beam" under Earthquake Action*, Master degree thesis: Hunan University, China (in Chinese).

Zhang, Y.P., Hao, Z.J., Shan, M.Y. and Ge, N. (2011). “Research on anti-seismic performance for reinforced concrete frame joint with slot around”, *Building Science*, 27(9), 7-11 (in Chinese).

Figure 1.1. Failure at column ends

(Courtesy of Prof. P. Feng, Tsinghua University, China)

Figure 1.2. Failure at beam ends

(Courtesy of Dr. D.H. Jing, Southeast University, China)

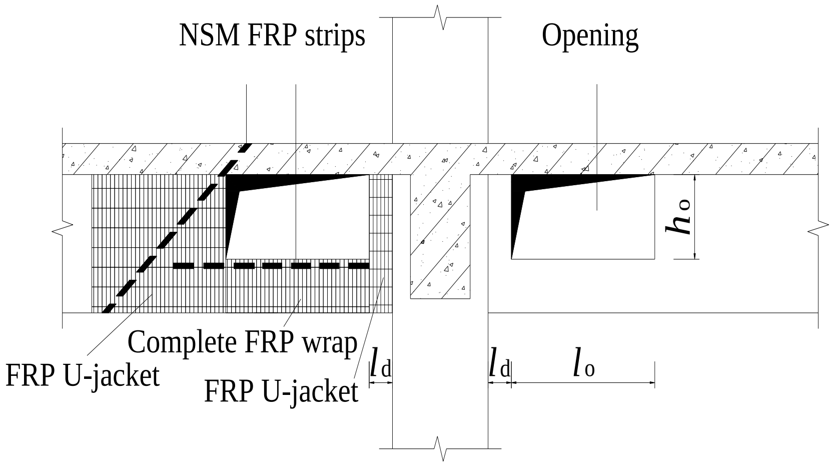

Figure 1.3. Beam opening (BO) technique

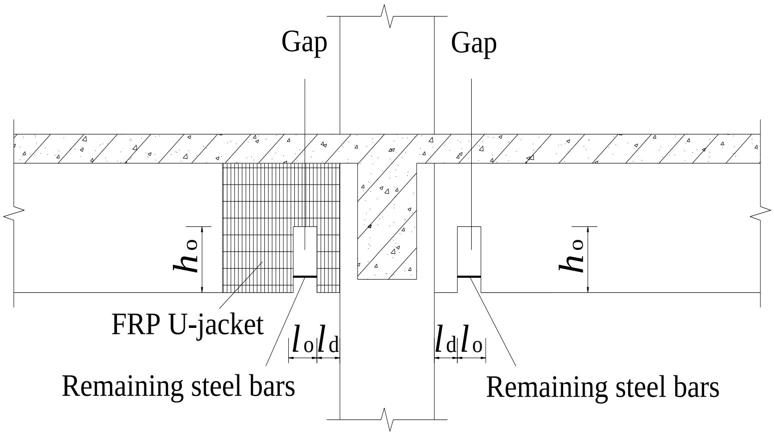

Figure 1.4. Section reduction (SR) technique

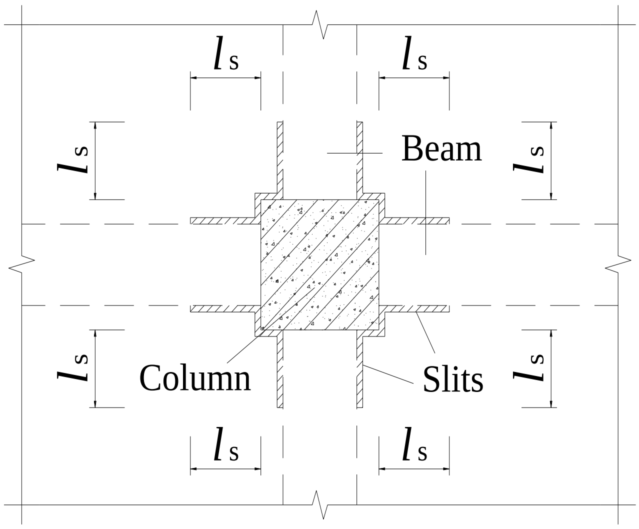

Figure 1.5. Slab slit (SS) technique

CHAPTER 2
LITERATURE REVIEW

2.1 INTRODUCTION

This chapter presents a literature review of existing research on relevant topics of the present PhD research programme. A comprehensive review of the strong column-weak beam design philosophy, including the research history of the strong column-weak beam philosophy and the development of design provisions for this design philosophy, is presented first. The implementation of strong column-weak beam hierarchy in real structural design is then discussed. Finally, existing experimental and numerical studies on RC beams with a web opening (to reduce the flexural capacity of the beam) are reviewed.

2.2 THE STRONG COLUMN-WEAK BEAM DESIGN PHILOSOPHY

The enforcement of a strong column-weak beam hierarchy based on the capacity design philosophy (Paulay 1979) is widely accepted as an effective way to realize the beam-sway mechanism (i.e., with plastic hinges forming first at beam ends) in a reinforced concrete (RC) frame structure when subjected to seismic loading. The beam-sway mechanism is preferred to the storey-sway mechanism (i.e., with plastic hinges forming first at column ends) as the former generally leads to better seismic performance. Beam failures are usually localized and will only influence limited parts of the structure, while column failures may cause progressive collapse of the entire structure and thus can lead to serious consequences. A large number of studies have been conducted in order to answer the following question: how to introduce the strong column-weak beam design philosophy into structural seismic design reasonably? This section and the several following sections give a review of relevant studies to shed light on the invention and development of the strong column-weak beam design philosophy as well as the adoption of this design philosophy in practical design.

The strong column-weak beam design philosophy was originally developed by Park and Paulay (1975) in New Zealand. In the late 70s of the 20th century, Park and Paulay (1975) proposed the capacity design method to ensure that RC structures develop sufficient global inelastic deformation before final failure. The capacity design method is a type of active seismic design method, which purposefully guides the failure mechanism of the structure and avoids undesirable failure modes.

The three main aspects covered by the capacity design method are: (1) strong column-weak beam design philosophy: to ensure that the beam sway mechanism could be realized in frame structures/frame-shear wall structures under seismic loading, that is, plastic hinges could be first formed at beam ends instead of column ends; (2) strong shear capacity-weak flexural capacity design philosophy: to ensure that the shear capacities of structural members (e.g. beams, columns, walls) are larger than their flexural capacities, in order to avoid the occurrence of brittle shear failure of the members; and (3) strong joint-weak member design philosophy: to ensure that the joints are stronger than the structural members, in order to avoid failure in the joints.

Although the present thesis is directly focused on the strong column-weak beam design philosophy, it is also related to the second aspect. For example, after making a web opening in the beam to reduce its flexural capacity to achieve the strong column-weak beam hierarchy in the structure, fiber-reinforced polymeric (FRP) strengthening system should be applied to make sure that the shear capacity of a weakened beam is still larger than its flexural capacity.

To achieve the strong column-weak beam hierarchy in an RC frame, the sum of the flexural capacities of the columns at a joint ($\sum M_C$) is required to be larger than that of the beams framing into the joint ($\sum M_B$), as expressed in the following equation:

$$\sum M_C = \eta_C \sum M_B \tag{2.1}$$

where η_C is called the column-to-beam flexural strength ratio and should be larger than 1. It has been reported that the strong column-weak beam mechanism may be violated due to the following two reasons: (1) underestimation of the flexural capacity of beams (i.e., actual flexural capacity of beams exceeds their flexural capacity calculated in design); and (2) the stipulated value of η_C is too low. Therefore, the related studies on the strong column-weak beam design philosophy have been mainly focused on the calculation of $\sum M_B$ and determination of a proper η_C, which will be introduced in the following sections.

2.3 CALCULATION OF THE FLEXURAL CAPACITY OF BEAMS $\sum \boldsymbol{M_B}$

Existing studies on the determination of $\sum M_B$ have mentioned that the value of $\sum M_B$ could be influenced by the existence of cast-in-place floor slabs, infill walls, over-reinforced beam ends, and so on.

2.3.1 Cast-in-place floor slabs

The effect of cast-in-place floor slabs on the flexural capacity of RC beams has attracted the most attention compared with other influencing factors. Cast-in-place floor slabs connect well with a rectangular beam to form a T-section beam with the rectangular beam acting as the web of the T-section beam and the slabs serving as the flange of the T-section beam, which can significantly enhance the bending stiffness and flexural capacity of the beam. A review of existing studies, including both experimental and numerical investigations, on the effect of cast-in-place slabs on the capacity of RC beams is given below.

2.3.1.1 Experimental studies

In the early 1980s, experimental studies on a full-scale 7-storey RC frame were jointly conducted by the researchers from the United States and Japan (Durrani and Wight 1982, Otani et al. 1984, JTCC 1988). The studies showed that in the RC frame under lateral loading, cast-in-place floor slabs could lead to a considerable increase in the flexural capacity of the beam. Such an increase was not taken into consideration in the design of the frame as such consideration was not available in design provisions at that time. Therefore, failure of the test frame was controlled by shear failure at joints.

Tests on RC column-beam joints conducted by Bertero et al. (1984), Otani et al. (1984), Suzuki et al. (1984) and Qi (1986) showed that while the joints were designed in strict accordance with the design codes to prevent failure in joints, plastic hinges formed first at the column ends. The reason was an unexpected increase in the flexural capacity of the beams mainly caused by cast-in-place floor slabs.

Leon (1984) reported two contrast specimens (Joint BCJ8 without a slab and Joint BCJ9 with a slab) to clarify the effect of cast-in-place floor slab on the behavior of RC joints. Again, there were no design provisions at that time to account for the increase in the flexural capacity of beams caused by slabs. Test results showed that the presence of a cast-in-place floor slab significantly affected the strength and behavior of the joints: the plastic hinges formed first at the beam ends in Joint BCJ8 which had no slab, while the plastic hinges formed first at columns ends in Joint BCJ9 which had a slab.

Researchers from Tongji University and the China Academy of Building Research in collaboration with those from Japan, New Zealand and the United States tested six full-scale two-way joints (Tang 1985), and reported that the cast-in-place floor slab significantly enhanced the negative flexural capacity of the beams.

Durrani and Zerbe (1987) tested a total of six 3/4-scale joints under cyclic lateral loading to study the effect of cast-in-place slabs on the behavior of exterior joints. The test results showed that the cast-in-place floor slab had a significant effect on the strength, stiffness and energy dissipation characteristics of the joints. Thus it was strongly suggested that the effect of cast-in-place floor slabs should be considered in the design of joints.

Durrani and Wight (1987) tested three interior joints to study the effect of cast-in-place slabs on the behavior of interior joints. The test results indicated that the cast-in-place slabs obviously affected the behavior of interior joints: at a drift level of 1.5%, the steel reinforcement in the slab began to yield, while all the steel reinforcement within the entire width of the slab had yielded at a drift level of 4%. Therefore they concluded that the contribution of the slab to the flexural capacity of the beam cannot be ignored.

French (1991) conducted analysis on the collected test data of 20 beam-slab-column joints (13 interior joints and 7 exterior joints). The results showed that the predicted strength of interior joints with the effect of the cast-in-place floor slab ignored was less than the test result by an average of 25%, while the predicted strength of exterior joints with the effect of the cast-in-place floor slab ignored was less than the test result by an average of 17%.

Qi and Pantazopoulou (1991) conducted a test on a 1/4-scale single-story RC frame with cast-in-place floor slabs under cyclic lateral loading. The test results showed that cast-in-place slabs significantly increased the flexural capacity of the beams, especially at the interior support.

Jiang et al. (1994) tested two contrast specimens, with one joint having cast-in-place floor slabs and the other one having no slabs. The test results showed that due to the contribution from the cast-in-place floor slab, the negative flexural capacity of the beam increased by as much as 30%.

Zhen et al. (2009) tested three groups of RC joints with different reinforcement schemes under cyclic lateral loading. Each group included a joint without a cast-in-place floor slab and one/four/two joints with a cast-in-place floor slab. Test results showed that the strengths of joints with a cast-in-place floor slab in group 1, 2 and 3 were respectively about 1.6, 2.0 and 2.3 times of those of the corresponding joints without a cast-in-place floor slab.

2.3.1.2 Numerical studies

In addition to experimental investigations, a large number of numerical studies on the effect of cast-in-place floor slabs on the seismic performance of RC frames have been conducted. Guan and Du (2005) conducted pushover analysis of a 3-storey-3-span RC frame using SAP2000 (1998). After the 2008 Wenchuan earthquake in China, Lin et al. (2009) conducted elastic-plastic time history analysis of a 6-storey RC frame structure damaged in the earthquake using MSC.Marc (2005). Comparison between two 3-dimentional (3-D) models (pure frame and frame with cast-in-place floor slabs) was carried out. Gao and Ma (2009) conducted pushover analyses of two 6-storey 4x4-span (the two span numbers in the two perpendicular directions in the plane) RC frames (one with floor slabs and one without floor slabs) using SAP2000. Yang (2010) conducted pushover analyses of five 6-storey 4x4-span RC frames with different slab widths using SAP2000. Chen (2010) conducted elastic-plastic time history analyses of two 6-storey 6x3-span RC frames (one with floor slabs and one without floor slabs) using SAP2000. Guo (2012) designed a 3-storey 3x4-span RC frame, established three FE models and conducted pushover analyses using SAP2000: one with cast-in-place slabs and slab reinforcement, one with cast-in-place slabs but without slab reinforcement and one without slabs.

Details of the above numerical analyses are given in Table 2.1. All these numerical results indicated that cast-in place floor slabs could significantly increase the negative flexural capacity of the beams and lead to the weak column-strong beam mechanism in RC frames.

2.3.1.3 Determination of effective flange width

A large number of experimental studies (e.g. Jiang 1994; Bijan and Aalami 2001; Huang et al. 2001) have indicated that the stresses of steel bars in a cast-in-place floor slab are not evenly distributed along the width direction of the beam. Instead, the stress in a steel bar in the floor slab deceases with an increase in the distance between the steel bar and the beam, due to the well-known shear lag effect. Therefore, only steel bars within a limited range of width away from the beam can reach their yield strength at the failure of the beam (Wu et al. 2002; Wang et al. 2009; Zhen et al. 2009). In order to quantify the effect of a cast-in-place floor slab on the flexural capacity of the beam, an effective flange width (b_f) has been proposed by previous researchers in the calculation of contribution from a cast-in-place floor slab to the flexural capacity of the beam supporting it (Wu et al.

2002; Wang et al. 2009). It is assumed that all longitudinal steel bars in the cast-in-place floor slab within the effective flange width can be equally strained in the bending of the beam. The suggested values of the effective flange width of floor slabs for interior and exterior joints (Durrani and Zerbe 1987; French 1991; Li 1994; Jiang et al. 1994; Wu et al. 2002; Wang et al. 2009; Zhen et al. 2009; Yang 2010; Sun 2010; Qi et al. 2010; and He 2010) are given in Table 2.2.

It can be seen from Table 2.2 that the factors which can influence the effective flange width include the inter-story drift angle (γ) (i.e. inter-story drift dived by the story height), joint types (i.e. interior joints and exterior joints), slab thickness (t), beam height (h), effective span of beam (l_0) and clear distance between two adjacent beams. Most existing studies only paid attention to interior joints, while three studies (Zhen et al. 2009; Sun 2010; and Qi et al. 2010) proposed effective flange widths for both interior joints and exterior joints. It was found that the effective flange width for interior joints is usually larger than that for exterior joints if the other parameters are the same. Most formulas proposed to calculate the value of effective flange width have the slab thickness as the main parameter (Li 1994; Jiang et al. 1994; Wu et al. 2002; Wang et al. 2009; Yang 2010; and He 2010), while several formulas related the effective flange width to more factors such as the beam height, the effective span of beam and the clear distance between two adjacent beams and so on (French 1991; Zhen et al. 2009; Sun 2010; and Qi et al. 2010). In addition, a large number of the existing studies (French 1991; Zhen et al. 2009; Sun 2010; Qi et al. 2010; and He 2010) examined the effective flange width when inter-story drift angle is equal to 1/50.

2.3.2 Infill walls

Ye et al. (2008) studied RC frames damaged in the 2008 Wenchuan earthquake in China and analyzed the factors that caused the violence of the strong column-weak beam mechanism. The effect of infill walls, which was not fully considered in structural design, was found to be one of the main causes. In most real structures, infill walls usually stand directly on the beams, which would cause the following effects (Ye et al. 2008): (1) infill walls can increase the stiffness and flexural capacity of the beam and reduce the deformation of the beam; (2) infill walls will be involved in the seismic performance of the overall structure, increasing the stiffness of the storeys with infill walls, leading to a non-uniform stiffness distribution of the structure, rendering storeys with no infill walls weak layers (usually at the ground floor) and thus resulting in the formation of the storey-sway mechanism; infill walls would also lead to an irregular distribution of the structural plane stiffness and cause a torsional effect; (3) due to the existence of infill walls, the total stiffness of the structure would increase, leading to a decrease in the basic period of the structure by about 40%-60% and thus an increase in the seismic loading; (4) infill walls would affect the internal force distribution and failure mode of RC frames. For example, the lateral deformation of a column can be restricted by the infill walls and thus the column would become a short column (Xiong 2011; Li 2015). The authors concluded that the effect of infill walls on the seismic performance of the whole structure was very complicated and should be considered in structural design.

Lin et al. (2009) conducted elastic-plastic time history analysis on a 6-storey 3x9-span RC frame structure damaged in the earthquake area by using MSC.Marc (2005). Comparisons between three schemes (pure frame, frame with cast-in-place floor slabs, and frame with both cast-in-place floor slabs and infill walls) were analyzed. The analysis results indicated that infill walls may significantly change the failure mechanism of the RC frame and the storey-sway mechanism may easily occur for a structure with non-uniformly distributed infill walls. The authors suggested that the effects of infill walls should be considered in seismic design of RC frames and structural elastic-plastic numerical analyses of RC frames should also take into account infill walls.

Chen (2010) designed four 6-storey 6x3-span RC frames and established FE models for them: one pure frame, one frame with floor slabs, one frame with both cast-in-place floor slabs and infill walls, and one frame with both cast-in-place floor slabs and infill walls except the ground floor. Results of linear and non-linear time history analyses conducted on these four frame models indicated that the existence of infill walls affected the failure mode of the structure. In particular, the non-uniform layout of infill walls led to the formation of a weak layer in the frame and the storey-sway mechanism.

Xiong (2011) established FE models for two 5-storey 2-span RC frames (one pure frame and one frame with infill walls) and conducted pushover analyses of these two frames. Analysis results indicated that the failure of RC frames without infilled walls for the ground level would occur at the ground level.

Shi (2012) tested two 1/4-scale 3-storey 2x2-span RC frames, one pure frame and one frame with infill walls, and then conducted elastic-plastic time history FE analyses of these two frames using PERFORM-3D (2011). Both test and numerical results showed that infill walls could significantly change the internal force distribution of the structure and increase bending moments at the column ends, leading to the failure of columns prior to the failure of beams.

A summary of the above studies is given in Table 2.3.

2.3.3 Over-reinforced beam ends

In structural design, over-reinforcement of beam ends is quite usual and could be caused by the following reasons (Ye et al. 2008; Liu et al. 2004; Wei et al. 2007): (1) the reinforcement of beam ends may be designed based on the bending moment at joint centre rather than at the beam end (i.e., omission of the width of column); (2) the reinforcement of the beam may be controlled by the limit of deformation or crack width rather than strength; (3) when the moments at the two beam ends of a joint is not equal, for ease of construction, the reinforcement at both beam ends is usually designed based on the larger value of the two moments; and (4) the real cross-sectional area of reinforcement is usually enlarged to certain extent by the designer to achieve a “safer” design. The adverse effects of the above factors can be avoided if the calculation of ΣM_B in Eq. 2.1 is based on the actual reinforcement. However, the calculation of ΣM_B is usually based on the design bending moments at the beam ends rather than the actual reinforcement (GB-50011 2010 or older versions). A summary of existing studies on the effect of over-reinforced beam ends in RC frames is given in Table 2.4. By using PL-AFJD (Yang 2000), Lei (2002) conducted elastic-plastic time history analyses of three RC frames. For two of the frames, the flexural capacities of beams and columns were calculated based on the actual reinforcement; and for one of the frames, the flexural capacities of beams and columns were calculated based on the design moments. Liu et al. (2004) conducted elastic-plastic time history analyses of two RC frames. For one of the frames, the flexural capacities of beams and columns were calculated based on the actual reinforcement; and for the other frame, the flexural capacities of beams and columns were calculated based on the design moments. By using OpenSees (2009), Han et al. (2010) conducted push-over analyses on two RC frames, with one having no over-reinforced beam ends and the other one having over-reinforced beam ends (the beam reinforcement at beam ends was increased by 10%). Analysis results showed that the RC frames which did not have over-reinforced beam ends exhibited beam-sway mechanism, while storey-sway mechanism was formed in RC frames which had over-reinforced beam ends.

2.4 DETERMINATION OF COLUMN-TO-BEAM FLEXURAL STRENGTH RATIO (η_C)

A proper value of the column-to-beam flexural strength ratio η_C in Eq. 2.1 is very important to achieve the strong column-weak beam mechanism in RC frames. By now, there have been a large number of studies on the determination of η_C, which are summarized in Table 2.5 and explained below.

Xu et al. (1986) conducted an experimental study on a 3-storey 2-span RC pure frame under cyclic lateral loading to investigate the relationship between the strengths of columns and beams framing into a joint. The test results showed that η_C of each joint in the frame was between 1.42 and 2.86 and the frame achieved beam-sway mechanism with good ductility. The elastic-plastic FE analyses of RC frames conducted by them indicated that a η_C of 1.25, which was the value recommended by the Chinese design manual (Manual for seismic design of industrial and civil buildings 1981), was not sufficient for a frame to achieve the strong column-weak beam hierarchy.

Dooley and Bracci (2001) evaluated the seismic performance of a 3-storey frame and a 6-storey frame with various η_C values (0.8, 1.0, 1.2, 1.6, 2.0, 2.4) using probabilistic measures. The results showed that an η_C value of 1.2, which was the requirement of ACI 318 (1999), led to only a 10% probability of preventing the formation of storey-sway mechanism, while an η_C value of 2.0 led to a much higher probability (roughly 80%) of preventing the formation of storey-sway mechanism. So η_C=2.0 was suggested by the authors.

Wei et al. (2003) designed 6 RC pure frames of Seismic Grade (SG) 2 in a Seismic Precautionary Intensity (SPI) 8 region [i.e. frames in this region whose height is not larger than 30 m following GB-50011 (2001)] in China and carried out seismic response analysis of these frame models using the nonlinear dynamic analysis program PL-AFJD (Yang 2000). The results indicated that for RC frames of SG 2 in an SPI 8 region in China, an η_C value of 1.2, which is prescribed in the old design code GB-50011 (2001), was not sufficient, and an η_C value of 1.4-1.5 was suggested.

Ma and Chen (2005) analyzed the reliability of strong column-weak beam design in a 6-storey RC pure frame with different values of η_C ranging from 1.0 to 2.0 and recommended a value of 1.6.

Cai et al. (2007) analyzed the failure probability of strong column-weak beam design for single RC joints using the theory of reliability, and conducted Monte Carlo simulation on a 3-storey and a 6-storey RC frames with floor slabs. Analysis results indicated that the acceptable probability of achieving the strong column-weak beam mechanism can be obtained if η_C is no less than 2.0.

Wei et al. (2007) designed five 6-storey 3-span RC frames in different SPI regions in China following the Chinese design code GB-50011 (2001) and carried out elastic-plastic time history analysis of these frames using FW-EPA (Wei 2005). The results showed that the frame of SG 1 in an SPI 9 region [i.e. a frame in this region whose height is not larger than 25 m following GB-50011 (2001)] achieved the beam-sway mechanism while the storey-sway mechanism formed in the frames of SG 2 in an SPI 8 region and SG 3 in an SPI 7 region [i.e. frames in this region whose height is not larger than 30 m following GB-50011 (2001)]. η_C=1.3 was suggested by the authors for frames of SG 3 in an SPI 7 region. For frames of SG 2 in an SPI 8 region, the authors suggested η_C=1.0, with the calculation of $\sum M_B$ being based on the actual reinforcement.

Based on structural reliability theory, Xia (2009) studied the strong column-weak beam design of RC frames following the Chinese design code GB-50011 (2001). According to the analysis results, the author gave some advice on the strong column-weak beam design method, with η_C=1.4, 1.3 and 1.2 being suggested respectively for RC frames of SG 2 in an SPI 8 region, SG 2 in an SPI 7 region [i.e. frames in this region whose height is larger than 30 m following GB-50011 (2001)], and SG 3 in an SPI 7 region.

Tao (2010) established an FE model of 2-storey 3x3-span RC frame with cast-in-place floor slabs using ANSYS (2007), and increased the value of η_C gradually until the beam-sway mechanism was achieved. Based on the analysis results, a value of η_C=1.7 was recommended.

Yang (2010) established 6 RC frame models with cast-in-place floor slabs and different η_C values and carried out static nonlinear analyses and nonlinear time-history analyses on these frames using SAP2000 (1998) to determine the reasonable value of η_C. Only RC frames of SG 2 in an SPI 8 region in China were taken into consideration in the analyses. The analysis results showed that the requirement η_C=1.2 in Chinese code GB-50011 (2001) was not sufficient for frames to achieve the beam-sway mechanism, and a value of η_C ranging from 1.6 to 2.0 was suggested by the author.

Ye et al. (2010) carried out elastic-plastic time history analysis on RC pure frames excited by 20 strong ground motions using THUFIBER (Lu et al. 2006) to study the required η_C values for the frames to achieve the beam-sway mechanism. Analysis results showed that the required η_C value increased with the earthquake intensity. Based on the analysis results, the values of η_C should be 2.0, 1.7 and

1.4 for RC frames respectively of SG 1, 2 and 3 in China. However, considering that the values of η_C stipulated in the latest Chinese seismic code (GB-50011 2008) for RC frames of SG 1, 2 and 3 are respectively 1.4, 1.2 and 1.1, moderate values of 1.7, 1.5 and 1.3 were suggested by Ye et al. (2010) for RC frames of SG 1, 2 and 3, respectively.

Sun (2010) conducted dynamic time history analysis on a series of RC frames with cast-in-place floor slabs and different η_C values using ABAQUS (2006) to study their displacements, storey drifts and distributions of plastic hinges under a rare earthquake. A value of η_C ranging from 1.8 to 2.0 was suggested by the author for RC frames of SG 2 in China (GB-50011 2001).

Yang (2011) established a group of 6-storey RC frame models with cast-in-place floor slabs and different η_C values, and conducted elastic-plastic time history analysis on these frames under three-dimensional earthquake actions using MSC.Marc (2005). A value of 2.4, 2.1, 1.9 and 1.6 were suggested for η_C of RC frames of SG 1, 2, 3 and 4 respectively in China (GB-50011 2010).

Yang (2012) established FE models of three 5-storey RC frames (with cast-in-place floor slabs) of SG 3 in China respectively with three different values of η_C: 1.3 (according to Chinese code GB-50011 2010), 1.4 and 1.5. Results from the pushover analyses carried out on these frames showed that the strong column-weak beam hierarchy was achieved when η_C=1.5.

Sunitha et al. (2014) established two 5-storey and one 10-storey RC pure frame models with various values of η_C and conducted nonlinear static pushover analysis on these three frames using SAP2000 (1998) to demonstrate the effect of η_C on the seismic behavior of frames. Analysis results showed that the η_C value required to achieve the beam-sway mechanism in these RC frames was between 2.5 and 3.0.

It can be concluded from these studies that, despite the use of different analysis methods (e.g. reliability analysis, elastic-plastic time history analysis and pushover analysis), the suggested values of η_C by the researchers from different countries (e.g. China, United States and India) are mostly much larger than 1.0.

2.5 DEVELOPMENT OF DESIGN PROVISIONS FOR THE STRONG COLUMN-WEAK BEAM DESIGN PHILOSOPHY

In this section, design provisions to implement the strong column-weak beam design philosophy in the design codes from New Zealand [NZS-3101 (2006) and previous versions], the United States [ACI 318 (2014) and previous versions], Europe [Eurocode 8 (2004) and previous versions] and China [GB-50011 (2010) and previous versions] are reviewed.

2.5.1 New Zealand

As mentioned in Section 2.2, the strong column-weak beam design philosophy was originally developed by Park and Paulay (1975) from New Zealand. Till now, New Zealand's structural design code is one of the most advanced codes in the world.

NZS-95 (1935) for the first time provided the seismic design method in New Zealand after a number of major earthquakes in late 1920s and early 1930s, while NZS-4203 (1976) for the first time adopted the capacity design method. NZS-3101 (1982) adopted the capacity design method and provided many requirements for capacity design (Gregory et al. 2011, Fenwick and MacRae 2009).

The consideration of the contribution from the cast-in-place floor slab to the flexural capacity of the beam first appeared in NZS-3101 (1982), and was improved in NZS-3101 (2006) to cover more factors. The stipulations on the strong column-weak beam design philosophy for RC frames in NZS-3101 are given in Table 2.6.

2.5.2 United States

The building code of the United States is one of the world's widely referenced codes. Different from the Chinese codes, however, there is not a unified national building code in the United States, and different regions use different building codes which are suitable for their local situations. These building codes are developed and managed by some professional groups, guilds and technology institutes.

Building Code Requirements for Structural Concrete is published by the American Concrete Institute (ACI) which was founded in 1904. ACI 318 [ACI 318 (2014) and previous versions] is an authoritative code for RC structures, and is also an important part or reference of most regional building codes in the United States. The concrete part of the *Uniform Building Code* [UBC (1997) and previous versions] drafted by the International Conference of Building Officials (ICBO) almost adopted all provisions of ACI 318 [ACI 318 (1995) and previous versions], the concrete part of the *National Building Code* [NBC (1999) and previous versions] drafted by the Building Officials Code Administrators (BOCA) and the *International Building Code* [IBC (2015) and previous versions] drafted by the International Code Council (ICC) also adopted a large number of clauses from ACI 318 (Liu 2006). Studies on American seismic design codes has mainly been focused on ACI 318 [ACI 318 (2014) and previous versions].

ACI published the *Standard Building Regulations for the Use of Reinforced Concrete* in 1910 (ACI 1910), which was named as ACI 318 in 1941. In the 1971 edition (ACI 318 1971), seismic design provisions were included. Afterwards, ACI 318 was revised every few years to reflect new scientific achievements and regulate their continuous development. The latest edition is ACI 318 (2014).

ACI 318 (1971) stipulated that the sum of the flexural capacities of the columns at a joint should be larger than that of the beams at the joint (i.e., the value of η_C in Eq. 2.1 should be larger than 1.0), while ACI 318 (1983) increased the value of η_C to be 1.2. ACI 318 (2002) for the first time stipulated that the effect of cast-in-place floor slabs on the negative flexural capacity of beams should be considered. Afterwards, stipulations based on the strong column-weak beam design philosophy in RC frames in ACI 318 almost kept unchanged (ACI 318 2005, 2014). A comparison between different versions of ACI 318 in terms of the strong column-weak beam design philosophy is given in Table 2.7.

2.5.3 Europe

As early as 1975, the Commission of the European Community (CEC) realized the situation that structural design among European countries was inconsistent with each other, which would lead to technical obstacles in engineering practice among the Member States. Thus CEC suggested compiling a set of structural design codes, making it forcibly used in the Member States first, coordinating the technical specifications of the Member States, and gradually replacing the previous design codes (Liu et al. 2006). Then Eurocodes appeared and the first Eurocodes were published by CEC in 1980.

In 1989, on the basis of an agreement between CEC and the European Committee for Standardization (CEN), CEC, the European Union (EU) and the European Free Trade Association (EFTA) decided to transfer the right of compilation and publication of Eurocodes to CEN. In 1990, CEN established a technical committee (CEN/TC 250) to be responsible for the compilation of Eurocodes, and stipulated that Eurocodes would be published first in the name of Euro Norm Vornorm (ENV), which would be tried out in the Member States and then modified to become Euro Norm (EN). The publication of ENVs was started by CEN in 1992 and was completed in 1998. Conversion of ENV to EN was started in 1998 and completed in 2006. (Yan 2010)

The EN is also referred to as the Eurocodes, which consists of 10 parts. Eurocode 0 gives the basic principles of structural design to ensure the structural safety, reliability and durability. Eurocode 1 provides a series of guidelines on structural calculation methods. Eurocode 2, Eurocode 3, Eurocode 4, Eurocode 5, Eurocode 6 and Eurocode 9 are respectively design rules for concrete structures, steel structures, composite steel and concrete structures, timber structures, masonry structures and aluminum structures, while Eurocode 7 and Eurocode 8 are respectively for geotechnical design and seismic design. Eurocode 8 comprises 6 parts, and seismic actions and general issues are stipulated in Part 1 (Eurocode 8-1).

In Eurocode 8 (1995, 2004), the strong column-weak beam design philosophy is adopted and the effect of cast-in-place floor slabs on the flexural capacity of beams is taken into account. The stipulations on the strong column-weak beam design philosophy for RC frames in Eurocode 8 (1995, 2004) are listed in Table 2.8.

2.5.4 China

Before the publication of the first Chinese seismic design code TJ11-74 (1974), the seismic design code of the Soviet Union was used for the structural design in China (Wang and Dai 2010). The historical highlights of Chinese seismic design codes are listed in Table 2.9. The strong column-weak beam design philosophy was adopted in GBJ11-89 (1989) for the first time and developed in the following versions. Comparisons of stipulation on the strong column-weak beam philosophy of RC frames in Chinese design codes are given in Table 2.10. After the 2008 Wenchuan Earthquake, the value of η_C was significantly increased in the latest version of Chinese seismic design code GB-50011 (2010), and RC frame structures of SG 1 need to meet the following requirement:

$$\sum M_C = 1.2 \sum M_B \tag{2.2}$$

where $\sum M_B$ is based on the actual reinforcement and the characteristic strength of materials, with the effect of cast-in-place floor slabs on the flexural capacity of beams considered.

2.6 IMPLEMENTATION OF THE STRONG COLUMN-WEAK BEAM DESIGN PHILOSOPHY IN STRUCTURAL DESIGN

2.6.1 Current situation

Structures designed using design codes which do not adopt the capacity design method cannot or can hardly achieve the strong column-weak beam hierarchy. Despite that the newer design codes adopt the capacity design method and specify the value of η_C, studies of failed structures after major earthquakes have shown that the beam-sway mechanism rarely occurred (ATC-40 1996) because most of the failed frames were designed according to codes (generally previous codes) which do not or do not adequately enforce the strong column-weak beam requirement. Moreover, although the current design codes investigated in Section 2.5 well consider the effect of cast-in-place floor slabs on the flexural capacity of the beam, the value of η_C given in these design codes are still smaller than those suggested by researchers (as discussed in Section 2.5). Therefore, structures designed based on the latest versions of design codes probably still cannot completely achieve the strong column-weak beam hierarchy.

For example, statistical results based on 48 frame structures which suffered damage from the 1976 Tangshan earthquake in China showed that most frame structures with cast-in-place floor slabs failed in the storey-sway mechanism, while frame structures without cast-in-place floor slabs failed in the beam-sway mechanism (Li 1994). In the magnitude (Ms) 8.0 Wenchuan earthquake in China in 2008 (Chinese Academy of Building Research 2008), failure of cast-in-place RC frames commonly occurred at column ends (Fig. 1.1); the beam-sway mechanism was normally found only in frames with no floor slabs or with precast floor slabs (Fig. 1.2). The prevalence of column end failures has been attributed to one major deficiency in GB-50011 (2001): the code does not include the contribution of the cast-in-place slab in tension to the flexural capacity of the beam in negative bending in its specification (Lin et al. 2009). As a result, it can be expected that in many RC frames in the Chinese mainland, the beams are stronger than the columns at a joint. The new Chinese seismic design code (GB-50011 2010), which came into force in December 2010, requires the consideration of the contribution of the cast-in-place slab to the beam flexural capacity in addition to the adoption of higher flexural strength ratios. Many existing RC buildings cannot meet these new requirements. Moreover, the suggested values of η_C by some researchers summarized in Table 2.6 are still much larger than those stipulated in GB-50011 (2010), and only for RC frame structures of SG 1, the calculation of $\sum M_B$ needs to be based on the actual reinforcement which considers the contribution of reinforcement in the slab. For RC frames of other

SGs, the calculation of $\sum M_B$ is still based on the designed reinforcement which does not consider the contribution of reinforcement in the slab. This situation indicates that structures built after 2010 probably still cannot completely meet the requirement of achieving the strong column-weak beam mechanism.

In other countries or regions, similar threats due to the violation of the strong column-weak beam hierarchy in the older existing buildings may also exist. For example, buildings designed in accordance with ACI 318 (1983) or older versions which did not consider the contribution of the cast-in-place slab in tension to the flexural capacity of the beam in negative bending are likely to violate this hierarchy.

2.6.2 Seismic retrofit of existing RC frames

To achieve the strong column-weak beam hierarchy in existing cast-in-place RC frames where such a hierarchy has not been satisfied, strengthening of columns might be an option. Common column retrofitting methods include concrete jacketing (e.g. Thermou et al. 2007), steel jacketing (e.g. Xiao and Wu 2003) and FRP jacketing (Teng et al. 2002; Pessiki et al. 2001; Xiao 2004; Al-Nimry et al. 2013; Teng et al. 2016). The former two methods may lead to increases in mass and/or stiffness and then increases in seismic forces, while FRP jacketing has been widely used in recent years as a simple but effective method for column strengthening. However, the strength enhancement due to FRP jacketing may be small, especially when FRP jacketing is applied to confine non-circular columns. And even when column strengthening can be sufficient, the location of failure may simply shift from column ends to the foundation and/or beam-column joints, which are both difficult to retrofit. Therefore, column strengthening alone is often not sufficient enough to change the strength hierarchy.

Instead of column strengthening, a novel seismic retrofit method for cast-in-place RC frames which violate the strong column-weak beam hierarchy has recently been proposed (Teng et al. 2013). This method is based on the concept of Beam-end Weakening in combination with FRP Strengthening (referred to as the BWFS method hereafter for simplicity), to implement the strong column-weak beam hierarchy. The technique is based on the weakening of the flexural capacities of the T-section beams at a joint, particularly when the flange (i.e. the cast-in-place slab) is in tension. The general concept of local weakening is not new in seismic retrofit or design. In steel structures, a typical weakening technique for new structures and seismic retrofit is adopting the dog-bone design to ensure a weak beam-strong connection strength hierarchy (Popov et al. 1998). For RC structures, local weakening by material removal for seismic retrofit as a concept is discussed in a preliminary and general manner in FEMA (2000) with little detail. Severing of bottom longitudinal steel reinforcement has recently been explored in detail as a seismic retrofit method to protect exterior beam-column joints (Pampanin 2006; Kam et al. 2009), but cutting bottom bars cannot solve the problem associated with the contribution of slab for T-section beams under negative bending. The proposed method represents an application/extension of the general selective local weakening approach to solve the slab contribution problem.

As presented in Chapter 1, three seismic retrofit techniques based on the concept of beam-end weakening in combination with FRP strengthening where necessary and/or appropriate to enforce the strong column-weak beam hierarchy are proposed (Teng et al. 2013): (1) the beam opening (BO) technique; (2) the beam section reduction (SR) technique; and (3) the slab slit (SS) technique. To the best of the candidate's knowledge, the first two techniques are new and no research is available on their effectiveness and the relevant design methods. Several studies on the effectiveness of the SS technique have been conducted, which are summarized in Table 2.11. All these studies indicated that joints/frames with slab slits can better achieve the strong column-weak beam mechanism than joints/frames without slab slits.

Recently, Feng et al. (2017) proposed a novel method using kinked rebars in the beams for improving the seismic performance and progressive collapse resistance of RC frame structures. The kinked rebar has locally curved regions (usually near the inflection points in beams) which can be gradually straightened under tension. Due to the lower initial yielding flexural capacity compared with that of a cross section reinforced with traditional straight bars, the beam section reinforced with kinked rebars will yield first when the RC frame is subjected to seismic loading, and thus the strong column-weak beam hierarchy can be realized. Although this method was originally proposed for new construction, the concept has the potential to be adopted in the BWFS method for existing structures. The feasibility and effectiveness of kinked rebars in reducing the flexural capacity of the beam is worth further investigations.

2.7 EXISTING STUDIES ON RC BEAMS WITH WEB OPENINGS

As discussed in Chapter 1, the present PhD thesis is focused on the BO technique, which involves the creation of an opening on the web in each end region of a T-section beam adjacent to the beam-column joint (as shown in Fig. 1.3), followed by the installation of a local strengthening system to avoid shear failure of the beam, with the aim being to assess its feasibility and to develop corresponding strength models/design methods. Externally bonded FRP shear reinforcement has been shown by many researchers to be an effective method for enhancing the shear capacity of RC beams (Teng et al. 2002; Triantafillou 1998; Chen and Teng 2003a, b; Bousselham and Chaallal 2004; Haddad et al. 2013).

It should be noted that creating web openings in RC beams is not a new thing. For the passage of utility ducts/pipes, such as electricity, heating, water supply systems as well as air conditioning, telephone, internet cables and sewage conduits, pre-formed rectangular or circular web openings in reinforced concrete (RC) beams have been widely used in new buildings (e.g. Kennedy and Abdalla 1992; Mansur 1998; Tan et al. 2001). With such web openings in beams, extra storey heights for accommodating ducts/pipes can be avoided. This can help reduce the overall height of the building, leading to a more cost-effective design. In the design of RC beams with a web opening, the detrimental effect of the web opening needs to be properly considered; steel reinforcement is usually adopted around such a web opening to prevent/mitigate the associated performance degradation (Kennedy and Abdalla 1992; Mansur 1998; Tan et al. 2001).

In an existing structure, if such ducts/pipes need to be installed, creating web openings in existing beams is an appealing solution that has been adopted in practical projects (e.g. Mansur et al. 1999; Maaddawy and Sherif 2009; Maaddawy and Ariss 2012). Cutting the web of an existing RC beam to form one or more openings, however, can cause significant degradation in its stiffness and load-carrying capacity (e.g. Mansur et al. 1999; Maaddawy and Sherif 2009; Maaddawy and Ariss 2012). This degradation usually results from two causes: (1) reduction in the beam cross-section; and (2) severing of some of the existing shear reinforcement. Therefore, a strengthening system (such as an externally bonded FRP strengthening system) generally needs to be applied around a post-formed web opening (referred to as “web opening” hereafter in the thesis) to ensure the safety of the beam (e.g. Mansur et al. 1999; Maaddawy and Sherif 2009; Maaddawy and Ariss 2012). A number of experimental studies on the behaviour of RC beams with a web opening have shown that the flexural and/or shear capacities of the beam can be significantly reduced and the degree of degradation is highly dependent on the size and location of the web opening (e.g. Mansur et al. 1999; Maaddawy and Sherif 2009; Maaddawy and Ariss 2012). A larger web opening usually causes a larger decrease in the load-carrying capacity and leads to a more brittle failure mode (Mansur et al. 1999; Maaddawy and Sherif 2009; Maaddawy and Ariss 2012). The location of the web opening influences the extent to which the natural force path in the beam is interrupted. A greater interruption of the natural force path in a beam usually leads to a larger decrease in the load-carrying capacity and a more brittle failure mode (Mansur et al. 1999; Maaddawy and Sherif 2009).

Although the purpose of creating openings in the beams in these studies is different from that of this thesis, these studies offer a useful source of information for the present work on beam-end weakening. The relevant existing experimental and numerical studies are summarised below to provide the necessary background to the present PhD research programme.

2.7.1 Experimental studies

Ten experimental studies on the topic have been found in the published literature (Mansur et al. 1999; Abdalla et al. 2003; Allam 2005; Maaddawy and Sherif 2009; Madkour 2009; Pimanmas 2010; Chin et al. 2012; Maaddawy and Ariss 2012; Suresh and Prabhavathy 2015; Chin et al. 2016). The first of these studies was conducted by Mansur et al. (1999), in which seven T-shaped RC beams were tested. One of the seven beams had no web openings and served as the control beam, while the other six beams had a circular web opening in each shear span. The parameters examined included the size and location of the circular web opening. The control beam failed by the crushing of the compressive concrete, which is a typical flexural failure mode; the other six specimens failed by the formation and propagation of a diagonal shear crack in each shear span that passed through the circular opening. Nearly all the subsequent studies on this topic were concerned with rectangular RC beams with a rectangular opening (Abdalla et al. 2003; Allam 2005; Maaddawy and Sherif 2009; Madkour 2009; Chin et al. 2012; Maaddawy and Ariss 2012; Suresh and Prabhavathy 2015； Chin et al. 2016), with the parameters examined being the length and height of the opening. The majority of these studies adopted beam specimens with two web openings of the same size that were symmetrically located in the two shear spans, respectively (Mansur et al. 1999; Maaddawy and Sherif 2009; Madkour 2009; Pimanmas 2010; Chin et al. 2012; Suresh and Prabhavathy 2015), while a smaller number of studies used beam specimens with only one web opening in one of the two shear spans (Abdalla et al. 2003; Allam 2005; Maaddawy and Ariss 2012). As mentioned earlier, regardless of the number of openings, all these beams are referred to as “beams with a web opening” or “beams with an opening” unless when the number of openings becomes an important factor.

Among these ten studies, nine experimental studies (Mansur et al. 1999; Abdalla et al. 2003; Allam 2005; Maaddawy and Sherif 2009; Pimanmas 2010; Chin et al. 2012; Maaddawy and Ariss 2012; Suresh and Prabhavathy 2015; Chin et al. 2016) addressed the effect of drilling an opening in an existing beam and the design of the associated strengthening measure. All nine studies except Suresh and Prabhavathy (2015) proposed the use of bonded FRP reinforcement for the strengthening intervention. These studies were motivated by the need to create openings in an existing structure for the passage of utility ducts and pipes, and were thus focused on restoring the strength of the beam through FRP strengthening. These studies confirmed the feasibility of FRP strengthening to compensate for the weakening effect of the opening. Among the different FRP strengthening schemes explored, the use of bonded U-jackets/complete wraps/side bonded FRP laminates (Mansur et al. 1999; Abdalla et al. 2003; Allam 2005; Maaddawy and Sherif 2009; Chin et al. 2012; Maaddawy and Ariss 2012; Chin et al. 2016) as well as diagonal near-surface mounted FRP bars at corners (Pimanmas 2010) were found to be effective in controlling shear cracks and shear failures emanating from the corners.

In addition to the published studies on this topic, two T-section beams with a rectangular opening in one of the two shear spans were tested by Prof. Teng's group to gain further insight into the behaviour of such RC beams (Teng et al. 2013): one beam had an un-strengthened rectangular opening of 150 mm (height) × 500 mm (length) (O-500×150) while the other one had an FRP-strengthened rectangular opening of 220 mm (height) × 500 mm (length) (FRP-500×220). The details of the test beams are shown in Fig. 2.1. In this study, both beams had a web width of 250 mm, a total height of 500 mm, a total flange width of 1,450 mm, a flange thickness of 100 mm, a beam clear span of 3,300 mm and a shear span of 1,650 mm.

A summary of the existing experimental studies together with the tests carried out by Teng et al. (2013) is given in Table 2.12. Table 2.12 indicates that although the concrete strength, the size and type of the beam (rectangular or T-section), and the size and number of openings adopted in these studies vary from one study to another, the following observations can be made based on the existing studies:

1) All control beams which had no web opening failed by the crushing of compressive concrete at the mid-span of the beam, which is the typical flexural failure mode for RC beams;
2) All beams with an un-strengthened web opening failed by the formation of a diagonal crack that started as small inclined cracks in the corners of the opening (a typical crack pattern is shown in Fig. 2.2a); all beams with an FRP-strengthened web opening except beams tested by Mansur et al. (1999), Abdalla et al. (2003) and Pimanmas (2010) whose opening size was quite small failed by shear in the opening region after the debonding/rupture of FRP (a typical failure mode is shown in Fig. 2.2b); and
3) A web opening/web openings reduced significantly both the strength and stiffness of the beam; after FRP-strengthening, the strength of the beam can be substantially restored.

2.7.2 Finite element modelling

Laboratory tests are usually time-consuming and costly. In this sense, finite element (FE) modelling is an efficient and cost-effective alternative to laboratory testing in studying the behaviour of concrete structures. So far, however, compared with the experimental studies on this topic, the numerical modelling of

RC beams with an un-strengthened/FRP-strengthened web opening has been very limited. Only three relevant studies can be found in the open literature (Pimanmas 2010; Chin et al. 2012; Hawileh et al. 2012).

Based on the smeared crack approach, Pimanmas (2010) conducted 2-D nonlinear FE analyses of RC beams with a rectangular web opening using the nonlinear FE program WCOMD (1998). Using ATENA (Cervenka et al. 2010), Chin et al. (2012) presented 2-D FE studies of RC beams with a rectangular web opening. Hawileh et al. (2012) proposed a 3-D nonlinear FE model for deep RC beams with a rectangular web opening which were strengthened in shear with externally bonded CFRP sheets. The general purpose FE program ANSYS (2007) was used in their study.

The features of the existing FE studies for RC beams with a web opening are summarized in Table 2.13 to highlight their differences and inadequacies. It can be seen from Table 2.13 that none of the existing FE studies included accurate modelling of the bond-slip behaviour between steel and concrete. Pimanmas (2010) also did not include accurate modelling of the bond-slip behaviour between FRP and concrete, and instead, a perfect bond was assumed. The perfect bond assumption will lead to inaccurate predictions of the crack pattern (Chen et al. 2012). Besides, none of the existing FE studies accurately modelled the behaviour of cracked concrete. Hawileh et al. (2012) did not mention the approach (discrete crack model or smeared crack model) used to model the cracked concrete, while the approaches proposed by Pimanmas (2010) and Hawileh et al. (2012) did not consider the tensile fracture energy in the modelling of the tensile behaviour of cracked concrete, implying that the predictions of the FE model were mesh-dependent. Furthermore, as one of the most important aspects in such simulation, the modelling of shear behaviour of cracked concrete (e.g. the shear retention factor) was not provided in one of the existing FE models (Hawileh et al 2012). Finally, the validity of the existing FE models needs to be verified with a larger test database containing also test results from other researchers. It can therefore be concluded that the limited existing numerical studies on RC beams with an un-strengthened/FRP-strengthened web opening have not been able to provide a well-established FE approach for predicting the behaviour of such RC beams.

2.8 CONCLUDING REMARKS

This chapter has provided a review of the existing knowledge on the strong column-weak beam design philosophy, covering the concept of strong column-weak beam design, factors affecting the accurate calculation of the flexural capacity of beams $\sum M_B$, the determination of the column-to-beam flexural strength ratio η_C, the development of design provisions for the strong column-weak beam design philosophy, the current situation of the implementation of the strong column-weak beam design philosophy in structural design and seismic retrofit of existing RC frames, and existing studies on RC beams with a web opening. Based on the review and discussions presented in this chapter, the following conclusions can be drawn:

1) The strong column-weak beam hierarchy has been widely adopted as one of the main design requirements in the seismic design of RC frame structures, in order to realize the beam-sway mechanism for RC frame structures subjected to seismic loading;
2) To achieve the strong column-weak beam hierarchy for an RC frame, the relationship $\sum M_C = \eta_C \sum M_B$ should be satisfied, where $\sum M_C$ and $\sum M_B$ are the sums of the flexural capacities of the columns and the beams framing into the joint, respectively, and η_C is the column-to-beam flexural strength ratio;
3) The main factors which can lead to under-estimation of the flexural capacity of RC beams include the effect of cast-in-place floor slabs, infill walls and over-reinforced beam ends. The existence of a cast-in-place floor slab can significantly enhance the stiffness and strength of the beam supporting it; infill walls may significantly alter the failure mechanism of an RC frames; and over-reinforced beam ends directly increase the flexural capacity of the beam at the ends. The under-estimation of the flexural capacity of RC beams may result in the violation of the strong column-weak beam hierarchy. Therefore, in the design of RC frame structures, the effect of the above factors on the flexural capacity of RC beams should be properly considered;
4) Structures designed using old versions of design codes which did not adopt the strong column-weak beam design philosophy cannot or can hardly

achieve the strong column-weak beam hierarchy. Although the newer design codes have adopted the strong column-weak beam design philosophy, existing studies have indicated that the values of η_C stipulated in these codes are still insufficient to ensure the strong column-weak beam hierarchy. Therefore, it can be expected that a large number of existing RC frame structures violate this hierarchy requirement and need to be retrofitted;

5) Existing studies have indicated that column strengthening alone is often not sufficient to achieve the strong column-weak beam hierarchy. Against this background, three strengthening techniques based on the concept of beam-end weakening in combination with FRP strengthening were proposed by Prof Teng's group: (a) the beam opening (BO) technique; (b) the beam section reduction (SR) technique; and (c) the slab slit (SS) technique. The proposed techniques can be used alone or in combination with column strengthening; and

6) The present study will only be focused on the BO technique. Although limited existing studies on RC beams with a web opening have shown that the flexural capacity of the beam can be substantially reduced by a web opening, they have not been able to provide a well-established FE modelling approach or a reliable strength model for such RC beams. Therefore, in-depth experimental, numerical and theoretical studies on RC beams with a web opening is the focus of the present PhD thesis.

2.9 REFERENCES

ABAQUS (2006). *ABAQUS Analysis User's Manual (Version 6.6)*, Dassault Systems SIMULIA Corporation, Providence, Rhode Island, USA.

Abdalla, H.A., Torkey, A.M., Haggag, H.A. and Abu-Amira A.F. (2003). "Design against cracking at openings in reinforced concrete beams strengthened with composite sheets", *Composite Structures*, 60(2), 197-204.

ACI (1910). *Standard Building Regulations for the Use of Reinforced Concrete*, American Concrete Institute, Farmington Hills, MI.

ACI 318 (1971). *Building Code Requirements for Structural Concrete and Commentary* (*ACI 318-71)*, ACI Committee 318, American Concrete Institute, Farmington Hills, MI.

ACI 318 (1983). *Building Code Requirements for Structural Concrete and Commentary* (*ACI 318-83)*, ACI Committee 318, American Concrete Institute, Farmington Hills, MI.

ACI 318 (2002). *Building Code Requirements for Structural Concrete and Commentary* (*ACI 318-02)*, ACI Committee 318, American Concrete Institute, Farmington Hills, MI.

ACI 318 (2005). *Building Code Requirements for Structural Concrete and Commentary* (*ACI 318-05)*, ACI Committee 318, American Concrete Institute, Farmington Hills, MI.

ACI 318 (2014). *Building Code Requirements for Structural Concrete and Commentary* (*ACI 318-14)*, ACI Committee 318, American Concrete

Institute, Farmington Hills, MI.

ADINA (2007). *ADINA Theory and Modeling Guide (Version 8.3)*, ADINA R&D, Inc.

Al-Nimry, H., Haddad, R., Afram, S. and Abdel-Halim, M. (2013). “Effectiveness of advanced composites in repairing heat-damaged RC columns”, *Materials and Structures*, 46 (11), 1843-1860.

Allam, S. M. (2005). “Strengthening of RC beams with large openings in the shear zone”, *Alexandria Engineering Journal*, *44*(1), 59-78.

ANSYS (2007). *A Finite Element Computer Software and User Manual for Nonlinear Structural Analysis*, Canonsburg, PA: ANSYS 2007 Inc.

ATC-40 (1996). *Seismic Evaluation and Retrofit of Concrete Buildings*, Applied Technology Council, Redwood City, California.

Bertero, V. V., Aktan, A. E., Charney, F. et al. (1984). *Earthquake Simulation Tests and Associated Studies of a 1/5th Scale Model of a 7-story RC Frame-wall Test Structure*, Earthquake Engineering Research Center, University of California at Berkeley.

Bijan, O. and Aalami (2001). *Effective Width in Post-Tensioned Flanged Beams*, Adapt Technical Note, ADAPT Corp.

Bousselham, A. and Chaallal, O. (2004). “Shear strengthening reinforced concrete beams with fiber-reinforced polymer: Assessment of influencing parameters and required research”, *ACI Structural Journal*, 101(2), 219-227.

Cai, J., Zhou, Q. and Fang, X.D. (2007). “Evaluation of influences of various moment magnifying coefficients at column ends of RC frames on seismic performance”, *China Civil Engineering Journal*, 40(1), 6-14. (in Chinese)

Cervenka, V., Jendele, L. and Cervenka, J. (2010). *ATENA Program Documentation Part 1- Theory*, Cervenka Consulting Ltd., Prague.

Chen, J.F. and Teng, J.G. (2003). “Shear capacity of FRP-strengthened RC beams: FRP debonding”, *Construction and Building Materials*, 17(1), 27-41.

Chen, J.G. and Teng, J.G. (2003). “Shear capacity of fiber-reinforced polymer-strengthened reinforced concrete beams: Fiber reinforced polymer rupture”, *Journal of Structural Engineerin*g, ASCE, 129(5), 615-625.

Chen, X.B. (2010). *The Effect of Floor Slab and Infill Walls on the Seismic Behavior of Reinforced Concrete Frames*, Master degree thesis: Fuzhou University, China. (in Chinese)

Chin, S.C., Shafiq, N. and Nuruddin, M.F. (2012). “Strengthening of RC beams with large openings in shear by CFRP laminates: experiment and 2D nonlinear finite element analysis”, *Research Journal of Applied Sciences Engineering and Technology*, 4(9), 1172-1180.

Chin, S.C., Shafiq, N. and Nuruddin, M.F. (2016). “Behaviour of RC beams with CFRP-strengthened openings”, *Structural Concrete*, 17(1), 32-43.

Chinese Academy of Building Research (2008). *Photo Collection of 2008 Wenchuan Earthquake Damage to Buildings*, China Architectural & Building Press, Beijing, China. (in Chinese)

DiFranco, M.A., Mitchell, M. and Paultre, P. (1995). "Role of spandrel beams on response of slab-beam-column connection", *Journal of Structural Engineering*, 121(3), 408-419.

Dooley, K.L. and Bracci, J.M. (2001). "Seismic evaluation of column-to-beam strength ratios in reinforced concrete frames", *ACI Structural Journal*, 98(6), 843-851.

Durrani, A. J. and Wight, J. K. (1982). *Experimental and Analytical Study of Internal Beam to Column Connections Subjected to Reversed Cyclic Loading*, Thesis Michigan Univ.

Durrani, A. J. and Wight, J. K. (1987). "Earthquake resistance of reinforced concrete interior connections including a floor slab", *ACI Structural Journal*, 84(5), 400-406.

Durrani, A.J. and Zerbe, H.E. (1987). "Seismic resistance of R/C exterior connections with floor slab", *Journal of Structural Engineering*, ASCE, 113(8), 1850-1864.

Ehsani, M.R. and Wight, J.K. (1982). *Behavior of External Reinforced Concrete Beam to Column Connections Subjected to Earthquake Type Loading*, Univ. of Michigan, Ann Arbor, Mich.

Eurocode 8 (1995). *Design Provisions for Earthquake Resistance of Structures - Part 1-3: General Rules - Specific Rules for Various Materials and Elements (ENV 1998-1.3: 1995)*, CEN, Brussels.

Eurocode 8 (2004). *Design of Structures for Earthquake Resistance – Part 1:*

General Rules, Seismic Actions and Rules for Buildings (EN 1998-1: 2004), CEN, Brussels.

FEMA-356 (2000). *Pre-Standard and Commentary for the Seismic Rehabilitation of Buildings.* Federal Emergency Management Agency, Washington, D.C.

Feng, P., Qiang, H., Qin, W. and Gao, M. (2017). "A novel kinked rebar configuration for simultaneously improving the seismic performance and progressive collapse resistance of RC frame structures", *Engineering Structures*, 147, 752-767.

Fenwick, R. and MacRae, G.A. (2009). "Comparison of New Zealand Standards used for seismic design of concrete buildings", *Bull of New Zealand Soc of Earthquake Eng.*, 42(3), 187-203.

French, C.W. (1991). *Effect of Floor Slab on Behavior of Slab-Beam-Column Connections*, Design of Beam-Column Joints for Seismic Resistance.

Gao, Z.R. and Ma, Q.L. (2009). "Effect of cast-in-place slab on column-beam strength ratio in frame structure", *Shanxi Architecture*, 35(17), 1-3. (in Chinese)

GBJ11-89 (1989). *Code for Seismic Design of Buildings*, Architectural & Building Press, Beijing, China. (in Chinese)

GB-50011 (2001). *Code for Seismic Design of Buildings*, Architectural & Building Press, Beijing, China. (in Chinese)

GB-50011 (2008). *Code for Seismic Design of Buildings*, Architectural & Building Press, Beijing, China. (in Chinese)

GB-50011 (2010). *Code for Seismic Design of Buildings*, Architectural & Building Press, Beijing, China. (in Chinese)

Gregory, M. R., Charles, C. and Les. M. (2011). *Review of NZ Building Codes of Practice*. (on-line) Available at: <canterbury.royalcommission.govt.nz> (Accessed 02 July 2015).

Guan, M.S. and Du, H.B. (2005). "Pushover analysis of effect of casting slab on RC frame structure", *Earthquake engineering and engineering vibration*, 5(5), 117-123. (in Chinese)

Guo, L. (2012). *Research on RC Structures with Cast-in-Place Slab*, Master degree thesis: Beijing University of Technology, China. (in Chinese)

Jiang, Y.S., Chen, Z.F., Zhou, X.P. et al. (1994). "Seismic studies of frame joints with cast-in-place slab", *Journal of Building Structures*, 15(6), 11-16. (in Chinese)

Haddad, R. H., Al-Rousan, R. Z. and Al-Sedyiri, B. K. (2013). "Repair of shear-deficient and sulfate-damaged reinforced concrete beams using FRP composites", *Engineering Structures*, 56, 228-238.

Han, J., Li, Y.M. and Ji, S.Y. (2010). "Realization of rational failure mechanism for the RC frame structure", *Journal of Harbin Institute of Technology*, 42(12), 2003-2008. (in Chinese)

Hawileh, R., El-Maaddawy, T. and Naser, M. (2012). "Nonlinear finite element modeling of concrete deep beams with openings strengthened with externally-bonded composites", *Materials & Design*, 10.1016/j.matdes.2012.06.004, 378-387.

He, J. (2010). *Study on Influence of Cast-in-situ Slab on RC Frame Structure Achieving "Strong Column Weak Beam"*, Master degree thesis: Huazhong University of Science and Technology, China. (in Chinese)

Huang, S.Y., Lou, W.J., Sun, B.B. et al. (2001). "Space prestressed slab system analysis and effective flange width", *Journal of Building Structures*, 31(2), 40-193. (in Chinese)

IBC (2015). *International Building Code*, International Code Council, INC.

Jiang, Y.S., Chen, Z.F., Zhou, X.P. et al. (1994). "Seismic studies of frame joints with cast-in-place slab", *Journal of Building Structures*, 15(6), 11-16. (in Chinese)

JTCC (1988). "U.S.-Japan research: seismic design implications", *Journal of Structural Engineering*, ASCE, 114(9), 2000-2016.

Kam, W.Y., Pampanin, S. and Bull, D. (2009). "Experimental validation of selective weakening approach for the seismic retrofit of exterior beam-column joints", *Proceedings, 2009 NZSEE Conference, Christchurch, New Zealand. April 2009 (Paper No: 32).*

Kennedy, J.B. and Abdalla, H. (1992). "Static response of prestressed girders with openings", *Journal of Structural Engineering*, ASCE, 118(2), 488-504.

Lei, J.C. (2002). *Verification Based on Inelastic Dynamic Analysis for Availability of Seismic Regulation Revised of Reinforced Concrete Framework*, Master degree thesis: Chongqing University, China. (in Chinese)

Leon, R.T. (1984). “The effect of floor member size on the behavior of reinforced concrete beam-column joints”. *Proceedings of 8th World Conference on Earthquake Engineering*, San Francisco, California.

Li, B.X. (2015). “Interaction mechanism between masonry infilled wall and bounding RC frame under earthquakes”, *Building Structure*, 45(4), 97-101. (in Chinese)

Li, W. (1994). “Study on the flexural bearing capacity of the beam end after the floor slab is considered”, *Jiangsu Architecture*, 01, 42-45. (in Chinese)

Lin, X.C., Pan, P., Ye, L.P. et al. (2009). “Analysis of the damage mechanism of a typical RC frame in Wenchuan Earthquake”, *China Civil Engineering Journal*, 42(5), 13-20. (in Chinese)

Liu, G.M. (2004). “Seismic assessment of RC frame structure based on new design codes”, *Journal of Chongqing Jianzhu University*, 26(1), 40-49. (in Chinese)

Liu, J.Y. (2006). *A Study on American Code-based Concrete Element Design and Comparison between American Codes and Chinese Codes*, Master degree thesis: China Academy of Building Research, China. (in Chinese)

Lu, X.Z., Miao, Z.W., Jiang, J.J. and Ye L.P. (2006). “Collapse simulation of high-rise structure of concrete under action of static and dynamic load”, *Earthquake Research in Shanxi*, 126(2), 7-11. (in Chinese)

Lu, X.Z., J.G. Teng, Ye, L.P. and Jiang, J.J. (2005). “Bond-slip models for FRP sheets /plates bonded to concrete”, *Engineering Structures*, 27(6), 920-

937.

Ma, H.W. and Chen, X.B. (2005). "Probability analysis for strong column-weak beam design of reinforced concrete frames", *Journal of Shanghai Jiaotong University*, 39(5), 723-726. (in Chinese)

Maaddawy, T. and Sherif, S. (2009). "FRP composite for shear strengthening of reinforced concrete deep beams with openings", *Composite Structures*, 89(1), 60-69.

Maaddawy, T. and El-Ariss, B. (2012). "Behavior of concrete beams with short shear span and web opening strengthened in shear with CFRP composites", *Journal of Composites for Construction*, ASCE, 16(1), 47–59.

Madkour, H. (2009). "Non-linear analysis of strengthened RC beams with web openings", *Proceedings of the Institution of Civil Engineers-Structures and Buildings*, 162(2), 115-128.

Mansur, M.A. (1998). "Effect of opening on the behaviour and strength of R/C beams in shear", *Cement and Concrete Composites*, 20(6), 477-486.

Mansur, M.A., Tan K.H. and Wei, W. (1999). "Effects of creating an opening in existing beams", *ACI Structural Journal*, 96(6), 899-906.

Manual for seismic design of industrial and civil buildings (1981). *Manual for Seismic Design of Industrial and Civil Buildings*, Institute of Earthquake Engineering of China Academy of Building Research.

MSC.Marc (2005). *MSC.Marc Volume D: User Subroutines and Special Routines (Version 2005)*, MSC. Software Corporation.

NBC (1999). *National Building Code*, Building Officials Code Administrators.

NZS-95 (1935). *New Zealand Standard Model Buildings By-laws*, New Zealand Standards Inst., Wellington, New Zealand.

NZS-4203 (1976). *Code of Practice for General Structural Design and Design Loadings for Buildings*, Standards New Zealand, Wellington, New Zealand.

NZS-3101 (1982). *Code of Practice for the Design of Concrete Structures*, Standards New Zealand, Wellington, New Zealand.

NZS-3101 (2006). *Concrete Structures Standard*, Standards New Zealand, Wellington, New Zealand.

OpenSees (2009). *Open System for Earthquake Engineering Simulation*, Pacific Earthquake Engineering Research Center, University of California at Berkeley, http://opensees.berkeley.edu.

Otani, S., Kabeyasawa, T., Shiohara, H. et al. (1984). "Analysis of the full-scale seven-story reinforced concrete test structure". *ACI SP-84*, 203-239.

Pampanin, S. (2006). "Controversial aspects in seismic assessment and retrofit of structures in modern times: understanding and implementing lessons from ancient heritage", *Bulletin of NZ Society of Earthquake Engineering*, 39(2), 120-133.

Park, R. and Pauly, T. (1975). *Reinforced Concrete Structures*, John Wiley and Sons, New York.

Paulay, T. (1979). "Developments in the design of ductile reinforced concrete frames", *Bulletin of the New Zealand National Society for Earthquake Engineering*, 12(1), 35-48.

PERFORM-3D (2011). *PERFORM-3D (Nonlinear Analysis and Performance Assessment for 3D Structures) User Guide*, Computers and Structures, Inc.

Pessiki, S., Harries, K.A., Kestner, J.T., Sause, R. and Ricles, J.M. (2001). "Axial behavior of reinforced concrete columns confined with FRP jackets", *Journal of Composites for Construction*, 5(4), 237-245.

Pimanmas, A. (2010). "Strengthening R/C beams with opening by externally installed FRP rods: Behavior and analysis", *Composite Structures*, 92(8), 1957-1976.

Popov, E.P., Yang, T.S. and Chang, S.P. (1998). "Design of steel MRF connections before and after 1994 Northridge earthquake", *Engineering Structures*, 20(12), 1030-1038.

Qi, C.H. et al. (2010). "Effect of floor slabs on the mechanical properties of reinforced concrete frame structures", *Journal of Catastrophology*, 25(S0), 105-110. (in Chinese)

Qi, X. (1986). *The Behavior of a R/C Slab-Beam-Column Subassemblage Under Lateral Load Reversals*, Department of Civil Engineering, University of California at Berkeley, California.

Qi, X. and Pantazopoulou, S.J. (1991). "Response of RC frames under lateral loads", *Journal of Structural Engineering*, ASCE, 117(4), 1167-1188.

SAP2000 (1998). *SAP2000 Analysis Reference*, Computers and Structures, Inc.

Shi, H.B. (2012). *Study on Infill Wall Function and Strong Beam-Weak Column Damage for Frame Structures*, Doctoral degree thesis: Institute of Engineering Mechanics, China Earthquake Administration, China. (in Chinese)

Sun, Y. (2010). *The effect of Slabs on Strong Column-Weak Beam Mechanism of RC Frame Structures*, Master degree thesis: Harbin Institute of Technology, China. (in Chinese)

Sunitha, P., Murty, C.V.R. and Goswami, R. (2014). "Quantifying parameters that ensure large deformability of earthquake resistant RC building in high seismic regions", *Network for Earthquake Engineering Simulation (distributor)*, Paper, DOI:10.4231/D3ZK55M8K.

Suresh, J. and Prabhavathy, R. A. (2015). "Behaviour of steel fibre reinforced concrete beams with duct openings strengthened by steel plates", *International Journal of Advanced Information in Arts, Science & Management*, 4(4).

Suzuki, N., Halim, J. K., Otani, S. et al. (1984). *Behavior of Reinforced Concrete Beam-Column Subassemblages with and without Slab*, Department of Architecture, Faculty of Engineering, University of ToKyo.

Tan, K.H., Mansur, M.A., and Wei, W. (2001). "Design of reinforced concrete beams with circular openings", *ACI Structural Journal*, 98(3), 407-415.

Teng, J.G., Chen, J.F., Smith S.T. and Lam L. (2002). *FRP-Strengthened RC Structures*, John Wiley and Sons Ltd, UK, November, 245pp.

Teng, J.G., Lam, L., Lin, G., Lu, J.Y. and Xiao, Q.G. (2016). "Numerical simulation of FRP-jacketed RC columns subjected to cyclic and seismic Loading", *Journal of Composites for Construction,* ASCE, 20(1), 04015021.

Teng, J.G., Zhang, S.S., Jing, D.H., Nie, X.F. and Chen, G.M. (2013). "Seismic retrofit of RC frames through beam-end weakening in conjunction with FRP strengthening", *Proceedings of the 4th Asia-Pacific Conference on FRP in Structures (APFIS 2013)*, 1-8.

Thermou, G.E., Pantazopoulou, S.J., Einashai, A.S. (2007). "Flexural behavior of brittle RC members rehabilitated with concrete jacketing", *Journal of Structural Engineering*, ASCE, 133(10), 1373-1384.

TJ-74 (1974). *Code for Seismic Design of Industrial and Civil Buildings*, Architectural & Building Press, Beijing, China. (in Chinese)

TJ-78 (1978). *Code for Seismic Design of Industrial and Civil Buildings*, Architectural & Building Press, Beijing, China. (in Chinese)

Triantafillou, T.C. (1998). "Shear strengthening of reinforced concrete beams using epoxy-bonded FRP composites", *ACI Structural Journal*, 95(2), 107-115.

UBC (1997). *Uniform Building Code*, Whittier, Calif.: International Conference of Building Officials.

Wang, S.G., Hang, X.L. and Ji, J. (2009). "The effect of slabs on the failure mode of reinforced concrete frame structures", *Journal of Civil, Architectural &*

Environmental Engineering, 31(1), 66-71.

Wang, X.G., Shan, M.Y., Ge, N. and Shu, Y.P. (2012). “Finite element analysis of efficiency of slot-cutting around RC frame joint for ‘strong column and weak beam’”, *Journal of Earthquake Engineering and Engineering Vibration*, 32(1), 121-127. (in Chinese)

Wang, Y.Y. and Dai, G.G. (2010). “Evolution and present updation of ‘Code for seismic design of buildings’”, *Journal of Building Structures*, 31(6), 7-16. (in Chinese)

WCOMD (1998). *Users Guide for WCOMD-SJ*, Concrete Engineering Laboratory, Department of Civil Engineering, University of Tokyo.

Wei, F. (2005). *Identification of Inelastic Seismic Responses of Reinforced Concrete Frame and Frame-Shear Wall Structure*, Doctoral degree thesis: Chongqing University. (in Chinese)

Wei, F., Yang, B., Bai, S.L. and Wang, Z. (2003). “Discussion on reasonable value of moment enhancement factor of bottom column section of seismic RC frames”, *Building Structure*, 33(5), 3-7. (in Chinese)

Wei, F., Fu, J.P. and Bai, S.L. (2007). “Actual control effect of strong-column and weak-beam measures of reinforced concrete frame structures in China”, *Building Structure*, 37(8), 5-9. (in Chinese)

Wu, Y., Lei, J.C., Y, H. et al. (2002). “Discussion on the problem that slab reinforcement getting involved in the negative moment capacity of beam end”, *Journal of Chongqing Jianzhu University*, 24(3), 33-37. (in Chinese)

Xia, Q. (2009). *Probability Analyses for Strong Column-Weak Beam Design of Reinforced Concrete Frames*, Master degree thesis: Xi'an University of Architecture and Technology, China. (in Chinese)

Xiao, Y. (2004). "Applications of FRP composites in concrete columns", *Advances in Structural Engineering*, 7(4), 335-343.

Xiao, Y. and Wu, H. (2003). "Retrofit of reinforced concrete columns using partially stiffened steel jackets", *Journal of Structural Engineering*, ASCE, 129(6), 725-732.

Xiong, Y.L. (2011). *Effect Analysis of Infilled wall on the Seismic Performance of Reinforced Concrete Frame Structure*, Master degree thesis: Changan University, China. (in Chinese)

Xu, X.P. and Needleman, A. (1994). "Numerical simulations of fast crack growth in brittle solids". Journal of the Mechanics and Physics of Solids, 42(9), 1397-1434.

Xu, Y.F., Hu, Q.C., Chen, Y.F., Shi, C., Hong, B.N., Lin, S.J. and Yu, H. (1986). "Experimental study on the mechanical properties of two-span three-layer RC frames under low cyclic loading", *Journal of Building Structures*, 7(2), 1-16. (in Chinese)

Yan, Y.L. (2010). *A Study on Eurocodes about the RC Elements Design and Comparison between Eurocodes and Chinese Codes*, Master degree thesis: China Academy of Building Research, China. (in Chinese).

Yang, B. (2012). *Study on Influence Factors of "Strong Column and Weak Beam"* *of Reinforced Concrete Frame Structures*, Master degree thesis: Hunan University, China. (in Chinese)

Yang, H. (2000). *Study on Nonlinear Dynamic Response of Reinforced Concrete Seismic Frame Based on Refined Rod Model*, Doctoral degree thesis: Chongqing Jianzhu University, China. (in Chinese)

Yang, H., Wang, Q.L. and Bai, S.L. (2010). “Strong column-weak beam mechanism for RC frames in China under bi-directional horizontal seismic excitation”, *Building Structure*, 40(8), 71-76. (in Chinese)

Yang, X.W. (2011). *Studies on Test of Earthquake Failure Mechanism of Beam-Column and Design Method of RC Frame Structures*, Doctoral degree thesis: China Academy of Building Research, China. (in Chinese)

Yang, Z.L. (2010). *Research on “Strong Column Weak Beam” Yield Mechanism Factors of Reinforced Concrete Frame Structure*, Master degree thesis: Qingdao Technological University, China. (in Chinese)

Ye, L.P., Ma, Q.L. and Miao, Z.W. (2010). “Study on weak beam-strong column design method of RC frame structures”, *Engineering Mechanics*, 12(12), 102-113. (in Chinese)

Ye, L.P., Qu, Z., Ma, Q.L., Lin, X.C, Lu, X.Z. and Pan, P. (2008). “Study on ensuring the strong column-weak beam mechanism for RC frames based on the damage analysis in the Wenchuan earthquake”, *Building Structure*, 38(11), 52-67. (in Chinese)

Zhang, J. (2013). *Research on Efficiency of Slot-cutting around Frame Joint for*

"Strong Column and Weak Beam" under Earthquake Action, Master degree Thesis: Hunan University, China. (in Chinese)

Zhang, Y.P., Hao, Z.J., Shan, M.Y. and Ge, N. (2011). "Research on anti-seismic performance for reinforced concrete frame joint with slot around", *Building Science*, 27(9), 7-11. (in Chinese)

Zhen, S.J., Jiang, L.X., Zhang, W.P. and Gu, X.L. (2009). "Experimental research and analysis of effective flange width of beam end section in cast-in-site concrete frames", *Structural Engineers*, 25(2), 134-140. (in Chinese)

Zhou, J.W., Zhao, F.H. and Wen, Z.W. (2012). "Effect of frame beam span on strong column-weak beam mechanism", *China Concrete and Cement Produc.*, (9), 49-51. (in Chinese)

Zhu, B.L., Wu, M.S. and Yuan, D. (1987). "Deformed state of masonry and reinforced concrete frame buildings", *Structural Engineer*, 01. (in Chinese)

Table 2.1. Summary of numerical studies on the effect of cast-in-place floor slabs on the behaviour of RC frames

Source	**Dimensions**	**FE Model**	**Modeling of floor slab**	**Analysis type**	**Software**
Guan and Du (2005)	2-D	A 3-storey 3-span RC frame	T-section beam	Pushover analysis	SAP2000 (1998)
Lin et al. (2009)	3-D	Two 6-storey 3x9-span RC frames, one with slabs and one without slabs	Elastic shell element	Elastic-plastic time history analysis	MSC.Marc (2005)
Gao and Ma (2009)	3-D	Two 6-storey 4x4-span RC frames, one with slabs and one without slabs	Layered shell element	Pushover analysis	SAP2000 (1998)
Yang (2010)	3-D	Five 6-storey 4x4-span RC frames with different slab widths	Shell element	Pushover analysis	SAP2000 (1998)
Chen (2010)	3-D	Two 6-storey 6x3-span RC frames, one with slabs and one without slabs	Shell element	Elastic-plastic time history analysis	SAP2000 (1998)
Guo (2012)	3-D	Three 3-storey 3x4-span RC frames, one with slabs and slab reinforcement, one with slabs but without slab reinforcement, and one without slabs	Shell element	Pushover analysis	SAP2000 (1998)

Table 2.2. Suggested effective flange widths

Source	**Value of b_f**	**Applicable condition**
Durrani and Zerbe (1987)	b_c + 2h	Exterior joints
French (1991)	min{l_0/4, b + 16t, s}	Interior joints (γ = 1/50)
Li (1994)	b + 8t	Interior joints
Jiang et al. (1994)	b + 12t	Interior joints
Wu et al. (2002)	b + 12t	Interior joints (γ =1.5%)
Wang et al. (2009)	b + 2t	Interior joints (γ =1/550)
Zhen et al. (2009)	min{b + 3.5h, l_0/3, s}	Interior joints (γ =1/50)
	min{b + 1.5h, l_0/6, s}	Exterior joints (γ =1/50)
Yang (2010)	b + (12~16)t	Interior joints
Sun (2010)	b + min{max(l_0/4, 2h), 1/2s}	Interior joints (γ =1/50)
	b + min{max(l_0/5, 1.5h), 1/2s}	Exterior joints (γ =1/50)
Qi et al. (2010)	b + min{l_0/4, 12t, s}	Interior joints (γ =1/50)
	b + min{l_0/5, 8t, s}	Exterior joints (γ =1/50)
He (2010)	b + 12t	Interior joints (γ =1/50)

Note: b_c=column width; b= beam width; h=beam height; l_0=effective span of beam; t=slab thickness; s=clear distance between two adjacent beams; γ = inter story drift angle.

Table 2.3. Studies on the effect of infill walls on the behavior of RC frames

Source	Experimental study	Numerical study			
		FE Model	**Modeling of infill walls**	**Analysis type**	**Software**
Lin et al. (2009)	NA	Three 6-storey 3x9-span RC frames, one pure frame, one frame with floor slab, and one frame with both floor slab and infill walls	Elastic-plastic model and fracture constitutive model	Elastic-plastic time history analysis	MSC.Marc (2005)
Chen (2010)	NA	Four 6-storey 6x3-span RC frames, one pure frame, one frame with floor slab, one frame with both floor slab and infill walls, and one frame with both floor slab and infill walls except the ground floor	Shell element	Linear and non-linear time history analysis	SAP2000 (1998)
Xiong (2011)	NA	Two 5-storey 2-span RC frames, one pure frame and one frame with infill walls	Cross spring supporting model	Pushover analysis	SAP2000 (1998)
Shi (2012)	Two 1/4-scale 3-storey 2x2-span RC frames, one pure frame and one frame with infill walls	Two 1/4-scale 3-storey 2x2-span RC frames, one pure frame and one frame with infill walls	Equivalent diagonal bracing model	Elastic-plastic time history analysis	PERFORM -3D (2011)

Table 2.4. Studies on the effect of over-reinforced beam ends on the behavior of RC frames

Source	FE Model	Analysis type	Software	Remarks
Lei (2002)	Three RC frames, frame A is a 6-storey 3-span frame of SG[(a)] 1 in SPI[(b)] 9 region in China, frame B is an 11-storey 3-span frame of SG 1 in SPI 8 region in China, frame C is an 8-storey 3-span frame C of SG 2 in SPI 8 region in China	Elastic-plastic time history analysis	PL-AFJD (2000)	According to the Chinese code GB-50011 (2001), the flexural capacities of beams and columns were calculated based on the actual reinforcement for frames A and B and the design bending moment for frame C
Liu et al. (2004)	Two 6-storey 3-span RC frames, frame A of SG 1 in SPI 9 region in China and frame B of SG 2 in SPI 8 region in China	Elastic-plastic time history analysis	PL-AFJD (2000)	According to the Chinese code GB-50011 (2001), the flexural capacities of beams and columns were calculated based on the actual reinforcement for frame A and the design bending moment for frame B
Han et al. (2010)	Two RC frames, frame A didn't have over-reinforced beam end while frame B had beam ends which were over-reinforced by 10%	Pushover analysis	OpenSees (2009)	NA

Note: (a) SG= Seismic Grade; (b) SPI= Seismic Precautionary Intensity.

Table 2.5. Suggested values of column-to-beam flexural strength ratio η_c

<table>
<tr><th rowspan="2">Source</th><th colspan="2">Calculation of flexural capacity of the beam</th><th rowspan="2">Value of η_c</th><th rowspan="2">Remarks</th></tr>
<tr><th>Reinforcement</th><th>Consideration of the effect of floor slabs</th></tr>
<tr><td>Xu et al. (1986)</td><td>Designed reinforcement</td><td>No</td><td>1.42 - 2.86</td><td>η_c of each joint in a tested frame</td></tr>
<tr><td>Dooley and Bracci (2001)</td><td>Actual reinforcement</td><td>Yes</td><td>2.0</td><td>For RC frames in the US</td></tr>
<tr><td>Wei et al. (2003)</td><td>Designed reinforcement</td><td>No</td><td>1.4-1.5</td><td>For RC frames of SG 2 in an SPI 8 region in China</td></tr>
<tr><td>Ma and Chen (2005)</td><td>Designed reinforcement</td><td>No</td><td>1.6</td><td>For RC frames in an SPI 8 region in China</td></tr>
<tr><td>Cai et al. (2007)</td><td>Actual reinforcement</td><td>Yes</td><td>2.0</td><td>For RC frames in an SPI 8 region in China</td></tr>
<tr><td rowspan="2">Wei et al. (2007)</td><td>Designed reinforcement</td><td>No</td><td>1.3</td><td>For RC frames of SG 3 in an SPI 7 region in China</td></tr>
<tr><td>Actual reinforcement</td><td>No</td><td>1.0</td><td>For RC frames of SG 2 in an SPI 8 region in China</td></tr>
<tr><td rowspan="3">Xia (2009)</td><td rowspan="3">Designed reinforcement</td><td rowspan="3">No</td><td>1.4</td><td>For RC frames of SG 2 in an SPI 8 region in China</td></tr>
<tr><td>1.3</td><td>For RC frames of SG 2 in an SPI 7 region in China</td></tr>
<tr><td>1.2</td><td>For RC frames of SG 3 in an SPI 7 region in China</td></tr>
<tr><td>Tao (2010)</td><td>Designed reinforcement</td><td>No</td><td>1.7</td><td>For RC frames of SG 2 in China</td></tr>
<tr><td>Yang (2010)</td><td>Designed reinforcement</td><td>No</td><td>1.6-2.0</td><td>For RC frames of SG 2 in an SPI 8 region in China</td></tr>
<tr><td rowspan="3">Ye et al. (2010)</td><td rowspan="3">Actual reinforcement</td><td rowspan="3">Yes</td><td>2.0 (1.7)</td><td>For RC frames of SG 1 (the latter one is the suggested moderate value of the former one)</td></tr>
<tr><td>1.7 (1.5)</td><td>For RC frames of SG 2 in China</td></tr>
<tr><td>1.4 (1.3)</td><td>For RC frames of SG 3 in China</td></tr>
<tr><td>Sun (2010)</td><td>Designed reinforcement</td><td>No</td><td>1.8-2.0</td><td>For RC frames of SG 2 in China</td></tr>
<tr><td rowspan="4">Yang (2011)</td><td rowspan="4">Actual reinforcement</td><td rowspan="4">Yes</td><td>2.4</td><td>For RC frames of SG 1 in China</td></tr>
<tr><td>2.1</td><td>For RC frames of SG 2 in China</td></tr>
<tr><td>1.9</td><td>For RC frames of SG 3 in China</td></tr>
<tr><td>1.6</td><td>For RC frames of SG 4 in China</td></tr>
<tr><td>Yang (2012)</td><td>Designed reinforcement</td><td>No</td><td>1.5</td><td>For RC frames of SG 3 in China</td></tr>
<tr><td>Sunitha et al. (2014)</td><td>Designed reinforcement</td><td>No</td><td>2.5-3.0</td><td>For RC frames in India</td></tr>
</table>

Table 2.6. Stipulations on the strong column-weak beam requirement of RC frames in NZS-3101

Time	Stipulation	Remarks
1982	$\Sigma M_C \geq (1.6\sim2.4)\Sigma M_B$	ΣM_C: sum of the moments at ideal strength in hinging columns at opposite faces of the joint, summed in the same vector sense, and related to the centre of the intersect-beam; ΣM_B: sum of the moments at ideal strength in non-yielding beams at opposite faces of the joint, summed in the same vector sense, and related to the centre of the intersecting beam. Slab reinforcement within an effective flange width d_f shall be assumed to contribute to M_B; $d_f = b + 8t$.[a]
2006	$\Sigma M_C = \omega\beta\Sigma M_B$ $\beta = 1.4 - \frac{\sum M'_o}{2.5\emptyset_{o,fy}\sum M'_n}$	ΣM_C: sum of nominal flexural strengths of the columns framing into that joint, evaluated at the faces of the joint; ΣM_B: sum of bending moments in beams sustained at the intersection of the beam and column centrelines when nominal moments act in the beams at the column faces. Slab reinforcement within an effective flange width d_f shall be assumed to contribute to M_B; $d_f = b + \min\{2h, 16t, 2s^*h_{b1}/(h_{b1}+h_{b2}), l_0/4\}$, where h_{b1} is the depth of the beam being considered and h_{b2} is the depth of the adjacent beam; ω: appropriate dynamic magnification factor, not less than 1.3 and not more than 1.8; β: appropriate modification factor; $\sum M'_o$ and $\sum M'_n$ are the sums of the beam overstrength and nominal strength moments respectively, acting at the column faces of the beam column joint being considered; $\emptyset_{o,fy}$ = 1.25 for Grade 300 reinforcement; = 1.35 for Grade 500 reinforcement.

Note: (a) The notation follows that in Table 2.2.

Table 2.7. Stipulations on the strong column-weak beam requirement of RC frames in ACI 318

Time	Stipulation	Remarks
1983	$\Sigma M_C \geq (6/5)\Sigma M_B$	ΣM_C: sum of moments, at the center of the joint, corresponding to the design flexural strength of the columns framing into that joint; ΣM_B: sum of moments, at the center of the joint, corresponding to the design flexural strengths of the girders framing into that joint.
2002	$\Sigma M_C \geq (6/5)\Sigma M_B$	ΣM_C: sum of moments at the face of the joint corresponding to the nominal flexural strength of the columns framing into that joint; ΣM_B: sum of moments at the face of the joint corresponding to the nominal flexural strength of the girders framing into that joint. In T-beam construction, where the slab is in tension under moments at the face of the joint, slab reinforcement within an effective flange width d_f shall be assumed to contribute to flexural strength if the slab reinforcement is developed at the critical section for flexure; $d_f = \min\{l_0/4, b + s, b + 16t\}$.(a)
2005	$\Sigma M_C \geq (6/5)\Sigma M_B$	ΣM_C: sum of nominal flexural strengths of the columns framing into that joint, evaluated at the faces of the joint; ΣM_B: sum of nominal flexural strengths of the beams framing into that joint, evaluated at the faces of the joint. In T-beam construction, where the slab is in tension under moments at the face of the joint, slab reinforcement within an effective flange width d_f shall be assumed to contribute to M_B if the slab reinforcement is developed at the critical section for flexure; $d_f = \min\{l_0/4, b + s, b + 16t\}$.(a)
2014	$\Sigma M_C \geq (6/5)\Sigma M_B$	Same as above except the stipulation for d_f. $d_f = b + \min\{l_0/4, s, 16t\}$.(a)

Note: (a) The notation follows that in Table 2.2.

Table 2.8. Stipulations on the strong column-weak beam requirement of RC frames in Eurocode 8

Time	Stipulation			Remarks
	DCL[a]	**DCM**[a]	**DCH**[a]	
1995	NA	$\Sigma M_C \geq 1.2 \Sigma M_B$	$\Sigma M_C \geq 1.35 \Sigma M_B$	ΣM_C: the sum of design values of the flexural capacity of the columns framing into a joint; ΣM_B: sum of design values of the flexural capacity of the beams framing into a joint; slab reinforcement parallel to the beam and within the effective flange width d_f should be assumed to contribute to the beam flexural capacities and taken into account for the calculation of ΣM_B, if it is anchored beyond the beam section at the face of the joint; $d_f = b_c + 8t$. [b]
2004	Same as above.			Same as above.

Note:

(a) Structural ductility class: DCL (Low ductility), DCM (Medium ductility), DCH (High ductility);

(b) The notation follows that in Table 2.2.

Table 2.9. Historical highlights of seismic design codes in China

Time	Title	Remarks
1959	Code for seismic design of buildings (draft)	Not published.
1964	Code for seismic design of buildings (draft)	Introduced the structural coefficient C to reduce seismic load of structures, in order to make up the gap between calculation results based on elastic theory and the fact that structure is elastic-plastic; not published.
1974	Code for seismic design of industrial and civil buildings (Trial) (TJ11-74 1974)	The first seismic design code in China.
1978	Code for seismic design of industrial and civil buildings (Trial) (TJ11-78 1978)	Revised on the basis of TJ11-74 (1974) after the Tangshan earthquake in 1976; used safety factor method or allowable stress method for seismic strength calculation, but safety factor was simplex, randomness of seismic action and discreteness of materials and strength of elements cannot be reflected.
1989	Code for seismic design of buildings (GBJ11-89 1989)	Implemented in 1990 and partially revised in 1993; changed from a single-level fortification to three-level fortification, and proposed target of three-level seismic fortification (i,e. not damaged under minor earthquake, repairable under medium earthquake, not collapse under large earthquake), marking China's seismic design theory and practice catch up with advanced countries.
2001	Code for seismic design of buildings (GB50011 2001)	Partially revised after the Wenchuan earthquake in 2008 and became GB50011 (2008).
2010	Code for seismic design of buildings (GB50011 2010)	Came into force in December 2010; adjusted the fortification intensity, improved the seismic design of buildings in mountain areas, supplemented seismic measures of RC, masonry and steel structures, and calculation and constructional measures of staircases.

Table 2.10. Stipulations on the strong column-weak beam requirement of RC frames in Chinese design codes

Time	Code	Stipulation				Remarks
		SG 1	SG 2	SG 3	SG 4	
1989	GBJ11-89	$\Sigma M_C=1.1\Sigma M_{Bua}$ or $\Sigma M_C=1.1\lambda_j\Sigma M_B$	$\Sigma M_C=1.1 \Sigma M_B$	NA		ΣM_C: sum of design flexural capacities of the columns framing into a joint; ΣM_B: sum of design flexural capacities of the beams framing into a joint; λ_j: amplified coefficient due to over-reinforcement, 1.1 can be used; ΣM_{Bua}: sum of flexural capacities of the beams framing into a joint calculated based on the actual reinforcement and the standard strength of materials, the effect of cast-in-place floor slab is not considered.
2001	GB-50011	$\Sigma M_C=1.4\Sigma M_B$ and $\Sigma M_C=1.2\Sigma M_{Bua}$	$\Sigma M_C=1.2 \Sigma M_B$	$\Sigma M_C=1.1 \Sigma M_B$	NA	Same as above.
2010	GB-50011	$\Sigma M_C=1.7\Sigma M_B$ and $\Sigma M_C=1.2\Sigma M_{Bua}$	$\Sigma M_C=1.5 \Sigma M_B$	$\Sigma M_C=1.3 \Sigma M_B$	$\Sigma M_C=1.2 \Sigma M_B$	Same as above except ΣM_{Bua}. When there is cast-in-place floor slab, actual reinforcement at beam end should include reinforcement in the slab within effective flange width d_f. $d_f = \min\{l_0/3, b + s, b + 12t\}$.[(a)]

Note: (a) The notation follows that in Table 2.2.

Table 2.11. Summary of studies on the effectiveness of the slab slit (SS) technique

Source	FE Model	Modeling of floor slab	Analysis type	Software
Zhang et al. (2011)	Three RC joints with a floor slab, joint A without slits, joint B with slits whose length was 200 mm, joint C with slits whose length was 300 mm	Solid element	Quasi-static analysis	ADINA (2007)
Wang et al. (2012)	Two 1/2 scale 6-storey 2-span RC frames, frame A without slits and frame B with slits whose length was 200 mm	NA	Linear and non-linear time history analysis	ADINA (2007)
Zhang (2013)	Three 6-storey 2x3-span RC frames, normal frame A, frame B with slits whose length was 200 mm and frame C whose columns were strengthened with FRP	Solid element	Elastic-plastic time history analysis	ABAQUS (2006)
	Two 5-storey 2x11-span RC frames, normal frame D and frame E with slits whose length was 200 mm	Solid element	Elastic-plastic time history analysis	SAP2000 (1998)

Table 2.12. Summary of experimental studies on RC beams with a web opening

Source	Beam dimensions			Web opening size (mm)	Load capacity reduction (%)	Strengthening method	Increase in load capacity due to strengthening (%)[a]	Observed failure mode		Remarks
	Span (mm)	Width (mm)	Height (mm)					Without strengthening	With strengthening	
Mansur et al. (1999)	2600	200[c]	500	r=100	22.9	NA	NA	Shear crack passing through the opening	Flexural at mid-span	Reversed T-section beams with circular openings (the flange is 100 mm in height and 700 mm in width)
				r=150	29.5	Bonded FRP plates	52.8			
Abdalla et al. (2003)	2000	100	250	100 × 100[b]	50.6	Bonded FRP sheets and wraps	109.8	Shear crack passing through the opening corners	Flexural at mid-span	NA
				200 × 100	48.2		76.7		Shear at opening	
				300 × 100	50.6		51.2		Shear at opening	
				300 × 150	73.5		59.1		Shear at opening	
Allam (2005)	3200	150	400	450 × 150	37.1	Bonded FRP sheets and U-jackets	49	Shear crack passing through the opening corners	Shear at opening after debonding of FRP	NA
Maaddawy and Sherif (2009)	1000	80	500	200 × 200	NA	Bonded FRP sheets and wraps	66.0	Shear crack passing through the opening corners, and shear crack in the chords	Shear at opening and chords after debonding of FRP	Deep beams, no control beam without opening was tested
				250 × 250	NA		65.3			
Madkour (2009)	2700	140	280	600 × 80	57.8	NA	NA	Shear crack passing through the opening corners	NA	NA
				600 × 100	66.7					
				600 × 120	75.6					
				600 × 140	81.7					
Pimanmas (2010)	2100	400	160	r=150	37.7	Near-surface mounted FRP rods	57.6	Shear crack passing through the opening	Flexural at mid-span	NA
				150 × 150	44.3		75.4			

								corners		
Chin et al. (2012)	1800	300	120	210 × 210	74.4	Bonded FRP sheets and wraps	80.1	Shear crack passing through the opening corners	Shear at opening	NA
				210 × 210	68.8		48.8			
Maaddawy and Ariss (2012)	2400	85	400	200 × 200	72.7	Bonded FRP sheets and U-jackets	276.2	Shear crack passing through the opening corners	Shear at opening and in chords after debonding and rupture of FRP	NA
				350 × 200	70.1		160.9			
				500 × 120	44.2		69.8	Shear crack passing through the opening corners, and shear crack in the chords		
				500 × 160	46.8		61.0			
				500 × 200	58.4		65.6			
Suresh and Prabhavathy (2015)	2200	150	300	150 × 150	44.8	NA	NA	Shear crack passing through the opening corners	NA	Strengthened with steel plates
				200 × 150	55.2					
				250 × 150	65.5					
				300 × 150	71.7					
Chin et al. (2016)	1800	120	300	800 × 140	58.4	Bonded FRP sheets	95.6	Shear crack passing through the opening corners	Shear at opening after debonding of FRP	NA
Teng et al. (2013)	3300	250(c)	500	500 × 150	NA	Bonded FRP plate, U-jackets and wraps	NA	Shear crack passing through the opening corners	Shear at opening	Reversed T- section beams whose flange is 100 mm in height and 1450 mm in width
				500 × 220						

Note: (a) Compared with beam specimen with an un-strengthened web opening; (b) Opening width × opening height; (c) Web width.

Table 2.13. Summary of numerical studies on RC beams with a web opening

Source	Software used	Modelling of concrete cracking			Modelling of bond behaviour	
		Crack modelling method	Tension-softening behavior	Shear stress transfer model	Steel-to-concrete	FRP-to-concrete
Pimanmas (2010)	WCOMD	Smeared crack model	$\sigma_t = f_t(\frac{\varepsilon_{tu}}{\varepsilon_t})^{0.4}$	$\tau_{cr} = 3.8(f_c')^{1/3}\frac{\delta^2}{1+\delta^2}$	Perfect bond	Perfect bond
Chin et al. (2012)	ATENA	Rotated crack model in the smeared crack approach	The slope of the ascending branch is equal to the concrete modulus of elasticity. In the descending branch of the stress-strain curve, a fictitious crack model based on a crack-opening law and fracture energy is used, where the cracks occur when the principal stress exceeds the tensile strength.	NA	Perfect bond	Bond-slip model developed by Lu et al. (2005)
Hawileh et al. (2012)	ANSYS ver. 11.0	NA	σ_t increases linearly to f_t, then suddenly drops to $0.6f_t$, finally descends linearly to zero at a strain value of $6\varepsilon_{tu}$	NA	Perfect bond	Bond-slip relationship proposed by Xu and Needleman (1994)

Note : σ_t=tensile stress of concrete; ε_t=tensile strain of concrete; ε_{tu}=cracking strain of concrete; f_t= tensile strength of concrete; $\varepsilon_{tu}=2f_t/E_c$, where E_c is initial elastic modulus of concrete; f_c'= cylinder compressive strength of concrete; τ_{cr}=shear stress of concrete; δ=normalized shear strain of concrete, defined as $\delta = \gamma_{cr}/\varepsilon_t$, where γ_{cr} is the shear strain of cracked concrete and ε_t is the tensile strain of cracked concrete.

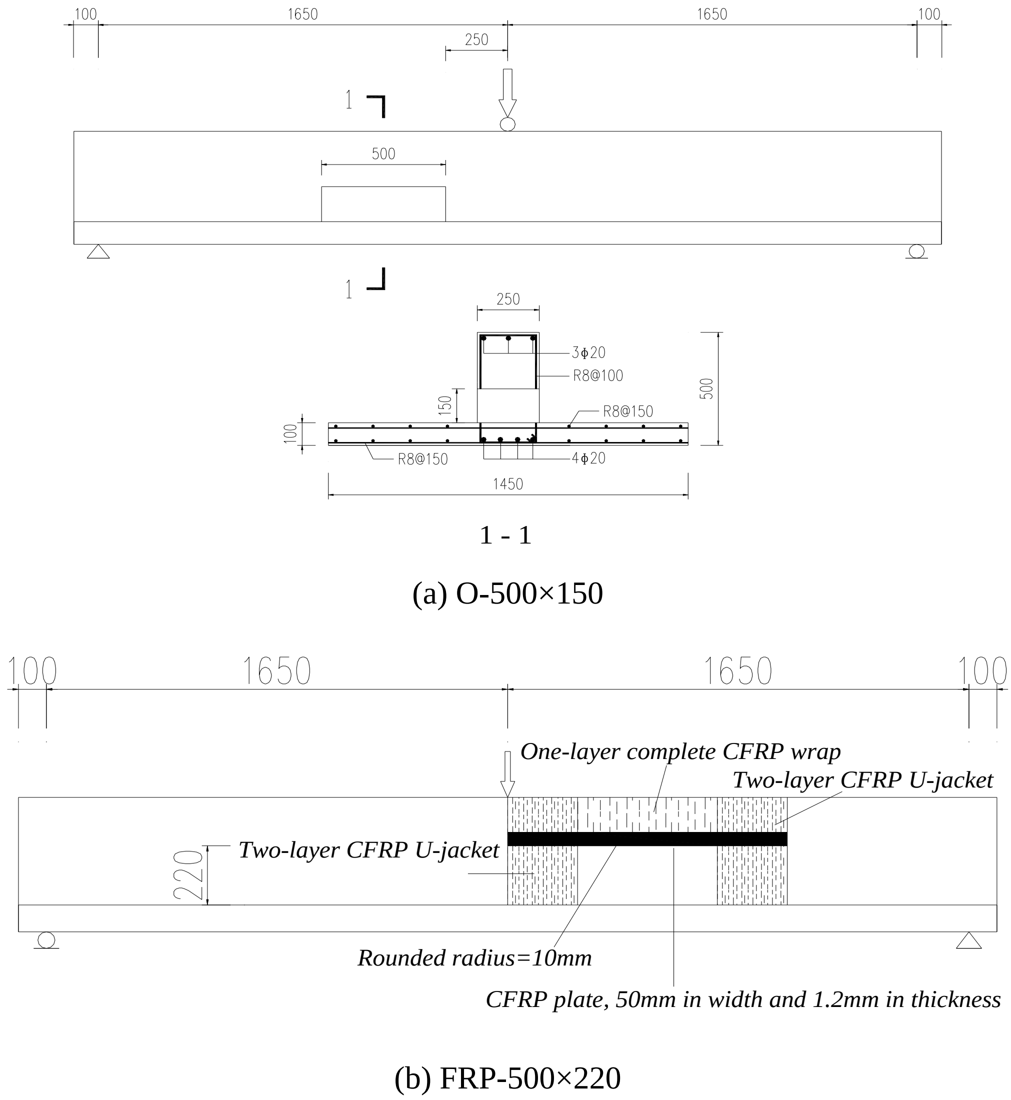

Figure 2.1. Layout of specimens tested by Prof. Teng's group (Teng et al. 2013)

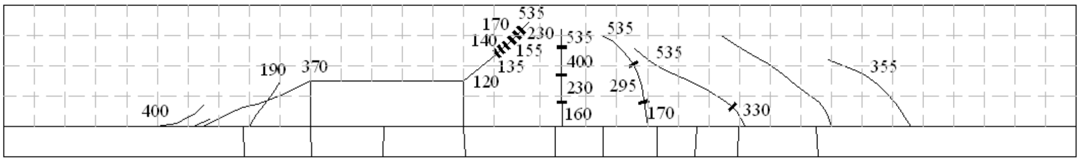

(a) O-500×150

(b) FRP-500×220

Figure 2.2. Failure modes of specimens tested by Prof. Teng’s group (Teng et al. 2013)

CHAPTER 3

FE MODELLING OF EXISTING TESTS ON RC BEAMS WITH A WEB OPENING

3.1 INTRODUCTION

As reviewed in Chapter 2, a number of experimental studies have been conducted to examine the behavior of RC beams with a web opening. Even though these studies were motivated by the need to create openings in an existing structure for the passage of utility ducts and pipes, a purpose different from that of the present study, these studies offered a useful source of information for the present work on beam-end weakening by the drilling of an opening. It can be concluded from these studies that a web opening can significantly reduce the shear and flexural capacities of a beam. Although the existing experimental studies have provided useful information on the behaviour of RC beams with a web opening, a reliable method for predicting the load-carrying capacity of such RC beams is not yet available. While experimental studies are essential in understanding the structural behaviour of RC beams with a web opening, many behavioural aspects can be better or more efficiently examined using a finite element (FE) model. Indeed, FE modelling can serve as a powerful and economical alternative to laboratory testing in understanding the structural behaviour of and in the development of a design method for RC beams with a web opening. However, most of the existing studies on the behavior of RC beams with a web opening were experimentally based, and only a very limited amount of research has been based on the numerical modeling of beams with a web opening using the FE method. As discussed in Chapter 2, the limited number of existing numerical studies on RC beams with a web opening have not led to a well-established FE modelling approach for predicting the behaviour of such RC beams. Thus, the study presented in this chapter was conducted with the aim of developing such an FE approach with the general purpose package ABAQUS (ABAQUS 2012). Three alterative FE approaches are presented in this chapter, and their predictions are compared with test results collected from the published literature to identify the most reliable approach. It should be noted that although the present study was conducted on RC beams with a rectangular web opening, the conclusions are also largely applicable to RC beams with a web opening of other shapes (e.g. a circular web opening).

3.2 PROPOSED FINITE ELEMENT APPROACH

3.2.1 FE meshes

Against the above background, a two-dimensional FE model was proposed in the present study by using the general purpose FE program ABAQUS (2012). In the proposed FE model, the concrete was modelled using 4-node plane stress elements CPS4R, and steel bars were modelled using 2-node truss elements T2D2. For rectangular beams, the thicknesses of the plane stress elements were set to be the width of the beam; and for T-section beams, the thicknesses of the plane stress elements for the beam flange were set to be the width of the flange, while those for the beam web were set to be the width of the web. The bond behaviour between concrete and steel reinforcement (longitudinal bars and stirrups) was modelled using 4-node interfacial elements COH2D4. All the elements employed a reduced integration scheme. The typical meshes are shown in Fig. 3.1. If the loads were symmetrically applied and the web openings were also symmetrically placed about the mid-span of the beam in the tests, only one half of the beam was modelled with horizontal displacements on the line of symmetry prevented (as shown in Fig. 3.1a). Otherwise the full beam was modelled (as shown in Fig. 3.1b). All concrete elements were square and the maximum side length of the concrete elements was chosen to be 10 mm based on the results of a convergence study. The steel element size was so determined that a maximum of one steel element would exist between two adjacent concrete element nodes. Therefore, all steel elements had a length of 10 mm. The applied boundary conditions and loads for both symmetrical and non-symmetric beam cases are shown in Fig. 3.1. In order to avoid premature local failure of concrete at the loading point and the two supports, four elastic elements with the same elastic modulus and element size as the beam concrete were placed near the loading point and each support respectively to simulate the rubber pads usually used in the tests, and then the imposed displacement at the loading point and displacement restraints at the two supports were applied through these elastic elements, as shown in Fig. 3.1.

3.2.2 Constitutive modelling of concrete

As have been mentioned earlier, it was found from experimental studies that RC beams with a web opening exhibited a shear failure mode, in which small inclined cracks first occurred at the corners of the opening and then propagated to form a diagonal crack in the shear span of the beam. Therefore, the modelling of the cracked concrete (especially the tensile and shear behaviour of the cracked concrete) is of most importance to accurately predict the behaviour of RC beams with a web opening. The crack band concept (Bazant and Oh 1983) was adopted with the fracture energy being that given by CEB-FIP (1993).

To achieve an accurate model for the simulation of cracked concrete, two concrete crack models available in ABAQUS/Explicit were examined in the present study: the brittle cracking model and the concrete damaged plasticity model. The concrete damaged plasticity model uses concepts of isotropic damaged elasticity in combination with isotropic tensile and compressive plasticity to represent the inelastic behaviour of concrete (ABAQUS 2012). This concrete damaged plasticity model has been successfully used by Prof. Teng’s group in the modelling of FRP-strengthened RC beams (Chen et al. 2011, 2012). On the other hand, the brittle cracking model is more competitive in applications where the brittle cracking behaviour (tensile and shear behaviour) of concrete governs. The shear retention factor of cracked concrete can be explicitly defined in the brittle cracking model for a more accurate modelling of the shear behaviour of cracked concrete (ABAQUS 2012). Both models have the potential to accurately simulate cracked concrete and thus were investigated in present study for comparison purpose.

3.2.2.1 Brittle cracking model

The brittle cracking model is proposed for applications where the tensile and shear behaviour of cracked concrete dominates the behaviour of the structure, and thus the behaviour of concrete is assumed to be linear elastic in compression. The brittle cracking model is a type of orthogonal fixed smeared crack model which allows the formation of a maximum of two orthogonal cracks in 2-D elements (ABAQUS 2012). The orientations of the cracks remain unchanged once the cracks are formed.

<u>*Initiation of cracking*</u>

The maximum tensile stress criterion (i.e., the Rankine criterion) (Eq. 3.1) is used to detect the initiation of cracking. Although the detection of cracking is only based on *Mode I* fracture considerations, the subsequent behaviour of cracked concrete includes both *Mode I* (i.e., tension softening behaviour) and *Mode II* (i.e., shear retention behaviour) behaviour (ABAQUS 2012).

$$f(I_1, J_2, \theta) = 2\sqrt{3}\sqrt{J_2}\cos\theta + I_1 - 3f_t = 0 \tag{3.1}$$

where I_1 and J_2 are the first invariant of stresses and the second invariant of deviatoric stresses, respectively; f_t is the tensile strength of concrete; and θ is the angle of similarity.

<u>*Tension-softening curve of cracked concrete*</u>

Following Chen et al. (2011, 2012), the exponential tension-softening curve of concrete in tension proposed by Hordijk (1991) (Eq. 3.2) was used to represent the tensile behaviour of cracked concrete.

$$\frac{\sigma_t}{f_t} = \left[1 + \left(3.0\frac{w}{w_0}\right)^3\right] e^{\left(-6.93\frac{w}{w_0}\right)} - 10\frac{w}{w_0} e^{(-6.93)} \tag{3.2}$$

$$w_0 = 5.14\frac{G_F}{f_t} \tag{3.3}$$

where σ_t (MPa) is the tensile stress normal to the crack, w (mm) is the crack opening displacement; w_0 (mm) is the crack opening displacement at the complete release of stress or fracture energy; G_F (N/m) is the tensile fracture energy required to create a stress-free crack over a unit area. The tensile strength of concrete f_t (MPa) and the tensile fracture energy of concrete G_F (N/m) are calculated by using the equations from CEB-FIP (1993) in the present study, as shown in Eq. 3.4 and Eq. 3.5, respectively.

$$f_t = 1.4\left(\frac{f_c - 8}{10}\right)^{\frac{2}{3}} \tag{3.4}$$

$$G_{ft} = (0.0469 D_a^2 - 0.5 D_a + 26)(\frac{f_c}{10})^{0.7} \tag{3.5}$$

where f_c (MPa) is the cylinder compressive strength of concrete and D_a (mm) is the maximum aggregate size, which is assumed to be 20 mm if no test data are given.

Shear retention factor model of cracked concrete

The shear retention factor β_s reflects the shear stress-shear strain (or slip) relationship after the cracking of concrete and significantly influences the predicted behaviour of cracked concrete. In the present study, Rots's (1988) model was employed to define the shear retention factor:

$$\beta_s = \left(1 - \frac{\varepsilon_{cr}}{\varepsilon_{cr,u}}\right)^n \tag{3.6}$$

where ε_{cr} is the concrete cracking strain, $\varepsilon_{cr,u}$ is the concrete cracking strain at the complete release of stress or fracture, which can be determined from w_0 based on the crack band concept [see Chen et al. (2011) for details], and n is the exponent controlling the rate of shear degradation, which were determined through parametric studies as shown later.

3.2.2.2 Concrete damaged plasticity model

Compressive behaviour of concrete

Following Chen et al. (2011), the concrete damaged plasticity model can simulate the inelastic behaviour of concrete in compression. In the present study, the uniaxial compressive stress-strain curve proposed by Saenz (1964) was employed:

$$\sigma = \frac{\alpha\varepsilon}{1+[(\alpha\varepsilon_p/\sigma_p)-2](\varepsilon/\varepsilon_p)+(\varepsilon/\varepsilon_p)^2} \tag{3.7}$$

where σ is the compressive stress, ε is the compressive strain; σ_p and ε_p are the maximum stress and the corresponding strain, respectively, and are assumed to be the compressive cylinder concrete strength and 0.002 respectively following Chen (1982) in absence of test data in the present study; α is the coefficient representing the initial tangent modulus and is set to be equal to the elastic modulus of the concrete E_0, calculated according to ACI-318 (2014) $E_0 = 4730\sqrt{f_c}$ where both E_0 and f_c are in *MPa*.

Tensile and shear behaviour of concrete

In the present study, the tension-softening curve and the shear retention factor model of cracked concrete adopted in the concrete damaged plasticity model are the same as those employed in the brittle cracking model (i.e., expressed in Eqs. 3.2 to 3.5). And the corresponding stiffness degradation variables of cracked concrete d_t is given by

$$d_t = 1 - \beta_s \tag{3.8}$$

where β_s is the shear retention factor given by Eq. 3.6. The exponent n in Eq. 3.6 is selected to be 5 for the concrete damaged plasticity model following Chen et al. (2012).

It should be noted that although the same tension-softening curve and shear retention factor model are used in the concrete damaged plasticity model and the brittle cracking model, the algorithms respectively adopted by these two concrete models to simulate cracked concrete are totally different. The brittle cracking model can be classified as an orthogonal fixed smeared crack model in which the orientations of cracks remain unchanged once the cracks are formed, while in the concrete damaged plasticity model there is only one active crack at one material integration point and the direction of crack keeps perpendicular to the direction of maximum tensile plastic strain of concrete. To some extent, therefore, the concrete damaged plasticity model can be seen as a rotating smeared crack model in terms of crack modelling.

3.2.3 Modelling of steel bars and bond behaviour between steel and concrete

The steel bars including the steel tension bars, steel compression bars and the stirrups were modelled as an elastic-perfectly plastic material.

In the present study, the normal stiffness between steel bars and concrete was simply assumed to be infinite (i.e. relative displacements in the normal direction are not allowed between steel bars and concrete). The shear bond behaviour between steel bars and concrete was represented using the bond-slip model of CEB-FIP (1993), as shown in Eq. 3.9.

$$\tau^s = \begin{cases} \tau^s_{\max}\left(\dfrac{s}{s_1}\right)^{\varphi} & for \;\; s \le s_1 \\ \tau^s_{\max} & for \;\; s_1 < s \le s_2 \\ \tau^s_{\max} - (\tau^s_{\max} - \tau^s_f)\dfrac{s - s_2}{s_3 - s_2} & for \;\; s_2 < s \le s_3 \\ \tau^s_f & for \;\; s > s_3 \end{cases} \tag{3.9}$$

where τ^s (*MPa*) is the local shear bond stress; s (*mm*) is the slip; φ =0.4 for deformed steel bars and 0.5 for plain steel bars; $s_1 = s_2 = 0.6$ mm and $s_3 = 1.0$ mm for deformed steel bars; $s_1 = s_2 = s_3 = 0.1$ mm for plain steel bars; $\tau^s_{\max} = 2\sqrt{f_{ck}}$ (*MPa*) and $\tau^s_f = 0.5\tau^s_{max}$ (*MPa*) for deformed steel bars; and $\tau^s_f = \tau^s_{max} = 0.3\sqrt{f_{ck}}$ (*MPa*) for plain steel bars.

3.2.4 Dynamic analysis approach

Following Chen et al. (2015), the dynamic analysis approach (i.e., the explicit central difference method available in ABAQUS) instead of the static analysis approach (e.g., the Newton-Raphson method and the arc-length method) was employed in the present study, in order to overcome the severe numerical convergence difficulties commonly encountered in the modelling of cracked concrete using static analysis approaches (e.g. Zheng et al. 2012; Chen et al. 2015). As has been shown in Chen et al. (2015), such convergence difficulties are mainly caused by the severe nonlinearities due to strain softening phenomena associated with concrete cracking. It should be noted that employing dynamic analysis approaches to solve static/quasi-static structural problems is not a new thing, but significant uncertainties existed in the use of the dynamic approach to achieve an efficient and reliable solution to an overall static structural problem involving concrete cracking-induced local dynamic effects before a recent study (Chen et al. 2015) of Prof. Teng's group. Chen et al. (2015) carried out a thorough review of the existing dynamic analysis approaches used to solve static/quasi-static structural problems and examined carefully the effectiveness of these approaches. Finally, an advanced dynamic approach was proposed by Prof. Teng's group to solve the static/quasi-static structural problems. This proposed dynamic approach, which has been proven to be capable of providing an accurate solution to the prediction of FRP debonding failure in FRP-strengthened RC beams, set a solid basis for the present study. As suggested by Chen et al. (2015), when the explicit central difference method is applied in the dynamic approach, key elements including the loading time and damping scheme should be carefully studied/chosen to achieve an accurate/reliable prediction, which is an important task of the present study.

3.3 CALIBRATION OF THE FE MODEL

In this section, the determination of parameters associated with the dynamic analysis approach, the elastic modulus of concrete and the exponent *n* in the shear retention factor model (Eq. 3.6) used in the brittle cracking model is discussed. Specimen CN-500×120 tested by Maaddawy and Ariss (2012) was selected as an example to calibrate the proposed FE model, because all needed details of the test were provided in the relevant paper.

3.3.1 Parameters in the dynamic analysis approach

In the present study, the explicit central difference method and displacement-controlled loading scheme were adopted to execute the dynamic approach, with the automatic mass scaling algorithm available in ABAQUS (2012) being deployed. The damping scheme and the loading time were determined through a paramedic study. In the parametric study, the exponent *n* in the shear retention factor model was chosen to be 5 and the secant modulus of concrete [half of the initial elastic modulus according to Ye (2005) and Pimanmas (2010)] was used in the brittle cracking model, as explained later.

3.3.1.1 Damping scheme

A vertical displacement of 12 mm was applied and the loading time was chosen to be 0.5 seconds which equals to $50T_1$, where T_1 is the period of the fundamental vibration mode of the beam (T_1=0.01 seconds from an eigenvalue analysis of the FE model). In the present study, the stiffness-proportional Rayleigh damping matrix C was used in the FE modelling, following the suggestion by Chen et al. (2015). Stiffness-proportional Rayleigh damping can be expressed as $C=\beta K$ (Clough and Penzien 1995), where K is the stiffness matrix and β is the damping factor to be defined in the FE model. Five values of the damping factor β were considered in the paramedic study, which were 0, 1×10^{-7}, 1×10^{-6}, 1×10^{-5} and 1×10^{-4}, respectively. The load-deflection curves, the kinetic energy history and the ratio between the kinetic energy and the internal energy are plotted in Fig. 3.2. As can be seen from Fig. 3.2, the damping factor of 1×10^{-5} gives the best prediction of the load-deflection curve (Fig. 3.2a), with the kinetic energy being kept in a relatively low range (Figs. 3.2b and c). The relatively large ratios between the kinetic energy and the internal energy at the beginning were because of the initial dynamic effect caused by applying the displacement versus the very small internal energy at the early loading stage. Other damping factors give either inaccurate predictions of the ultimate load or very high values of kinetic energy, as shown in Fig. 3.2. When the damping factor is relatively small (i.e., 0 and 1×10^{-7}), the dynamic effects cannot be quickly damped out. As a result, large fluctuations exist in the load-deflection curves, and the ultimate load is underestimated, which is probably because the inertia forces associated with the dynamic analysis caused the earlier failure of the beam. When the damping factor is relatively large (i.e., 1×10^{-4}), the ultimate load is significantly overestimated due to the existence of high damping forces which are proportional to damping ($C\dot{d}$, where $\dot{d}$ is velocity). The damping factor of 1×10^{-6} leads to slight overestimation of the ultimate load and a worse prediction of the load-deflection curve than the damping factor of 1×10^{-5}. In the later comparisons, therefore, the damping factor of 1×10^{-5} was adopted.

3.3.1.2 Loading time

Loading time determines the loading rate when a certain displacement is specified as the latter is defined as the ratio (d/t) of the applied maximum displacement (d) to the loading time (t). When the loading rate (d/t) is too high, the dynamic response of the beam cannot be ignored (i.e., the kinetic energy is relatively large) and thus the purpose of conducting a quasi-static analysis might not be achieved. On the other hand, it is not practical to significantly increase the loading time for a much lower loading rate, as a larger loading time will lead to a much heavier computing effort and much larger accumulated errors due to the explicit nature of the central difference method (Chen et al. 2015). Therefore, an optimized loading time, which not only minimizes the computing effort but also still ensures an overall static response of the beam, should be determined first. In the present study, five values of the loading time (t) were considered in the paramedic study, which were 200T_1 (i.e., 2 seconds), 100T_1 (i.e., 1 seconds), 50T_1 (i.e., 0.5 seconds), 25T_1 (i.e., 0.25 seconds) and 12.5T_1 (i.e., 0.125 seconds), respectively, where T_1 is the period of the fundamental vibration mode of the beam studied. The load-deflection curves, the kinetic energy values and the ratios between the kinetic energy and the internal energy are plotted in Fig. 3.3. As can be seen from Fig. 3.3a, the loading time of 50T_1 gives a quite acceptable prediction of the load-deflection curve which is very close to the prediction obtained with the loading time of 100T_1, while loading times of 25T_1 and 12.5T_1 result in large fluctuations in the load-deflection curve, which indicates that the dynamic response in the beam is very large (i.e. the obtained structural solution is not an essentially static response). The loading time of 200T_1 lead to an overestimation of the ultimate load and causes an unexpected drop of the load at a deflection of 3 mm, which may be due to the larger error accumulation of displacement than that of load caused by the central different method as explained in Chen (2010). It can be seen from Figs. 3.3b and c that the values of kinetic energy and the ratio between the kinetic energy and the internal energy decrease with the loading time (lower than 1%) even through that the ratio is quite large at the beginning of loading, which implies that the solution is essentially static except for the short initial loading stage. Therefore, the loading time of 50T_1 was adopted in the later comparisons.

3.3.1.3 Hourglass control

When reduced-integration elements are used in FE modelling, the hourglass phenomenon which leads to severe mesh distortion may exist. To avoid the hourglass phenomenon, hourglass control needs to be applied. Applying hourglass control will introduce an artificial strain energy to the analysis, and a commonly adopted criterion is that if the artificial strain energy caused by the hourglass control is within 5% of the internal energy during the whole analysis process, the analysis results can be deemed to be reliable. In ABAQUS (2012), three hourglass scaling factors (i.e., displacement hourglass scaling factor s^s, rotational hourglass scaling factor s^r and out-of-plane displacement hourglass scaling factor s^w) are available for hourglass control. The effect of the hourglass scaling factors on the analysis result was examined in a preliminary study not shown here and it was found that the default values of these three factors (i.e., 1) could offer quite acceptable predictions of the studied specimens. It should be noted that when the default values do not work well, a trial-and-error process should be performed to find proper values of the hourglass scaling factors, in order that the hourglass phenomenon can be well controlled and the requirement on the ratio of the artificial strain energy to the internal energy can also be met.

3.3.2 The elastic modulus of concrete

The behaviour of RC beams with a web opening is dominated by the tensile and shear behaviour of the concrete. In the brittle cracking model, before reaching the tensile strength (i.e., before initiation of cracking), the concrete is assumed to be linear elastic. However, the real tensile stress-strain relationship before reaching the tensile strength of concrete is not linear and the modulus (slope of stress-strain curve) of concrete is decreases continuously as the tensile stress goes up, as shown in Fig. 3.4 (Ye 2005). Therefore, using the initial elastic modulus [e.g. $E_0 = 4730\sqrt{f_c}$ according to ACI-318 (2014)] might not be reasonable anymore. For these reasons, both the secant modulus and the initial elastic modulus of concrete were used in the definition of the brittle cracking model in later studies for comparison purpose. The secant modulus is defined as the ratio between the maximum tensile stress and the corresponding tensile strain of concrete (i.e., $\sigma_{to}/\varepsilon_{to}$ shown in Fig. 3.4). In the present study, the secant modulus of concrete is assumed to be half of its initial elastic modulus, following Ye (2005) and Pimanmas (2010). It should be noted that for the brittle cracking model available in ABAQUS (2012), the elastic modulus of concrete in compression was automatically set to be same as that in tension.

3.3.3 Shear retention factor model of concrete

The shear retention factor of concrete is given by Eq. 3.6, in which the exponent *n* in the shear retention factor model governs the shape of the shear stress-strain relationship of cracked concrete. It is an exponent controlling the rate of shear degradation of cracked concrete: a larger value of *n* means a faster drop of the shear stress with the increase of the crack opening. To examine the effect of the exponent *n* on the predicted behaviour of cracked concrete, five values were considered in a paramedic study, which were 2, 3, 4, 5 and 6, respectively. The comparison between the test results and the predicted load-defection curves is plotted in Fig. 3.5. It can be seen from Fig. 3.5 that: (1) when the exponent *n* is equal to 2, 3 or 4, the ultimate load of the beam is overestimated to different extents with a smaller value of n giving a larger gap between the test result and the prediction; (2) when the exponent n is equal to 6, the predicted load-deflection curve has a lower stiffness than the test result; (3) when the exponent n is equal to 5, the predicted load-deflection curve agrees very well with the test result, in terms of the stiffness, the ultimate load and the corresponding deflection. Finally, the value of 5 is recommended for the exponent n in such modelling and was thus adopted in later studies.

3.4 RESULTS AND COMPARISON

3.4.1 Test database

A total of 16 RC beams with a rectangular web opening were collected from existing studies. These tests were chosen because sufficient geometric and material properties had been provided. Both the specimens tested by Mansur et al. (1999), in which the web opening was circular, and the specimens tested by Maaddawy and Sherif (2009), which were concerned with very deep beams, were not considered in the comparison as they are out of the scope of present study. Details of the collected specimens are given in Table 3.1 and Fig. 3.6. The details of the beam O-500×150 tested by Prof. Teng's group (Teng et al. 2013) are also shown in Fig. 3.6. In this thesis, for T-section beams, the concrete chord in the beam web is referred to as the web chord while the concrete chord containing the beam flange is referred to as the flange chord for brevity.

3.4.2 Load-deflection curves

In the FE analyses, the damping factor β was set to be 1×10^{-5}, the loading time was set to be $50T_1$, and the hourglass scaling factors were chosen to be the default values (i.e., 1), according to the findings described in the preceding section. The exponent n in the shear retention factor model (Eq. 3.6) was chosen to be 5 for the brittle cracking model based on the parametric study and also 5 for the concrete damaged plasticity model following Chen et al. (2012). In the comparison of load-deflection curves, three schemes were examined: (1) Scheme-1: the brittle cracking model, with the secant modulus of concrete recommended by Ye (2005) and Pimanmas (2010) being used, was employed to simulate cracked concrete (referred to as the ***BC model with SECANT modulus*** hereafter for simplicity); (2) Scheme-2: the brittle cracking model, with the initial elastic modulus of concrete given by Eq. 3.6 being used, was employed to simulate cracked concrete (referred to as the ***BC model with INITIAL modulus*** hereafter); and (3) Scheme-3: the concrete damaged plasticity model was adopted to simulate the behaviour of cracked concrete (referred to as the ***DP model*** hereafter). As the explicit central difference method available in ABAQUS instead of the static analysis approach (e.g., the Newton-Raphson method or the arc-length method) was employed in the present study, there was no convergence criterion in the three modelling schemes (BC model with SECANT or INITIAL modulus and DP model).

The load-deflection curves obtained from the above three schemes are compared with the test results in Fig. 3.7. It can be seen from Fig. 3.7 that for specimens tested by Maaddawy and Ariss (2012), Madkour (2009), Suresh and Prabhavathy

(2015), Allam (2005), Chin et al. (2012) and Teng et al. (2013), the brittle cracking model with SECANT modulus gives the most accurate predictions of the load-deflection curves in terms of both the predicted ultimate load and stiffness. The brittle cracking model with INITIAL modulus consistently overestimates the ultimate load as well as the stiffness of the beam, while the DP model either significantly overestimates or underestimates the ultimate load and significantly overestimates the stiffness for most specimens. For the three specimens tested by Abdalla et al. (2003), however, all three models greatly overestimate the ultimate load of the beam. The brittle cracking model with SECANT modulus gives the closest ultimate loads to the test values for two (i.e., UO7 and UO8) of the three specimens while the DP model gives the closest ultimate load for the remaining one (i.e., UO9) of the three specimens. The stiffness of the beam obtained from the brittle cracking model with SECANT modulus agrees very well with the test result while those obtained from other two models consistently overestimate the test results. Such big difference of the ultimate loads between the prediction and test for the specimens tested by Abdalla et al. (2003) cannot be well explained with the information currently available to the candidate. However, considering that the brittle cracking model with SECANT modulus can provide quite accurate predictions to specimens from all the collected sources except for Abdalla et al. (2003), it is not unreasonable to suspect that the test data from Abdalla et al. (2003) may not be reliable.

A comparison of the ultimate loads between FE analyses and tests for all the collected specimens are given in Fig. 3.8 and Table 3.2. As can be seen from Fig. 3.8 and Table 3.2, which show that the brittle cracking model with SECANT modulus gives the closest predictions of the ultimate loads from tests, with an average prediction-to-test ratio of 1.09, a standard deviation (STD) of 0.155, and a coefficient of variation (CoV) of 0.142. The brittle cracking model with INITIAL modulus gives an average prediction-to-test ratio of 1.46, a STD of 0.173, and a CoV of 0.119. Although the CoV obtained from the brittle cracking model with INITIAL modulus is slightly better than that obtained from the brittle cracking model with SECANT modulus, it substantially overestimates the ultimate load with an error of around 50%. The DP model either significantly overestimates (for 7 specimens) or underestimates (for 9 specimens) the ultimate loads, leading to an average prediction-to-test ratio of 1.01. The scatter of the predictions, however, is very large, with a STD of 0.316, and a CoV of 0.314. The better performance of the brittle cracking model with SECANT modulus can also be evidenced by the much smaller scatter in its predictions of test results as shown in Fig. 3.8.

The better performance of the brittle cracking model with SECANT modulus over the concrete damaged plasticity model can be attributed to the following reasons: (1) the failure of RC beams with a web opening is governed by the tensile and shear behaviour of cracked concrete but not the compressive behaviour of concrete, due to the existence of web opening(s). Therefore, the assumed linear elastic behaviour of concrete in compression does not compromise the accuracy of the modelling; (2) the brittle cracking model is a type of orthogonal fixed smeared crack model while the concrete damaged plasticity model is similar to the rotating smeared crack model in terms of crack modelling. The orthogonal fixed smeared crack model assumes that once a crack forms at a material integration point, its direction will not change anymore, while the concrete damaged plasticity model can have a maximum of one active crack whose direction changes according to the direction of maximum tensile plastic strain. The orthogonal fixed smeared crack model is closer to the observations in tests and has a clearer physical meaning, and therefore is more suitable for the modelling of tension and shear-dominated behaviour of concrete; (3) the shear retention factor of cracked concrete, which is crucial for the accurate modelling of cracked concrete, can be defined directly as a function of concrete cracking strain in the brittle cracking model but can only be indirectly defined through the tensile damage variable in the concrete damaged plasticity model. In the present study, the tensile damage variable in the concrete damaged plasticity model was so defined that the shear retention factor model (i.e., Eq. 3.6) of cracked concrete can be achieved (i.e., not based on the cyclic tensile test of concrete), which may result in unexpected errors in the modelling of cracked concrete.

3.4.3 Failure process and failure mode

Specimen O-500×150 (T-section beam) tested by Prof. Teng's group (Teng et al. 2013) is selected as the example to demonstrate the initiation and propagation of cracks. The failure mode of the specimen is shown in Fig. 3.9a, while the predicted crack patterns (represented by the maximum principal cracking strain) at different load levels are shown in Figs. 3.9b-e. As can be seen from Figs. 3.9b-e, when the load reaches 121 kN, an inclined crack (around 45 degrees above the horizontal direction) occurs at the top-right corner of the web opening (i.e., the one closer to the loading point) (Fig. 3.9b). This prediction agrees well with the test observation in which the recorded load is 120 kN (as shown in Fig. 3.9a). When the load increases to 176 kN, a major flexural crack is formed at the mid-span of the beam (Fig. 3.9c), which also agrees well with the test observation as shown in Fig. 3.9a. As the load continues to increase to higher levels, small inclined cracks gradually happen near the top-left corner of the web opening and the existing cracks become larger, and at the same time, shear cracks gradually happen in the right shear span of the beam (i.e. the shear span without web opening). When the load reaches 370 kN, a large inclined crack is formed near the top-left corner of the web opening (Fig. 3.9d), agreeing well with the test observation in which the recorded load is 370 kN (Fig. 3.9a). When the load further increases to 545 kN, the failure of the beam is achieved. The inclined crack at the top-right corner of the web opening reaches the loading point (Fig. 3.9e). A comparison between Fig. 3.9e and Fig. 3.9a shows that the predicted crack pattern of the beam is very close to the observed cracking pattern in the test. The failure modes of the test specimen and the modelled specimen are both dominated by the inclined crack at the top-right corner of the web opening, which reaches the loading point.

The predicted crack patterns at failure of the other 15 collected specimens are plotted in Fig. 3.10. The test crack patterns at failure of 6 specimens (out of the 15 specimens) whose crack patterns are given in relevant publications are also shown in Fig. 3.10 for the purpose of comparison. It can be seen from Fig. 3.10, at failure of the specimen, substantial shear cracks are formed near the corners of the web opening. The predicted crack patterns also agree well with the observed cracking patterns in the tests.

3.5 CONCLUDING REMARKS

This chapter has presented an FE study of RC beams with a rectangular opening. A total of three numerical approaches, all utilizing the explicit central difference solution method available in ABAQUS (2012), have been examined. Parametric studies were first conducted to achieve a proper determination of parameters for the dynamic analysis approach as well as the shear-retention factor model in order to achieve accurate predictions for the quasi-static behaviour of RC beams with a rectangular opening under monotonic loading. In addition, the predictions based on respectively the initial elastic modulus of concrete given by ACI-318 (2014) and the secant elastic modulus of concrete recommended by Ye (2005) and Pimanmas (2010) were compared. Based on the results presented in this chapter, the following conclusions can be drawn:

1) The dynamic method used is efficient for obtaining the static structural responses of RC beams with a rectangular opening;
2) The approach employing the brittle cracking model with SECANT modulus of concrete gives the best predictions of load-deflection curves of collected tests. This approach is thus recommended for the modelling of RC beams with a rectangular web opening;
3) The approach employing the brittle cracking model with INITIAL modulus of concrete overestimates the ultimate load as well as the stiffness, indicating that the secant elastic modulus of concrete is more suitable for use in such modelling owing to the intrinsic nonlinear behavior of concrete in tension;

4) The approach employing the concrete damaged plasticity model is found to overestimate the stiffness and underestimate or overestimate the ultimate load, although this model has shown good performance in the modelling of RC beams without a web opening and strengthened in flexure with FRP. This indicates that the concrete damaged plasticity model might not be suitable for the modelling of RC structures whose failure is dominated by the tensile and shear behavior of concrete; and
5) The proposed approach employing the brittle cracking concrete model with SECANT modulus of concrete is a powerful and economical alternative to laboratory testing to gain a full understanding of the behaviour of RC beams with a web opening and can be used to generate numerical results for the development of a reliable strengthening method for such RC beams.

3.6 REFERENCES

ABAQUS (2012). *ABAQUS Analysis User's Manual (Version 6.12)*, Dassault Systems SIMULIA Corporation, Providence, Rhode Island, USA.

Abdalla, H.A., Torkey, A.M., Haggag, H.A. and Abu-Amira, A.F. (2003). "Design against cracking at openings in reinforced concrete beams strengthened with composite sheets", *Composite Structures*, 60(2), 197-204.

Allam, S. M. (2005). "Strengthening of RC beams with large openings in the shear zone", Alexandria Engineering Journal, 44(1), 59-78.

American Concrete Institute (ACI) (2014). *Building Code Requirements for Structural Concrete and Commentary*, ACI 318-14, Farmington Hills, MI.

Bazant, Z.P. and Oh, B.H. (1983). "Crack band theory for fracture of concrete", *Materials and Structures*, 16(3), 155-177.

CEB-FIP. (1993). *CEB-FIP Model Code 90*, Thomas Telford, London.

Chen, G.M. (2010). *Shear Behaviour and Strength of RC Beams Shear-Strengthened with Externally Bonded FRP Reinforcement*, Hong Kong (China): The Hong Kong Polytechnic University.

Chen, G.M., Teng, J.G. and Chen, J.F. (2011). "Finite element modeling of intermediate crack debonding in FRP-plated RC beams", *Journal of Composites for Construction*, ASCE, 15(3), 399-353.

Chen, G.M., Chen, J.F. and Teng, J.G. (2012). "On the finite element modelling of RC beams shear-strengthened with FRP", *Construction and Building Materials*, 32, 13-26.

Chen, G.M., Teng, J.G., Chen, J.F. and Xiao, Q.G. (2015). "Finite element modeling of debonding failures in FRP-strengthened RC beams: A dynamic approach", *Computers and Structures*, 158, 167-183.

Chen, W. F. (1982). *Plasticity in Reinforced Concrete*, McGraw-Hill, New York.

Chin, S.C., Shafiq, N. and Nuruddin, M.F. (2012). "Strengthening of RC beams with large openings in shear by CFRP laminates: experiment and 2D nonlinear finite element analysis", *Research Journal of Applied Sciences Engineering and Technology*, 4(9), 1172-1180.

Clough, R. W. and Penzien, J. (1995). *Dynamics of Structures*, Computers & Structures, Inc.

Hordijk, D.A. (1991). *Local Approach to Fatigue of Concrete*, PhD thesis, Delft University of Technology.

Maaddawy, T. and Sherif, S. (2009). "FRP composite for shear strengthening of reinforced concrete deep beams with openings", *Composite Structures*, 89(1), 60-69.

Maaddawy, T. and El-Ariss, B. (2012). "Behavior of concrete beams with short shear span and web opening strengthened in shear with CFRP composites", *Journal of Composites for Construction*, ASCE, 16(1), 47-59.

Madkour, H. (2009). "Non-linear analysis of strengthened RC beams with web openings", *Proceedings of the Institution of Civil Engineers-Structures and Buildings*, 162(2), 115-128.

Mansur, M.A., Tan K.H. and Wei, W. (1999). "Effects of creating an opening in existing beams", *ACI Structural Journal*, 96(6), 899-906.

Rots, J. G. (1988). *Computational Modeling of Concrete Fracture*, Ph.D. thesis, Delft University of Technology.

Saenz, L. P. (1964). "Discussion of 'Equation for the stress-strain curve of concrete' by P. Desayi and S. Krishan", *ACI Journal*, 61(9), 1229-1235.

Suresh, J. and Prabhavathy, R. A. (2015). "Behaviour of steel fibre reinforced concrete beams with duct openings strengthened by steel plates", *International Journal of Advanced Information in Arts, Science & Management*, 4(4).

Ye, L.P. (2005). *Concrete Structures (Second Edition)*, Tsinghua University Press, Beijing, China (in Chinese).

Zheng, Y., Robinson, D., Taylor, S. and Cleland, D. (2012). "Non-linear finite-element analysis of punching capacities of steel-concrete bridge deck slabs", *Proceedings of the Institution of Civil Engineers-Structures and Buildings*, 165(5), 255-69.

Table 3.1. Geometry and material properties of existing RC test beams with a web opening

Source	Specimen	Shape of cross section	Beam dimensions			Opening size		Cylinder compressive strength of concrete f_c' (MPa)	Steel reinforcement						
			Span (mm)	Width (mm)	Height (mm)	Width (mm)	Height (mm)		Tension steel bars	Yield strength of tension bars f_{yt} (MPa)	Compression steel bars	Yield strength of compression bars f_{yc} (MPa)	Stirrups	Yield strength of stirrups f_{vy} (MPa)	Elastic modulus of all steel bars E_s[c] (GPa)
Maaddawy and Ariss (2012)	CN-200×200	Rectangular	2400	85	400	200	200	20	4Φ16 (deformed, and placed in two rows)	520	2Φ12 (deformed)	520	Φ6@80 (plain)	300	200
	CN-350×200		2400	85	400	350	200								
	CN-500×120		2400	85	400	500	120								
	CN-500×160		2400	85	400	500	160								
Madkour (2009)	E2	Rectangular	2700	140	280	600	80	20[a]	3Φ13 (deformed)	470	2Φ10 (deformed)	470	Φ6@130 (deformed)	470	200
	E3		2700	140	280	600	100								
	E4		2700	140	280	600	120								
	E5		2700	140	280	600	140								
Suresh and Prabhavathy (2015)	NS250	Rectangular	2200	150	300	250	150	20	3Φ12 (deformed)	415	2Φ10 (deformed)	415	Φ8@200 (deformed)	415	200
	NS300		2200	150	300	300	150								
Chin et al. (2012)	B3	Rectangular	1800	120	300	210	210	35	2Φ12 (deformed)	410	2Φ10 (deformed)	410	Y6@300 (plain)	275	200
Abdalla et al. (2003)	UO7	Rectangular	2000	100	250	100	100	34.4[a]	4Φ10 (deformed, and placed in two rows)	400	2Φ10 (deformed)	400	Φ8@150 (deformed)	240	200
	UO8		2000	100	250	200	100	39.2[a]							
	UO9		2000	100	250	300	100	41.6[a]							
Allam (2005)	B2	Rectangular	3200	150	400	450	150	28[a]	3Φ16 (deformed)	400	2Φ12 (deformed)	380	Φ8@150 (plain)	250	200
Teng et al. (2013)	O-500×150	T-section	3300	250[b]	500	500	150	33.2	4Φ20 (deformed)	482	3Φ20 (deformed)	482	Φ8@100 (plain)	375	200

Note:

(a) Calculated using $f_c^{'} = 0.8 f_{cu}$ when only f_{cu} is given in the paper, where f_{cu} is the concrete cube compressive strength;

(b) Web width (Specimen O-500×150 is a reversed T-section beam whose flange is 100 mm in height and 1450 mm in width);

(c) E_s is assumed to be 200 GPa as test data are not available in the relevant publications.

Table 3.2. Test and predicted ultimate loads

Source	Specimen	Test result (kN)	BC model with SECANT modulus (kN)		BC model with INITIAL modulus (kN)		DP model (kN)	
			Prediction	Prediction / test	Prediction	Prediction / test	Prediction	Prediction / test
Maaddawy and Ariss (2012)	CN-200×200	21	22.1	1.05	31.7	1.51	30.1	1.43
	CN-350×200	23	21.3	0.925	38.6	1.68	23.9	1.04
	CN-500×120	43	43.3	1.01	63.4	1.47	32.4	0.754
	CN-500×160	41	32.3	0.787	50.8	1.24	25.9	0.632
Madkour (2009)	E2	39	42.9	1.10	54.2	1.39	26.1	0.669
	E3	30	31.9	1.06	44.8	1.49	23.3	0.777
	E4	23	24.4	1.06	33.7	1.46	18.5	0.805
	E5	17	19.1	1.12	23.7	1.39	15.1	0.888
Suresh and Prabhavathy (2015)	NS250	49	48.7	0.994	65.5	1.34	37.5	0.766
	NS300	40	42.4	1.06	62.2	1.55	32.7	0.817
Chin et al. (2012)	B3	20	22.1	1.10	31.9	1.60	21.6	1.08
Abdalla et al. (2003)	UO7	43	61.7	1.44	76.9	1.79	75.1	1.75
	UO8	49	67.3	1.37	76.4	1.56	70.4	1.44
	UO9	52	63.1	1.21	71.3	1.37	60.6	1.17
Allam (2005)	B2	105	117	1.11	148	1.41	122	1.16
Teng et al. (2013)	O-500×150	535	545	1.02	561	1.05	498	0.931
Statistical characteristics	**Average =**			1.09		1.46		1.01
	STD =			0.155		0.173		0.316
	CoV =			0.142		0.119		0.314

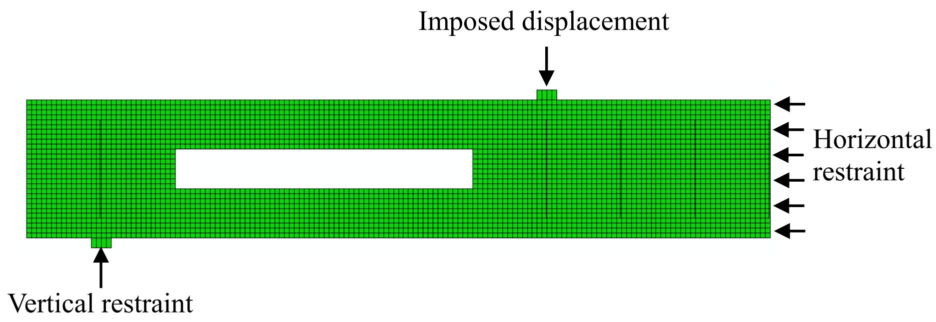

(a) Symmetrical beam

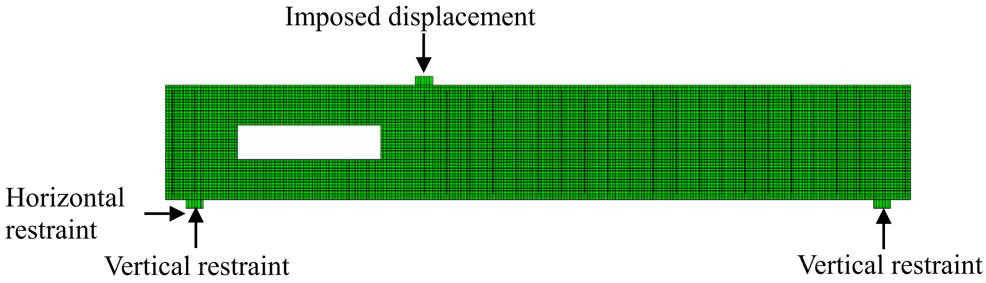

(b) Non-symmetric beam

Figure 3.1. Typical FE meshes

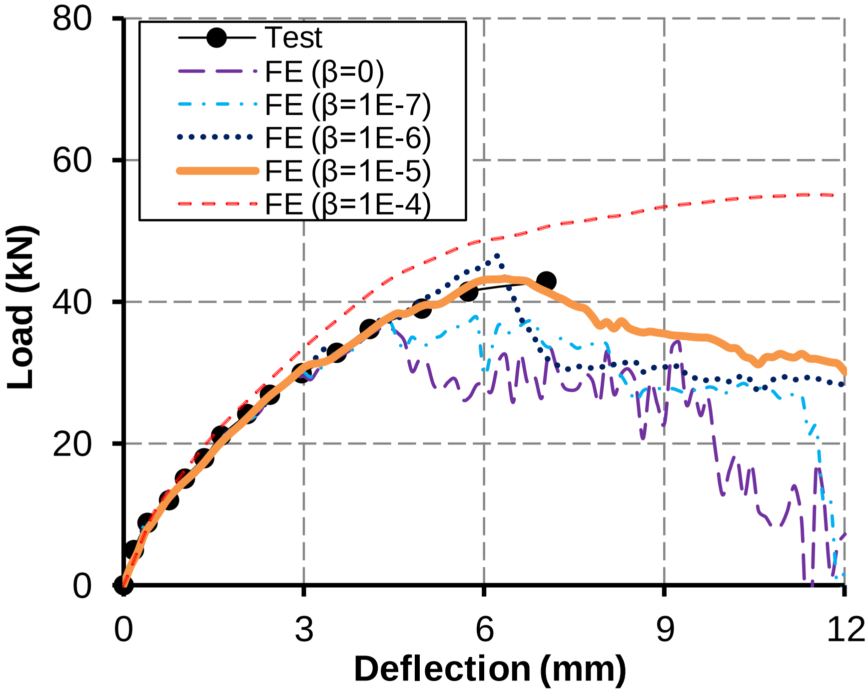

(a) Load-deflection curves

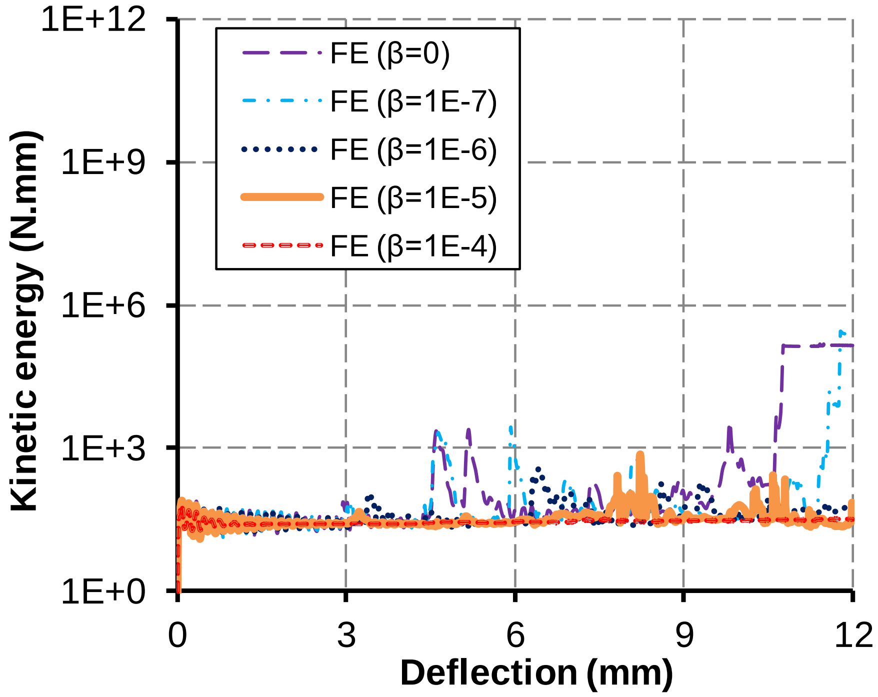

(b) Kinetic energy history

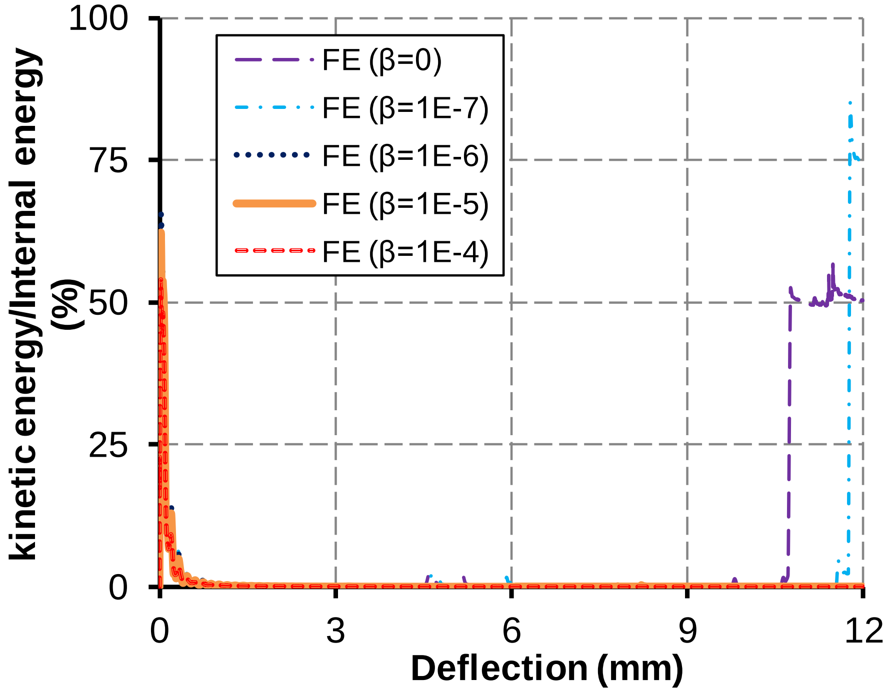

(c) Ratio between kinetic energy and internal energy

Figure 3.2. Effect of damping factor β on the FE prediction

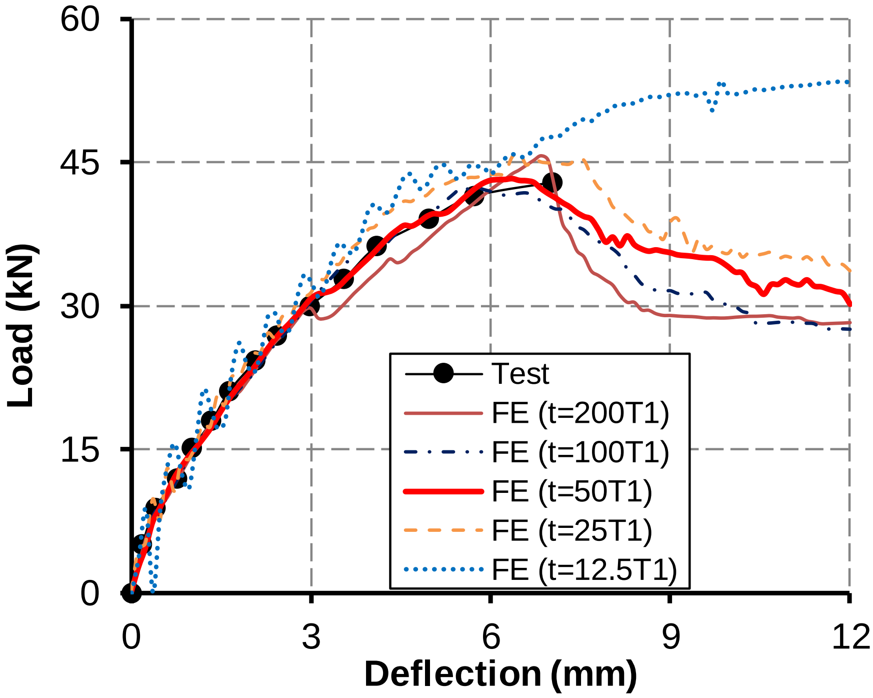

(a) Load-deflection curves

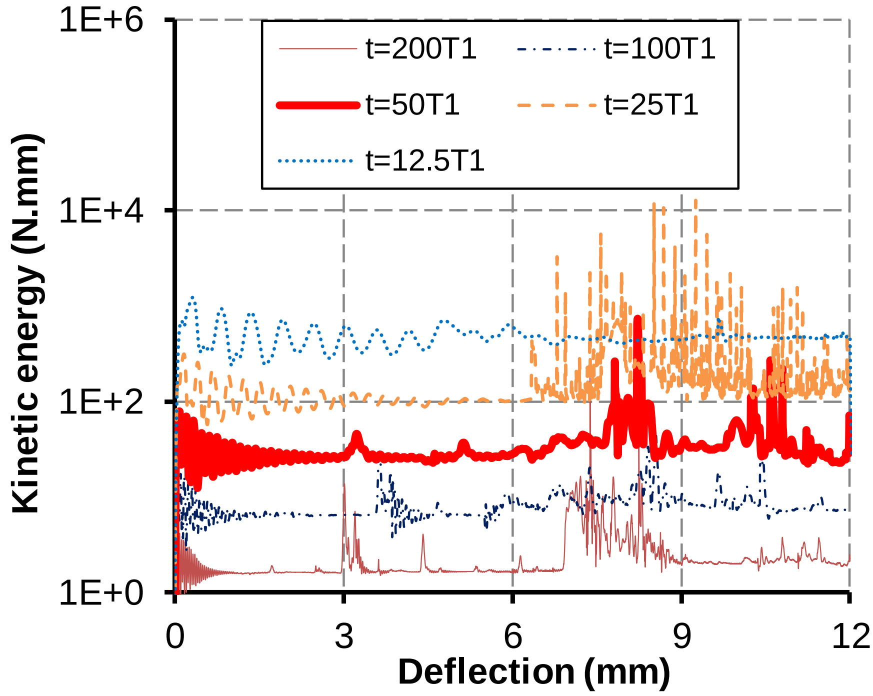

(b) Kinetic energy history

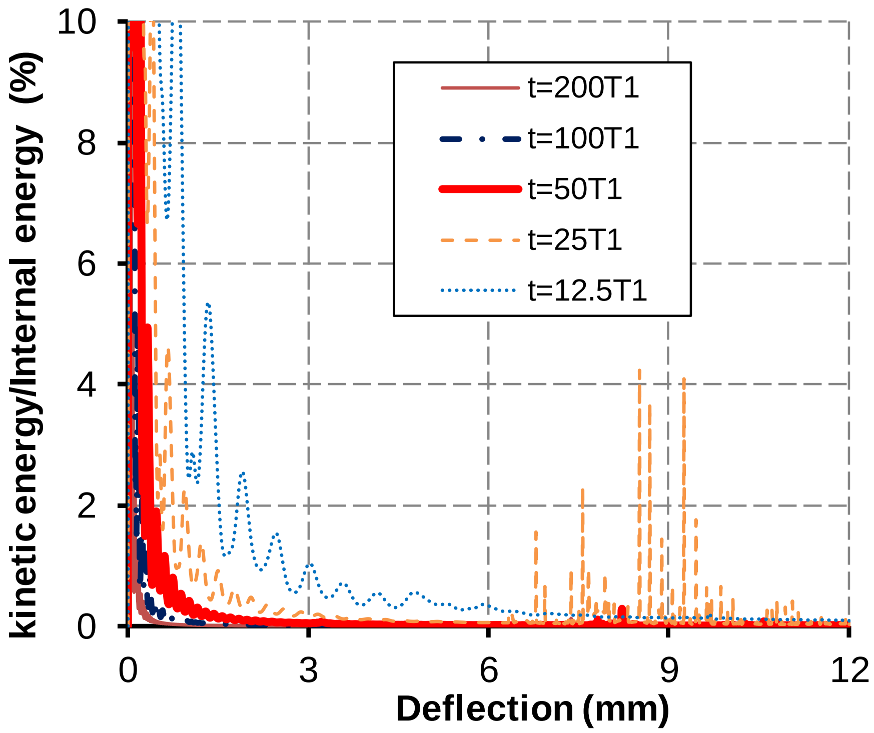

(c) Ratio between kinetic energy and internal energy

Figure 3.3. Effect of loading time on the FE prediction

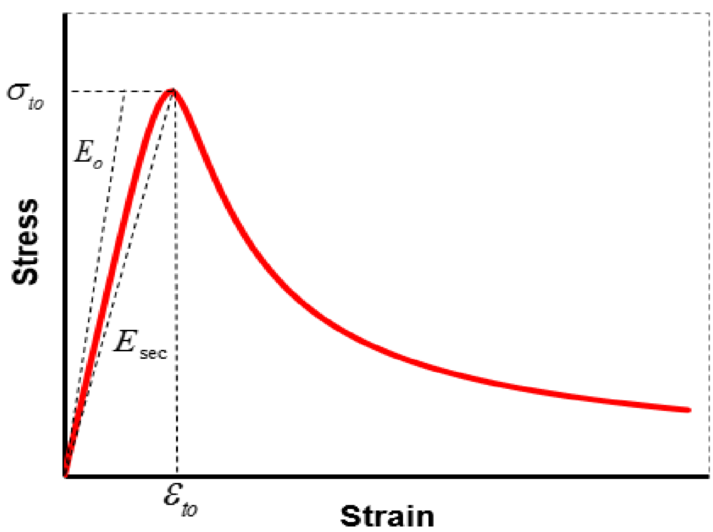

(Note: E_0=initial modulus; E_{sec}=secant modulus)

Figure 3.4. Tensile stress-strain curve of concrete

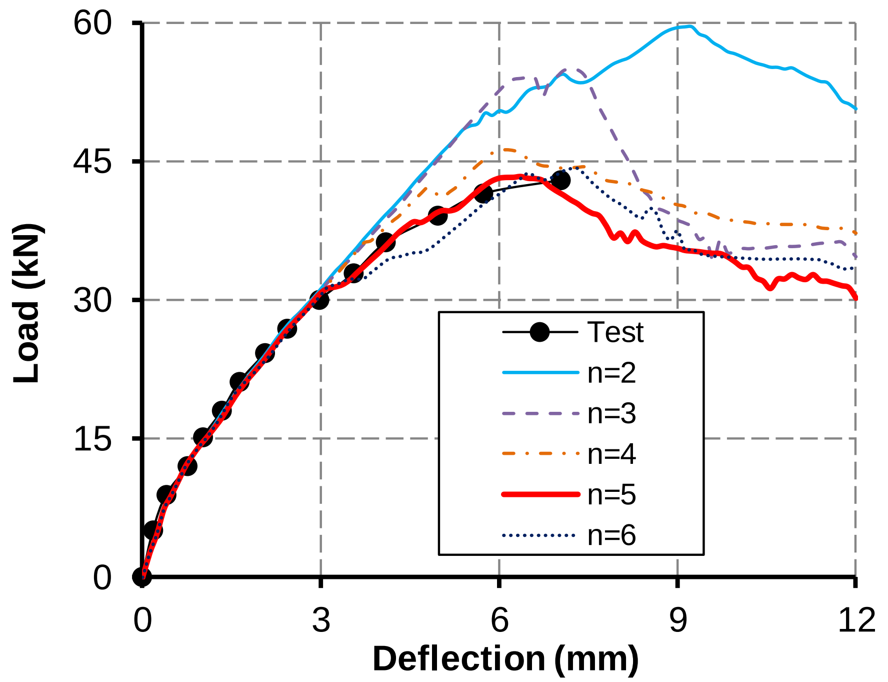

Figure 3.5. Effect of *n* in the shear retention factor model (Eq. 3.6) on the FE prediction

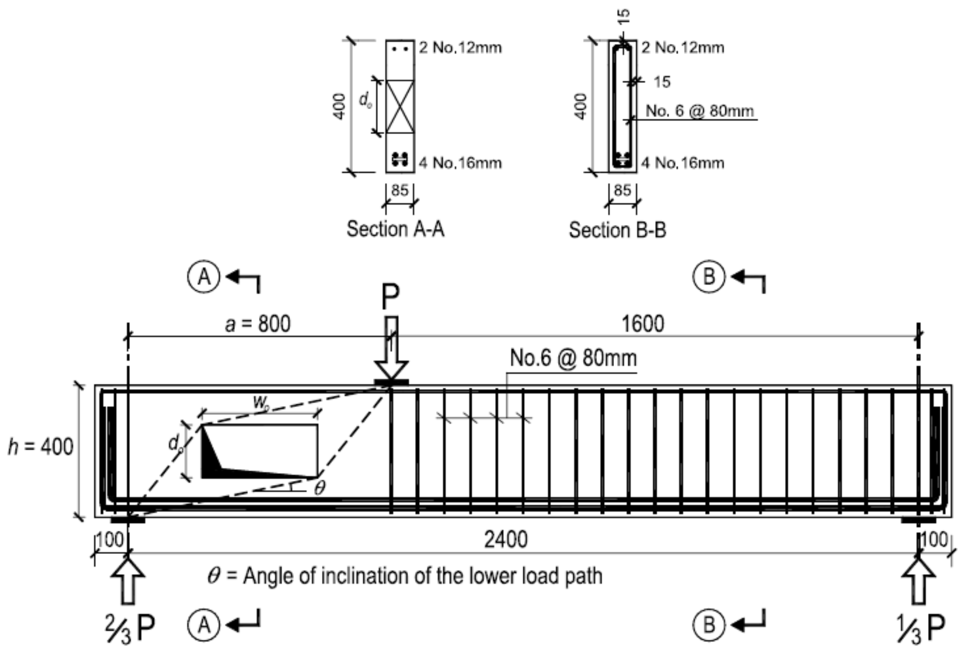

(a) Maaddawy and Ariss's (2012) specimens (extracted from Maaddawy and Ariss 2012)

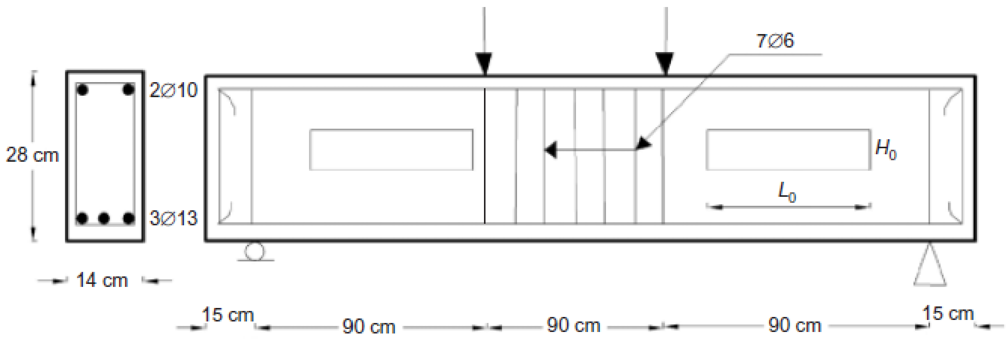

(b) Madkour's (2009) specimens (extracted from Madkour 2009)

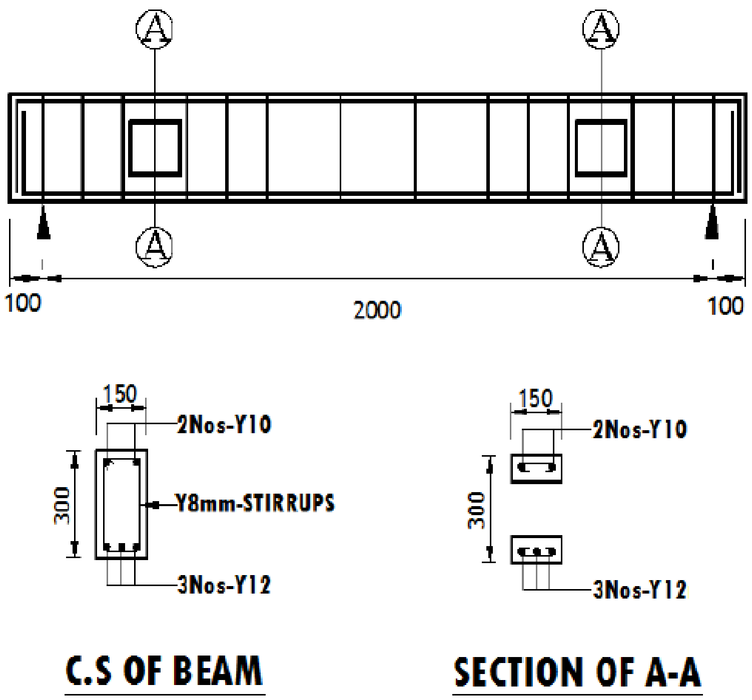

(c) Suresh and Prabhavathy's (2015) specimens (extracted from Suresh and Prabhavathy 2015)

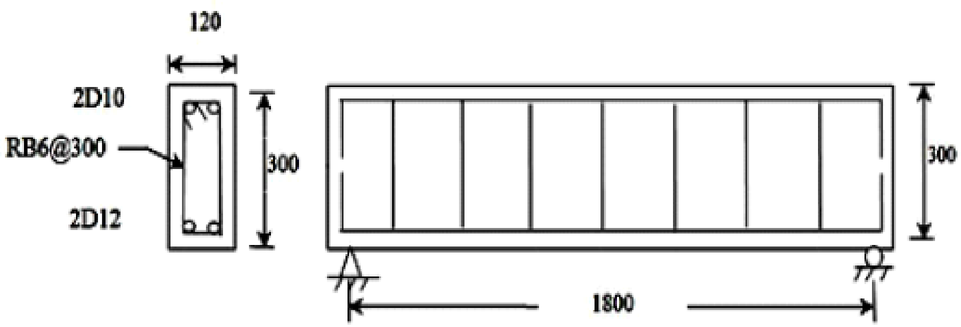

(d) Chin et al.'s (2012) specimens (extracted from Chin et al. 2012)

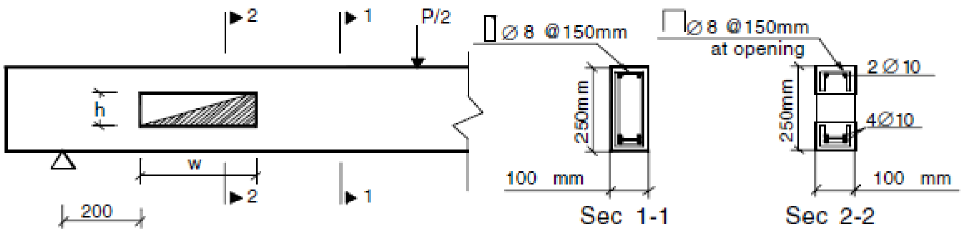

(e) Abdalla et al.'s (2003) specimens (extracted from Abdalla et al. 2003)

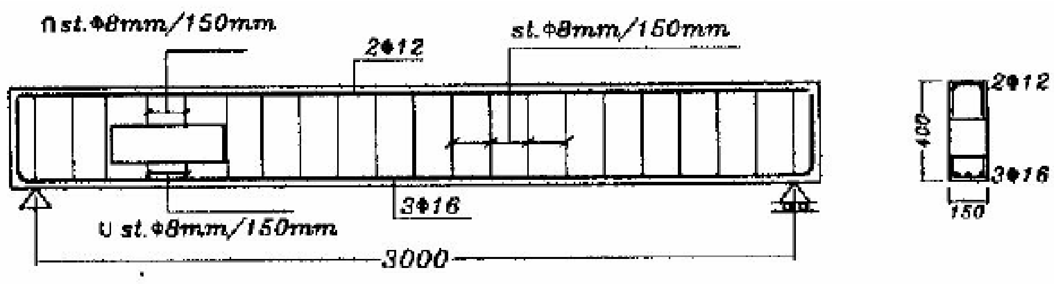

(f) Allam's (2005) specimens (extracted from Allam 2005)

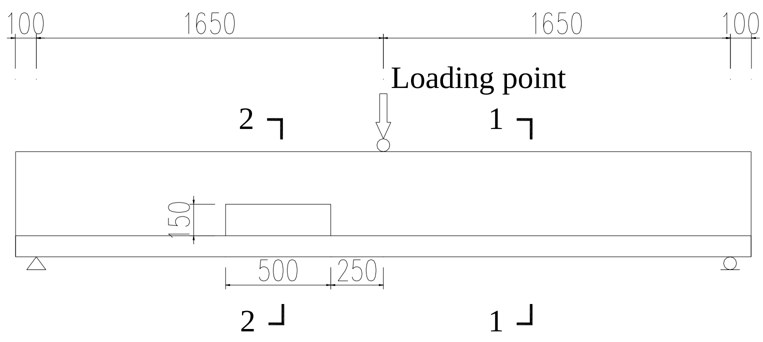

Elevation view of the beam

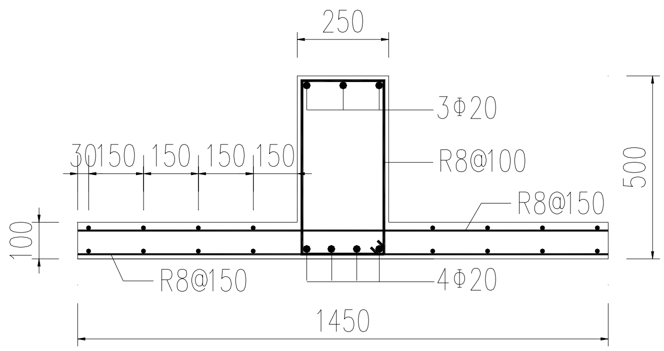

Section 1-1

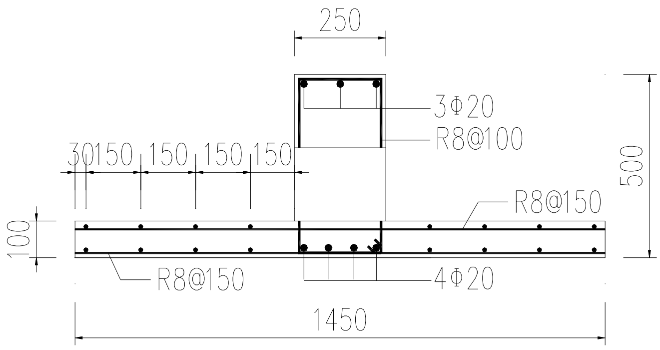

Section 2-2

(g) Teng et al.’s (2013) specimen (O-500×150) (Dimensions in mm)

Figure 3.6. Details of the collected specimens

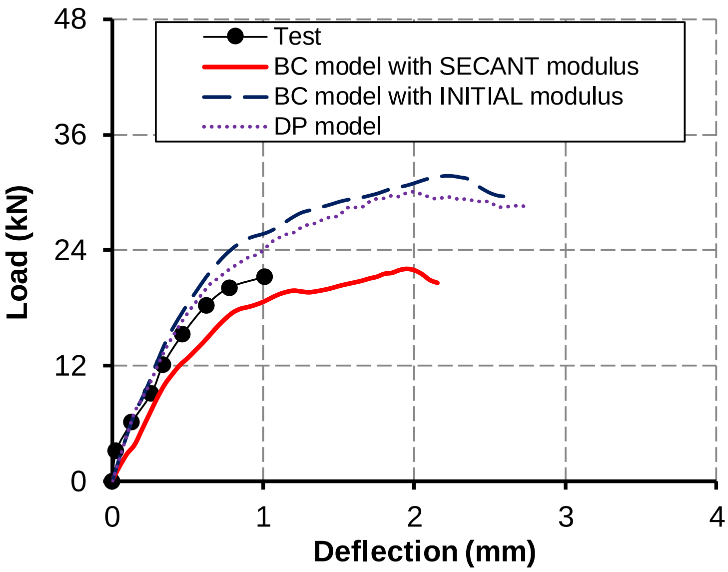

(a) CN-200×200 (Maaddawy and Ariss 2012)

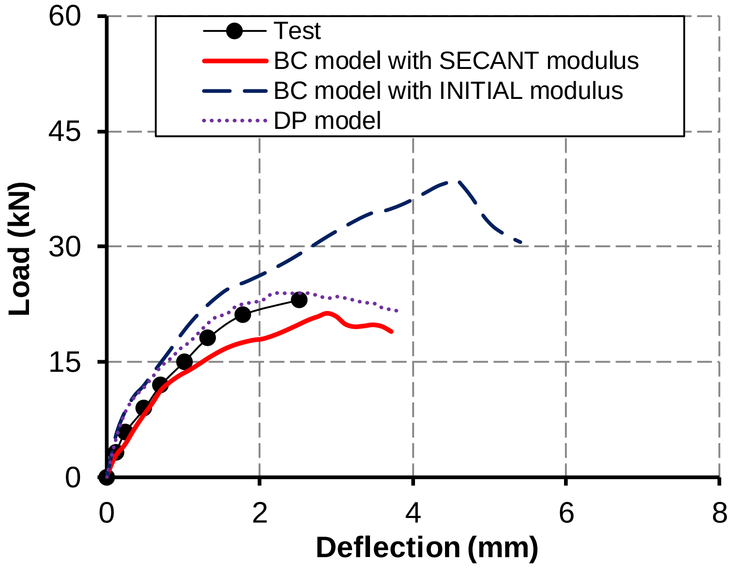

(b) CN-350×200(Maaddawy and Ariss 2012)

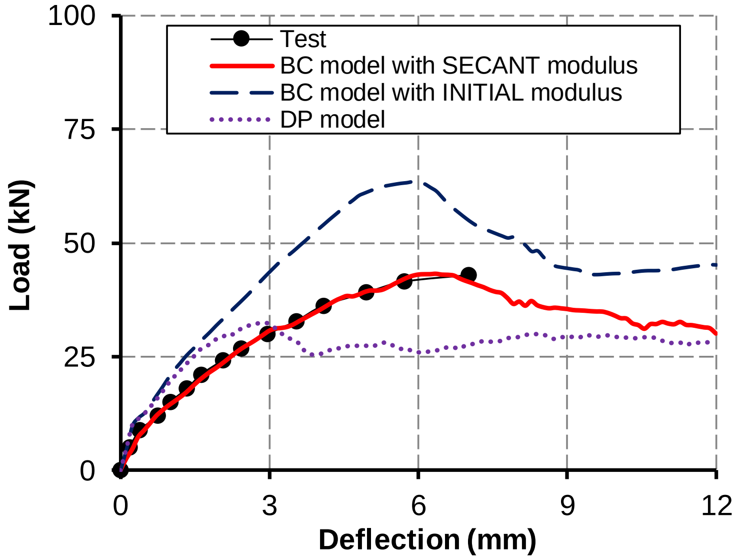

(c) CN-500×120 (Maaddawy and Ariss 2012)

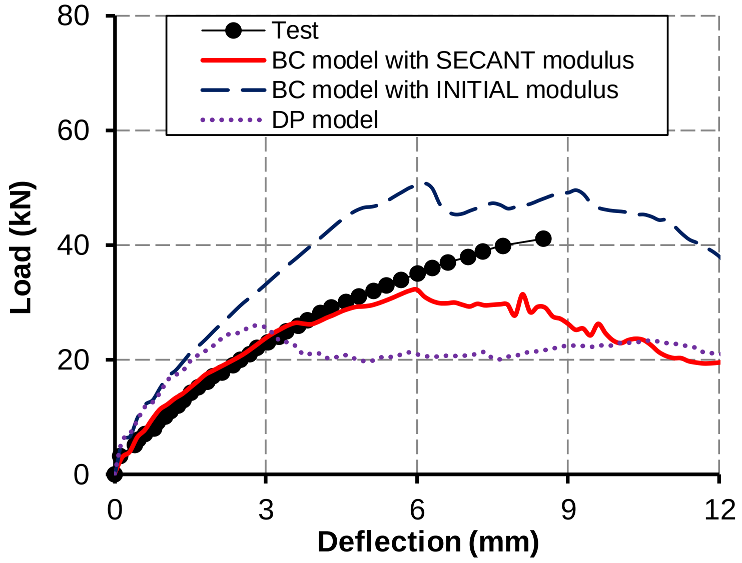

(d) CN-500×160 (Maaddawy and Ariss 2012)

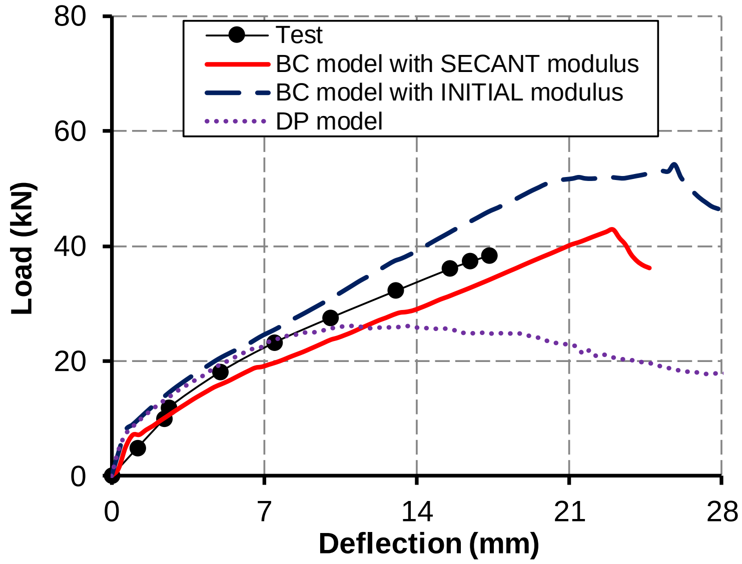

(e) E2 (600×80) (Madkour 2009)

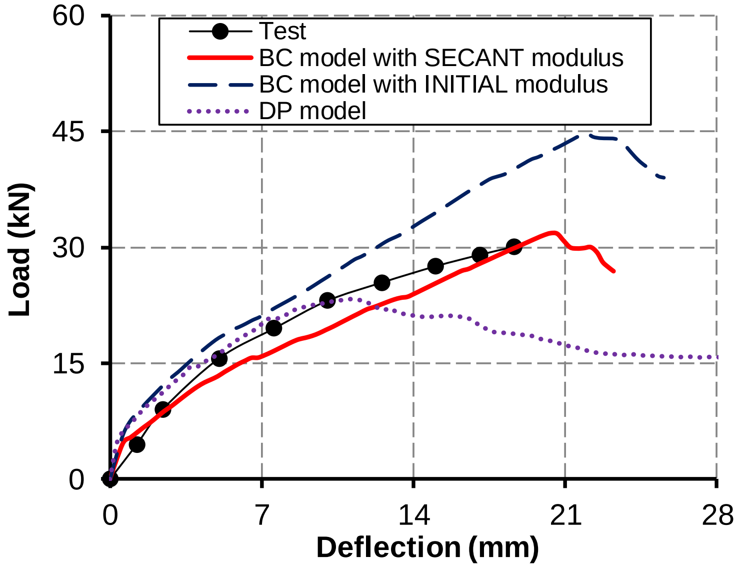

(f) E3 (600×100) (Madkour 2009)

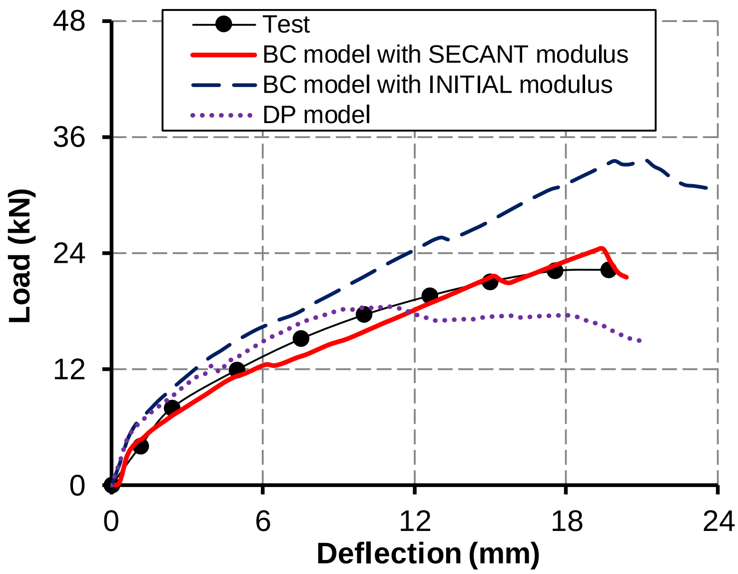

(g) E4 (600×120) (Madkour 2009)

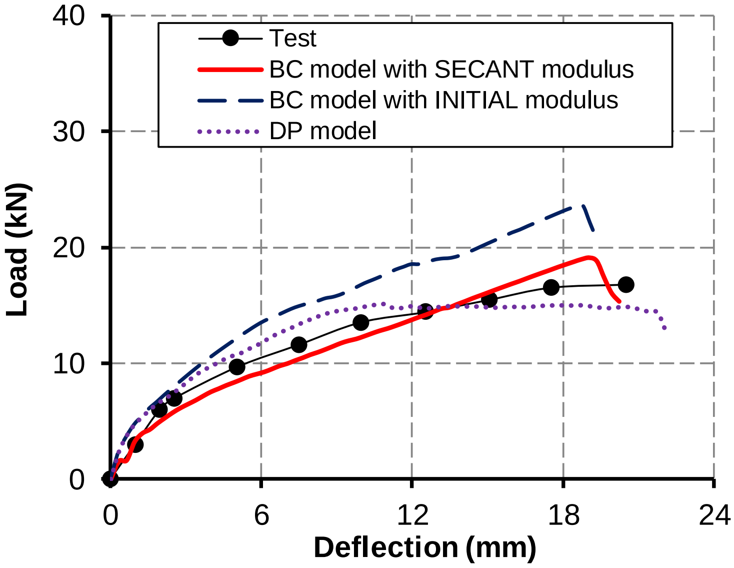

(h) E5 (600×140) (Madkour 2009)

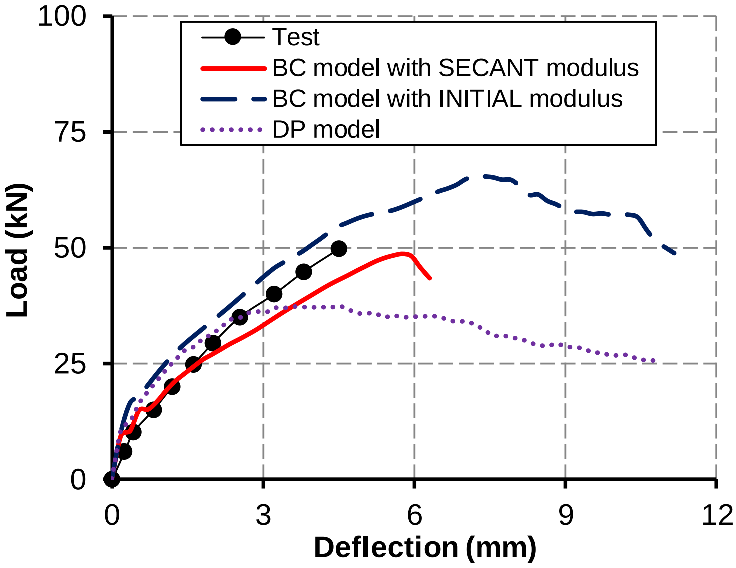

(i) NS250 (250×150) (Suresh and Prabhavathy 2015)

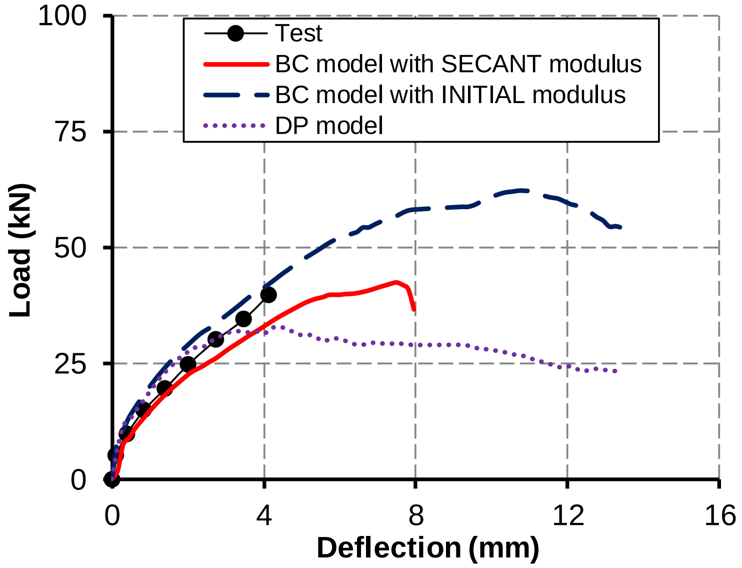

(j) NS300 (300×150) (Suresh and Prabhavathy 2015)

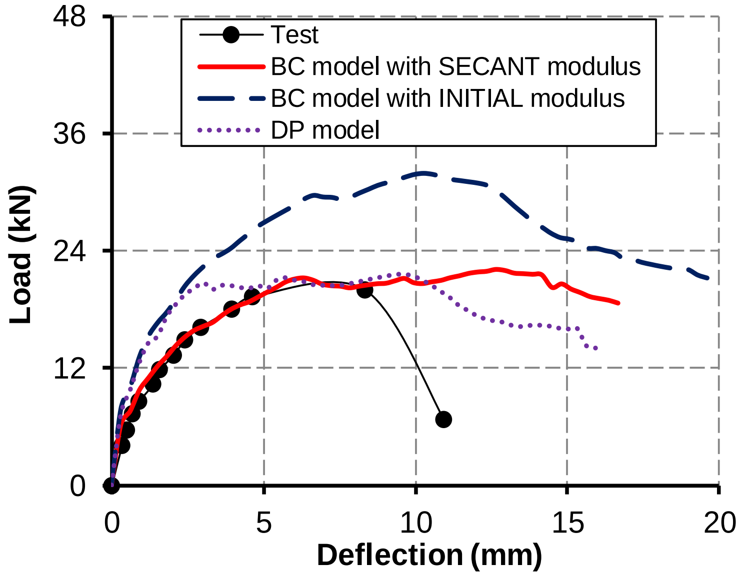

(k) B3 (210×210) (Chin et al. 2012)

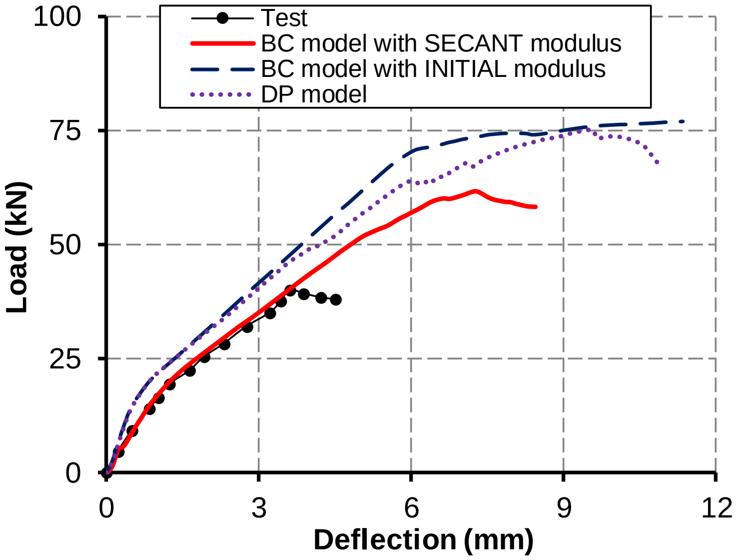

(l) UO7 (100×100) (Abdalla et al. 2003)

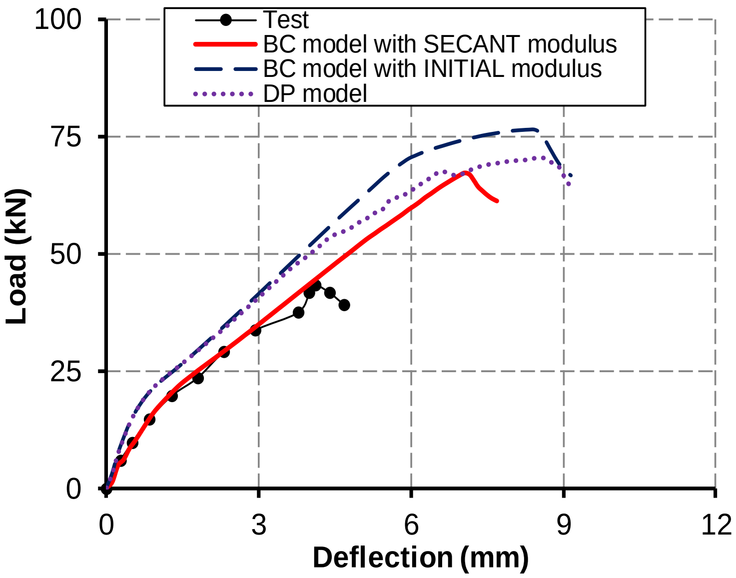

(m) UO8 (200×100) (Abdalla et al. 2003)

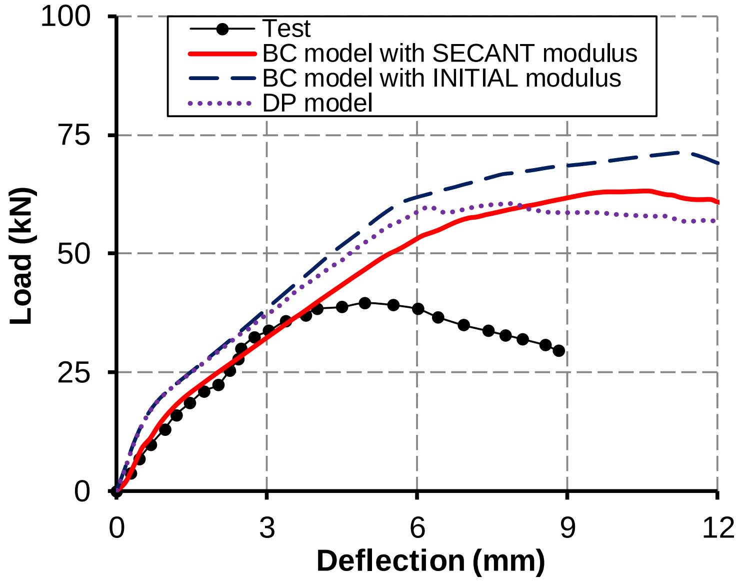

(n) UO9 (300×100) (Abdalla et al. 2003)

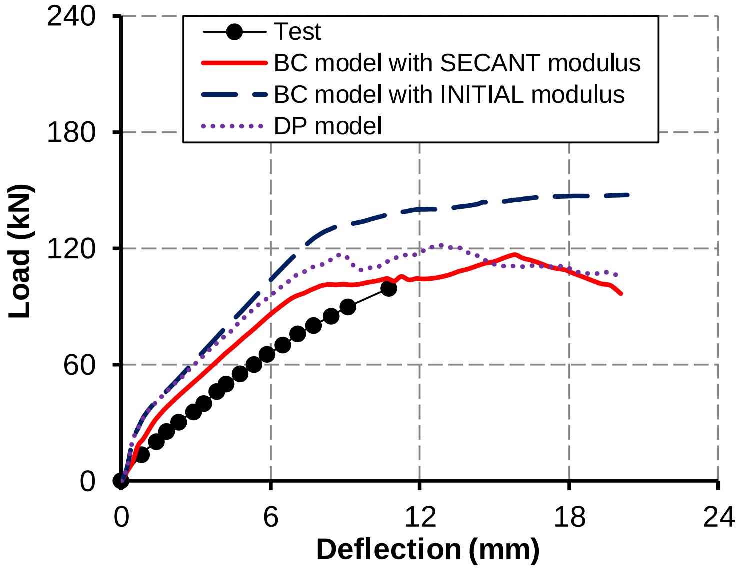

(o) B2 (450×150) (Allam 2005)

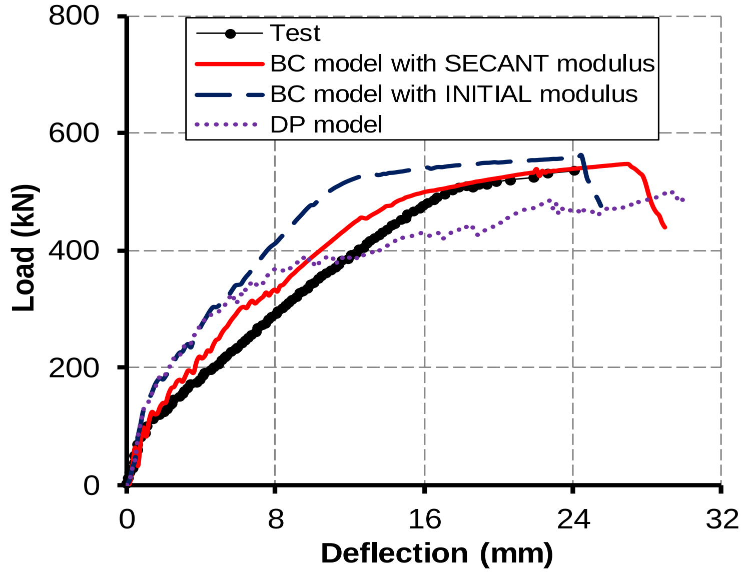

(p) O-500×150 (Teng et al. 2013)

Figure 3.7. Load-deflection curves

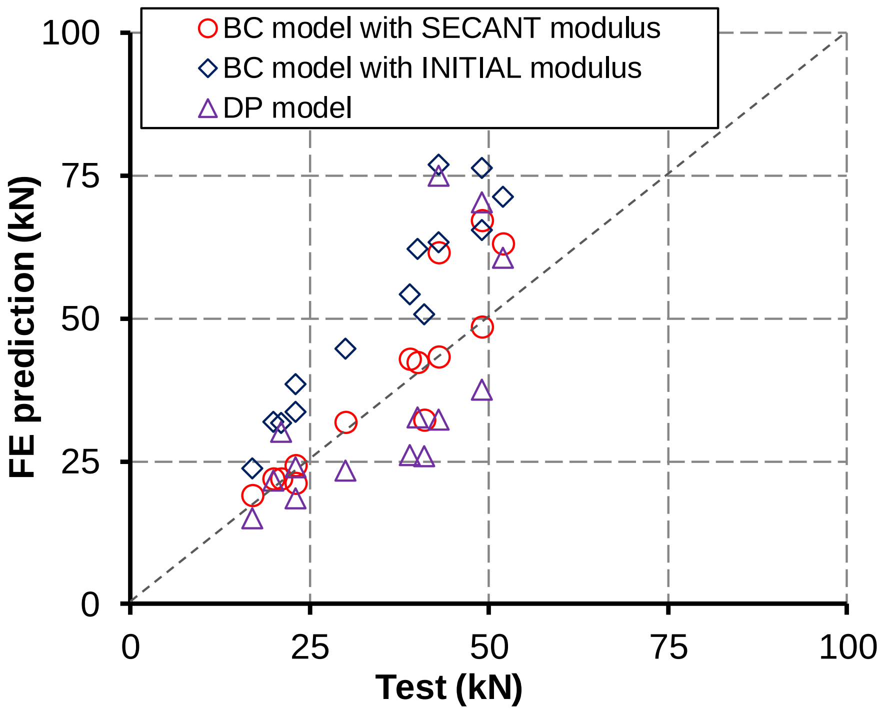

Figure 3.8. Comparison of ultimate loads between FE predictions and tests

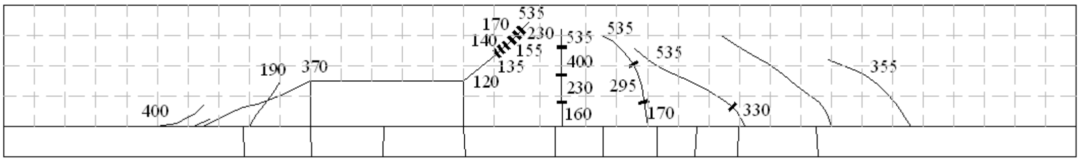

(a) Crack pattern (forces in kN)

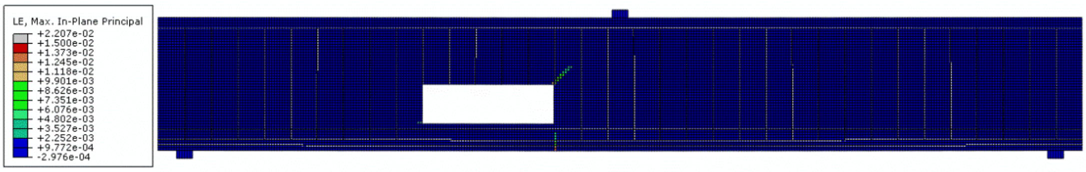

(b) FE prediction at 121 kN

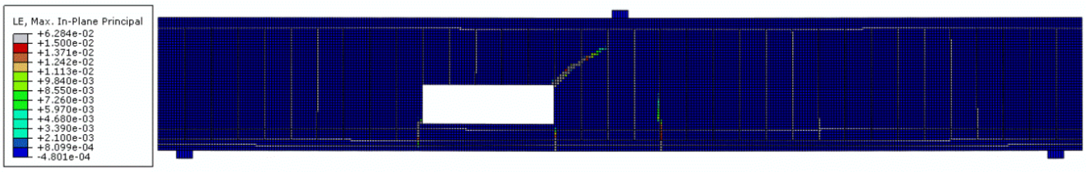

(c) FE prediction at 176 kN

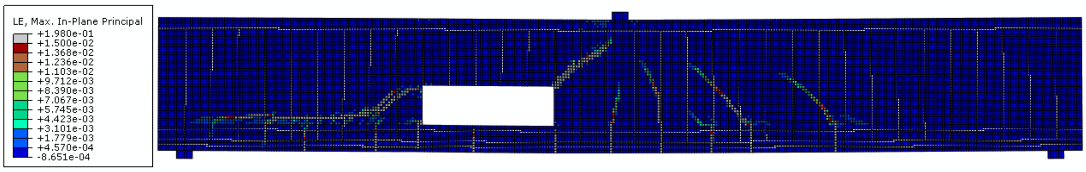

(d) FE prediction at 370 kN

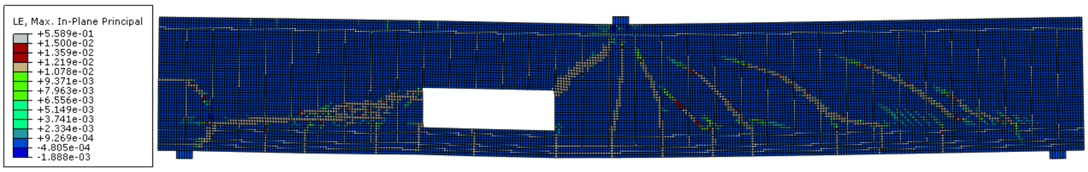

(e) FE prediction at 545 kN

Figure 3.9. Crack pattern at failure and predicted development of cracks of the specimen tested by Prof. Teng's group (Teng et al. 2013)

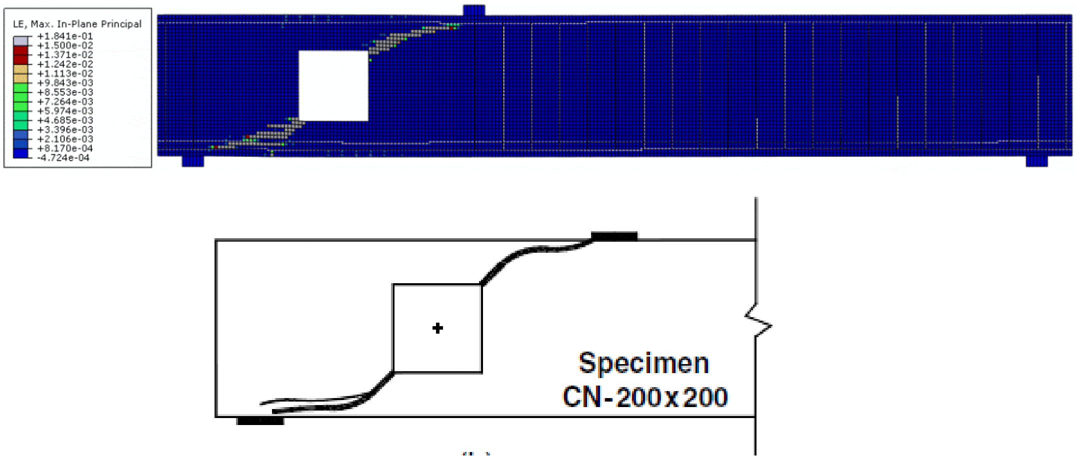

(Extracted from Maaddawy and Ariss 2012)

(a) CN-200×200

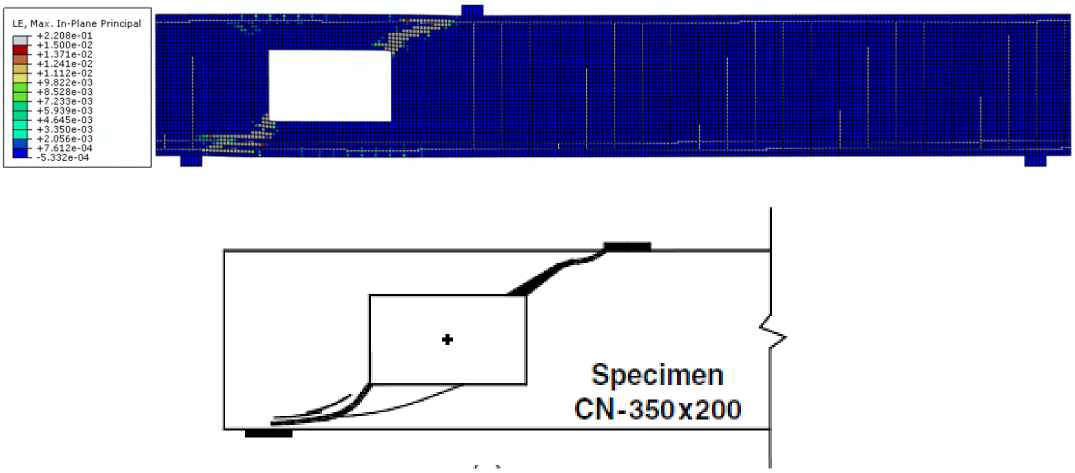

(Extracted from Maaddawy and Ariss 2012)

(b) CN-350×200

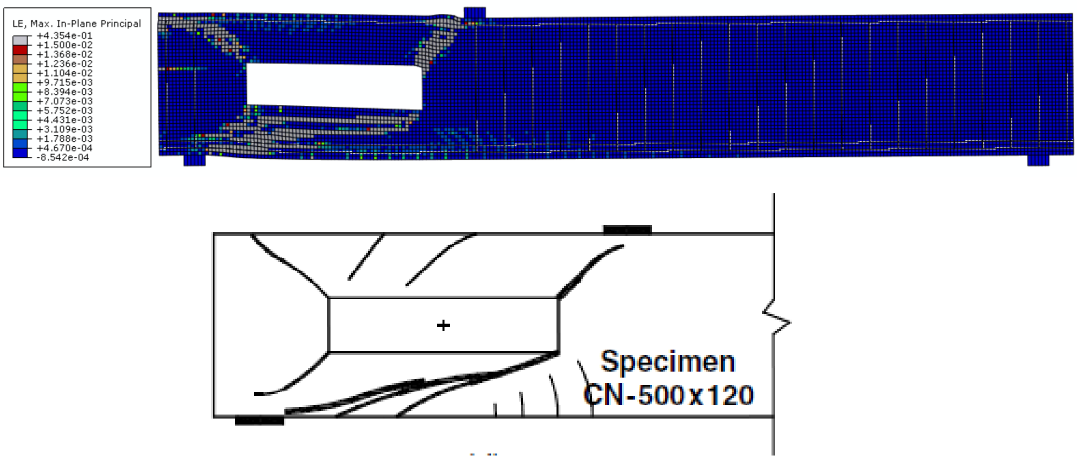

(Extracted from Maaddawy and Ariss 2012)

(c) CN-500×120

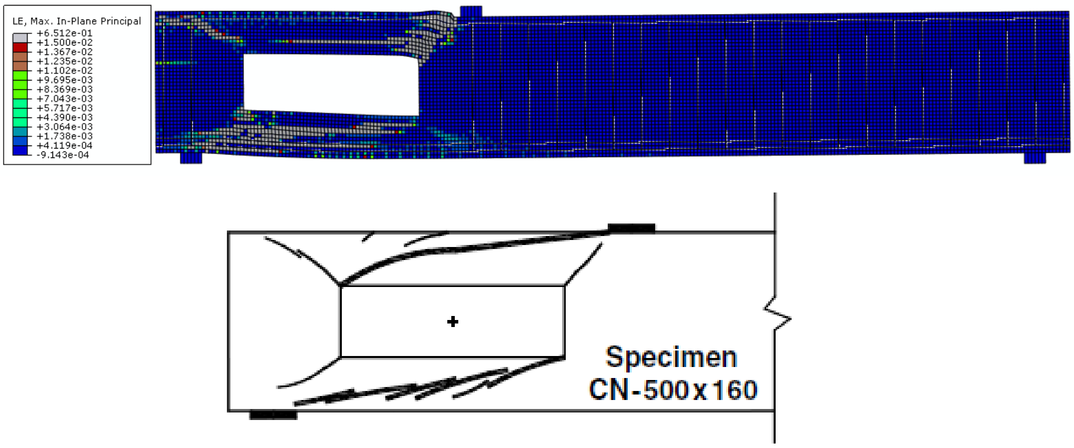

(Extracted from Maaddawy and Ariss 2012)

(d) CN-500×160

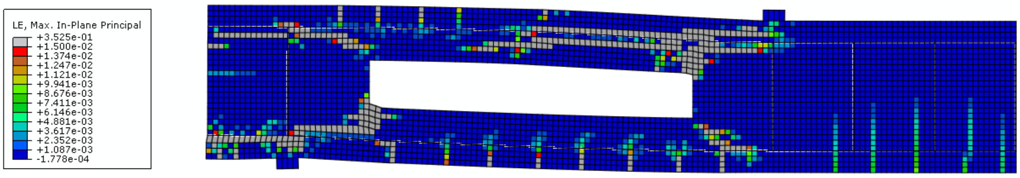

(e) E2 (600×80) (Madkour 2009)

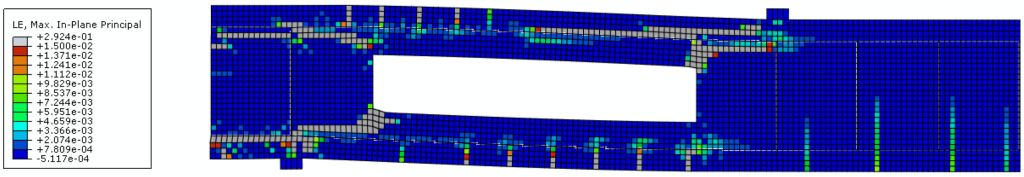

(f) E3 (600×100) (Madkour 2009)

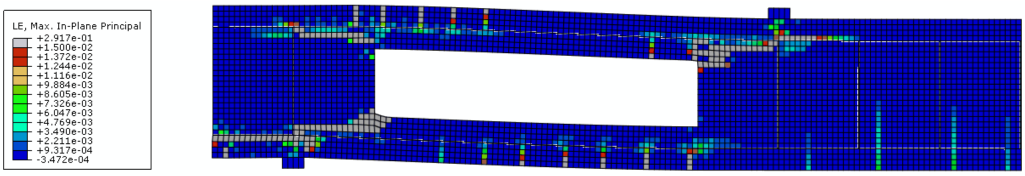

(g) E4 (600×120) (Madkour 2009)

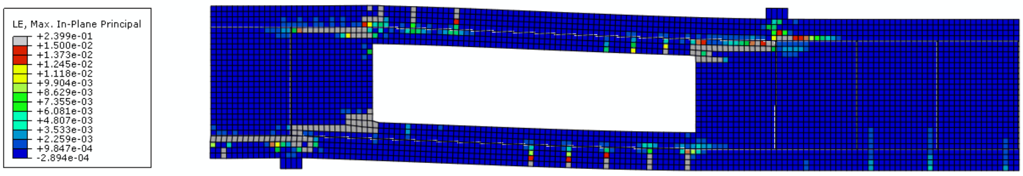

(h) E5 (600×140) (Madkour 2009)

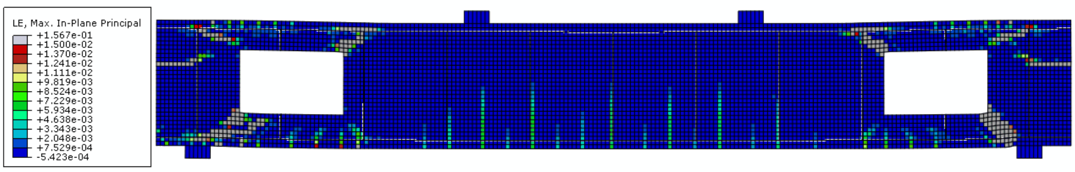

(i) NS250 (250×150) (Suresh and Prabhavathy 2015)

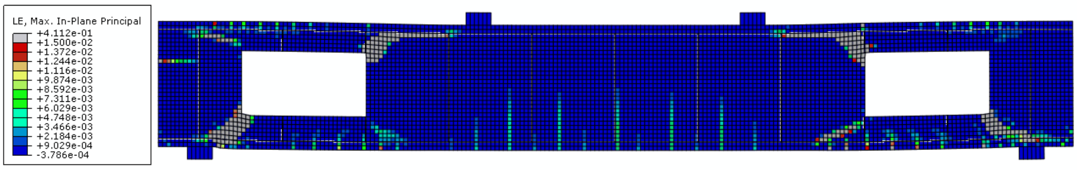

(j) NS300 (300×150) (Suresh and Prabhavathy 2015)

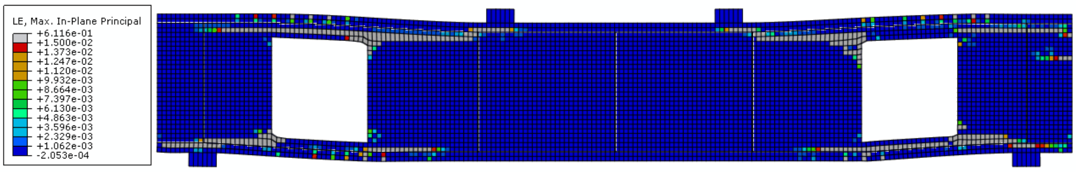

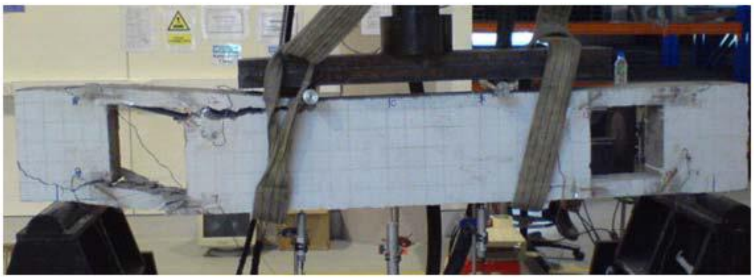

(Extracted from Chin et al. 2012)

(k) B3 (210×210)

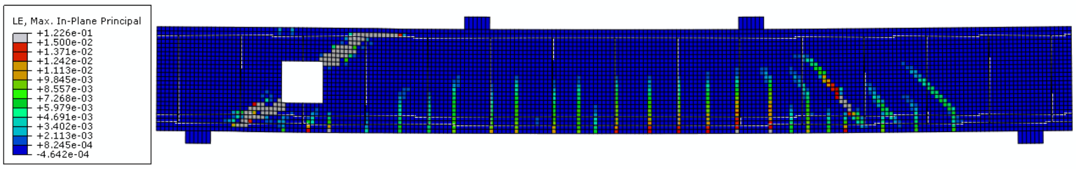

(l) UO7 (100×100) (Abdalla et al. 2003)

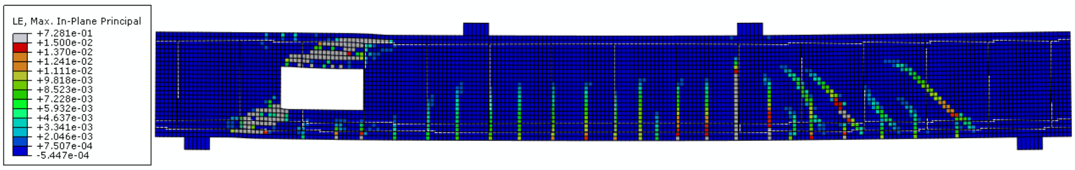

(m) UO8 (200×100) (Abdalla et al. 2003)

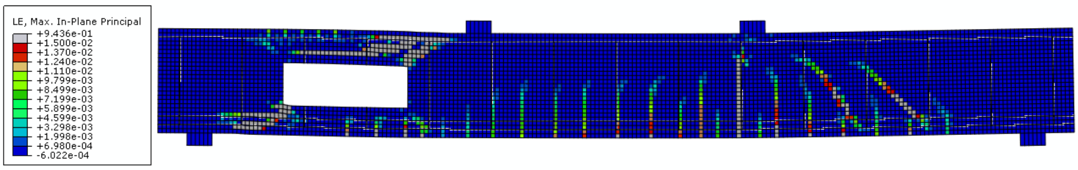

(n) UO9 (300×100) (Abdalla et al. 2003)

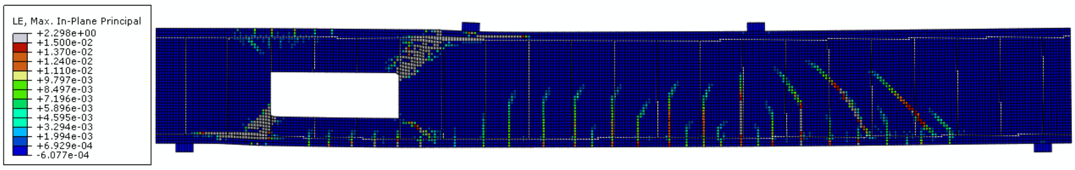

(Extracted from Allam 2005)

(o) B2 (450×150)

Figure 3.10. Predicted crack patterns at failure of existing tests

CHAPTER 4

FE MODELLING OF EXISTING TESTS ON RC BEAMS WITH AN FRP-STRENGTHENED WEB OPENING

4.1 INTRODUCTION

As reviewed in Chapter 2, most existing studies on RC beams with a web opening confirmed the feasibility of use of externally bonded FRP to compensate for the strength loss of the beam caused by the creation of a web opening (Mansur et al. 1999; Abdalla et al. 2003; Allam 2005; Maaddawy and Sherif 2009; Chin et al. 2012; Maaddawy and Ariss 2012; Chin et al. 2016). These studies were motivated by the need to create web openings in an existing structure for the passage of utility ducts and pipes, and were thus focused on restoring the strength of the beam through FRP strengthening. Compared with the experimental studies, only very limited research has been conducted on the finite element (FE) modeling of beams with an FRP-strengthened web opening. Therefore, a well-established FE approach for predicting the behaviour of such RC beams is not yet available. Against this background, this chapter presents a study on the FE modelling of RC beams with an FRP-strengthened web opening using the general purpose package ABAQUS (ABAQUS 2012).

In Chapter 3, three alterative FE approaches, including the brittle cracking model with SECANT modulus, the brittle cracking model with INITIAL modulus and the concrete damaged plasticity model, have been examined for the modelling of RC beams with an un-strengthened web opening. The brittle cracking model with SECANT modulus was finally identified to be the most reliable approach and thus adopted in the present study.

In the existing studies, the externally bonded FRP system has been adopted as the main measure to strengthen the web opening (e.g., externally bonded FRP U-jackets/FRP complete wraps/FRP sheets/FRP plates) (as shown in Fig. 4.1). Therefore, the bond-slip model for externally bonded FRP reinforcement proposed by Lu et al. (2005) was adopted to simulate the bond behaviour between FRP and concrete. This bond-slip relationship has been successfully used by Chen et al. (2011) and many others (e.g. Kotynia et al. 2008; Chen et al. 2012; Zhang and Teng 2014) in the modelling of RC beams strengthened with externally bonded FRP reinforcement, and is thus expected to be able to give accurate predictions in the present modelling work. Comparisons between the numerical predictions and the test results verified the accuracy of the proposed FE model for RC beams with an FRP-strengthened web opening.

4.2 THE PROPOSED FE APPROACH

4.2.1 FE approach for RC beams with an un-strengthened web opening

A reliable FE approach has been proposed in Chapter 3 for the simulation of RC beams with an un-strengthened web opening. In that FE approach, a dynamic analysis method (i.e., the explicit central difference method available in ABAQUS) instead of a static analysis method (e.g. the Newton-Raphson method and the arc-length method) was employed, and the brittle cracking model with SECANT modulus was adopted for the modelling of cracked concrete. In the present study, the FE approach proposed in Chapter 3 was further developed to simulate RC beams with an FRP-strengthened web opening, by incorporating proper bond-slip relationship for modelling the bond behaviour between externally-bonded FRP and concrete.

4.2.2 Modelling of FRP

In the FE approach, the externally bonded FRP is assumed to be linear-elastic-brittle and is modeled using 2-node truss elements (T2D2). The 2-node truss elements share the same nodes of the concrete elements and are arranged in the fiber direction of the FRP. The cross-sectional area of a truss element is determined by the thickness of the FRP and the spacing of the truss elements (i.e., the width of the corresponding concrete elements).

For FRP U-jackets, one end of the lowest FRP truss elements (i.e., nearest to the soffit of the beam) is fixed onto the bottom surface of the beam (i.e. to the corresponding concrete node). For FRP complete wraps, one end of the lowest FRP truss elements is fixed onto the bottom of the beam, while one end of the highest FRP truss elements (i.e., nearest to the top surface of the beam) is fixed onto the top surface of the beam. A typical FE mesh is shown in Fig. 4.2, in which the red lines stand for the FRP reinforcement.

4.2.3 Modelling of bond behaviour between FRP and concrete

The bond behavior between FRP and concrete is modeled using the 4-node interfacial element COH2D4, and the simplified bond-slip model developed by Lu et al. (2005) for externally bonded FRP is adopted, as expressed in Eq. 4.1.

$$\tau = \begin{cases} \tau_{\max}\sqrt{\dfrac{s}{s_0}} & for \;\; s \le s_0 \\ \tau_{\max} e^{-\alpha(\frac{s}{s_0}-1)} & for \;\; s > s_0 \end{cases} \tag{4.1}$$

$$s_0 = 0.0195\beta_{\mathrm{w}} f_t \tag{4.2}$$

$$\tau_{\max} = \alpha_1 \beta_{\mathrm{w}} f_t \tag{4.3}$$

$$\beta_{\mathrm{w}} = \sqrt{\frac{2\text{-}\mathrm{b}_f / b_c}{1+\mathrm{b}_f / b_c}} \tag{4.4}$$

$$\mathrm{f}_t = 0.395(f_{cu})^{0.55} \tag{4.5}$$

$$\alpha = \frac{1}{\dfrac{G_{\mathrm{f}}}{\tau_{\max} s_0} - \dfrac{2}{3}} \tag{4.6}$$

$$G_{\mathrm{f}} = 0.308\beta_w^2\sqrt{f_t} \tag{4.7}$$

where τ (*MPa*) is the local shear bond stress; $\tau_{\max}$ (*MPa*) is the local bond strength; s (*mm*) is the slip; s_0 (*mm*) is the slip when the bond stress reaches $\tau_{\max}$; β_{w} is the width ratio factor; $\mathrm{b_f}$ (*mm*) is the width of FRP; $\mathrm{b_c}$ (*mm*) is the width of beam; f_t (*MPa*) is the tensile strength of concrete; f_{cu} (*MPa*) is the cube compressive strength of concrete; G_{f} is the interfacial fracture energy; α_1=1.5. Lu et al.'s (2005) simplified bond-slip model was developed based on a combination of the numerical results of a meso-scale finite element model and relevant experimental results. This bond-slip model consists of an ascending branch with continuous stiffness degradation and a descending branch which drops to zero bond stress when the slip is sufficiently large. The key parameters were determined based on a parametric study using the meso-scale finite element model and relevant experimental results.

In the normal direction of the FRP-to-concrete interface, the interfacial elements are assumed to be linear-elastic with a very large stiffness, which is based on the assumption that the interaction of bond between the normal and shear directions is insignificant and can be ignored, and the debonding between FRP and concrete depends only on the bond-slip behavior parallel to the FRP-to-concrete bonded interface.

4.3 VERIFICATION OF THE PROPOSED FE APPROACH

4.3.1 Test database

As reviewed in Chapter 2, nine experimental studies in the published literature (Mansur et al. 1999; Abdalla et al. 2003; Allam 2005; Maaddawy and Sherif 2009; Pimanmas 2010; Chin et al. 2012; Maaddawy and Ariss 2012; Suresh and Prabhavathy 2015; Chin et al. 2016) have addressed the effect of drilling an opening in an existing beam and the design of the associated strengthening measure; all nine studies except Suresh and Prabhavathy (2015) proposed the use of externally bonded FRP reinforcement for the strengthening of the web opening. As shown in Fig. 4.1, five main strengthening schemes have been proposed in the existing studies: (1) vertically bonded FRP U-jackets on the chords (Figs. 4.1c, d and g) or on the two sides of the opening (Fig. 4.1g); (2) vertically bonded FRP complete wraps on the chords (Figs. 4.1d and g) or on the two sides of the opening (Fig. 4.1b); (3) vertical side bonded FRP sheets/plates on the two sides of the opening (Figs. 4.1b, c, d and f) or diagonal side bonded FRP plates on the two sides of the opening (Fig. 4.1a); (4) horizontally bonded FRP sheets/plates on the side surfaces of chords (Figs. 4.1a, b, c, d, f, g and h) or on the top and bottom surfaces of the beam (Fig. 4.1f); and (5) diagonal near-surface mounted FRP bars at corners (Fig. 4.1e). The above listed strengthening schemes were adopted together or alone by the researchers. For example, Maaddawy and Ariss (2012) used FRP U-jackets on the top chord, FRP complete wraps on the bottom chord, vertical side bonded FRP sheets on the two sides of the opening and horizontally bonded FRP sheets on the side surfaces of two chords together to strengthen their beams with a web opening; while the beam with a web opening tested by Chin et al. (2016) was strengthened only by horizontally bonded FRP plates on the side surfaces of chords. The above summarised strengthening schemes were found to be effective in preventing/mitigating shear cracks initiating from the corners of the web opening.

As reviewed in Chapter 2, in addition to the existing published studies on this topic, Prof. Teng's group recently conducted a test on a T-section beam with an FRP-strengthened rectangular opening in one of the two shear spans to further investigate the behaviour of such RC beams (Teng et al. 2013). The layout of the tested beam is shown in Fig. 2.1b. In the test, the beam had a web width of 250 mm, a total height of 500 mm, a total flange width of 1,450 mm, a flange thickness of 100 mm, a beam clear span of 3,300 mm, a shear span of 1,650 mm and a rectangular opening of 220 mm (height) × 500 mm (length).

A total of 12 RC beams with an FRP-strengthened web opening were collected from the above studies to verify the accuracy of the proposed FE approach. These tests were chosen because sufficient geometric and material properties had been provided. The specimens tested by Mansur et al. (1999) in which the web opening was circular and the specimens tested by Maaddawy and Sherif (2009) which were concerned with very deep beams were not considered in the comparison as they are out of the scope of present study. The present study is only concerned with RC beams with a web opening strengthened with externally bonded FRP sheets/plates, so the specimens tested by Pimanmas (2010), in which diagonal near-surface mounted FRP bars at corners were adopted as the FRP strengthening scheme, are also out of the scope of present study. Details of the collected specimens are given in Table 4.1 and material properties of the collected specimens are given in Table 4.2.

4.3.2 Load-deflection curves

In the FE analyses, the damping factor β was chosen to be 1×10^{-5}, the loading time was chosen to be $50T_1$ (where T_1 is the period of the fundamental vibration mode of the beam and can be found from an eigenvalue analysis of the FE model), and the hourglass scaling factors were chosen to be the default values (i.e., 1), following the findings in Chapter 3. The exponent n in the shear retention factor model was chosen to be 5 for the brittle cracking model based on the parametric study presented in Chapter 3. For comparison purposes, the three schemes adopted in Chapter 3 are also examined in the present study: (1) Scheme-1: the brittle cracking model, with the secant modulus of concrete recommended by Ye (2005) and Pimanmas (2010) being used, was employed to simulate cracked concrete (referred to as the ***BC model with SECANT modulus*** in Fig. 4.3); (2) Scheme-2: the brittle cracking model, with the initial elastic modulus of concrete being used, was employed to simulate cracked concrete (referred to as the ***BC model with INITIAL modulus*** in Fig. 4.3); and (3) Scheme-3: the concrete damaged plasticity model was adopted to simulate the behaviour of cracked concrete (referred to as the ***DP model*** in Fig. 4.3).

The load-deflection curves obtained from the above three schemes are compared with the test results in Fig. 4.3. As can be seen from Fig. 4.3, for all 12 specimens tested by Maaddawy and Ariss (2012), Abdalla et al. (2003), Allam (2005), Chin et al. (2012), Chin et al. (2016) and Teng et al. (2013), the brittle cracking model with SECANT modulus gives the most accurate predictions of the load-deflection curves in terms of both the predicted ultimate load and the stiffness. The brittle cracking model with INITIAL modulus consistently overestimates the ultimate load as well as the stiffness of the beam, while the DP model usually significantly underestimates the ultimate load but overestimates the stiffness. These findings fully coincide with findings from FE modelling of RC beams with an un-strengthened web opening as presented in Chapter 3.

A comparison of the ultimate loads between FE analyses and tests for all the collected specimens are given in Fig. 4.4 and Table 4.3. As can be seen from Fig. 4.4 and Table 4.3, the brittle cracking model with SECANT modulus gives close predictions of the ultimate loads from tests, with an average prediction-to-test ratio of 1.00, a standard deviation (STD) of 0.079, and a coefficient of variation (CoV) of 0.079. On the contrary, the brittle cracking model with INITIAL modulus substantially overestimates the ultimate load, with an average prediction-to-test ratio of 1.17, a STD of 0.175, and a CoV of 0.150; the DP model significantly underestimates the ultimate load, with an average prediction-to-test ratio of 0.796, a STD of 0.228, and a CoV of 0.287. The better performance of the brittle cracking model with SECANT modulus is also evidenced by the much smaller scatter in its predictions of test results as shown in Fig. 4.4.

4.3.3 The initiation of FRP debonding

For RC beams with an FRP-strengthened web opening, the initiation of FRP debonding commonly occurs at the corners of the opening due to the development of inclined cracks initiating at these regions. As explained in Chapter 3, the adopted dynamic analysis approach can not only overcome the severe numerical convergence difficulties commonly encountered in the modelling of cracked concrete using static analysis approaches, but also capture the local dynamic responses caused by a sudden release of energy, such as the initiation and development of FRP debonding. Therefore, the development history of the kinetic energy during the whole loading process of the specimens is examined to identify the initiation of FRP debonding in the present study. Specimen S1-500×120 tested by Maaddawy and Ariss (2012) is selected as an example to illustrate the detailed process, as its test results were clearly reported. The predicted development history of the kinetic energy using the brittle cracking model with

SECANT modulus is plotted in logarithmic scale in Fig. 4.5, in which the test and predicted load-deflection curves are also shown for reference. As shown in Fig. 4.5, the kinetic energy remains in a low range at the early loading stage, and experiences a sudden increase at a deflection of 8.6 mm. Such a sudden increase indicates the initiation of FRP debonding. Afterwards, the kinetic energy starts fluctuating, caused by the gradual debonding of FRP. When the deflection further increases to about 12 mm, the kinetic energy steps into a higher level and fluctuation becomes more severe, which indicates that failure of the beam happens. The development of the kinetic energy reflects well the changes in the predicted load-deflection curve. As shown in Fig. 4.5, the predicted load-deflection curve keeps ascending at the early loading stage and achieves a local peak value at the deflection of 8.6 mm, corresponding to the initiation of FRP debonding. When the deflection further increases to about 12 mm, the load experiences a sudden drop, indicating the failure of the beam. The initiation of FRP debonding predicted by the FE analysis is marked by a circle in the predicted load-deflection curve, and the initiation of FRP debonding obtained from test (Maaddawy and Ariss 2012) is marked by a square in the test load-deflection curve. It can be seen from Fig. 4.5 that the predicted and test points of initiation of FRP debonding are quite close to each other.

The predicted points of the initiation of FRP debonding of the collected specimens are shown in Fig. 4.6, in which the test points of initiation of FRP debonding are also shown for comparison if they were reported in the relevant publications. As can be seen from Fig. 4.6, the predicted and the test points of initiation of FRP debonding are very close to each other for all the compared specimens.

4.3.4 Failure process and failure mode

The failure mode of Specimen FRP-500×220 (T-section beam) tested by Prof. Teng's group (Teng et al. 2013) was recorded in detail and available to the candidate, thus this specimen is selected as the example in the comparison of failure process and failure mode between test and prediction from the brittle cracking model with SECANT modulus.

The failure mode of the specimen is shown in Fig. 4.7, from which it can be seen that the failure of the beam was dominated by the debonding of CFRP U-jackets on the opening side closer to the loading point. After removing the debonded CFRP U-jackets, an inclined crack (around 45 degrees above the horizontal direction), which initiated from the opening corner nearest the loading point and extended to the loading point was found (Fig. 4.7b). In addition, flexural cracks were observed in the flange chord near both its bottom surface (closer to the loading point, as shown in Fig. 4.7c) and its top surface (closer to the corresponding support, as shown in Fig. 4.7d).

The predicted crack patterns (represented by the maximum principal cracking strain) of Specimen FRP-500×220 at different load levels are shown in Fig. 4.8. As can be seen from Fig. 4.8, when the load reaches 110 kN, an inclined crack (around 45 degrees above the horizontal direction) occurs at the opening corner closer to the loading point. Meanwhile, one flexural crack occurs at one end (closer to the loading point) of the flange chord near its bottom surface, while another one occurs at the other end (i.e., closer to the corresponding support) of the flange chord near its top surface (Fig. 4.8a). At the load of 224 kN, a major flexural crack is formed at the mid-span of the beam (Fig. 4.8b). As the load increases to higher levels, the existing cracks become wider, and at the same time, shear cracks gradually appear in the shear span of the beam without a web opening. When the load reaches 384 kN, a large inclined crack is formed near the top corner of the web opening nearer to the support (Fig. 4.8c). When the load further increases to 455 kN, the failure of the beam is achieved. The inclined crack at the opening corner closer to the loading point which reaches the loading point can be obviously seen (Fig. 4.8d). A comparison between Fig. 4.8d and Fig. 4.7 shows that the predicted crack pattern of the beam agrees well with the observation in the test.

The predicted crack patterns at failure of the other 11 collected specimens by using the brittle cracking model with SECANT modulus are plotted in Fig. 4.9. The test crack patterns at failure of 6 specimens (out of the 11 specimens) whose crack patterns are given in relevant publications are also shown in Fig. 4.9 for the purpose of comparison. As can be seen from Fig. 4.9, at failure of the specimens, substantial shear cracks are formed near the corners of the web opening. The predicted crack patterns also agree well with the test observations.

4.3.5 Comparison between un-strengthened and FRP-strengthened beams

The test and predicted (using the brittle cracking model with SECANT modulus) load-deflection curves of the RC beams with an un-strengthened web opening and the corresponding beams with an FRP-strengthened web opening are plotted in Fig. 4.6. As can be seen from Fig. 4.6, after FRP strengthening, both the predicted strength and stiffness of the beam increase, which is as expected and as observed in the tests. In addition, it can also be seen from Fig. 4.6 that the agreement between predictions and tests is better for RC beams with an FRP-strengthened web opening than for the corresponding specimens with an un-strengthened web opening.

Specimens CN-500 $\times$ 120 (un-strengthened beam) and S1-500 $\times$ 120 (FRP-strengthened beam) tested by Maaddawy and Ariss (2012) are taken as examples to illustrate the effect of FRP strengthening on the crack patterns, as shown in Fig. 4.10. As can be seen from Fig. 4.10, after FRP strengthening, the development of the localized cracks near the corners of the web opening obtained from the FE modelling are well restricted by the FRP and thus forced into a larger region of the beam.

4.4 CONCLUDING REMARKS

In this chapter, an FE approach for RC beams with an FRP-strengthened web opening has been proposed based on the FE approach developed in Chapter 3 for RC beams with an un-strengthened web opening. The bond behaviour between FRP and concrete was modelled using the simplified bond-slip relationship proposed by Lu et al. (2005). By comparing it with 12 collected tests from the existing studies, it was found that the brittle cracking model with SECANT modulus gives the most accurate predictions of the load-deflection curves in terms of both the ultimate load and the stiffness, the brittle cracking model with INITIAL modulus consistently overestimates the ultimate load as well as the stiffness of the beam, and the DP model usually significantly underestimates the ultimate load but overestimates the stiffness. The brittle cracking model with SECANT modulus is thus recommended for the modelling of RC beams with an FRP-strengthened web opening.

4.5 REFERENCES

ABAQUS (2012). *ABAQUS Analysis User's Manual (Version 6.12)*, Dassault Systems SIMULIA Corporation, Providence, Rhode Island, USA.

Abdalla, H.A., Torkey, A.M., Haggag, H.A. and Abu-Amira, A.F. (2003). "Design against cracking at openings in reinforced concrete beams strengthened with composite sheets", *Composite Structures*, 60(2), 197-204.

Allam, S. M. (2005). "Strengthening of RC beams with large openings in the shear zone", *Alexandria Engineering Journal*, *44*(1), 59-78.

Chen, G.M., Teng, J.G. and Chen, J.F. (2011). "Finite element modeling of intermediate crack debonding in FRP-plated RC beams", *Journal of Composites for Construction*, ASCE, 15(3), 399-353.

Chen, G.M., Chen, J.F. and Teng, J.G. (2012). "On the finite element modelling of RC beams shear-strengthened with FRP", *Construction and Building Materials*, 32, 13-26.

Chin, S.C., Shafiq, N. and Nuruddin, M.F. (2012). "Strengthening of RC beams with large openings in shear by CFRP laminates: experiment and 2D nonlinear finite element analysis", *Research Journal of Applied Sciences Engineering and Technology*, 4(9), 1172-1180.

Chin, S.C., Shafiq, N. and Nuruddin, M.F. (2016). "Behaviour of RC beams with CFRP-strengthened openings", *Structural Concrete*, 17(1), 32-43.

Kotynia, R., Abdel Baky, H., Neale, K.W. and Ebead, U.A. (2008). "Flexural strengthening of RC beams with externally bonded CFRP systems: Test results and 3D nonlinear FE analysis", *Journal of Composites for Construction*, 12(2), 90-201.

Lu, X.Z., J.G. Teng, Ye, L.P. and Jiang, J.J. (2005). "Bond-slip models for FRP sheets /plates bonded to concrete", *Engineering Structures*, 27(6), 920-937.

Maaddawy, T. and Sherif, S. (2009). "FRP composite for shear strengthening of reinforced concrete deep beams with openings", *Composite Structures*, 89(1), 60-69.

Maaddawy, T. and El-Ariss, B. (2012). "Behavior of concrete beams with short shear span and web opening strengthened in shear with CFRP composites." *Journal of Composites for Construction*, ASCE, 16(1), 47-59.

Mansur, M.A., Tan K.H. and Wei, W. (1999). "Effects of creating an opening in existing beams", *ACI Structural Journal*, 96(6), 899-906.

Pimanmas, A. (2010). "Strengthening R/C beams with opening by externally installed FRP rods: behavior and analysis", *Composite Structures*, 92(8), 1957-1976.

Suresh, J. and Prabhavathy, R. A. (2015). "Behaviour of steel fibre reinforced concrete beams with duct openings strengthened by steel plates", *International Journal of Advanced Information in Arts, Science &*

Management, 4(4).

Ye, L.P. (2005). *Concrete Structures* (Second Edition), Tsinghua University Press, Beijing, China. (in Chinese)

Zhang, S.S. and Teng, J.G. (2014). "Finite element analysis of end cover separation in RC beams strengthened in flexure with FRP", *Engineering Structures*, 75, 550–560.

Table 4.1. Summary of experimental studies on RC beams with an FRP-strengthened web opening

Source	Specimen	Shape of cross section	Beam dimensions			Opening size		Number of web opening	FRP strengthening configuration		Observed failure mode
			Span (mm)	Width (mm)	Height (mm)	Width (mm)	Height (mm)		Opening chords	Sides of opening	
Abdalla et al. (2003)	RO3	Rectangular	2000	100	250	200	100	1	One-layer horizontal CFRP sheet	One-layer CFRP wrapping	Shear at opening
	RO4					300	100				
Allam (2005)	B8	Rectangular	3000	150	400	450	150	1	One-layer horizontal CFRP sheet	One-layer vertical CFRP sheet	Shear at opening
	B9					450	150		One-layer vertical CFRP U-jacket and one-layer horizontal CFRP sheet	One-layer horizontal CFRP U-jacket and one-layer vertical CFRP sheet	
Chin et al. (2012)	B5	Rectangular	1800	120	300	210	210	2	One-layer horizontal CFRP plate	One-layer vertical CFRP plate	Shear at opening
	B6					210	210				
Maaddawy and Ariss (2012)	S1-500×120	Rectangular	2400	85	400	500	120	1	One-layer horizontal CFRP sheet and one-layer vertical CFRP U-jacket/complete wrap	One-layer vertical CFRP U-jacket	Shear at opening
	S1-500×160					500	160				
	S2-500×120					500	120		One-layer horizontal CFRP sheet and two-layer vertical CFRP U-jacket/complete wrap	Two-layer vertical CFRP U-jacket	
	S2-500×160					500	160				
Chin et al. (2016)	SBRO	Rectangular	1800	120	300	800	140	1	One-layer horizontal CFRP plate	NA	Shear at opening
Teng et al. (2013)	FRP-500×220	T-section	3300	250[(a)]	500	500	220	1	One-layer vertical CFRP wrap and one-layer horizontal CFRP plate	Two-layer vertical CFRP U-jacket	Shear at opening

Note: (a) Web width (Specimen FRP-500×220 is a reversed T-section beam whose flange is 100 mm in height and 1450 mm in width).

Table 4.2. Material properties of RC test beams with an FRP-strengthened web opening

Source	Specimen	Cylinder compressive strength of concrete f'_c (MPa)	Steel reinforcement							FRP reinforcement		
			Tension steel bars	Yield strength of tension bars f_{yt} (MPa)	Compression steel bars	Yield strength of compression bars f_{yc} (MPa)	Stirrups	Yield strength of stirrups f_{vy} (MPa)	Elastic modulus of all steel bars E_s[a] (GPa)	Nominal thickness (mm)	Tensile strength (MPa)	Elastic modulus (GPa)
Maaddawy and Ariss (2012)	S1-500×120 S2-500×120 S1-500×160 S2-500×160	20	4Φ16 (deformed, and placed in two rows)	520	2Φ12 (deformed)	520	Φ6@80 (plain)	300	200	0.381	3450	230
Abdalla et al. (2003)	RO3	39.2	4Φ10 (deformed, and placed in two rows)	400	2Φ10 (deformed)	400	Φ8@150 (deformed)	240	200	0.13	3500	230
	RO4	40.8										
Allam (2005)	B8 B9	28	3Φ16 (deformed)	400	2Φ12 (deformed)	380	Φ8@150 (plain)	250	200	0.13	3500	230
Chin et al. (2012)	B5 B6	35	2Φ12 (deformed)	410	2Φ10 (deformed)	410	Φ6@300 (plain)	275	200	1.4	2200	170
Chin et al. (2016)	SBRO	29.75	2Φ12 (deformed)	460	2Φ10 (deformed)	460	Φ6@300 (plain)	275	200	1.4	2200	170
Teng et al. (2013)	FRP-500×220	33.2	4Φ20 (deformed)	482	3Φ20 (deformed)	482	Φ8@100 (plain)	375	200	0.337 (sheet) 1.2 (plate)	2738 (sheet) 2450 (plate)	238 (sheet) 131 (plate)

Note: (a) E_s is assumed to be 200 GPa as test data are not available in the relevant publications.

Table 4.3. Test and predicted ultimate loads

Source	Specimen	Test result (kN)	BC model with SECANT modulus (kN)		BC model with INITIAL modulus (kN)		DP model (kN)	
			Prediction	Prediction / test	Prediction	Prediction / test	Prediction	Prediction / test
Maaddawy and Ariss (2012)	S1-500×120	72	74.2	1.03	90.6	1.26	44.4	0.617
	S2-500×120	73	75.7	1.04	104.6	1.45	45.6	0.624
	S1-500×160	57	62.7	1.09	87.0	1.53	32.5	0.571
	S2-500×160	66	64.0	0.970	75.8	1.15	33.5	0.507
Abdalla et al. (2003)	RO3	73	72.2	0.989	78.3	1.07	77.3	1.06
	RO4	62	65.9	1.06	70.5	1.14	65.6	1.06
Allam (2005)	B8	120	131.5	1.10	152.3	1.27	136.5	1.14
	B9	147	144.4	0.983	149.1	1.01	139.3	0.947
Chin et al. (2012)	B5	36	32.1	0.891	36.6	1.02	33.6	0.934
	B6	37	30.5	0.825	36.6	0.989	32.4	0.875
Chin et al. (2016)	SBRO	83	82.0	0.988	87.1	1.05	52.6	0.634
Teng et al. (2013)	FRP-500×220	475	488.2	1.03	520.5	1.10	275.8	0.581
Statistical characteristics	**Average =**			1.00		1.17		0.796
	STD =			0.079		0.175		0.228
	CoV =			0.079		0.150		0.287

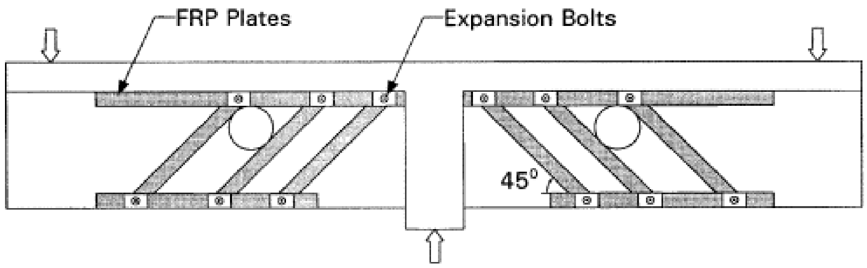

(a) Mansur et al.'s (1999) specimens (extracted from Mansur et al. 1999)

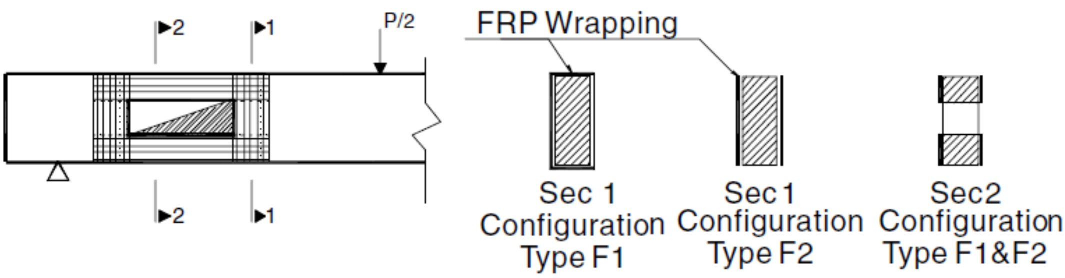

(b) Abdalla et al.'s (2003) specimens (extracted from Abdalla et al. 2003)

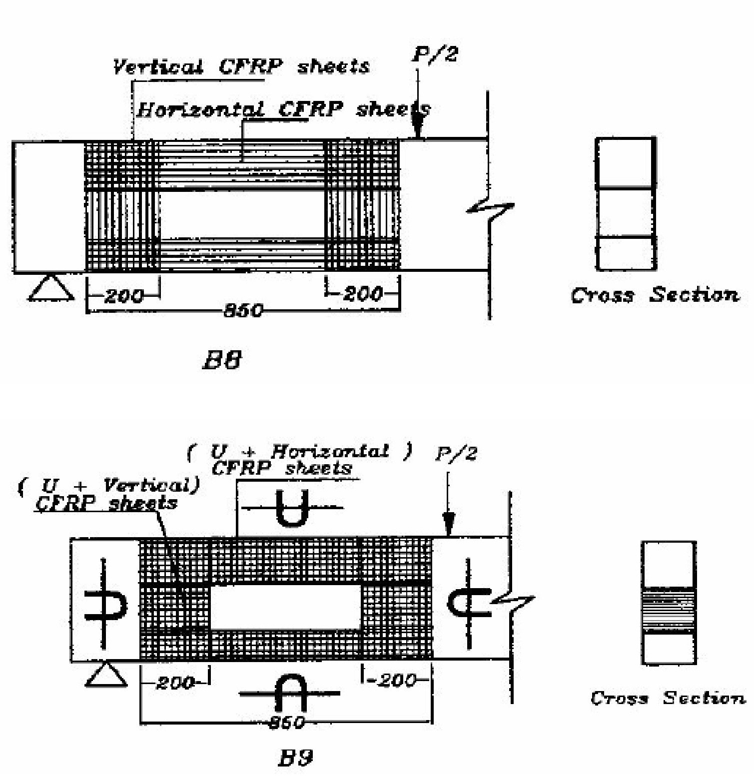

(c) Allam's (2005) specimens (extracted from Allam 2005)

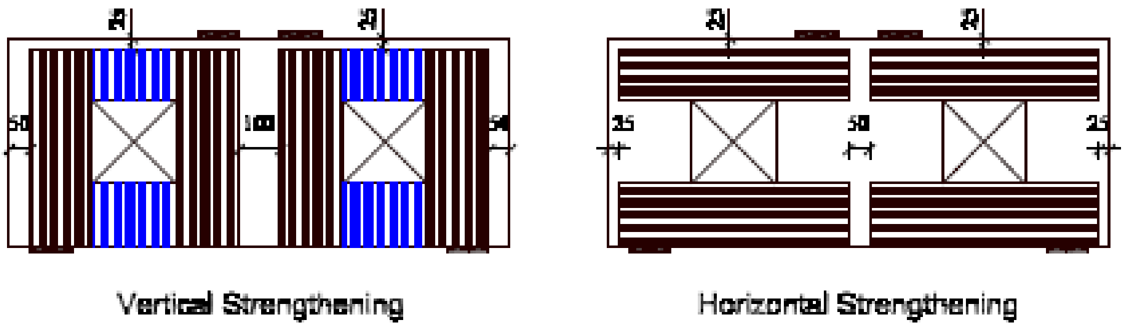

(d) Maaddawy and Sherif's (2009) specimens (extracted from Maaddawy and Sherif 2009)

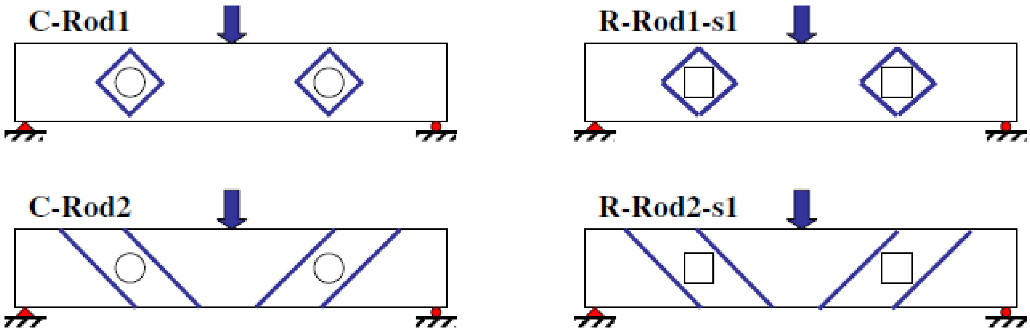

(e) Pimanmas's (2010) specimens (extracted from Pimanmas 2010)

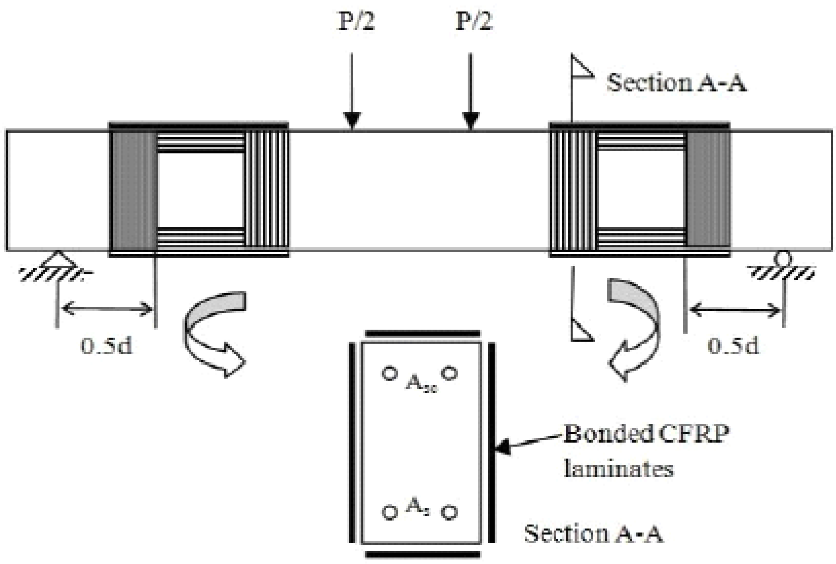

(f) Chin et al.'s (2012) specimens (extracted from Chin et al. 2012)

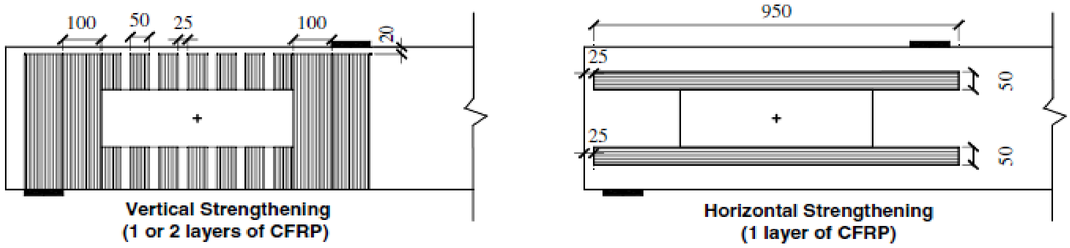

(g) Maaddawy and Ariss's (2012) specimens (extracted from Maaddawy and Ariss 2012)

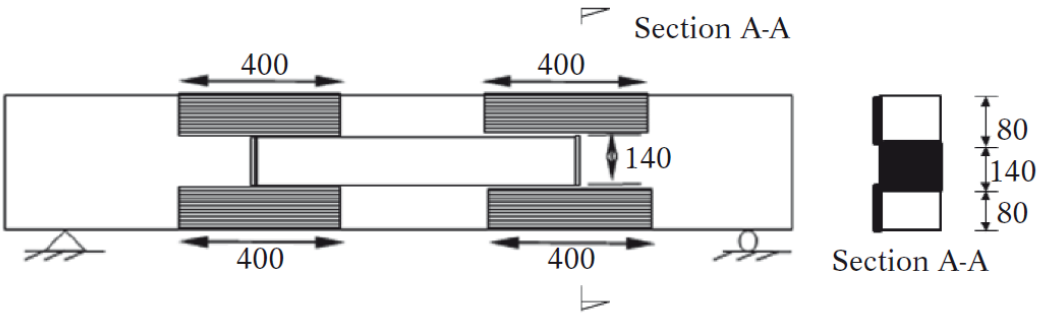

(h) Chin et al.'s (2016) specimen (Extracted from Chin et al. 2016)

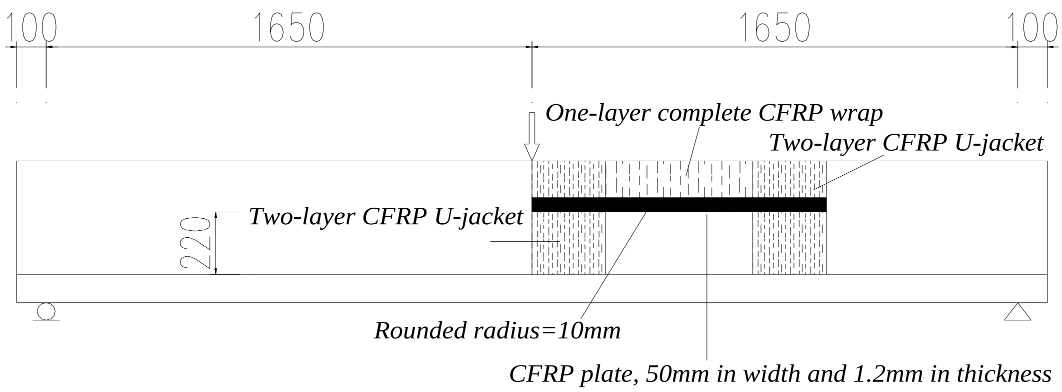

(i) Teng et al.'s (2013) specimen (FRP-500×220)

Figure 4.1. Layout of the CFRP-strengthening configuration of the beam specimens

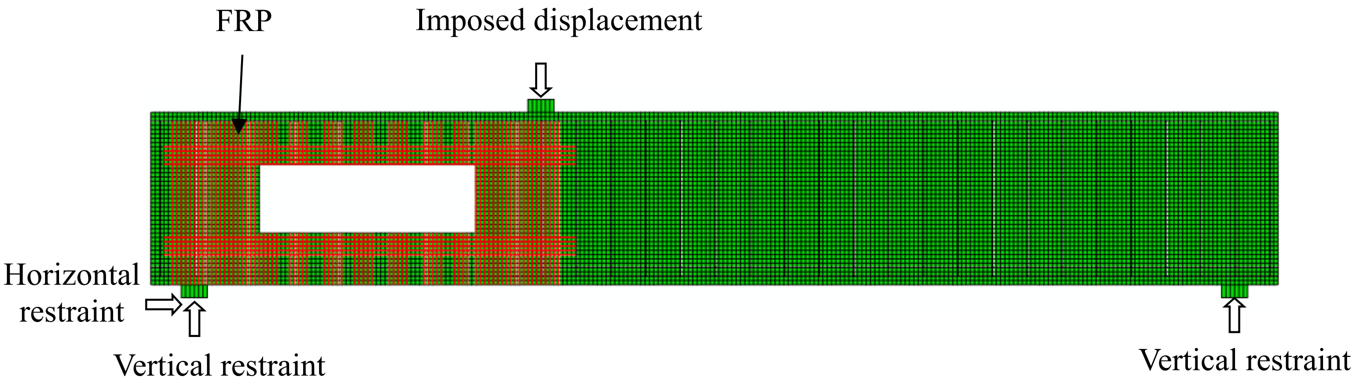

Figure 4.2. Typical FE mesh

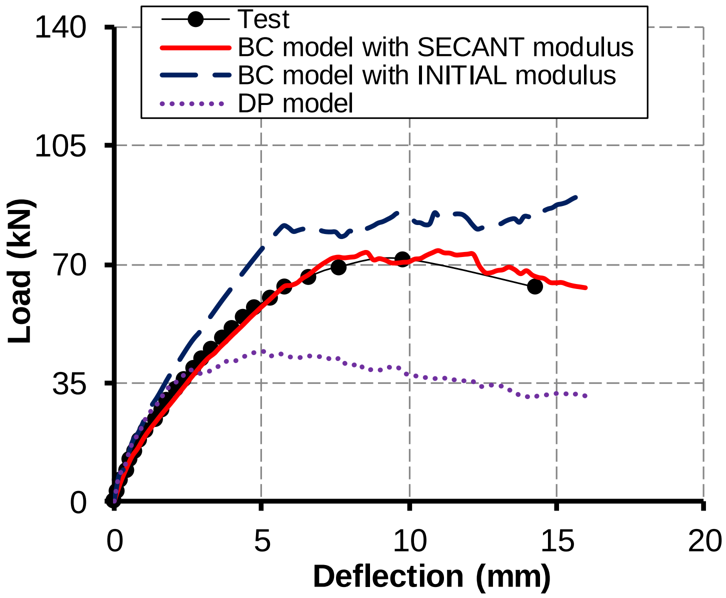

(a) S1-500×120 (Maaddawy and Ariss 2012)

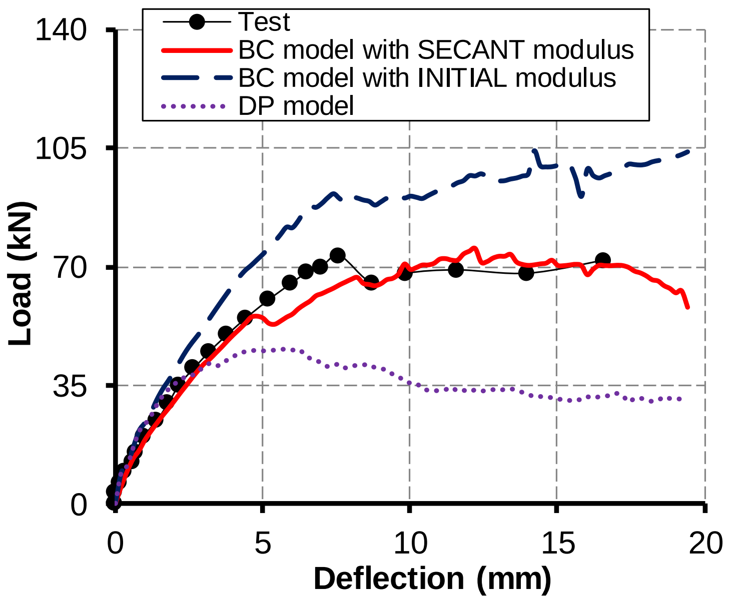

(b) S2-500×120 (Maaddawy and Ariss 2012)

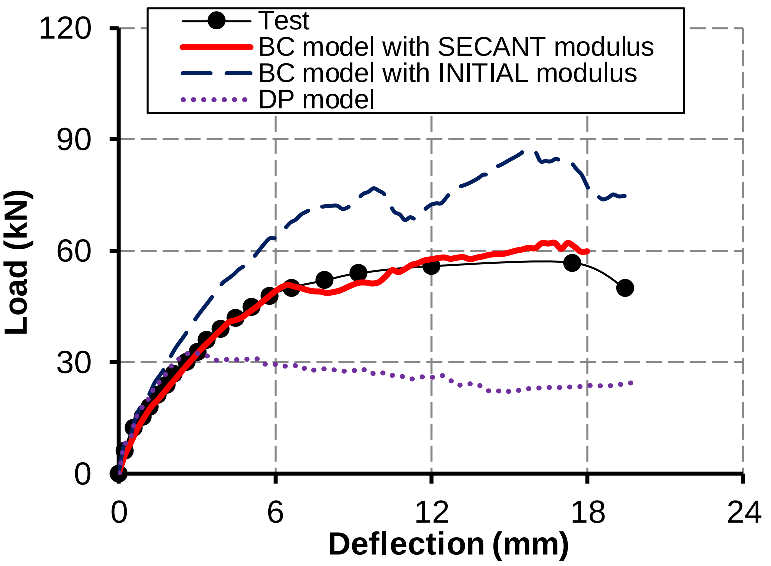

(c) S1-500×160 (Maaddawy and Ariss 2012)

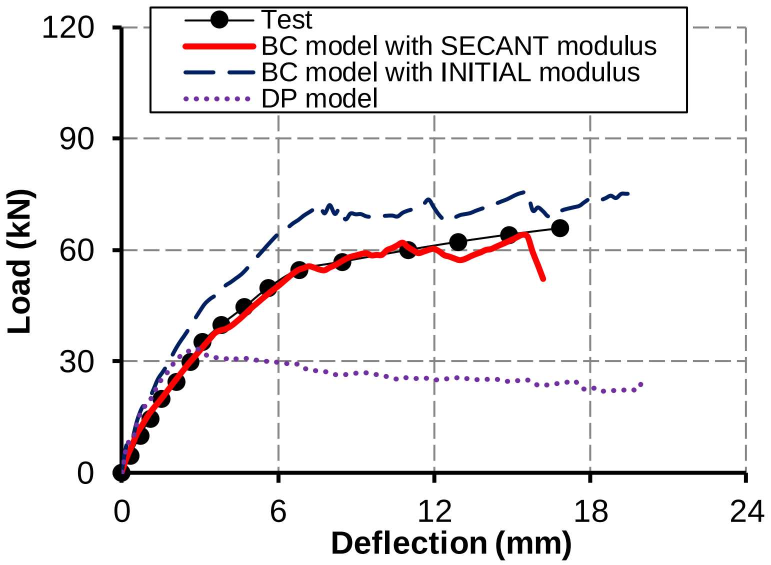

(d) S2-500×160 (Maaddawy and Ariss 2012)

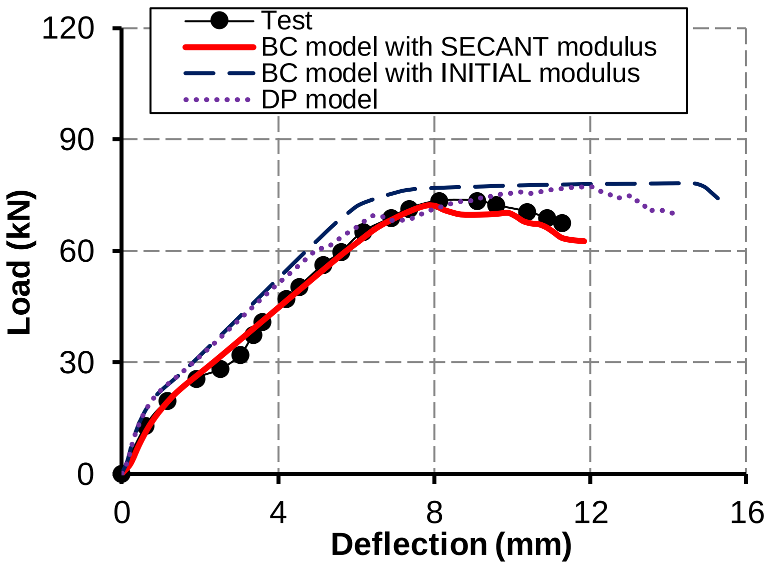

(e) RO3 (200×100) (Abdalla et al. 2003)

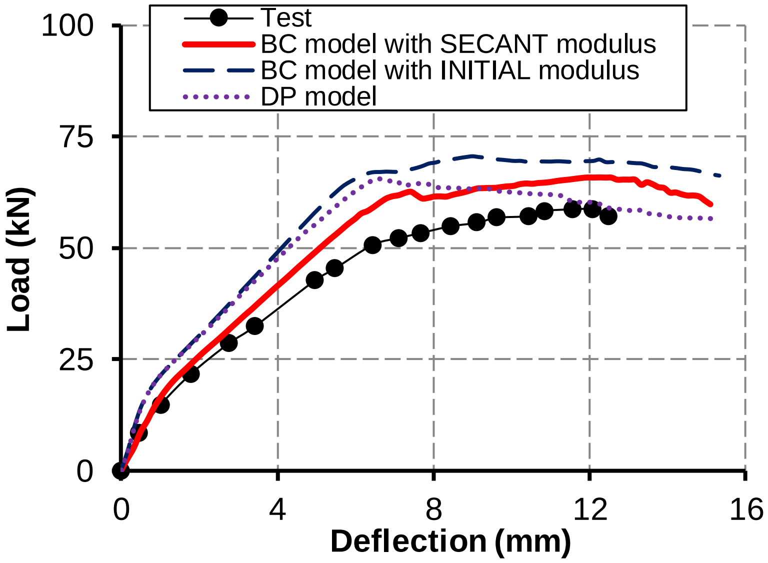

(f) RO4 (300×100) (Abdalla et al. 2003)

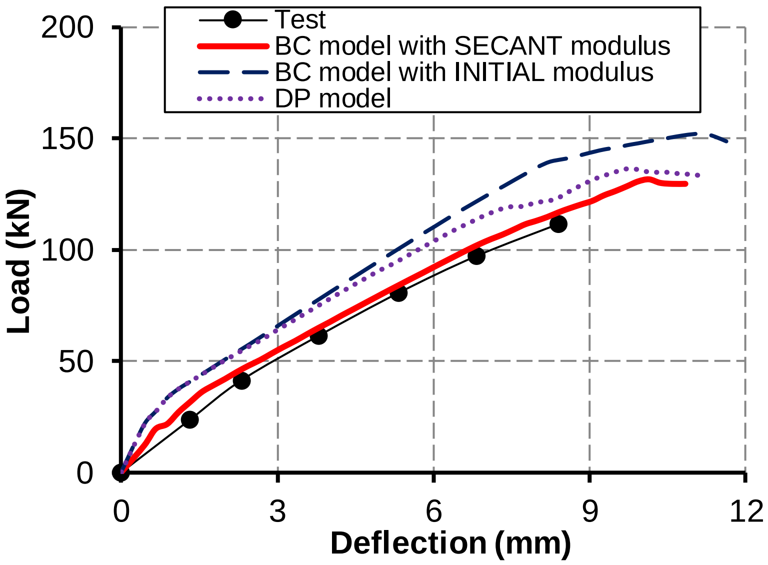

(g) B8 (450×150) (Allam 2005)

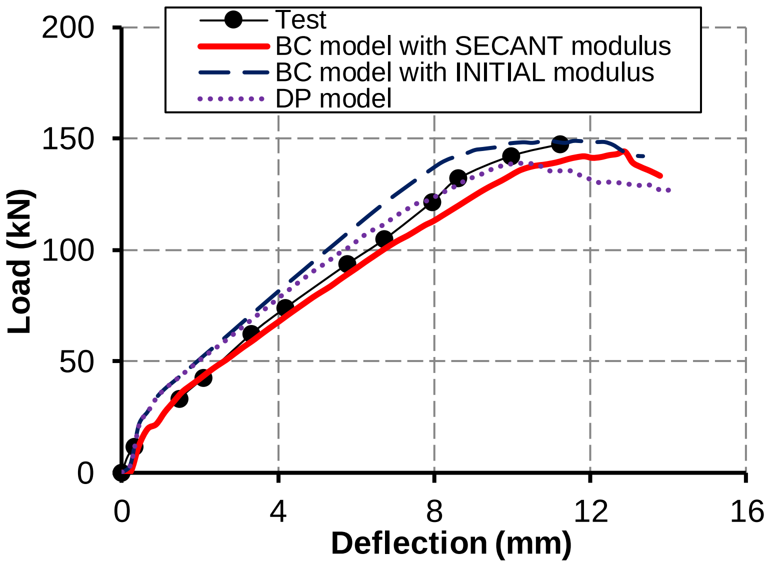

(h) B9 (450×150) (Allam 2005)

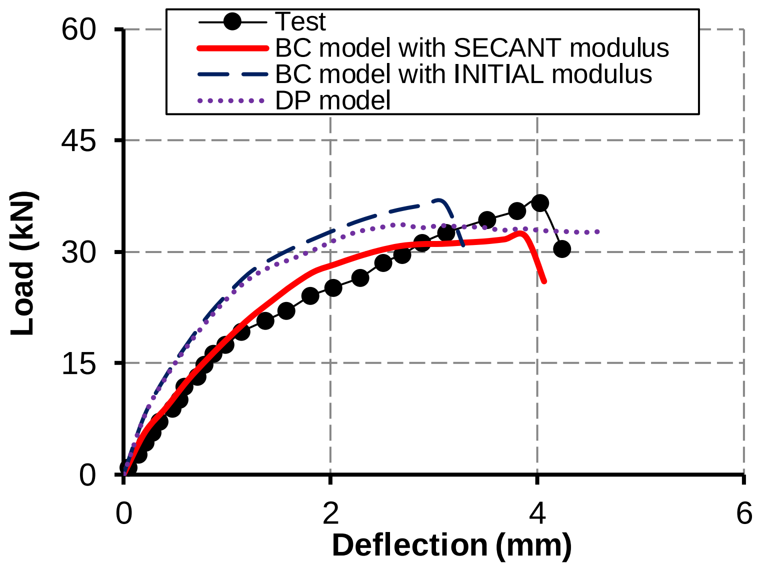

(i) B5 (210x210) (Chin et al. 2012)

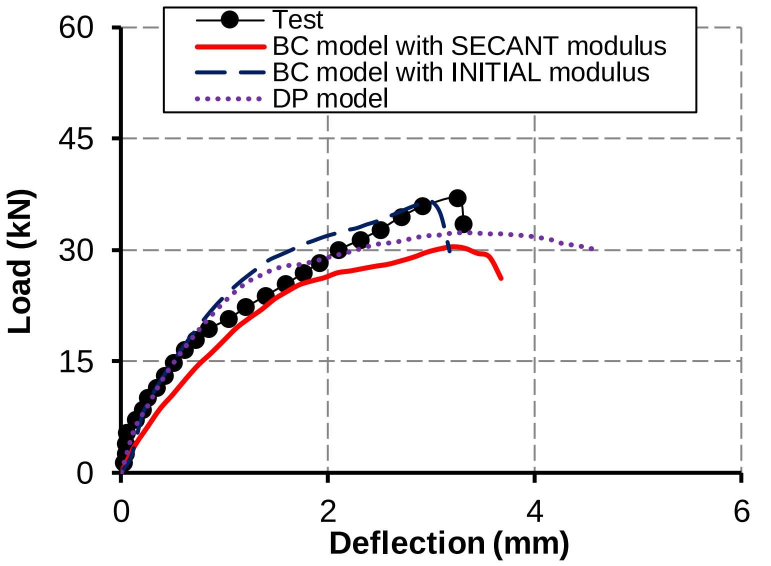

(j) B6 (210x210) (Chin et al. 2012)

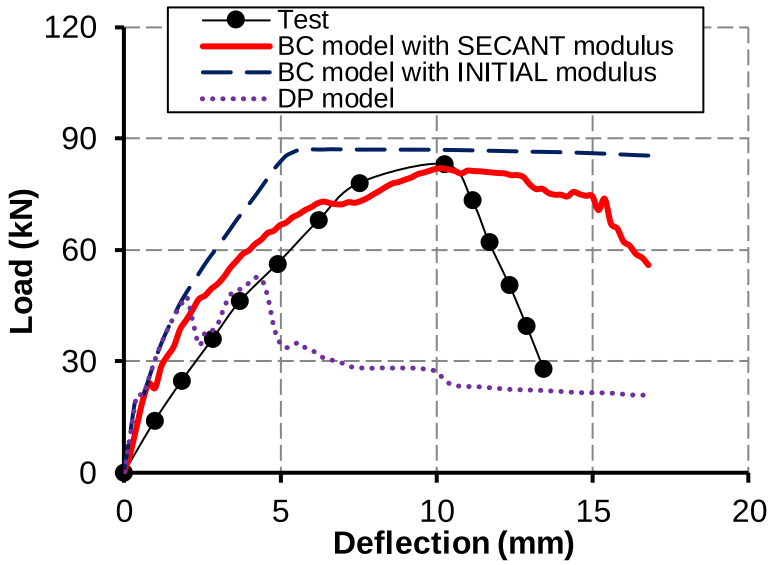

(k) SBRO (800x140) (Chin et al. 2016)

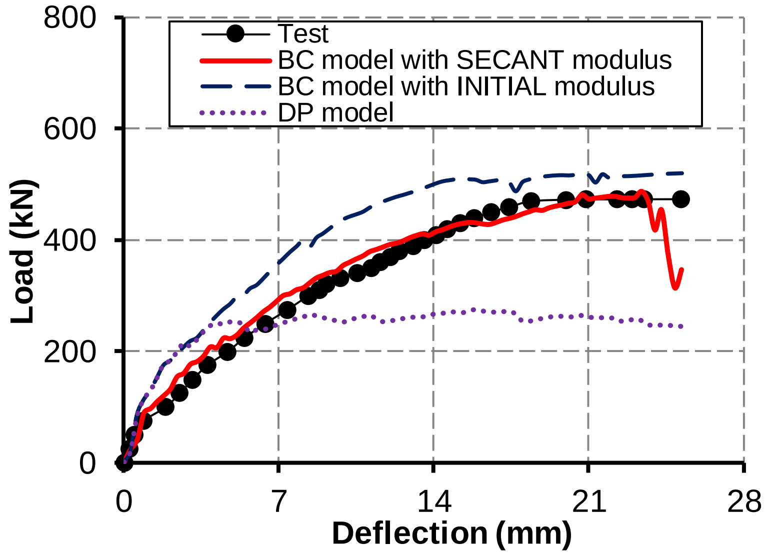

(l) FRP-500×220 (Teng et al. 2013)

Figure 4.3. Load-deflection curves

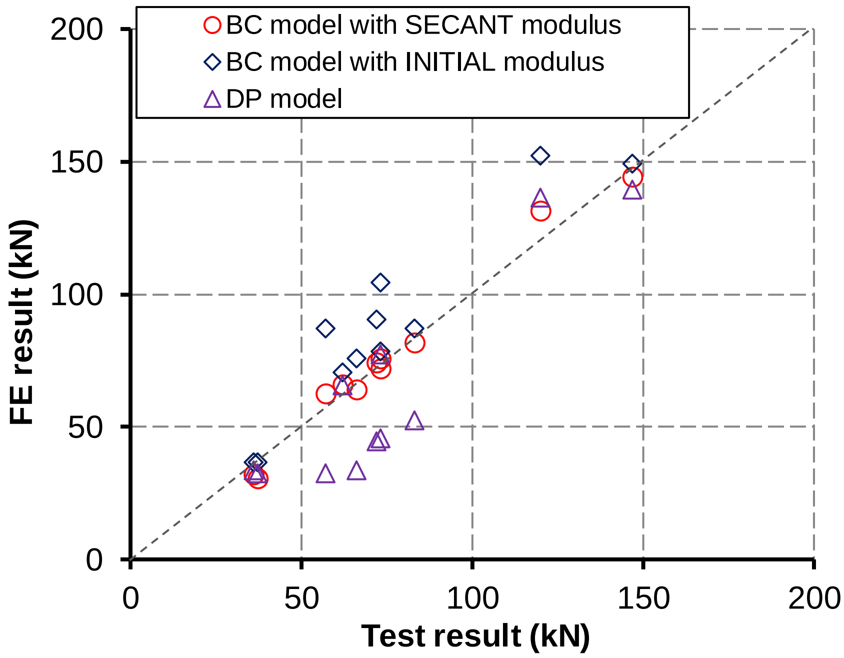

Figure 4.4. Comparison of ultimate loads between FE predictions and tests

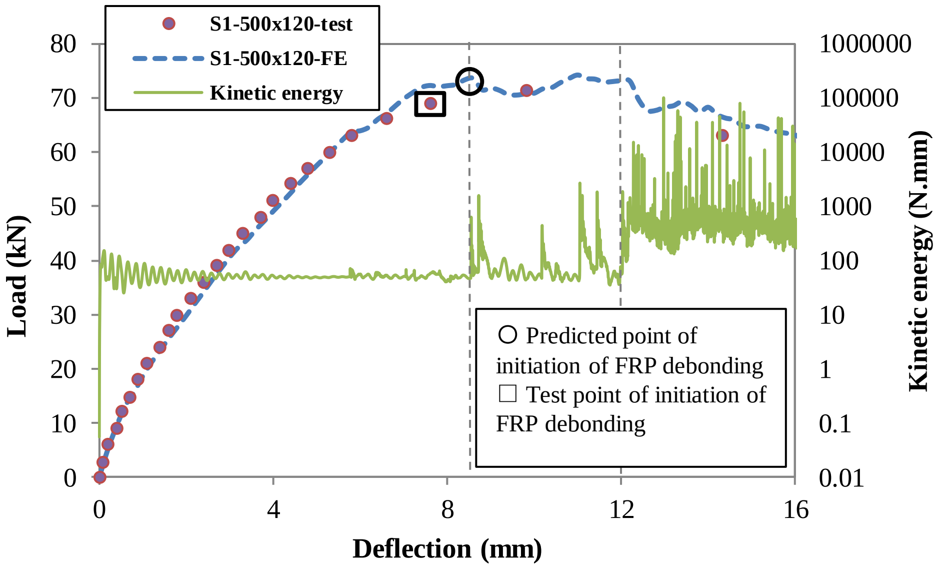

Figure 4.5. Development history of kinetic energy (S1-500×120)

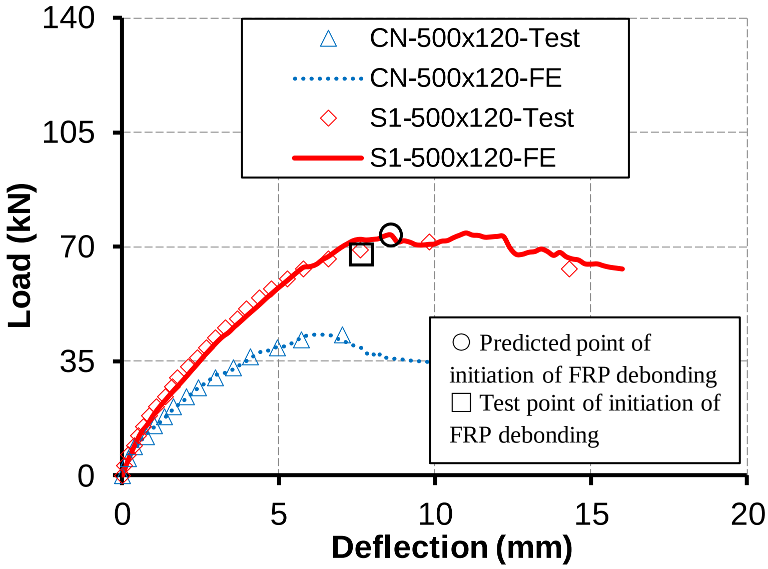

(a) S1-500×120 versus CN-500×120 (Maaddawy and Ariss 2012)

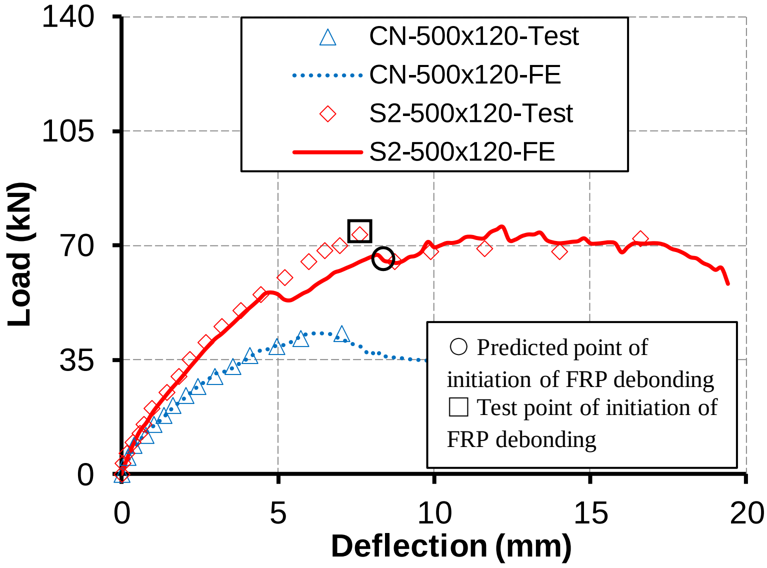

(b) S2-500×120 versus CN-500×120 (Maaddawy and Ariss 2012)

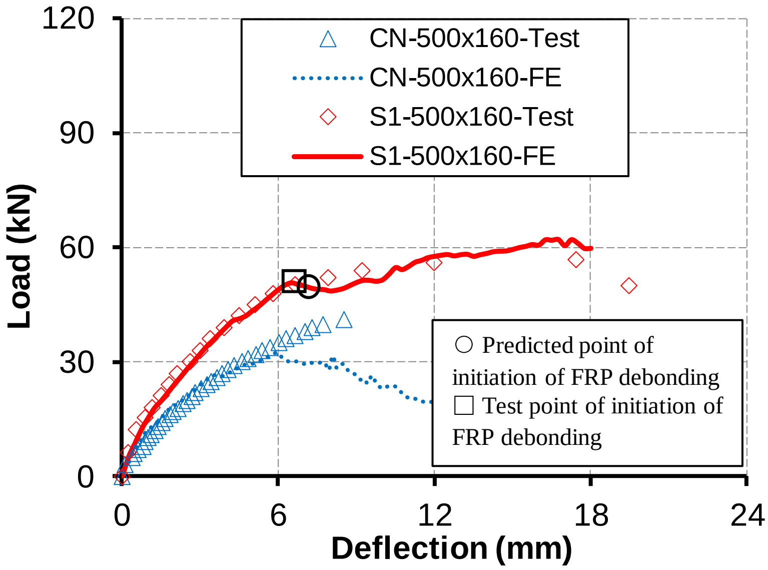

(c) S1-500×160 versus CN-500×160 (Maaddawy and Ariss 2012)

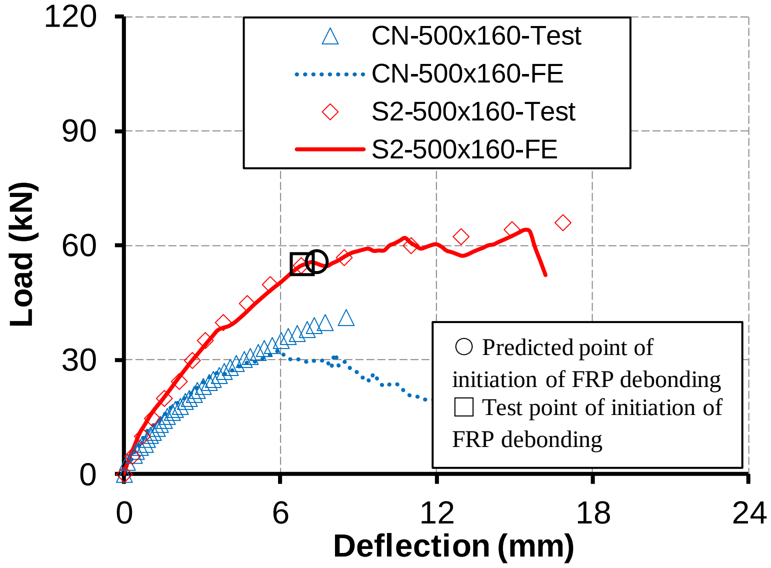

(d) S2-500×160 versus CN-500×120 (Maaddawy and Ariss 2012)

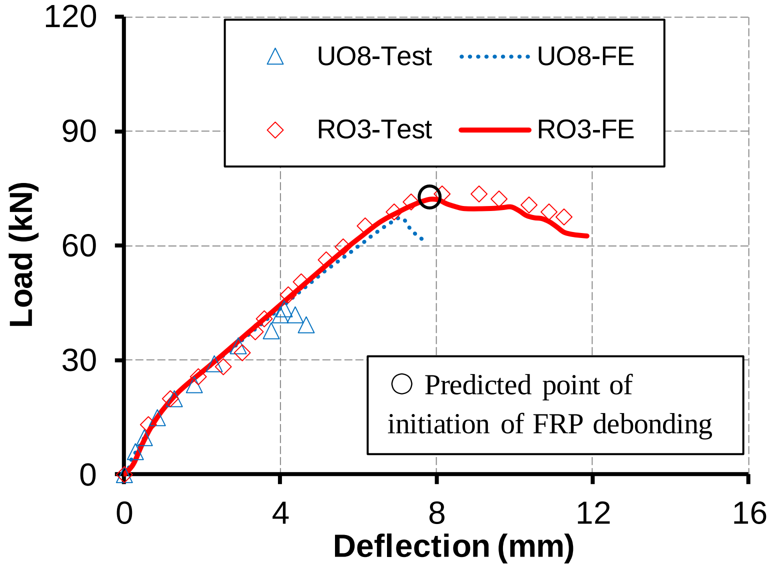

(e) RO3 versus UO8 (200×100) (Abdalla et al. 2003)

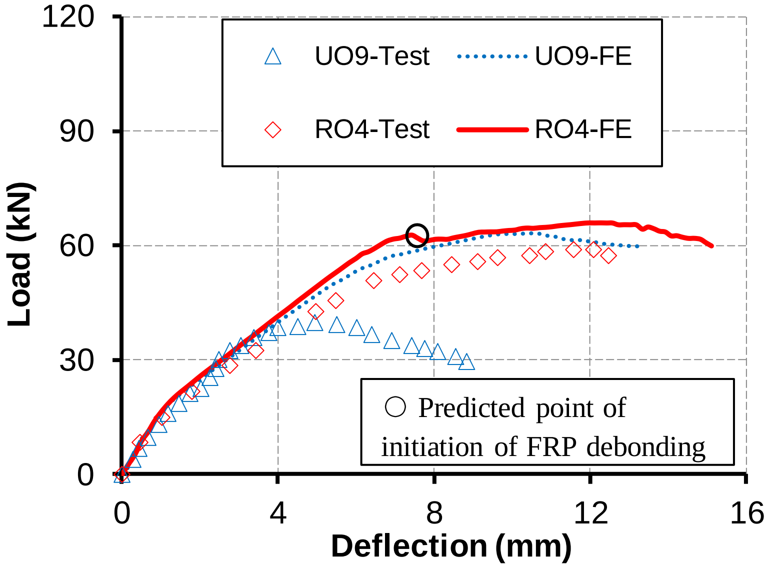

(f) RO4 versus UO9 (300×100) (Abdalla et al. 2003)

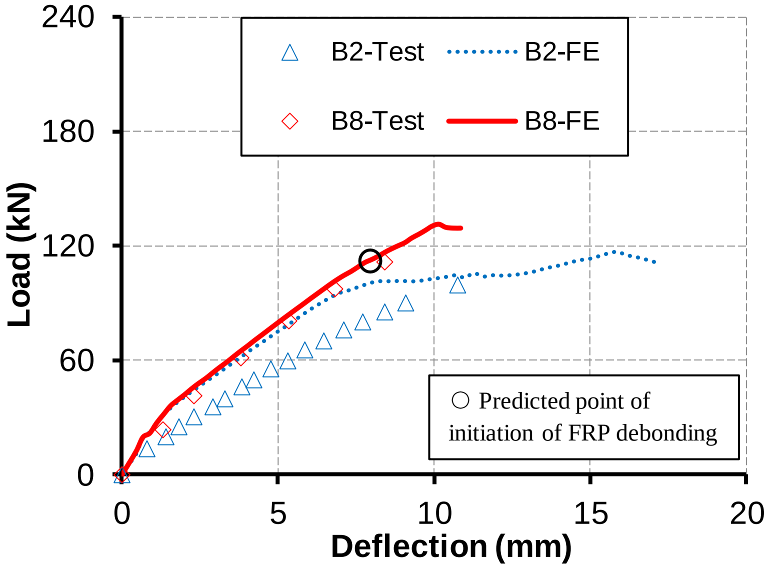

(g) B8 versus B2(450×150) (Allam 2005)

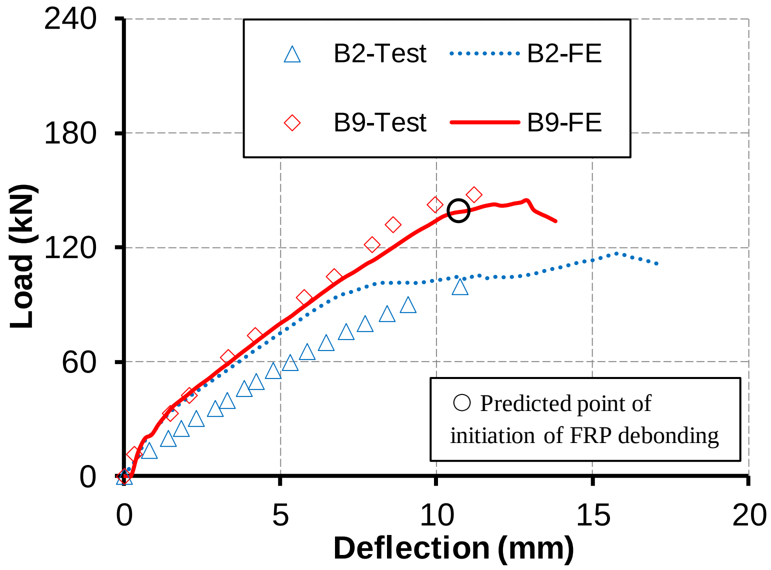

(h) B9 versus B2 (450×150) (Allam 2005)

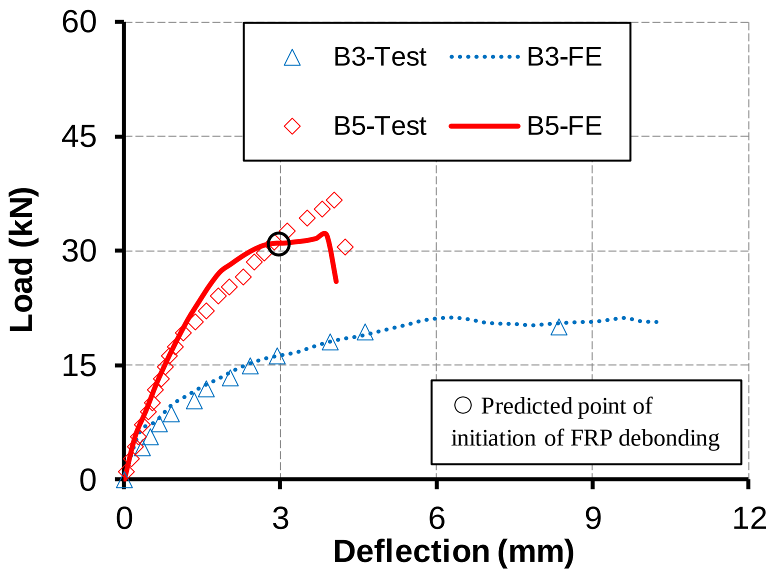

(i) B5 versus B3 (210x210) (Chin et al. 2012)

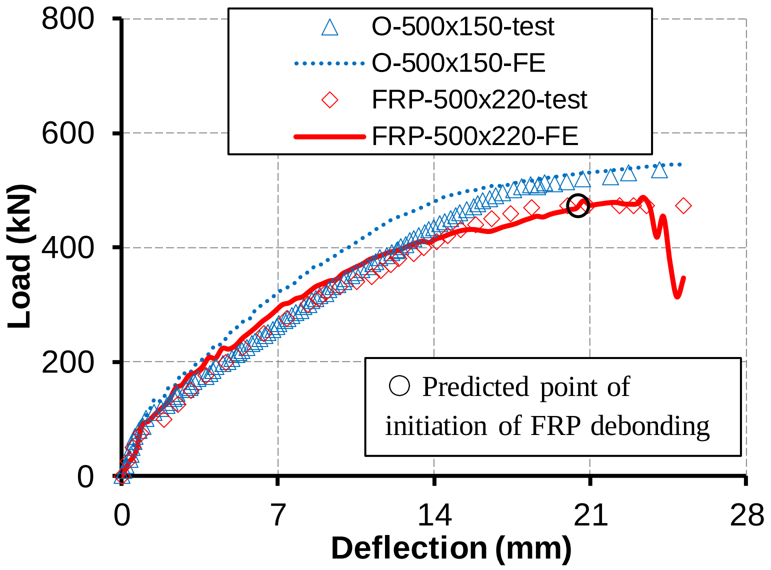

(j) FRP-500×220 versus O-500×150 (Teng et al. 2013)

Figure 4.6. Comparison between un-strengthened and FRP-strengthened beams

(a) FRP debonding at the opening corner nearest to the loading point

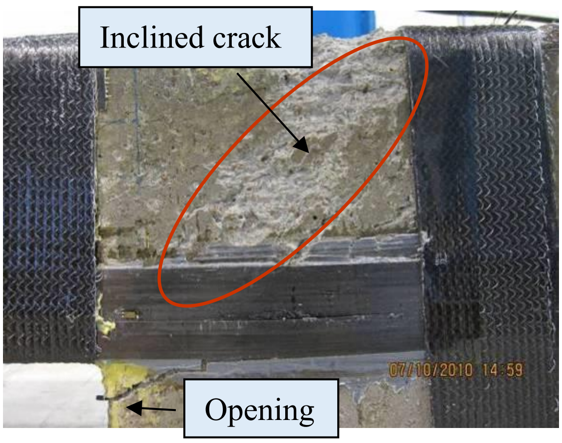

(b) Inclined crack at the opening corner nearest to the loading point

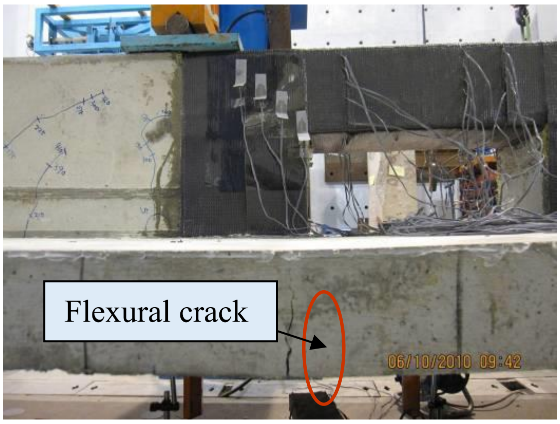

(c) Flexural crack at one end (closer to the loading point) of the flange chord near its bottom surface

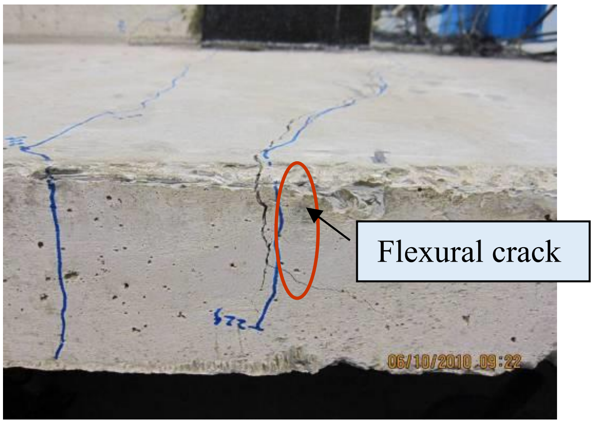

(d) Flexural crack at the other end (i.e., closer to the corresponding support) of the flange chord near its top surface

Figure 4.7. Failure mode of Specimen FRP-500×220 tested by Prof. Teng's group (Teng et al. 2013)

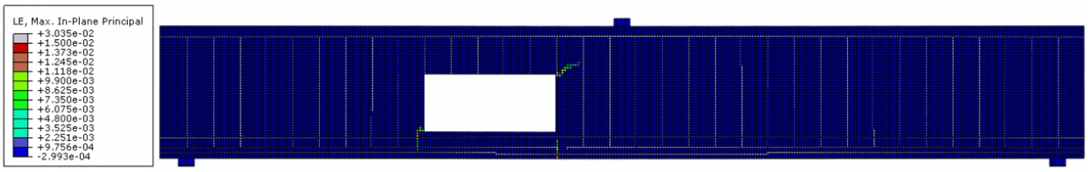

(a) 110 kN

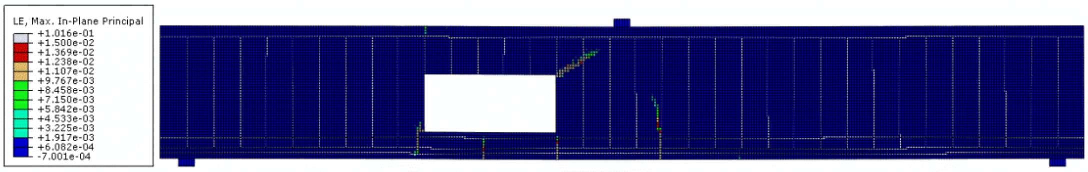

(b) 224 kN

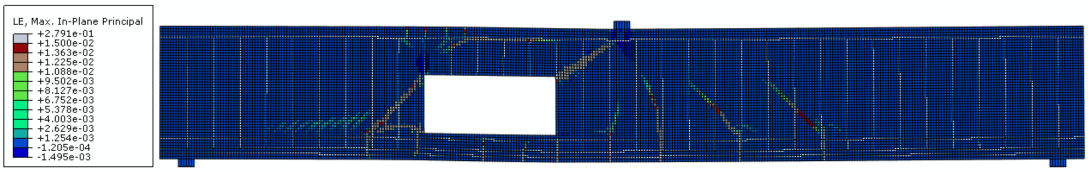

(c) 384 kN

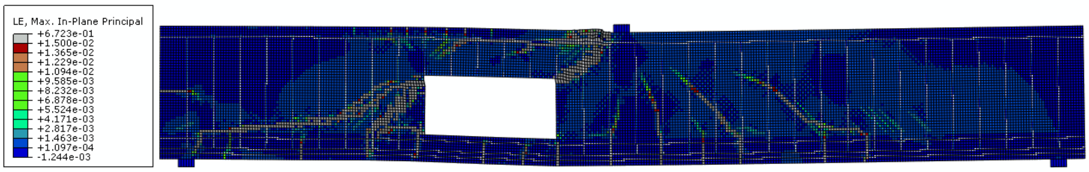

(d) 455 kN

Figure 4.8. Predicted failure process of Specimen FRP-500×220 tested by Prof. Teng's group (Teng et al. 2013)

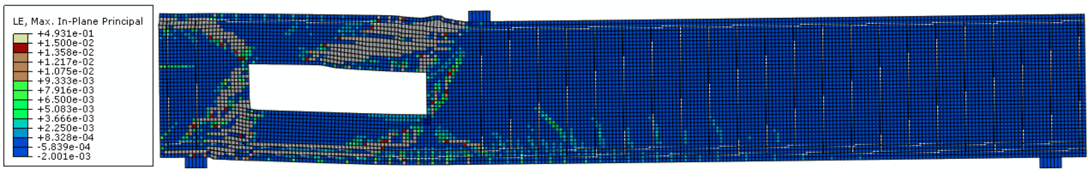

(a) S1-500×120 (Maaddawy and Ariss 2012)

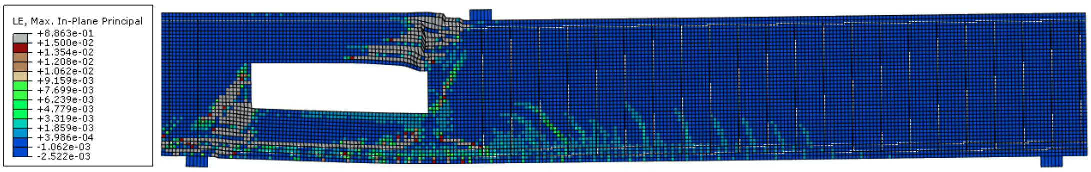

(b) S2-500×120 (Maaddawy and Ariss 2012)

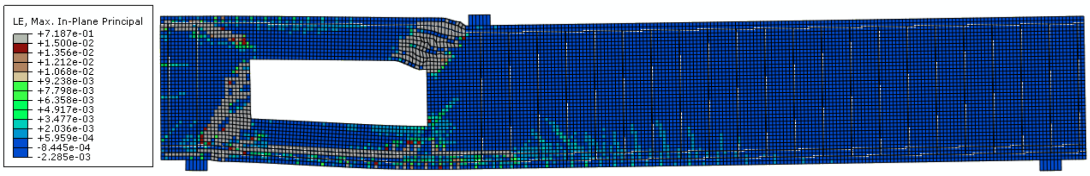

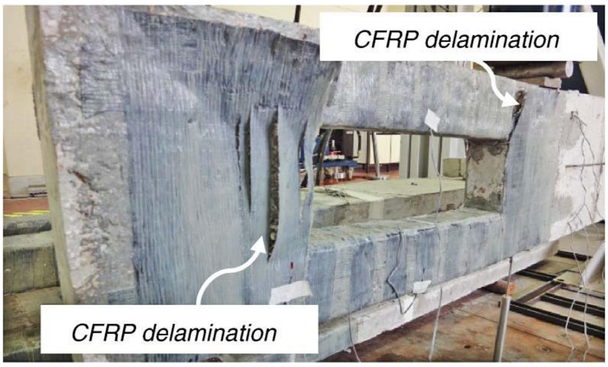

(Extracted from Maaddawy and Ariss 2012)

(c) S1-500×160

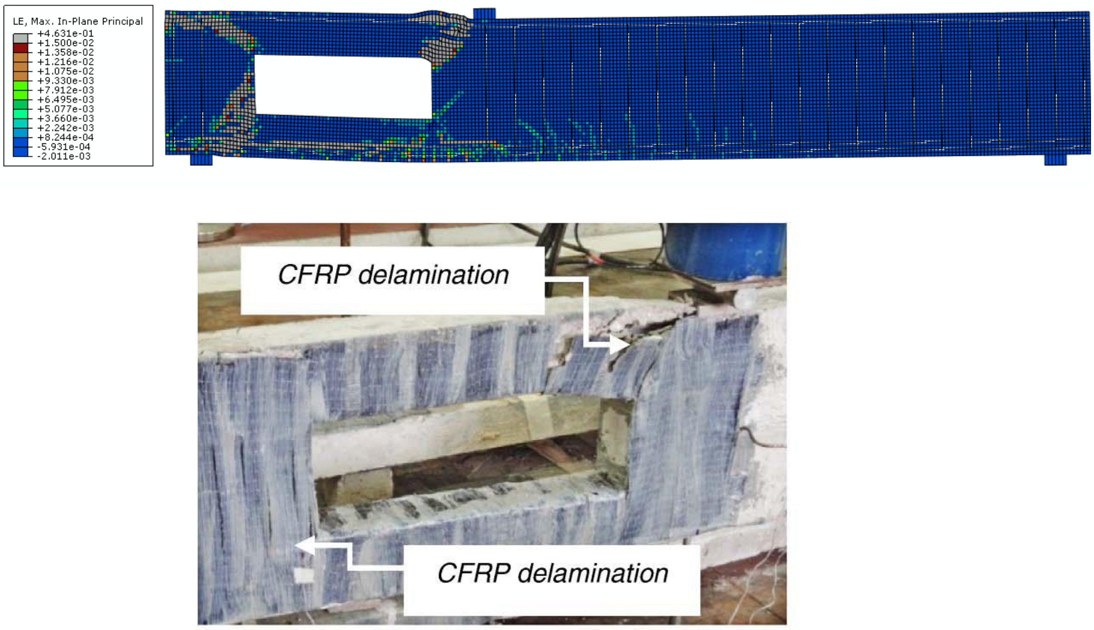

(Extracted from Maaddawy and Ariss 2012)

(d) S2-500×160

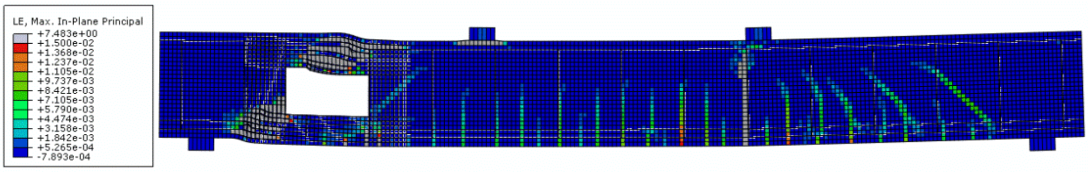

(e) RO3 (200×100) (Abdalla et al. 2003)

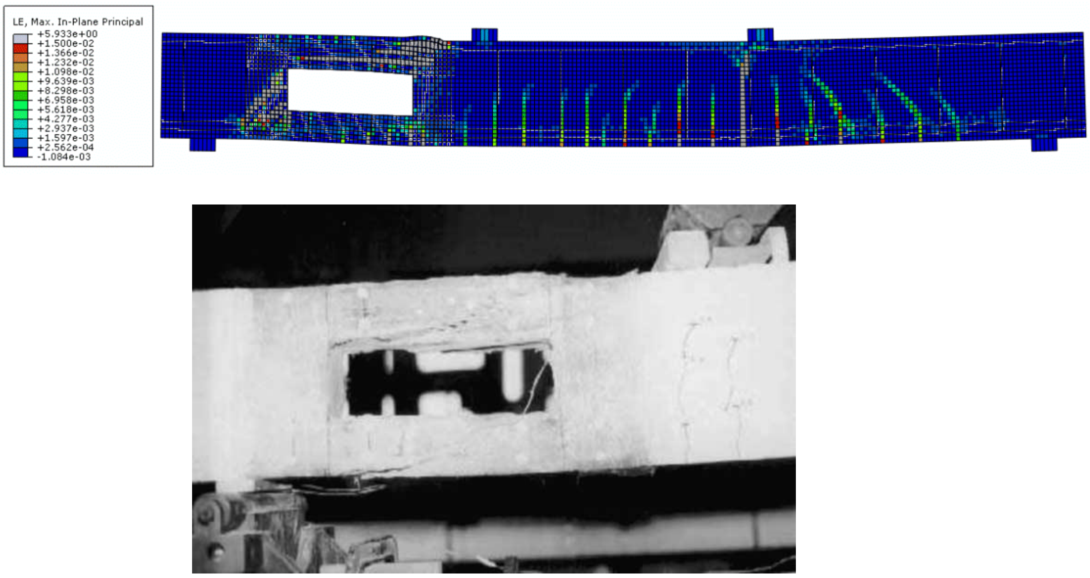

(Extracted from Abdalla et al. 2003)

(f) RO4 (300×100)

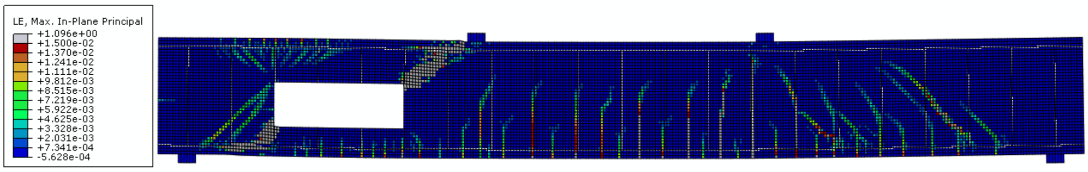

(g) B8 (450×150) (Allam 2005)

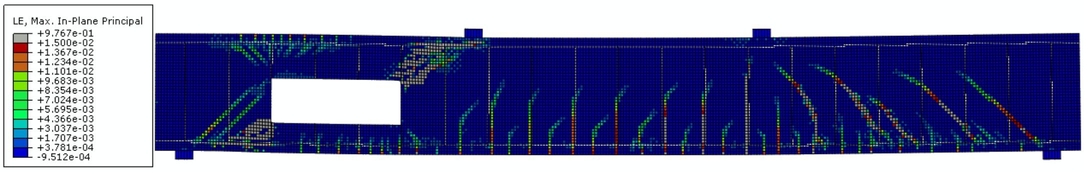

(h) B9 (450×150) (Allam 2005)

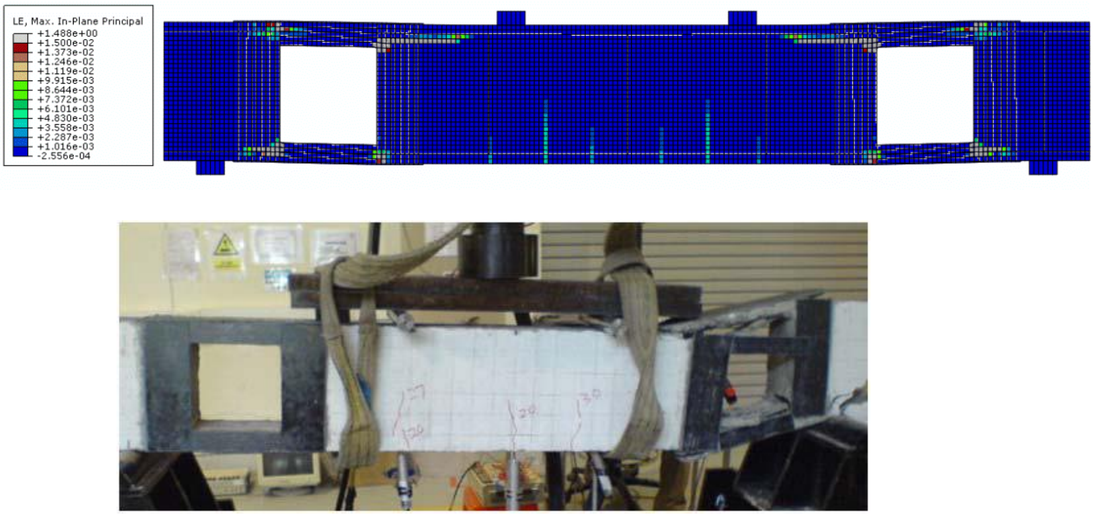

(Extracted from Chin et al. 2012)

(i) B5 (210×210)

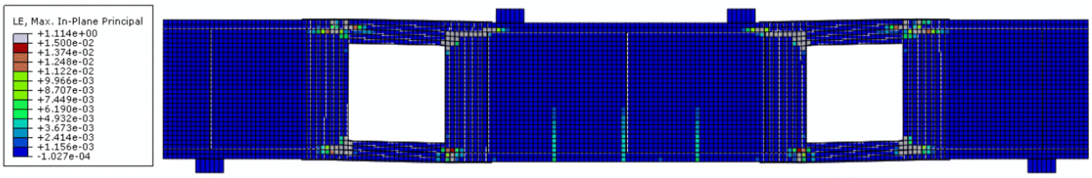

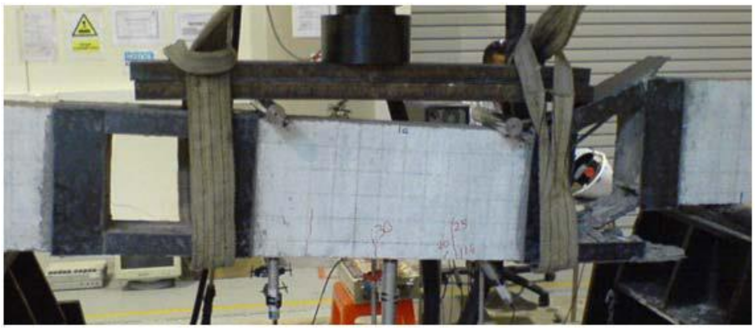

(Extracted from Chin et al. 2012)

(j) B6 (210×210)

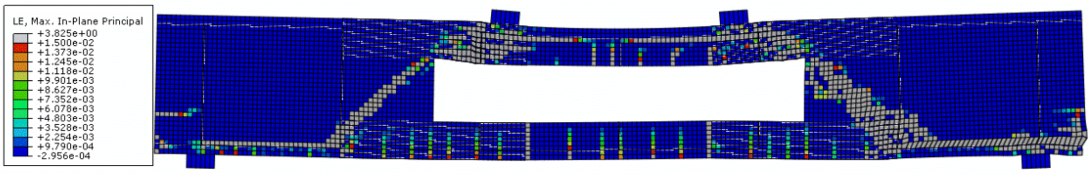

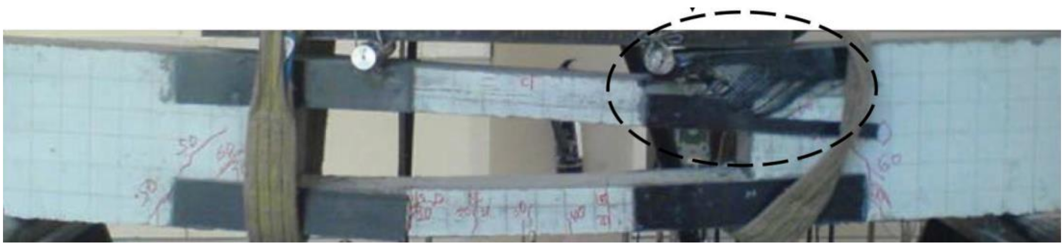

(Extracted from Chin et al. 2016)

(k) SBRO (800×140)

Figure 4.9. Predicted crack patterns at failure

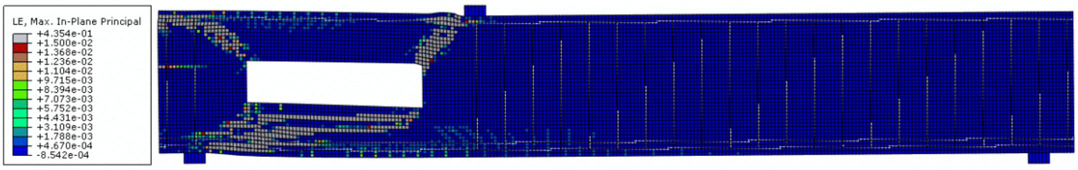

(a) CN-500×120

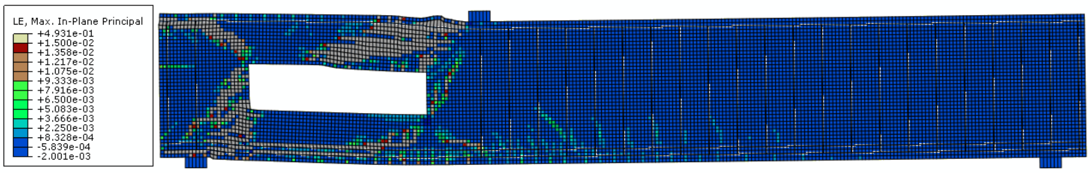

(b) S1-500×120

Figure 4.10. Comparison of predicted crack patterns at failure between un-strengthened and FRP-strengthened beams

CHAPTER 5

RC T-SECTION BEAMS WITH A WEB OPENING FOR FLEXURAL WEAKENING AND CFRP SHEAR STRENGTHENING: TESTS

5.1 INTRODUCTION

As reviewed in Chapter 2, nine experimental studies in the open literature (Mansur et al. 1999; Abdalla et al. 2003; Allam 2005; Maaddawy and Sherif 2009; Pimanmas 2010; Chin et al. 2012; Maaddawy and Ariss 2012; Suresh and Prabhavathy 2015; Chin et al. 2016) have addressed the effect of drilling an opening in an existing beam and the design of the associated strengthening measure. All nine studies except Suresh and Prabhavathy (2015) proposed the use of bonded FRP reinforcement for the strengthening intervention. These studies were motivated by the need to create openings in an existing structure for the passage of utility ducts and pipes, and were thus focused on restoring the strength of the beam through FRP strengthening. These studies confirmed the significant strength reduction due to the creation of an opening in the beam and the feasibility of FRP strengthening to compensate for the weakening effect of the opening. Among the different FRP strengthening schemes explored, the use of bonded U jackets/complete wraps/FRP laminates (Mansur et al. 1999; Abdalla et al. 2003; Allam 2005; Maaddawy and Sherif 2009; Chin et al. 2012; Maaddawy and Ariss 2012; Chin et al. 2016) as well as diagonal near-surface mounted FRP bars at corners (Pimanmas 2010) were found to be effective in controlling shear cracks and shear failures emanating from the corners. However, most existing experimental studies focused on rectangular beams, with only the study of Mansur et al. (1999) being concerned with T-section beams, so more experimental studies are obviously needed to investigate the effectiveness of drilling a web opening in T-section beams to deduce their flexural capacity substantially and local strengthening using CFRP to avoid shear failure. Thus, an experimental study on full-scale RC T-section beams with a web opening and local FRP strengthening was conducted. The test results are presented and interpreted in the present chapter.

In the present chapter, unless otherwise specified: (1) in presenting the results, it is assumed that the beam is so positioned that the web opening is located in the right shear span of the beam. Therefore, the left end of a web/flange chord is the end closer to the loading point while the right end of a web/flange chord is the end closer to the right support; and (2) the position terms “top” and “bottom” refer to the actual positions in the beam in the testing configuration: the flange of the beam is at the bottom of the beam in a negative bending test but at the top of the beam in a positive bending test.

5.2 EXPERIMENTAL PROGRAM

5.2.1 Specimen details

A total of 14 full-scale RC beams, including one rectangular beam and 13 T-section beams, were tested in three-point bending in this experimental program. The tests were conducted in two batches and the studied parameters covered the dimension of web opening (i.e., length × height) and the effect of FRP strengthening. Batch-1contained 8 specimens, in which 2 specimens (i.e., CB-Rec and CB-T) did not have web openings and were treated as control specimens. CB-Rec was a rectangular beam which was used to simulate the situation where the contribution from cast-in-place slab was ignored in the design, while CB-T was a T-section beam which was used to represent the real situation in the structure where the slab makes an important contribution to the flexural capacity of the beam. The remaining 6 specimens were T-section RC beams which had the same dimensions as CB-T but had a web opening in one of the two shear spans. These specimens were used to study the effect of web openings on the behaviour of T-section RC beams, and web openings of two different sizes (length × height being 700 mm × 300 mm and 800 mm × 280 mm, respectively) were investigated. For each web opening size, three specimens were tested, with one having an un-strengthened web opening tested in negative bending, and the other two having an FRP-strengthened web opening and tested in negative bending and positive bending, respectively. In the present context, the web opening in a T-section RC beam should ideally reduce the sum of the negative flexural capacity and the positive flexural capacity of the T-section beam to that of the rectangular beam CB-Rec (i.e., to offset the flexural contribution from the cast-in-place slab ignored in design). For the same reason, the FRP strengthening of the web opening should ideally compensate only the loss of shear capacity of the beam due to a web opening. All the T-section beams had the same dimensions: a clear span of 3300 mm, an overall depth of 500 mm, a web thickness of 250 mm, a flange thickness of 100 mm and a flange width of 1450 mm [i.e., designed according to Chinese design code for concrete structures GB-50010 (2010)]. The control specimen CB-Rec had a clear span of 3300 mm, a depth of 500 mm and a width of 250 mm.

The test results to be discussed in later sections showed that the two web opening sizes studied in Batch-1 could reduce the flexural capacity of the T-section RC beams to a much lower value than that of CB-Rec, indicating that the web opening sizes were too large. Therefore, tests of Batch-2 with smaller web openings were conducted to further investigate the effect of web opening on the flexural behaviour of T-section RC beams. Batch-2 consisted of 6 specimens covering four different web opening sizes (length × height being 600 mm × 220 mm, 700 mm × 200 mm, 600 mm × 280 mm and 700mm × 260 mm, respectively). For web openings of 600 mm × 220 mm and 700 mm × 200 mm, each web opening size contained two specimens with one having an un-strengthened web opening and the other one having an FRP-strengthened web opening. For web openings of 600 mm × 280 mm and 700 mm × 260 mm, only specimens with an FRP-strengthened web opening were tested. The specimens in Batch-2 were all tested in negative bending. As examined in Chapters 3 and 4, the BC model with SECANT modulus provides the best predictions for the existing RC beams with a web opening. Thus, this model was used to design the first batch of the test specimens. After testing the first batch of the test specimens, in which all specimens exhibited the flexural mode of failure, it was found that the BC model with SECANT modulus highly overestimated the strength of all specimens, while the DP model could well predict the strength of all specimens (the details will be explained in Chapter 6). Therefore, the DP model was used to design the second batch of the test specimens. It was found from the preliminary FE predictions that the reduction in the strength of the beam caused by an increase of 20 mm in the height of the web opening was comparable to that caused by an increase of 100 mm in the length of the web opening (e.g, O-700×300-N and O-800×280-N; F-700×300-N and F-800×280-N). Therefore, for each kind of opening size (i.e. large, medium or small opening), two opening sizes (e.g, 700×300 and 800×280) were chosen for examination. In this sense, the two specimens can be regarded as repeated tests.

Details of all tested beams in Batch-1 and Batch -2 are listed in Table 5.1, in which the specimens are named as follows: (1) for specimens with an un-strengthened web opening, the name starts with a letter of “O”, followed by a three-digit number to represent the length of the opening, another three-digit number to represent the height of the opening, and the letter “N” for a specimen tested in negative bending or the letter “P” for a specimen tested in positive bending; and (2) specimens with an FRP-strengthened web opening are similarly named but with “O” being replaced by “F” as the first letter.

The details of Specimens CB-Rec, CB-T and O-700×300-N are shown as examples in Fig. 5.1, in which the layout of the longitudinal/shear steel reinforcement and the locations of web openings are clearly given. The rectangular beam CB-Rec had three longitudinal steel bars of 20 mm in the compression zone, four longitudinal steel bars of 20 mm in the tension zone and transverse steel bars (stirrups) of 8 mm with a spacing of 200 mm. For the T-section beams, in each side of the flange six steel bars of 8 mm with a spacing of 200 mm were used as the longitudinal steel reinforcement, with three near the top surface of the flange and the other three near the bottom surface. The transverse steel reinforcement in the flange was also steel bars of 8 mm with a spacing of 200 mm. The concrete cover to the longitudinal steel reinforcement was 30 mm for the rectangular beam or the web of a T-section beam and 15 mm for the flange of a T-section beam. A web opening was created in only one of the two shear spans of each beam. The web opening was such located that (Fig. 5.1): (1) the horizontal distance from the loading point to the nearer vertical edge of the web opening was 250 mm, considering that the distance between the edge of the column and the nearer edge of the opening was assumed to be 250 mm; and (2) one of the horizontal edges of the web opening coincided with the web-flange intersection for ease of making the opening and subsequent theoretical studies.

5.2.2 Preparation of specimens

5.2.2.1 Formation of web opening

Two approaches were adopted in the present study to make the web openings. In the first approach, the web openings were pre-formed by manipulating the formwork for casting the concrete. The stirrups intersected with the web opening were carefully cut according to the size of the web opening. One of the pre-formed web openings is shown in Fig. 5.2. This approach is suitable for the new construction of RC beams with web openings but does not suit the scenario of web weakening of existing RC beams. Therefore, another approach was also examined in the present study to verify the feasibility of post-cutting web openings in the existing RC beams. In the second approach, the web openings were post-cut after 28 days' curing of the concrete by adopting the following three steps: (1) drill small round holes along the boundary of the opening and cut the stirrups passing through the opening (Fig. 5.3a); (2) remove the concrete chunk to form a rough opening (Fig. 5.3b); (3) chip away the extrusive concrete by using an electric chisel along the boundary of the opening (Fig. 5.3c); and (4) polish the boundary of the opening by using a grinding machine (Fig. 5.3d). The web openings in most specimens were prepared by using the first approach and the rest ones by using the second approach, as shown in Table 5.1. The web openings in most specimens tested in this study were prepared by using the pre-forming method as the pre-forming method is much easier to operate. And to verify the feasibility of post-cut web openings in the existing RC beams, the web openings in some specimens were post-cut. The candidate was very careful in cutting the openings in the cast specimens, and no cracks were found in the opening region after cutting the openings. Moreover, for each kind of opening size (i.e. large, medium or small openings), two opening sizes (e.g, 700×260 and 600×280 for medium openings) were examined. In this sense, they can be regarded as repeated tests. For example, the openings of Specimens F-700×260 and F-600×280 were respectively pre-formed and post-cut, but the load-deflection curves of these two specimens almost coincide with each other, which indicates that the two approaches of making openings are almost equivalent. Therefore, both approaches were proved to be feasible in fabricating the web opening.

5.2.2.2 Installation of FRP jackets

For all specimens with an FRP-strengthened web opening, CFRP was used and the strengthened regions are shown in Fig. 5.4. The web chord was wrapped with one layer of CFRP having a nominal thickness of 0.334 mm after the rounding of its corners to a radius of 25 mm. In addition, to mitigate the possible development of diagonal cracks at the corners of the web opening, a vertical CFRP U-jacket with a nominal thickness of 0.334 mm was installed onto the beam web within 200 mm from each vertical edges of the web opening, as shown in Fig. 5.4a. CFRP strengthening was applied through wet-layup process by adopting the following steps: (1) roughening the concrete surface with a needle gun (Fig. 5.5a); (2) applying a well-mixed primer (Sikadur 330) onto the concrete surface using a clean brush (Fig. 5.5b); (3) laying carbon fibre sheets impregnated with well-mixed epoxy (Sikadur 300) onto the concrete surface (Fig. 5.5c); and (4) slowly rolling the FRP sheet to achieve an even distribution of the resin and release air bubbles (Fig. 5.5d).

5.2.2.3 Fabrication and installation of CFRP spike anchors

To avoid premature debonding of the bonded CFRP U-jacket, CFRP spike anchors were used to anchor the CFRP U-jackets to the flange of the beam (Fig. 5.4). Such spike anchors were first used by Teng and his associates (Teng et al. 2000; Lam and Teng 2001) to mitigate debonding failures of externally bonded FRP reinforcement and have received much recent attention (Kim and Smith 2010; Smith et al. 2011; Zhang and Smith 2012). As shown in Fig. 5.4c, the spike anchors, which were made of the same materials as the CFRP U-jackets, consisted of a hardened bundle of carbon fibres (referred to as the anchor dowel) with a diameter of around 11 mm and a length of 90 mm as well as an 80 mm-long loose fibre tail (referred to as the anchor fan). The anchor dowel was inserted into a predrilled hole in the flange with epoxy at an inclination angle of 20 degree with respect to the side surface of the beam web, while the anchor fan was bonded onto the outer surface of CFRP U-jacket during the wet-layup process. Eight spike anchors were installed on each CFRP U-jacket with four at each end of the CFRP U-jacket. The spike anchors were evenly distributed across the width of a CFRP U-jacket with a spacing of 50 mm (as shown in Fig. 5.4a).

5.2.3 Material properties

Normal strength commercial concrete was used in the present study. For each beam, three plain concrete cylinders (150 mm × 300 mm) were tested on the same day of beam test to determine the concrete cylinder compressive strength. The averaged concrete cylinder compressive strength for each beam specimen is given in Table 5.1.

Standard tensile tests according to BS-18 (1987) were conducted to determine the material properties of steel bars used in the test. Batch-2 was conducted one year later than Batch-1, and unfortunately the candidate could not buy the same type of steel rebars for Batch-2. Therefore, the strengths of steel rebars used in Batch-1 and Batch-2 were different. In Batch-1, the yield stress and ultimate stress of steel bars with a diameter of 8 mm were found to be 307 MPa and 447 MPa, respectively, and those of steel bars with a diameter of 20 mm were 475 MPa and 625 MPa, respectively. In Batch-2, the yield stress and ultimate stress of steel bars with a diameter of 8 mm were found to be 349 MPa and 526 MPa, respectively, and those of steel bars with a diameter of 20 mm were 434 MPa and 559 MPa, respectively. The average measured elastic modulus of all steel bars was 203 GPa.

Tensile tests on 7 coupons were conducted to determine the material properties of

CFRP sheet according to ASTM-3039 (2008). The test region of the FRP coupons had a width of 25 mm and a length of 250 mm, respectively. The tensile strength and elastic modulus were calculated based on the nominal thickness of CFRP sheet (i.e., 0.334 mm per ply as provided by the manufacturer) and the values averaged from the 7 specimens were found to be 2820 MPa and 227 GPa respectively.

5.2.4 Test set-up and instrumentation

A large number of strain gauges were used in the tests to monitor strain development in steel bars and FRP. The arrangement of strain gauges in all specimens with a web opening was the same, so Specimen F-700×300-N is used as an example here to explain the layout of strain gauges. As shown in Fig. 5.6a, the longitudinal steel bars are divided into three groups: the longitudinal steel bars near the bottom surface of the flange (i.e., six bars in the flange and four in the web) are termed as “bottom steel bars”, those near the top surface of the flange (i.e., six bars in the flange) are termed as “middle steel bars”, and those near the upper end of the web (i.e., three bars in the web) are termed as “top steel bars”. By taking advantage of symmetry, half of the bottom steel bars on the same side of the beam (i.e., three bars in the flange and two in the web) were monitored using strain gauges (Fig. 5.6b). In addition, the outmost bottom steel bar on the other side of the flange was also monitored using strain gauges. For each selected longitudinal steel bar, four strain gauges, corresponding to the following critical positions respectively were installed: the mid-span of the beam as well as the two vertical edges and mid-length of the web opening. Of the three top steel bars, two steel bars, including the middle one, were monitored using strain gauges (Fig. 5.6c); for each steel bar, the arrangement of the strain gauges is the same as that for the monitored bottom steel bars. For middle steel bars, the two middle bars on each side of the flange were monitored, and for each bar a single strain gauge was installed at the mid-span of the beam (Fig. 5.6d).

The layout of strain gauges on the CFRP is shown in Fig. 5.7. For the CFRP wrap on the web chord, a total of 15 strain gauges were installed near the following three positions: the two ends and the mid-span of the web chord. At each position, five strain gauges were employed: two on the bottom surface of the chord, two on the top surface of the chord and one on the side surface of the chord, as shown in Fig. 5.7. The two strain gauges on the top or bottom surface of the chord were placed near the mid-length of the chord with one being in the longitudinal direction and the other being in the hoop direction. The strain gauge on the side surface of the chord was placed at the mid-height of the chord in the hoop direction. For each of the two CFRP U-jackets, four evenly distributed strain gauges were installed vertically (i.e., along the fibre direction of the CFRP) on one of the two legs of the jacket, leading to a total of eight strain gauges on two CFRP U-jackets as shown in Fig. 5.7.

The arrangement of linear variable displacement transducers (LVDTs) is shown in Fig. 5.8. For the T-section beams in negative bending, three LVDTs were placed on the bottom surface of the flange at the mid-span of the beam, with one being at the mid-width of the flange and the other two being at 300 mm away from the nearer edge of the flange, respectively (i.e., 01, 02 and 03 shown in Fig. 5.8);

similarly, three LVDTs were installed on the bottom surface of the flange at the mid-length of the web opening (i.e., 04, 05 and 06 in Fig. 5.8). For the rectangular beam and T-section beams in positive bending, only one LVDT was applied on the bottom surface of the web at the mid-span of the beam and mid-width of the web. In addition, five LVDTs were installed on the top surface (for specimens in negative bending) or bottom surface (for specimens in positive bending) of the web chord and evenly distributed over the web chord, as shown in Fig. 5.8.

All beam specimens except Specimens F-700×300-P and F-800×280-P were tested in three-point negative bending, in which the beam was so placed that the flange of the beam was at the bottom, and thus the flange was in tension under the downward point load (Fig. 5.9). For specimens F-700×300-P and F-800×280-P, the beam was placed in the opposite direction. The downward point load was applied at the mid-span of the beam by a hydraulic jack.

5.3 FAILURE MODES

The failure modes of all specimens are shown in Fig. 5.10. The two control specimens (i.e., CB-Rec and CB-T) failed by crushing of compressive concrete at the mid-span of the beam after the yielding of tension steel bars, which is the typical flexural failure mode of RC beams (Figs. 5.10a and b).

For the four specimens with an un-strengthened web opening (i.e., Specimens O-700x300-N, O-800x280-N, O-600x220-N and O-700x200-N), an inclined crack (at around 45 degrees to the horizontal direction) appeared first at the top-left corner of the web opening (i.e., the corner nearest to the loading point), followed by the occurrence of a horizontal crack between the web and the flange at the bottom-right corner of the web opening (i.e., the corner nearest to the right support) (Figs. 5.10c, d, i and j), and then vertical flexural cracks in the flange which was in tension happened and developed. Afterwards, the development of cracks diverged depending on the size of web opening. For O-700×300-N and O-800×280-N which had larger web openings, subsequent major cracks happened near the right end of the web chord, including vertical cracks near the top surface of the chord and nearly horizontal cracks near the bottom surface of the chord. The final failure of these two beams was controlled by local flexural failure at the right end of the web chord and the left end of the flange chord (i.e., crushing of compressive concrete of the web and flange chords) and local mixed flexural and shear failure at the left end of the web chord and the right end of the flange chord, as shown in Figs. 5.10c and d. For Specimens O-600×220-N and O-700×200-N with smaller web openings (i.e., a larger height of the top chord), diagonal cracks (at around 30 to 45 degrees to the horizontal direction) initiated and developed in span of the web chord and finally controlled the failure of the specimens (Figs. 5.10i and j).

For the eight beam specimens with a CFRP-strengthened web opening, due to the existence of CFRP wraps and CFRP U-jackets, the shear cracks near the ends of the web chord were well prevented/mitigated. All these specimens failed by local flexural failure at the two ends of web chord as well as flange chord; the formation of plastic hinges at the ends of the web and flange chords can be clearly seen (Figs. 5.10e-h, k-n).

5.4 LOAD-DEFLECTION RESPONSE OF BEAMS

5.4.1 Load-deflection curves

Control specimens

The load-deflection (mid-span deflection) curves of test specimens are shown in Fig. 5.11, and the key load levels (i.e., cracking load, yield load and ultimate load) are listed in Table 5.2. The mid-span deflection shown in Fig. 5.11 was averaged from the readings of three LVDTs (i.e., 01, 02 and 03 as shown in Fig. 5.8). The two control specimens (i.e., CB-Rec and CB-T) exhibited flexural load-deflection responses typical of conventional RC beams with three typical segments: (1) the first segment: before cracking of the bottom concrete in tension, the load increased nearly linearly with the mid-span deflection; (2) the second segment: after tensile cracking of the concrete, the load still increased with the mid-span deflection but at a much smaller slope (i.e. stiffness); (3) the third segment: after yielding of bottom longitudinal steel bars, the load only showed a very slight increase with the mid-span deflection, where the slight load increases can be attributed to the hardening of the steel bars. Due to the existence of a flange, Specimen CB-T had a much larger cracking load (around 160 kN) as well as a much larger yield load (478 kN) than Specimen CB-Rec which had a cracking load of 55 kN and a yield load of 340 kN, indicating that the flange (i.e., floor slab in a real structure) can significantly enhance the negative flexural capacity of a beam. It should be noted that the test results of Specimens CB-Rec and CB-T can only be used for comparisons of Batch-1's specimens tested in negative bending, as the yielding and ultimate strength of the longitudinal steel bars with a diameter of 20 mm used in Batch-2 were a little smaller than those used in Batch-1. Therefore, numerical results obtained using the finite element (FE) approach well-established by Chen et al. (2011) will be used for the comparisons of Batch-1's specimens tested in positive bending and Batch-2's specimens. To demonstrate the accuracy of the FE approach, the load-deflection curves of Specimens CB-Rec and CB-T predicted by the FE approach are also plotted in Fig. 5.11a, from which it can be seen that FE predictions are in close agreement with the test results. In the present comparisons, the overall trend of the predicted load-deflection curves and the predicted load-carrying capacities of the two control beams without a web opening were most important. Only the predicted load-carrying capacities of the control beams were used in the subsequent comparisons. Therefore, the applied maximum displacements in the FE modelling were not sufficiently large to save the computing time and thus the ending points of the predicted load-deflection curves did not correspond to the ultimate deflection at failure.

In the remainder of the section, comparisons are focused on differences in load-carrying capacity between the rectangular control beam CB-Rec and the T-section beams with an un-strengthened or FRP-strengthened web opening to see which of the studied web opening sizes could most efficiently reduce the capacity of the beam from the value of Specimen CB-T to that of Specimen CB-Rec.

Specimens with a large web opening

The load-deflection curves of Specimens O-700×300-N and O-800×280-N, which had a large size un-strengthened web opening, also have three segments

(Fig. 5.11a), but their second-segment slopes are much smaller than that of either CB-Rec or CB-T; in addition, the third segment indicates slight decreases in the load (i.e., with a negative slope). It should be noted that for RC beams with either an un-strengthened web opening or an FRP-strengthened web opening, the bottom steel bars at the mid-span of the beam did not yield during the loading process. Therefore, the yield load F_y listed in Table 5.2 for the control specimens does not exist in RC beams with a web opening. Instead, the load corresponding to the yielding of bottom steel bars at the left end of the flange chord F_{y1} and the load corresponding to the yielding of steel bars at the right end of the web chord F_{y2} are listed in Table 5.2 for RC beams with a web opening in negative bending. As shown in Table 5.2, the cracking loads F_{cr} of Specimens O-700×300-N and O-800×280-N are 61 kN and 50 kN respectively which are very close to that of Specimen CB-Rec and much smaller than that of Specimen CB-T. The yield loads F_{y1} are respectively 37% and 42% of that of Specimen CB-Rec, and the ultimate loads F_u are respectively around 47% and 46% of that of Specimen CB-Rec. After FRP strengthening (i.e., Specimens F-700×300-N and F-800×280-N), the cracking loads of F-700×300-N and F-800×280-N are nearly unchanged, the slopes of the second segment are slightly increased, the yield loads F_{y1} are respectively increased to 44% and 45% of that of Specimen CB-Rec, and the ultimate loads F_u are respectively increased to 53% and 56% of that of Specimen CB-Rec. Furthermore, the third segments of load-defection curves of an FRP-strengthened specimen is much flatter than that of an un-strengthened beam, indicating that the deformation capacity and ductility of the specimen were also improved by FRP strengthening. However, the yield and ultimate loads of FRP-strengthened specimens are still much lower than those of Specimen CB-Rec, revealing that the web opening sizes in these specimens were too large so that the T-section beams were overly weakened.

Specimens with a small web opening

The load-deflection curves of Specimens O-600×220-N and O-700×200-N which had a small size un-strengthened web opening are shown in Fig. 5.11b. As mentioned earlier, the numerical results of two control beams of Batch 2 (referred to as CB-Rec-2 and CB-T-2 respectively) obtained by using the FE model are used in the comparisons, as shown in Fig. 5.11b. The stiffness of Specimens O-600×220-N and O-700×200-N after cracking of concrete was still lower than that of either CB-Rec-2 or CB-T-2 but much larger than that of specimens with large web openings (i.e., O-700×300-N and O-800×280-N). Shortly after yielding of the specimen, the load experienced an abrupt drop (around 30%-35% of the yielding load) due to the brittle shear failure in the top chord and then gradually dropped to around half of the yielding load. As shown in Table 5.2, the cracking loads of Specimens O-600×220-N and O-700×200-N are respectively 160 % and 120% of that of Specimen CB-Rec-2, the yield loads are respectively around 74% and 79% of that of Specimen CB-Rec-2, and the ultimate loads are respectively around 99% and 94% of that of Specimen CB-Rec-2. With FRP strengthening (i.e., Specimens F-600×220-N and F-700×200-N), the load did not experience a sudden drop after yielding of the specimens, revealing a significantly improved deformation capacity and ductility of the specimens. As can be seen from Table 5.2, the cracking loads of Specimens F-600×220-N and F-700×200-N are both around 202% of the corresponding un-strengthened specimens, the yielding loads are both around 89% of that of Specimen CB-Rec-2, and the ultimate loads are respectively around 121% and 128% of that of Specimen CB-Rec-2. The results indicate that the web opening sizes of 600 mm×220 mm and 700 mm×200 mm are too small to result in satisfactory reductions in the flexural capacity of the T-section beam (i.e., Specimen CB-T-2).

Specimens with a medium web opening

To further investigate the effect of web opening size on the behaviour of the beam, two specimens with a medium size FRP-strengthened web opening (i.e., Specimens F-600×280-N and F-700×260-N) were tested. It can be seen from Fig. 5.11c that the shapes of the load-deflection curves of Specimens F-600×280-N and F-700×260-N are quite similar to those of the two control specimens (i.e., CB-Rec-2 and CB-T-2). As shown in Table 5.2, the cracking loads of the two specimens are both 76 kN which is around 152% of that of Specimen CB-Rec-2, and the ultimate loads are respectively around 81% and 84% of that of Specimen CB-Rec-2. The results reveal that the web opening sizes of 600 mm×280 mm and 700 mm×260 mm are a little larger to meet the desired reduction in the flexural capacity of the T-section beam (i.e., Specimen CB-T-2).

Specimens tested in positive bending

For the two specimens with an FRP-strengthened web opening (i.e., F-700×300-P and F-800×280-P) tested in positive bending, the numerical results of the two corresponding control beams in positive bending [referred to as CB-Rec-P (FE) and CB-T-P (FE), respectively], obtained from FE analyses, are used for comparison (Fig. 5.11d). It can be seen from Fig. 5.11d that the shapes of the load-deflection curves of Specimens F-700×300-P and F-800×280-P are quite similar to those of the two control specimens [i.e., CB-Rec-P (FE) and CB-T-P (FE)]. It should be noted that for specimens tested in positive bending, F_{y1} listed in Table 5.2 corresponds to the yielding of steel bars at the left end of the web chord and F_{y2} corresponds to the yielding of steel bars at the right end of the flange chord. As shown in Table 5.2, the cracking loads of Specimens F-700×300-P and F-800×280-P are respectively around 110% and 120% of that of CB-Rec-P (FE), the yield loads F_{y1} are respectively around 53% and 62% of that of CB-Rec-P (FE), and the ultimate loads F_u are respectively around 84% and 80% of that of CB-Rec-P (FE). Compared with the test results of corresponding specimens in negative bending (i.e., F-700×300-N and F-800×280-N, whose negative bending capacities are respectively around 53% and 56% of that of the control beam CB-Rec), it is obvious that the effect of a web opening on the positive flexural capacity of the beam is much less substantial than that on the negative flexural capacity of the beam. To clarify the influence of web openings on the positive flexural capacity of T-section beams, further experimental studies are needed.

5.4.2 Sum of negative and positive flexural capacities of the beam

In the seismic retrofit of an internal beam-column joint (the simplest and common case) of a plane RC frame to convert a strong beam-weak column scenario to a weak beam-strong column scenario, the sum of reductions in flexural capacity of both beams on the two sides of the joint needs to ensure that the sum of flexural capacities of the two beams is smaller than that of the two columns above and below the joint. In this comparison, the two beams are in negative or positive bending, respectively, so the sum of the negative flexural capacity and the positive flexural capacity of the beam section is the key parameter (referred to as the sum of flexural capacities or SFC). Obviously, the column above and below the joint are also bent in opposite directions, but this is generally not a significant issue as the column are typically symmetrically reinforced.

The SFCs of the two control specimens (i.e., CB-Rec, CB-T) as well as the two T-section beams with a large size of FRP-strengthened web opening (700 mm × 300 mm and 800 mm × 280 mm) are listed in Table 5.3. It should be noted that for web openings of small/medium sizes, there were no specimen tested in positive bending. Therefore, the SFCs of specimens with a small/medium FRP-strengthened web opening are not available from the test, but will be examined in Chapter 7 with the help of the proposed strength model. It can be seen from Table 5.3 that the SFC of Specimen CB-T is 124% of that of the rectangular control beam CB-Rec, which indicates that the flange (i.e., the existence of a floor slab in a real structure) has a substantial effect on the SFC. With the presence of an FRP-strengthened web opening of 700 mm × 300 mm or 800 mm × 280 mm, the SFC of the T-section beam can be reduced to around 66% of that of the control beam CB-Rec, indicating that the proposed beam opening technique is very effective in reducing the SFC. These results also indicate that in many practical cases, web opening sizes smaller than those examined here are sufficient to achieve the necessary degree of reduction in the SFC for the purpose of seismic retrofit.

5.4.3 Effect of web opening size

From the above comparisons, it can be seen that a larger web opening unusually gives a lower load-carrying capacity and stiffness of the beam but a better ductility of the beam (as the failure mode may be changed from brittle shear failure in the top chord to the local flexural or mixed-mode failure at the ends of the chords). Increasing either the length of web opening or the height of web opening could reduce the load-carrying capacity of the beam. However, increasing the height of web opening was found to be more efficient in reducing the load-carry capacity than increasing the length, as evidenced by the result that the reduction in the load-carrying capacity of the beam caused by an increase of 20 mm in the height of the web opening is comparable to that caused by an increase of 100 mm in the length of the web opening (e.g, O-700×300-N and O-800×280-N; F-700×300-N and F-800×280-N). Considering that the height of the web opening directly influences the height of the top chord, it is not unreasonable to suppose that the reduction in the load-carrying capacity of the beam is highly dependent on the height of the top chord.

5.4.4 Effect of FRP strengthening

The FRP strengthening system, including the CFRP wrap on the web chord and the CFRP U-jackets with spike anchors on the beam web, not only enhanced the load-carrying capacity and stiffness of the beam but also significantly improved the deformation capacity as well as ductility of the beam. The performance improvement due to bonded FRP reinforcement can be attributed to the following reasons: (1) the CFRP wrap on the web chord enhances its shear resistance and provides confinement to the chord when it is in compression, thus enhancing the compressive strength and ductility of the web chord; and (2) the FRP U-jackets with spike anchors restrain the development of cracks at the two ends of the web chord and the horizontal crack between the web and the flange of the beam, thus mitigating the brittle failure of the beam induced by these cracks.

5.5 DEFLECTION SHAPES OF THE WEB CHORD

The vertical deflections of the web chord recorded by the five LVDTs evenly distributed over the chord length (i.e. 09-13 in Fig. 5.8) are shown in Fig. 5.12. It can be seen from Fig. 5.12 that the deflected shapes of the web chord are nearly linear for all the selected load levels no matter whether FRP strengthening was provided or not. Specimens with an FRP-strengthened web opening experienced a larger ultimate deflection than the corresponding specimens with an un-strengthened web opening. This can be attributed to two reasons: (1) the CFRP U-jackets prevented the shear failure of the beam and thus improved the deformation capacity of the beam; (2) the FRP wrap on the web chord provided confinement to the web chord and thus directly enhanced its deformation capacity.

It is interesting to notice that some specimens (i.e., Specimens O-700×200-N, F-700×200-N, O-600×220-N and F-600×220-N) only have downward defections (i.e., negative values in the figures) of the web chord over its span while some specimens (i.e., Specimens O-800×280-N, F-800×280-N, O-700×300-N, F-700×300-N, F-700×260-N, F-600×280-N, F-800×280-P and F-700×300-P) have a zero-deflection point (where the deflection of the chord is equal to zero) in the deflected shapes of the web chord, with the deflections being downward on the left side of the zero-deflection point (i.e., closer to the loading point) while upward (i.e., positive values in the figures) on the right side (i.e., closer to the right support). A further investigation of these deflected shapes indicates that a larger length-to-height ratio of the web chord gives a higher possibility of the formation of zero-deflection point in the span of the web chord. Furthermore, the relative position of the zero-deflection point is also dependant on the length-to-height ratio of the web chord: a larger ratio gives a larger relative distance from the zero-deflection point to the right end of the top chord (defined as the distance from the zero-deflection point to the right end of the top chord divided by the total length of the chord). For example, the relative distance from the zero-deflection point to the right end of the top chord of F-800×280-N is 0.25 (i.e., 200 mm/800 mm), which is larger than that of Specimen F-600×280-N (i.e., 0.17 =100 mm/600 mm). This is because the former specimen has a length-to-height ratio of the top chord of 6.7 (i.e., 800 mm/120 mm), which is larger than that of the latter specimen (i.e., 5.0= 600 mm/120 mm).

5.6 STRAINS IN THE FRP AND THE STEEL BARS

5.6.1 Strains in the FRP

An examination of the strain readings in the FRP revealed that the general features (e.g. shapes) of strain distributions are similar for all specimens with an FRP-strengthened web opening, thus Specimen F-700×300-N is discussed herein as an example to demonstrate the development of strains in the FRP during the loading process. The strain distributions in the CFRP wrap and CFRP U-jackets are shown in Figs. 5.13, 5.14 and 5.15, respectively; the layout of strain gauges is shown in Fig. 5.7.

Fig. 5.13a shows the readings from the three longitudinal strain gauges installed on the bottom surface of the web chord. It can be seen that all the readings are negative, indicating that the bottom surface of the web chord was in compression. The readings from the three longitudinal strain gauges installed on the top surface of the web chord are shown in Fig. 5.13b. These strain readings indicate that the right end of web chord was subjected to a hogging moment while the left end of the web chord was subjected to a sagging moment; in addition, the mid-span of the web chord was subjected to a small hogging moment. Due to the large bending moments at the two ends of the web chord, plastic hinges developed at the two ends and controlled the final failure of the beam.

The readings from the three hoop strain gauges (on the bottom surface, side surface and top surface of the web chord, respectively) at the right end of the web chord are shown in Fig. 5.14a. These strain readings are positive (i.e., in tension) and small except when the load reached 205.8 kN (corresponding to a mid-span deflection of 17.7 mm), indicating that the FRP wrap was little mobilized to confine the web chord. When the load reached 205.8 kN, the hoop strain on the bottom surface became much larger and reached around 3400 $\mu\varepsilon$. This phenomenon corresponds well to the large compressive readings measured by the longitudinal strain gauge at the same position. The hoop strain readings at the left end shown in Fig. 5.14b indicate that the concrete near the top surface of the web chord was more effectively confined, which again is consistent with the large compressive strains measured by the longitudinal strain gauge located at the same position. The hoop strain readings at the mid-span of the web chord are much smaller, as shown in Fig. 5.14c. The hoop strain readings on the top surface reveal that the FRP was in compression in the hoop direction, which might be because that the concrete near the top surface of the web chord at the mid-span was in tension in the longitudinal direction as recorded by strain gauge WM2 (Fig. 5.13b). In summary, the strain readings indicate that the FRP wrap provided significant confinement to the compressive concrete at both ends of the web chord, where plastic hinges formed. That is, the deformation capacity and ductility of the web chord were much improved by confinement from the FRP wrap.

The readings from the four vertical strain gauges installed on each CFRP U-jacket (see Fig. 5.7) are shown in Fig. 5.15. In general, the strain in the FRP increases from the beam flange to the tip end of the beam web. The larger FRP strain near the tip end of the beam web was due to the development of cracks near the top corners of the web opening. The maximum strain in the CFRP U-jacket closer to the loading point is around 1000 $\mu\varepsilon$, which is larger than that in the U-jacket on the other side of the web opening (around 550 $\mu\varepsilon$). This is because the cracks near the top left corner of the web opening (i.e., the corner closer to the loading point) were wider than those at the top right corner of the web opening, as a result of the larger bending moment acting on the beam cross section passing through the former.

5.6.2 Strains in the steel bars

Due to space limitation, the development of strains in the steel bars is not shown in this chapter. The key observations of the strain readings, however, are summarized in this section. The position of top steel bars, middle steel bars and bottom steel bars can be found in Fig. 5.6a, which indicate that the top steel bars were placed close to the top surface of the web chord, and bottom steel bars were placed close to the bottom surface of the flange chord. It should be noted that the following observations are for specimens in negative bending. For specimens in positive bending, the development of strains in steel bars is similar except the web chord and the flange chord swap their roles.

For the two control specimens (Specimens CB-Rec and CB-T), all top steel bars were in compression while all the bottom and middle steel bars were in tension during the loading process. The yielding of the beam was controlled by the yielding of the bottom and middle steel bars at the mid-span of the beam. On contrary, the yielding of beams with an un-strengthened web opening was not due to the yielding of the bottom/middle steel bars at the mid-span of the beam, instead it was due to the yielding of steel bars at the ends of web/flange chord (i.e., the formation of plastic hinges at their ends). Generally, as the left end of the web/flange chord was under a sagging moment, the top steel bars at the left end of the web chord were in compression while the bottom steel bars at the left end of the flange chord were in tension during the early stage of loading. As the applied load increased, cracking occurred near the bottom surface of web/flange chord, and the natural axis of the cross-section of the web/flange chord at the left end gradually moved towards the top surface of chord. Subsequently, the top steel bars at the left end of the web chord changed from being in compression to being in tension while the tensile strains in the bottom steel bars at the left end of the flange chord further increased. By contrast, the right end of the web/flange chord was under a hogging moment, thus the top steel bars at the right end of the web chord were in tension while the bottom steel bars at the right end of the flange chord were in compression during the early stage of loading. With increases in the applied load, cracking occurred near the top surface of web/flange chord, and the natural axis of the cross-section of the web/flange chord at the right end gradually moved towards the bottom surface of the chord. Subsequently, the tensile strains in the top steel bars at the right end of the web chord kept increasing while the strains in the bottom steel bars at the right end of the flange chord diverged: the bottom steel bars within the beam web were changed from being in compression to being in tension while the bottom steel bars within the flange remained in compression and the strains remained very small.

The process of development of strains in steel bars in specimens with an FRP-strengthened web opening was similar to that in specimens with an un-strengthened web opening, but with two significant differences: (1) due to the existence of CFRP, the development of cracks near the top left corner of web opening was restrained and thus the movement of natural axis was mitigated. As a result, the top steel bars at the left end of the web chord remained in compression till the failure of the beam; and (2) due to the existence of CFRP spike anchors, the development of horizontal cracks between the web and flange was restrained, and thus a larger hogging moment could be resisted at the right end of the flange chord. Therefore, the bottom steel bars at the right end of the flange chord within both the beam web and the flange were finally changed from being in compression to being in tension.

5.7 Concluding remarks

To demonstrate the effectiveness of the proposed beam opening (BO) technique, a total of 14 full-scale RC beams, including one rectangular beam and 13 T-section beams, were tested. Based on the test results, the following conclusions can be drawn:

1) There is no significant behavioural difference between the specimens prepared by the pre-forming and post-cutting methods. The proposed BO technique (referred to as the post-cutting method) can effectively reduce both the negative flexural capacity (i.e., with the beam flange in tension) and the positive flexural capacity (i.e., with the beam flange in compression) of T-section RC beams;
2) Increasing either the length or the height of web opening reduces the negative flexural capacity of a T-section beam, with the latter being more effective than the former;
3) The proposed FRP strengthening system, including a complete CFRP wrap on the web chord and two properly anchored CFRP U-jackets on the beam web, not only enhances the shear capacity of the beam but also significantly improves the ductility of the failure process; and
4) This experimental study was mainly focused on the influence of web openings on the negative flexural capacity of T-section beams, while the

results of two specimens with an FRP-strengthened web opening tested in positive bending showed that web opening can also reduce the positive flexural capacity of T-section beams. To clarify the influence of web openings on the positive flexural capacity of T-section beams, further experimental studies are needed.

5.8 REFERENCES

Abdalla, H.A., Torkey, A.M., Haggag, H.A. and Abu-Amira, A.F. (2003). "Design against cracking at openings in reinforced concrete beams strengthened with composite sheets", *Composite Structures*, 60(2), 197-204.

Allam, S. M. (2005). "Strengthening of RC beams with large openings in the shear zone", *Alexandria Engineering Journal*, *44*(1), 59-78.

Chin, S.C., Shafiq, N. and Nuruddin, M.F. (2012). "Strengthening of RC beams with large openings in shear by CFRP laminates: experiment and 2D nonlinear finite element analysis", *Research Journal of Applied Sciences Engineering and Technology*, 4(9), 1172-1180.

Chin, S.C., Shafiq, N. and Nuruddin, M.F. (2016). "Behaviour of RC beams with CFRP-strengthened openings", *Structural Concrete*, 17(1), 32-43.

Kim, S.J. and Smith, S.T. (2010). "Pullout strength models for FRP anchors in uncracked concrete", *Journal of Composites for Construction*, 14(4), 406-414.

Lam, L. and Teng, J.G. (2001). "Strength of RC cantilever slabs bonded with GFRP strips", *Journal of Composites for Construction*, ASCE, 5(4), 221-227.

Maaddawy, T. and Sherif, S. (2009). "FRP composite for shear strengthening of reinforced concrete deep beams with openings", *Composite Structures*, 89(1), 60-69.

Maaddawy, T. and El-Ariss, B. (2012). "Behavior of concrete beams with short shear span and web opening strengthened in shear with CFRP composites", *Journal of Composites for Construction*, ASCE, 16(1), 47–59.

Madkour, H. (2009). "Non-linear analysis of strengthened RC beams with web openings", *Proceedings of the Institution of Civil Engineers-Structures and Buildings*, 162(2), 115-128.

Mansur, M.A., Tan K.H. and Wei, W. (1999). "Effects of creating an opening in existing beams", *ACI Structural Journal*, 96(6), 899-906.

Pimanmas, A. (2010). "Strengthening R/C beams with opening by externally installed FRP rods: Behavior and analysis", *Composite Structures*, 92(8), 1957-1976.

Smith, S.T., Hu, S., Kim, S.J. and Seracino, R. (2011). "FRP-strengthened RC slabs anchored with FRP anchors", *Engineering Structures*, 33(4), 1075-1087.

Suresh, J. and Prabhavathy, R. A. (2015). "Behaviour of steel fibre reinforced concrete beams with duct openings strengthened by steel plates", *International Journal of Advanced Information in Arts, Science & Management*, 4(4).

Teng, J.G., Lam, L, Chan, W. and Wang, J. (2000). "Retrofitting of deficient RC cantilever slabs using GFRP strips", *Journal of Composites for Construction*, ASCE, 4(2), 75-84.

Zhang, H.W. and Smith, S.T. (2012). "Influence of FRP anchor fan configuration and dowel angle on anchoring FRP plates", *Composites Part B: Engineering*, 43(8), 3516-3527.

Table 5.1. Specimen details

Batch	Specimen	Opening size Length (mm)	Opening size Height (mm)	Web/flange chord height (mm)	FRP strengthening	Bending direction	Fabrication of web opening	Cylinder compressive strength of concrete f_c (MPa)
[1]	CB-Rec	NA	NA	NA	No	Negative bending[(a)]	NA	42.5
	CB-T	NA	NA	NA	No	Negative bending	NA	55.2
	O-700×300-N	700	300	100/100	No	Negative bending	Pre-formed	42.5
	F-700×300-N				Yes	Negative bending	Pre-formed	41.0
	F-700×300-P				Yes	Positive bending[(b)]	Pre-formed	44.1
	O-800×280-N	800	280	120/100	No	Negative bending	Pre-formed	42.5
	F-800×280-N				Yes	Negative bending	Pre-formed	41.0
	F-800×280-P				Yes	Positive bending	Pre-formed	44.1
[2]	O-600×220-N	600	220	180/100	No	Negative bending	Post-cut	40.3
	F-600×220-N				Yes	Negative bending	Post-cut	40.3
	O-700×200-N	700	200	200/100	No	Negative bending	Pre-formed	36.2
	F-700×200-N				Yes	Negative bending	Pre-formed	39.6
	F-600×280-N	600	280	120/100	Yes	Negative bending	Post-cut	42.0
	F-700×260-N	700	260	140/100	Yes	Negative bending	Pre-formed	42.0

Note: (a) The beam flange was in tension; (b) The beam flange was in compression.

Table 5.2. Key test results

Specimen	Cracking load F_{cr} (kN)	Yield load F_y (kN)	Yield load F_{y1} (a) (kN)	Yield load F_{y2} (b) (kN)	Ultimate load F_u (kN)	Cracking load ratio (c) (%)	Ratio of yield load F_{y1} (c) (%)	Ultimate load ratio (c) (%)	Gain in flexural capacity due to CFRP (%)
CB-Rec	55	340			390				
CB-T	160	478			510				
O-700×300-N	61		125	NA(d)	182	110.9	36.8	46.7	
F-700×300-N	60		150	175	207	109.1	44.1	53.1	13.7
O-800×280-N	50		143	160	181	90.9	42.1	46.4	
F-800×280-N	55		154	200	219	100.0	45.3	56.2	21.0
CB-Rec-P (FE)	50	270			270				
CB-T-P (FE)	109	310			310				
F-700×300-P	55		142	NA(d)	228	110.0	52.6	84.4	
F-800×280-P	60		168	176	215	120.0	62.2	79.6	
CB-Rec-2 (FE)	50	320			320				
CB-T-2 (FE)	146	500			500				
O-600×220-N	80		238	316	316	160.0	74.4	98.8	
F-600×220-N	101		284	NA(d)	388	202.0	88.8	121.3	24.0
O-700×200-N	60		253	291	300	120.0	79.1	93.8	
F-700×200-N	101		284	NA(d)	410	202.0	88.8	128.1	31.3
F-600×280-N	76		NA(d)	211	260	152.0	NA(d)	81.3	
F-700×260-N	76		196	199	270	152.0	61.3	84.4	

Note:
(a) F_{y1}= load at yielding of bottom steel bars at the left end of flange chord for specimens in negative bending or web chord for specimens in positive bending;
(b) F_{y2}= load at yielding of steel bars at the right end of web chord for specimens in negative bending or flange chord for specimens in positive bending;
(c) Ratio between weakened T-section beam and rectangular control beam;
(d) The relevant strain gauge was damaged during loading.

Table 5.3. Sum of negative and positive flexural capacities

Specimen	Negative flexural capacity (kN)	Positive flexural capacity (kN)	Sum of flexural capacities (kN)	Ratio of sum between T-section beams and CB-Rec
CB-Rec	390	270	660	100%
CB-T	510	310	820	124%
T-section beam with an FRP-strengthened web opening of 700 mm × 300 mm	207	228	435	65.8%
T-section beam with an FRP-strengthened web opening of 800 mm × 280 mm	219	215	434	65.6%

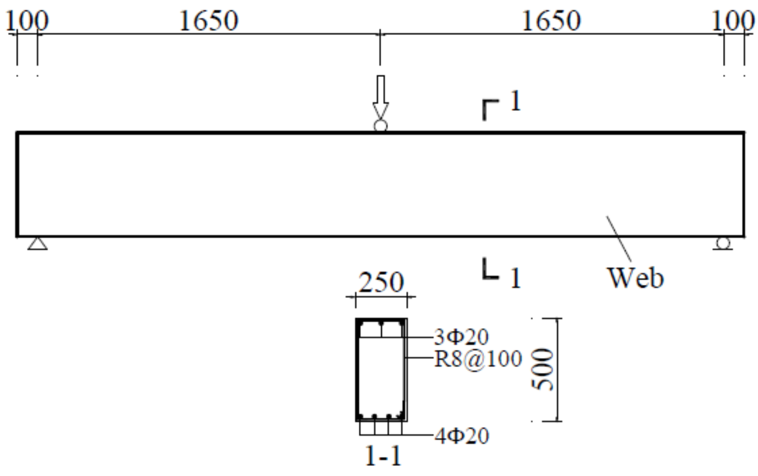

(a) CB-Rec

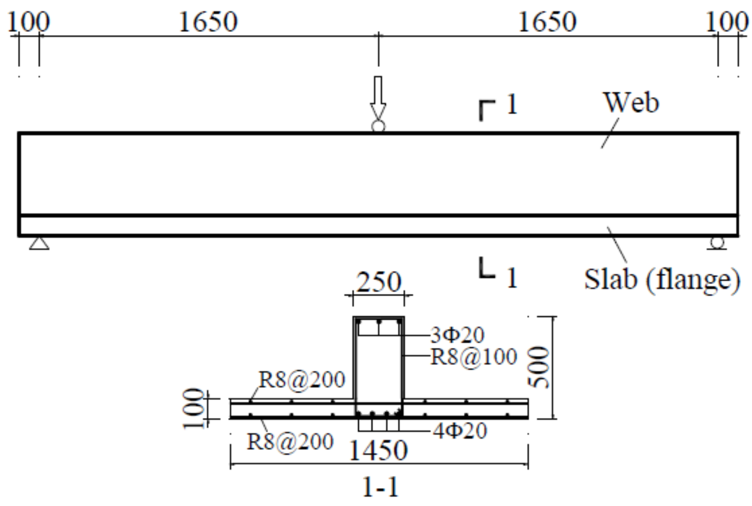

(b) CB-T

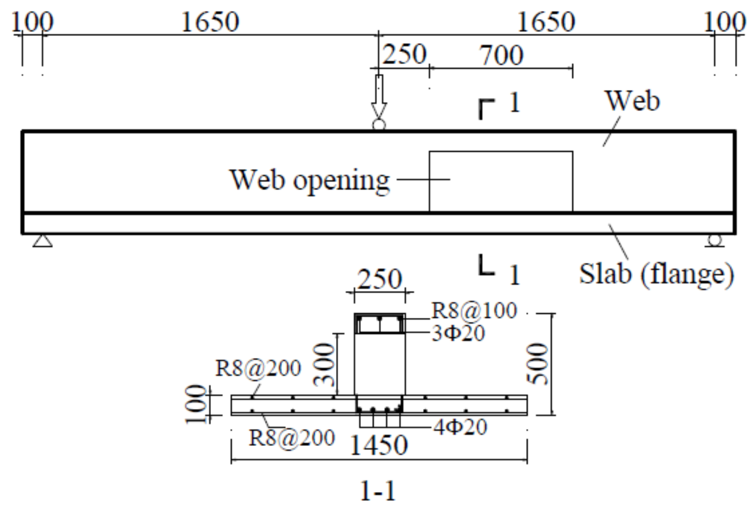

(c) O-700×300-N

Figure 5.1. Details of the tested specimens (dimensions in mm)

Figure 5.2. Making a pre-formed opening on a T-section beam

(a)

(b)

(c)

(d)

Figure 5.3. Making a post-cut opening on a T-section beam

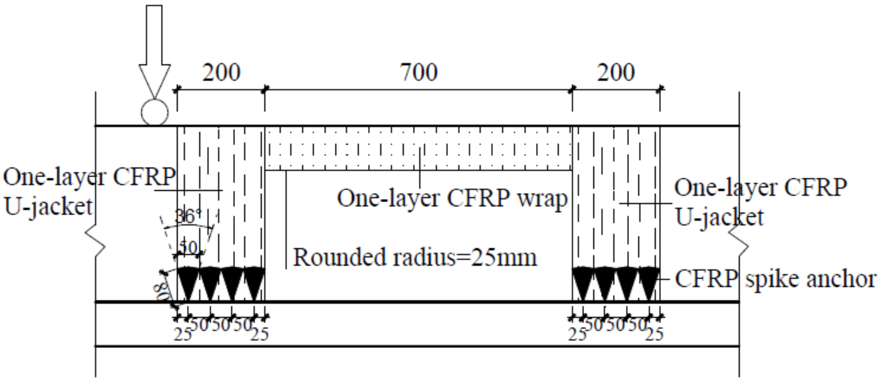

(a) CFRP-strengthened regions

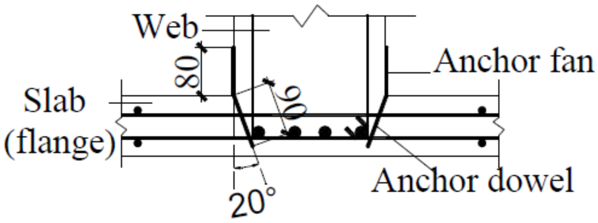

(b) CFRP spike anchors shown on beam cross-section

(c) CFRP spike anchor

Figure 5.4. CFRP strengthening system (F-700×300-N) (dimensions in mm)

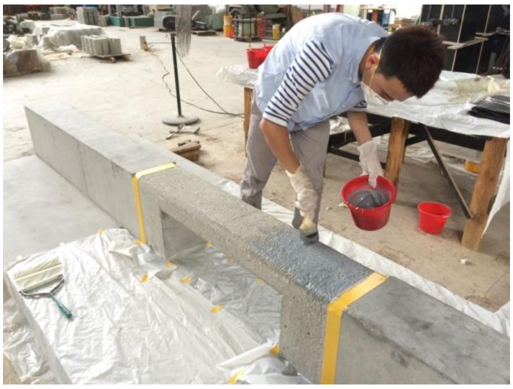

(a) (b)

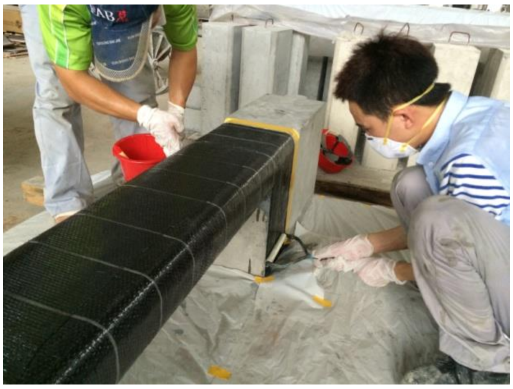

(c) (d)

Figure 5.5. Installation of CFRP

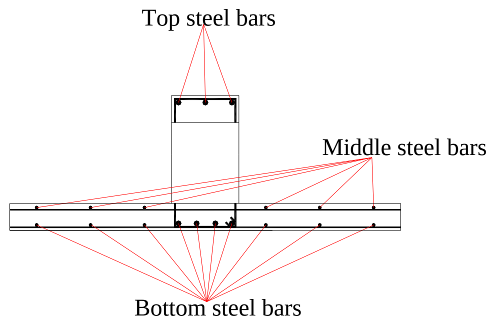

(a) Grouping of steel bars

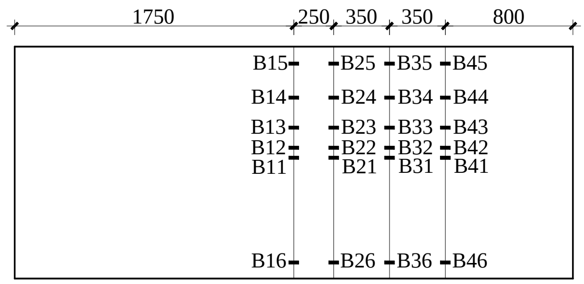

(b) Strain gauges on bottom steel bars

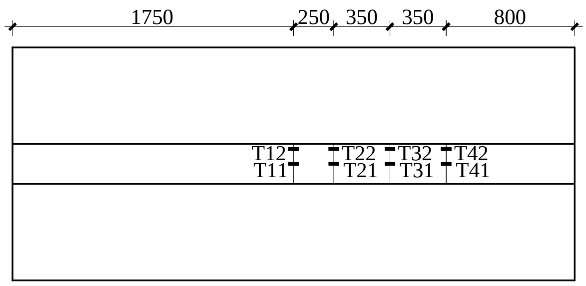

(c) Strain gauges on top steel bars

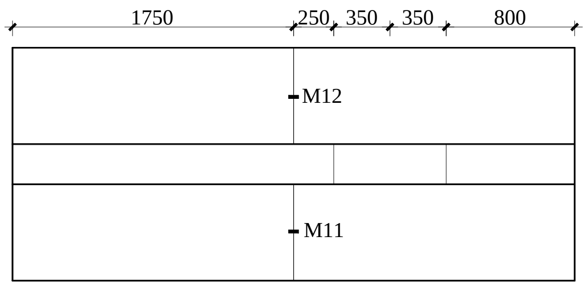

(d) Strain gauges on middle steel bars

Figure 5.6. Layout of strain gauges on steel bars (F-700×300-N) (dimensions in mm)

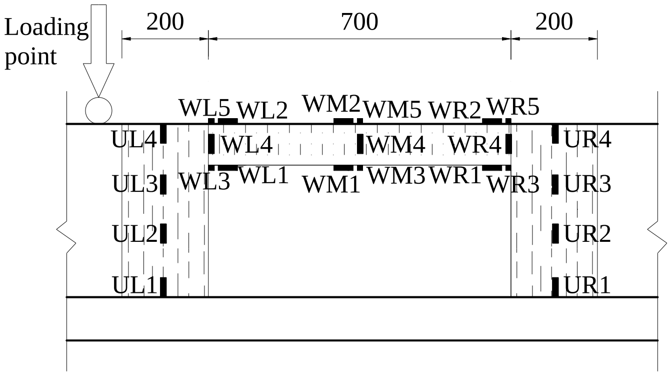

Figure 5.7. Layout of strain gauges on FRP (F-700×300-N) (dimensions in mm)

(Note: W-wrap; U-U-jacket; L-left; M-middle; R-right; W*1,2-strain gauges in the longitudinal direction on the web chord, with 1 representing the strain gauge on the bottom surface, 2 representing the strain gauge on the top surface; W*3,4 or 5-strain gauges in the hoop direction on the web chord, with 3 representing the strain gauge on the bottom surface, 4 representing the strain gauge on the side surface, 5 representing the strain gauge on the top surface.)

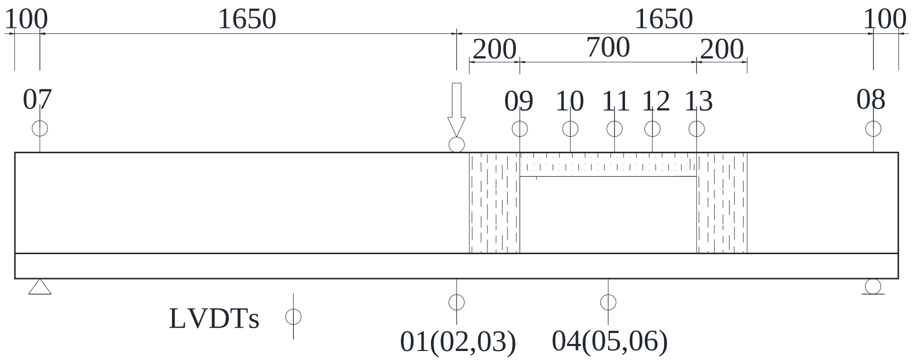

Figure 5.8. Layout of LVDTs (F-700×300-N) (dimensions in mm)

Figure 5.9. Test set-up

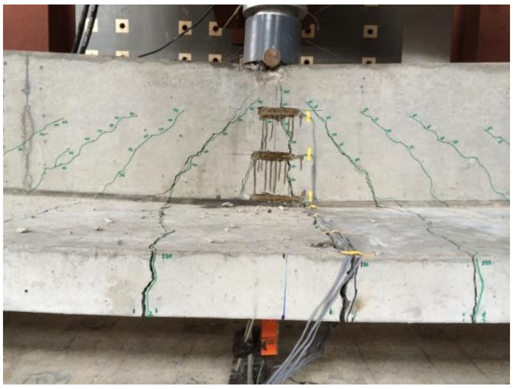

(a) CB-Rec

(b) CB-T

(c) O-700×300-N

(d) O-800×280-N

(e) F-700×300-N

(f) F-800×280-N

(g) F-700×300-P

(h) F-800×280-P


(i) O-600×220-N (j) O-700×200-N


(k) F-600×220-N (l) F-700×200-N


(m) F-600×280-N (n) F-700×260-N

Figure 5.10. Failure modes of tested specimens

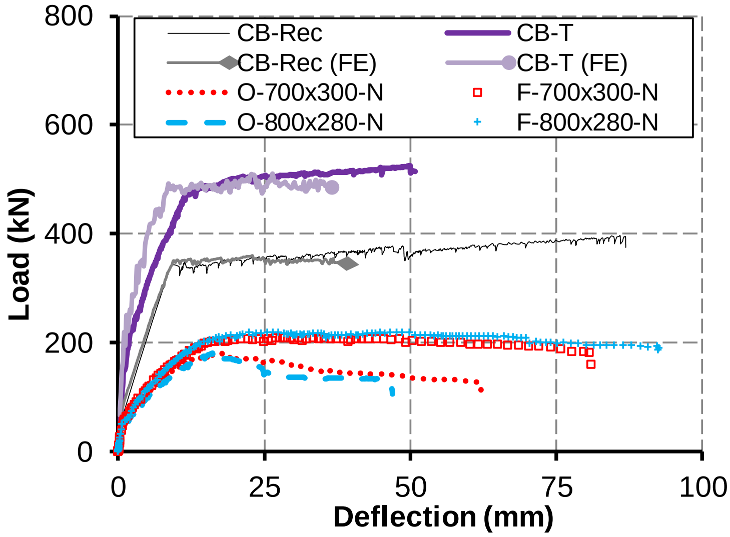

(a) Specimens with a large web opening

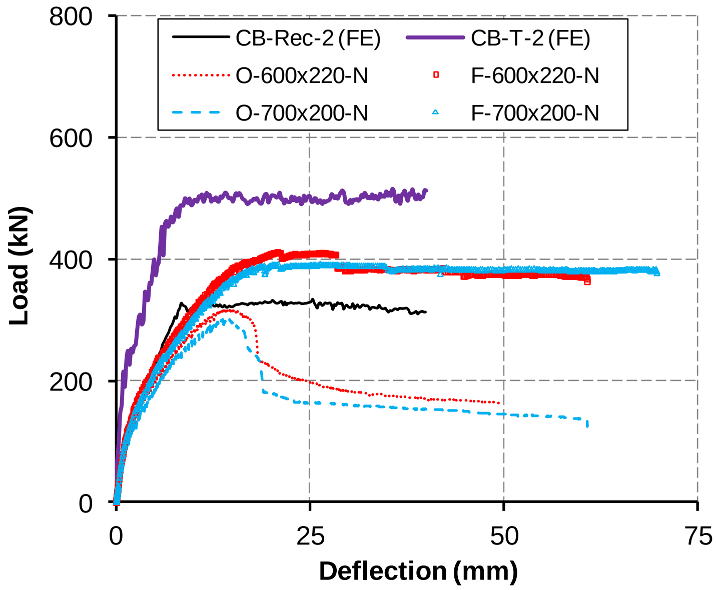

(b) Specimens with a small web opening

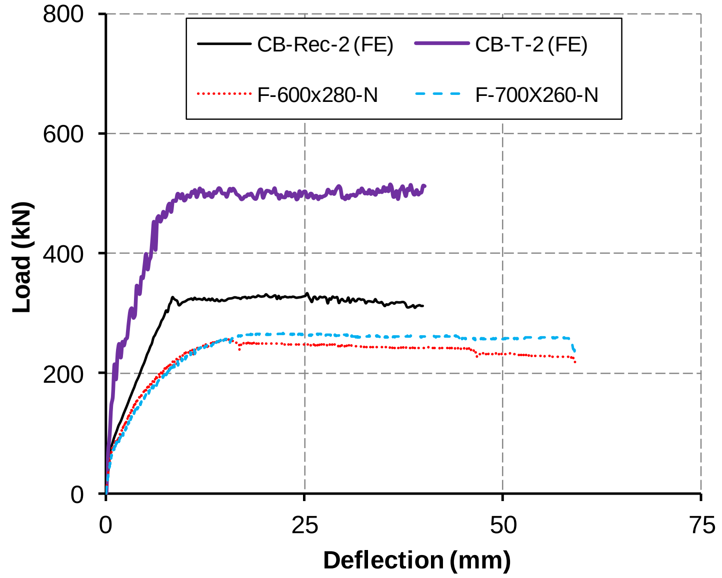

(c) Specimens with a medium web opening

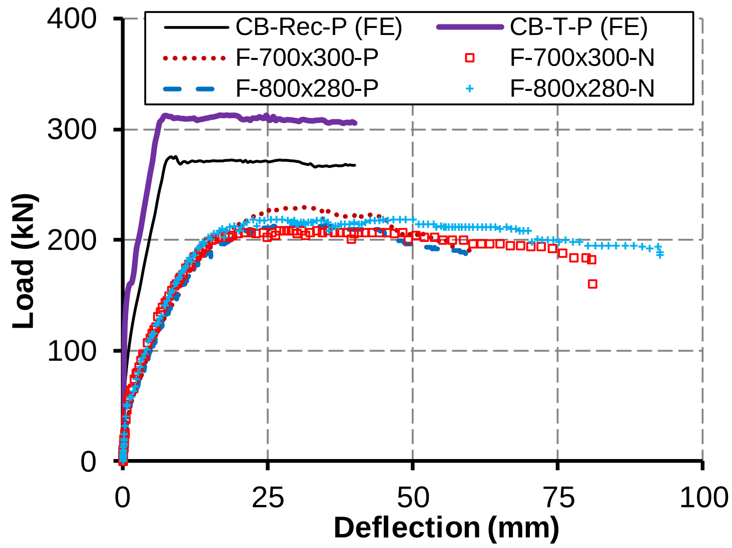

(d) Specimens tested in positive bending

Figure 5.11. Load-deflection curves of tested specimens

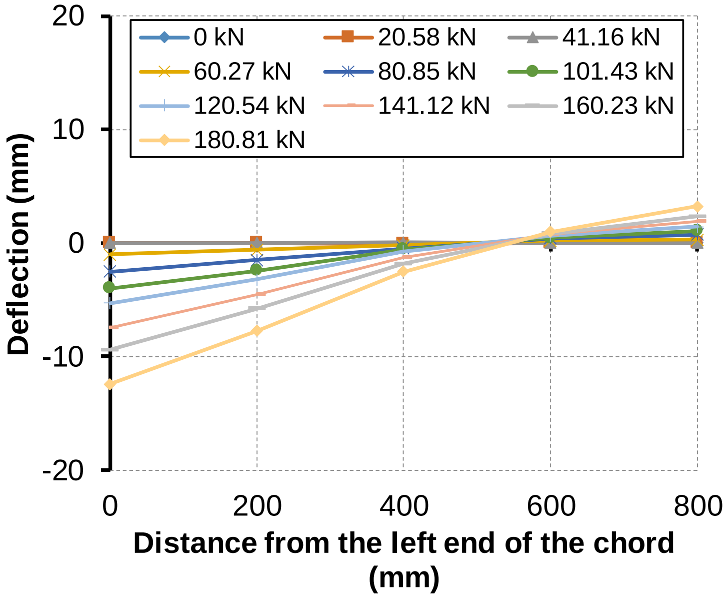

(a) O-800×280-N

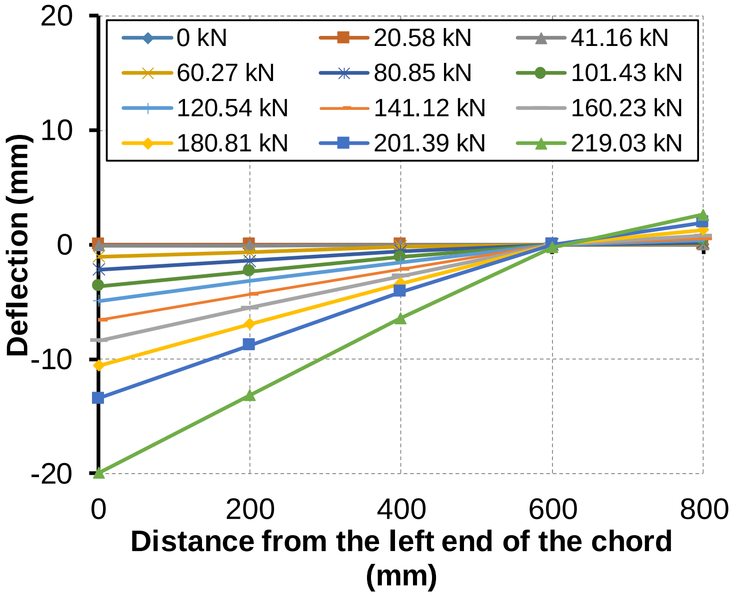

(b) F-800×280-N

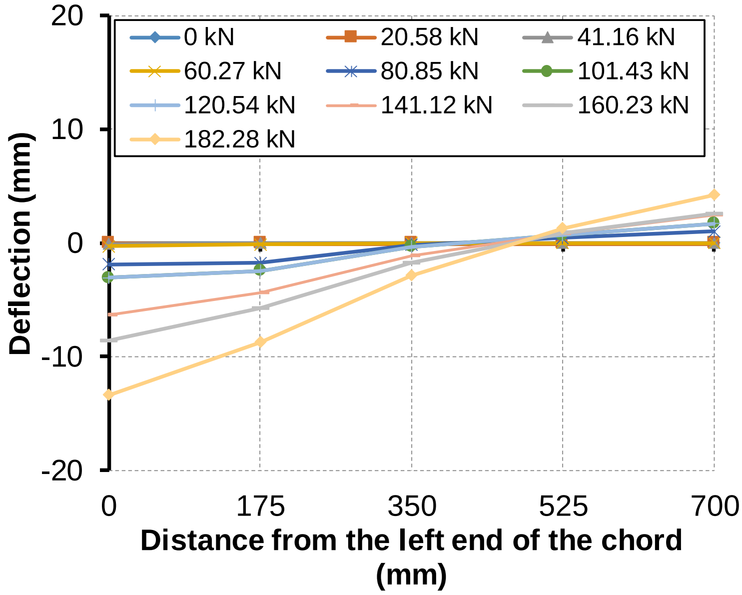

(c) O-700×300-N

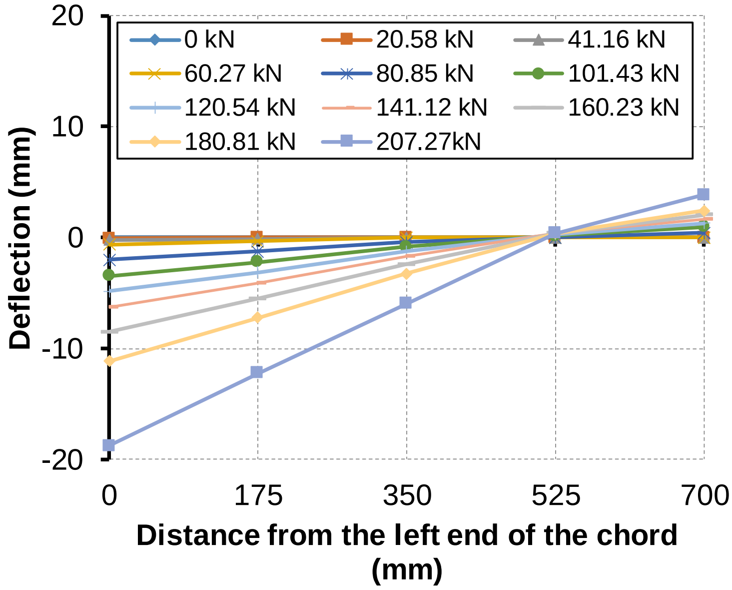

(d) F-700×300-N

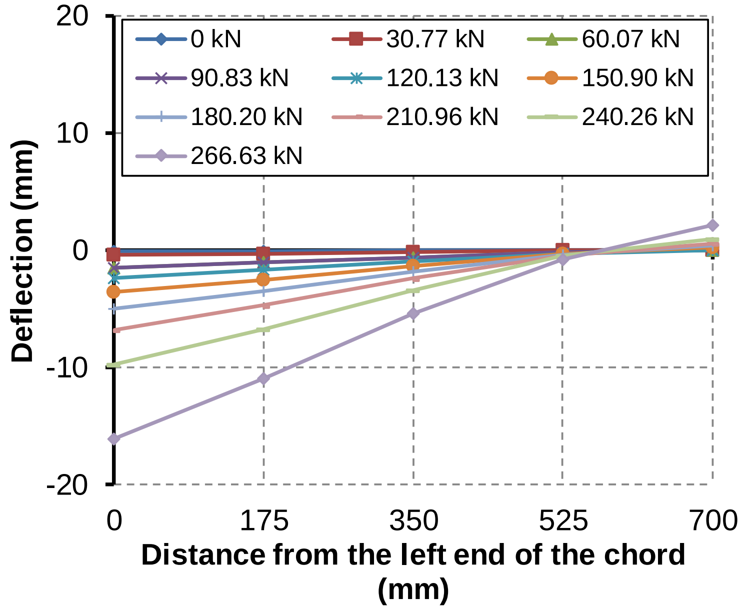

(e) F-700×260-N

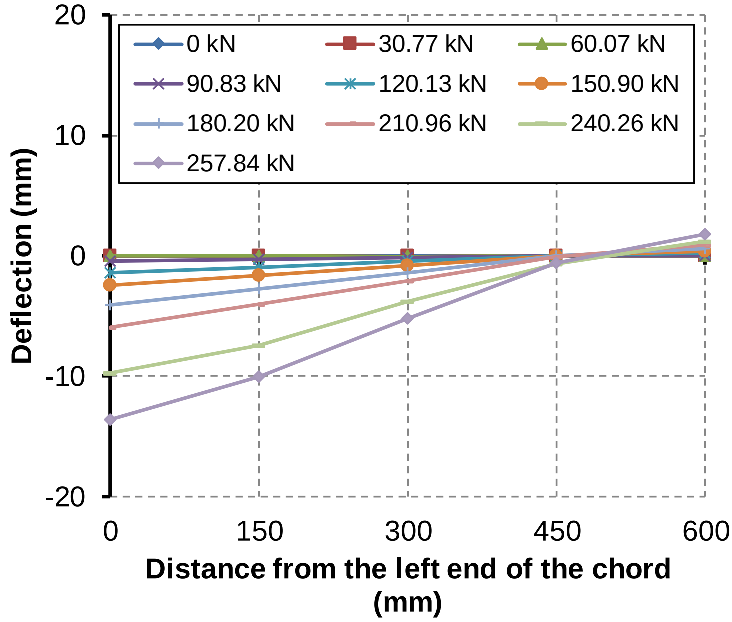

(f) F-600×280-N

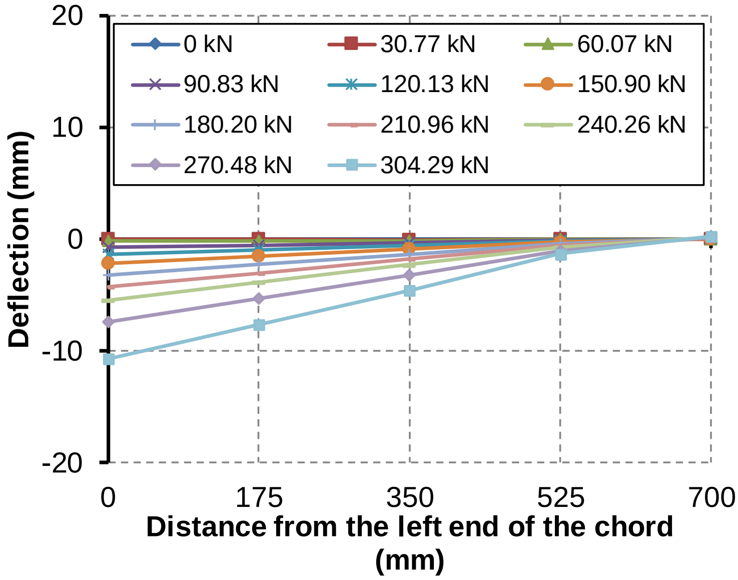

(g) O-700×200-N

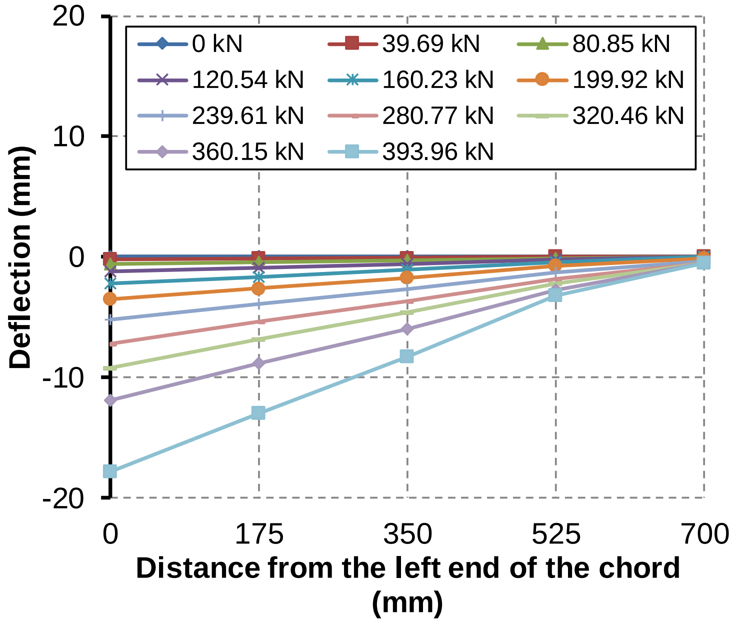

(h) F-700×200-N

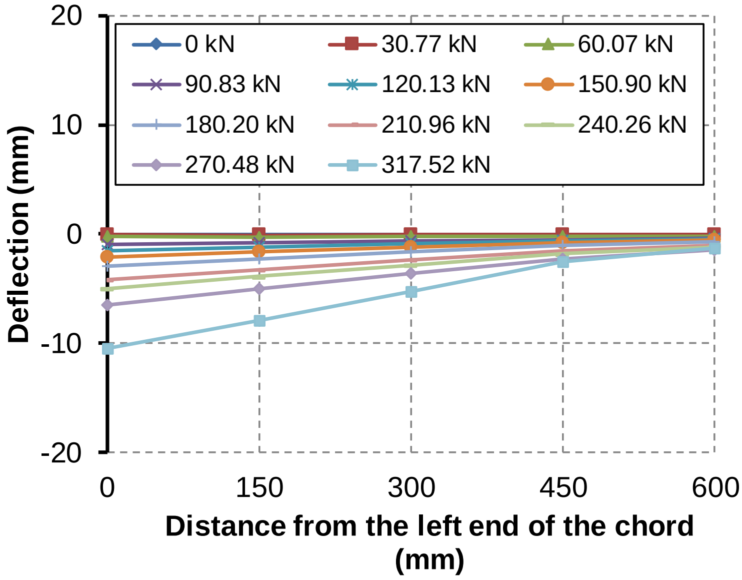

(i) O-600×220-N

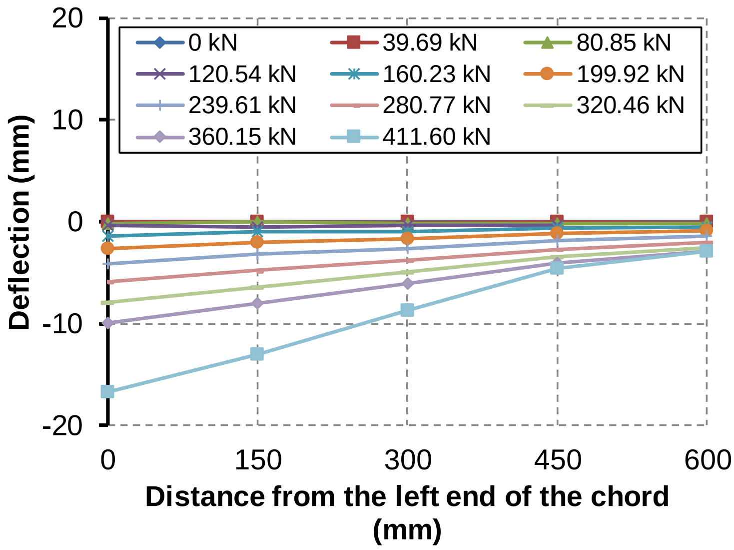

(j) F-600×220-N

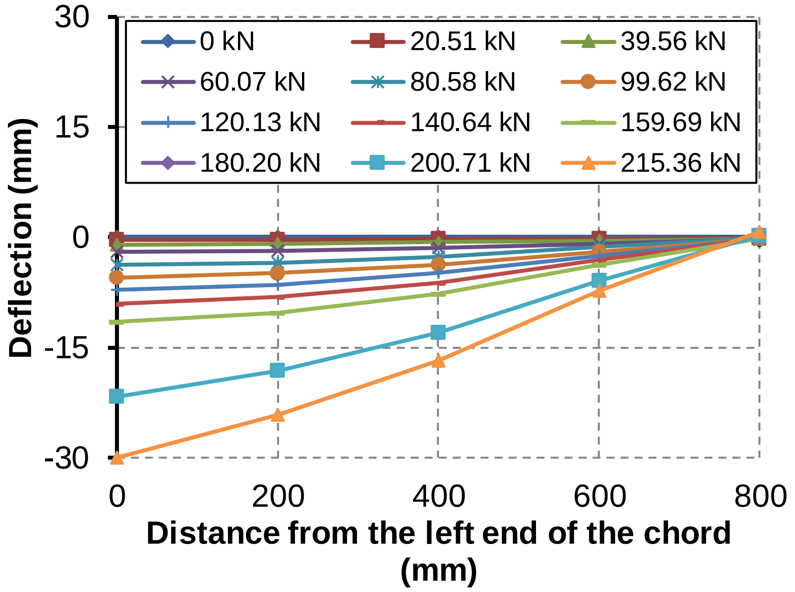

(k) F-800×280-P

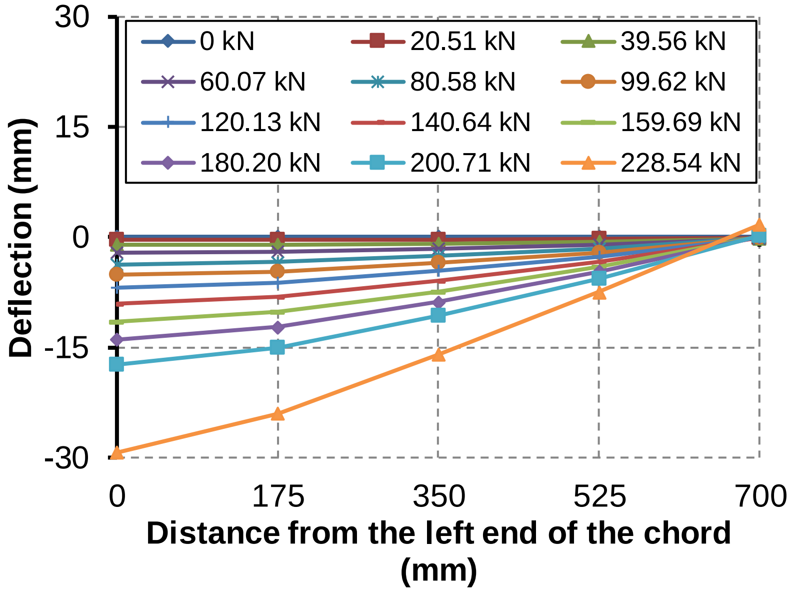

(l) F-700×300-P

Figure 5.12. Deflection of the web chord

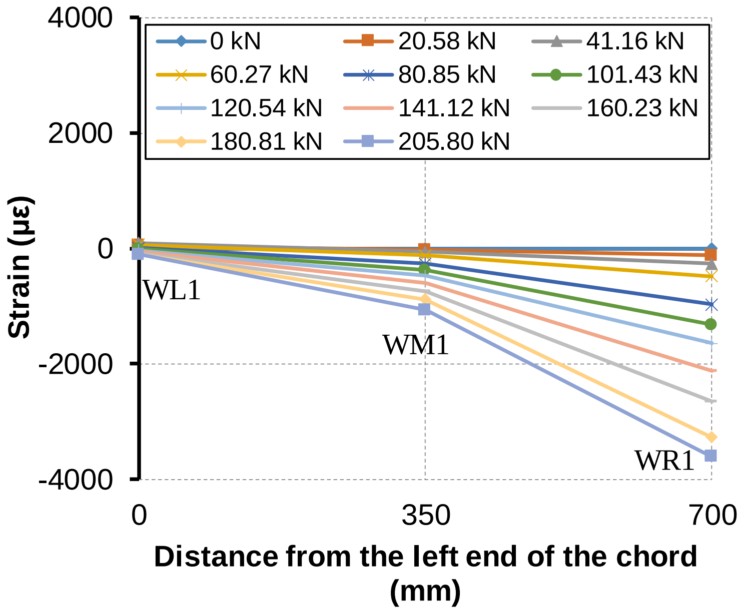

(a) On the bottom surface of web chord

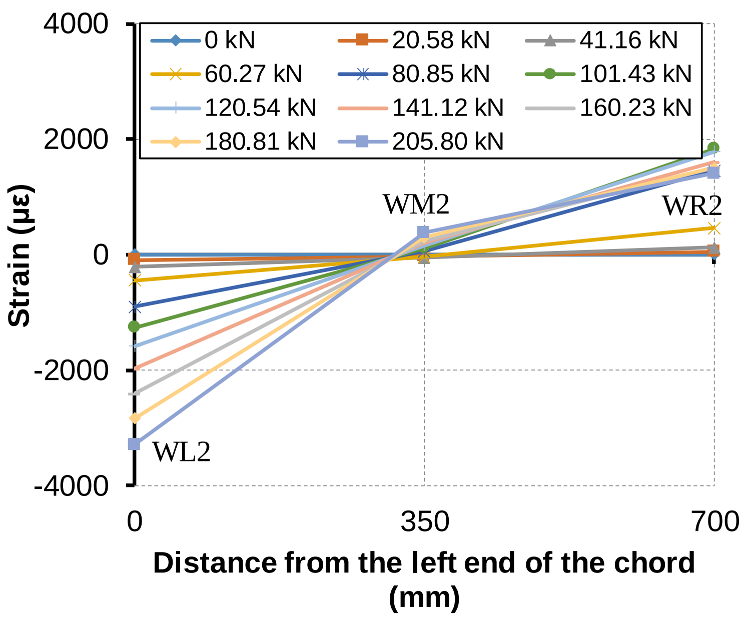

(b) On the top surface of web chord

Figure 5.13. Longitudinal strains in the FRP wrap (F-700×300-N)

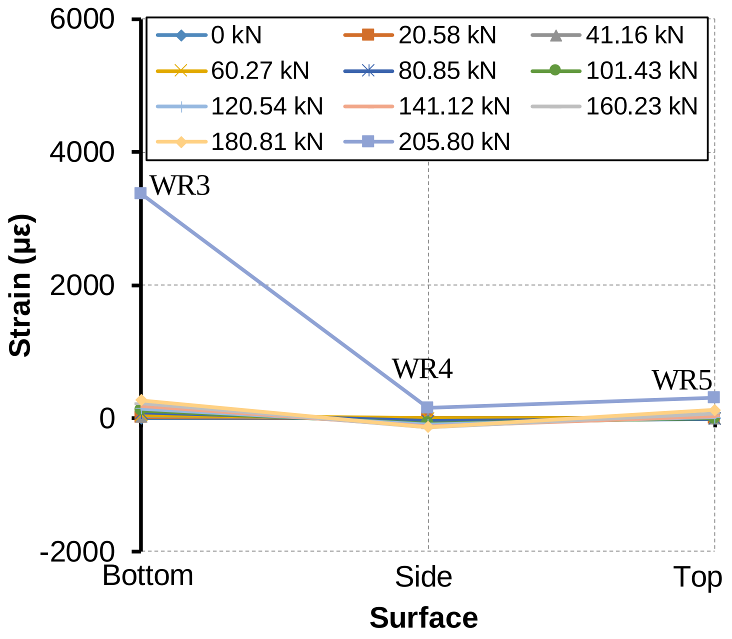

(a) At the right end of web chord

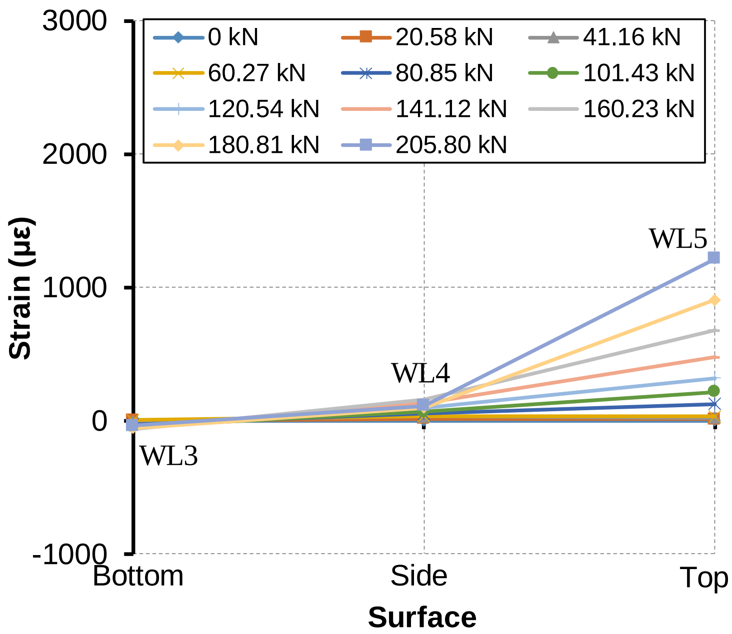

(b) At the left end of web chord

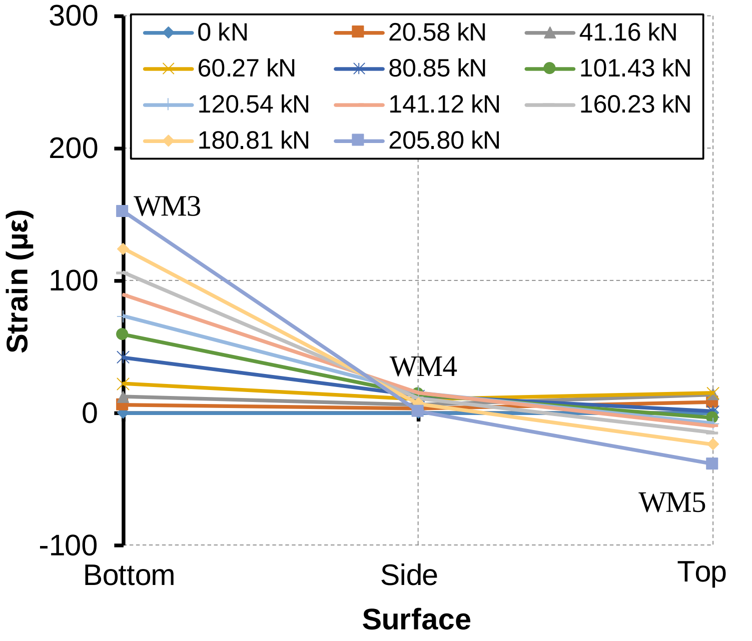

(c) At the mid-span of web chord

Figure 5.14. Hoop strains in the FRP wrap (F-700×300-N)

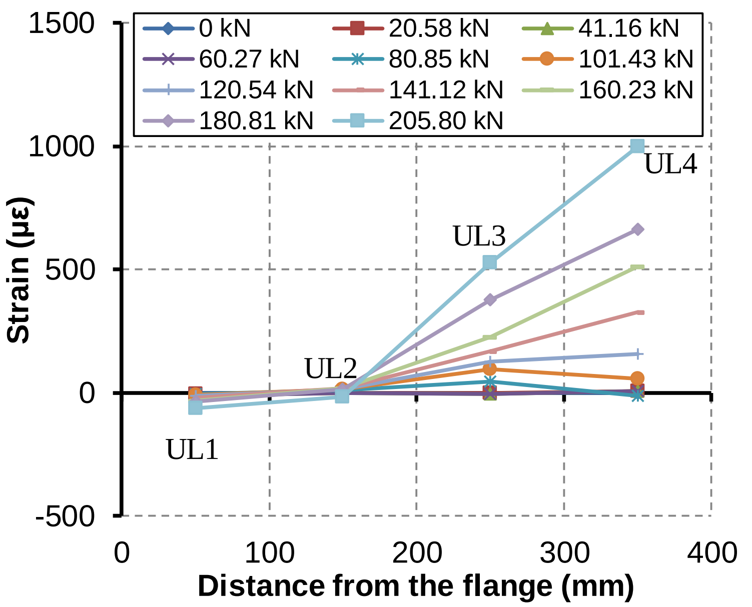

(a) Left CFRP U-jacket

(i.e., closer to the loading point)

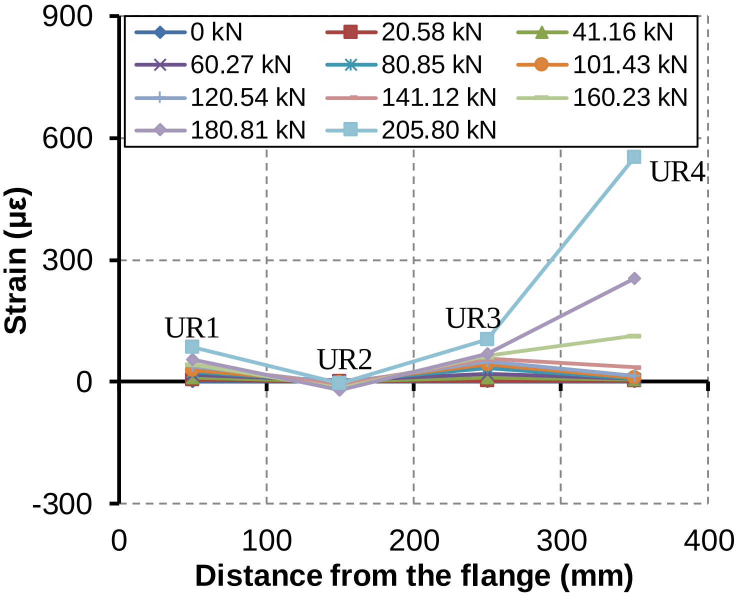

(b) Right CFRP U-jacket

(i.e., closer to the right support)

Figure 5.15. Strains in FRP U-jackets (F-700×300-N)

CHAPTER 6

RC T-SECTION BEAMS WITH A WEB OPENING FOR FLEXURAL WEAKENING AND CFRP SHEAR STRENGTHENING: FE MODELLING

6.1 INTRODUCTION

Existing experimental studies on rectangular RC beams with an un-strengthened/FRP-strengthened web opening (Abdalla et al. 2003; Allam 2005; Maaddawy and Sherif 2009; Madkour 2009; Pimanmas 2010; Chin et al. 2012; Maaddawy and Ariss 2012; Suresh and Prabhavathy 2015; Chin et al. 2016) and T-section RC beams with a relatively small un-strengthened/FRP-strengthened web opening [specimens tested by Mansur et al. (1999) and Teng et al. (2013)] indicated that the beam usually failed in a shear mode, i.e., the formation of diagonal cracks (near the corners of the web opening or the top and/or bottom chords) that initiated at the corners of the web opening. All the 12-full scale T-section RC beams with a large web opening tested by the candidate except two beams with a relatively small un-strengthened web opening, however, exhibited a flexural failure mode, i.e., the formation of four plastic hinges at the two ends of top and bottom chords. In Chapters 3 and 4, three FE approaches have been assessed for the modelling of RC beams with an un-strengthened/FRP-strengthened web opening which failed in a shear mode, and it was found that the brittle cracking model with the SECANT modulus of concrete provided the best predictions of the test results. It has been well acknowledged that, however, the brittle cracking model was proposed for applications where the tensile and shear behaviours of cracked concrete dominate the behaviour of the structure. Whether it is also able to give acceptable predictions for the tests that failed in a flexural mode has not been clarified yet. Therefore, the predictions from the three FE approaches examined in Chapters 3 and 4 are compared in this chapter with the results of the specimens tested by the candidate, in order to identify the most suitable approach for the FE modelling of T-section RC beams with an FRP-strengthened web opening that failed in a flexural mode.

6.2 PROPOSED FE APPROACH

6.2.1 General

As presented in Chapters 3 and 4, the proposed approach is a two-dimensional FE approach implemented with ABAQUS (2012). The typical mesh is shown in Fig. 6.1, in which the red lines stand for FRP sheets. It should be noted that as the ends of the FRP U-jackets were anchored into the beam flange through spike anchors, for the modelling of FRP U-jackets, the end of the lowest FRP truss elements (i.e., nearest to the upper surface of the beam flange) is fixed onto the upper surface of the beam flange (i.e. to the corresponding concrete node). The applied boundary conditions and loads are shown in Fig. 6.1. The load was applied at the midspan of the beam using the displacement-controlled method. The dynamic analysis approach, already presented in Chapters 3 and 4, was employed in the present study. The key factors including the time integration method, damping factor, loading time and hourglass scaling factors were all chosen following the studies in Chapter 3. The modelling of steel, FRP reinforcement, and interfaces (i.e., the FRP-to-concrete interface and the steel-to-concrete interface) was the same as explained in Chapters 3 and 4, while the modelling of concrete is explained as follows.

6.2.2 Constitutive modelling of concrete

Both the brittle cracking (BC) model and concrete damaged plasticity (DP) model employed in Chapters 3 and 4 are examined in the present study. For the brittle cracking model, the tension-softening curve and shear retention factor model are all the same as those adopted in Chapters 3 and 4. For the concrete damaged plasticity model, the uniaxial compressive stress-strain curve, tension-softening curve and tensile damage model are also the same as those adopted in Chapters 3 and 4. In addition to the power law model (see Eq. 3.8, referred to as the PL model for simplicity), however, another tensile damage model (i.e. elastic model, referred to as the ELA model for simplicity) is also examined in the present study for comparison purposes. For existing RC beams with a web opening, the DP model could not well predict their behaviour (Chapters 3 and 4); while for the T-section beams with an FRP-strengthened web opening tested by the candidate, which were modelled in the study presented in this chapter, the DP model provided the best predictions of their behaviour. Therefore, the effect of different damage models is considered in the present chapter but was not considered in Chapters 3 and 4. For the ELA model, it is assumed that the unloading path of the tensile stress-tensile strain curve of concrete passes through the origin of the coordinate system for all post-cracking values of tensile stress σ_t. The corresponding tensile damage factor of cracked concrete d_t can thus be expressed as

$$d_t = \frac{w_t}{[w_t + (h_c\sigma_t)/E_c]} \tag{6.1}$$

where w_t *(mm)* is crack opening displacement, E_c *(MPa)* is the elastic modulus of the concrete, and h_c *(mm)* is crack band which is defined as the characteristic crack length of an element in ABAQUS and regarded as equaling to the element size for elements with a reduced integration scheme in the present study [following Rots's (1988) recommendation].

For RC beams with an FRP-strengthened web opening, to consider the confinement effect from FRP wraps to the concrete of the web chord, the design-oriented stress-strain model developed by Lam and Teng (2003) for FRP-confined concrete in rectangular columns is employed in DP model in the present study:

$$\sigma_c = \begin{cases} E_c\varepsilon_c - \dfrac{(E_c - E_2)^2}{4f_{co}^{'}}\varepsilon_c^2 & (0 \le \varepsilon_c \le \varepsilon_t) \\ f_{co}^{'} + E_2\varepsilon_c & (\varepsilon_t \le \varepsilon_c \le \varepsilon_{cu}) \end{cases} \tag{6.2}$$

$$E_2 = \frac{f_{cc}^{'} - f_{co}^{'}}{\varepsilon_{cu}} \tag{6.3}$$

$$\varepsilon_t = \frac{2f_{co}^{'}}{E_c - E_2} \tag{6.4}$$

$$\frac{f_{cc}^{'}}{f_{co}^{'}} = 1 + k_1 k_{s1}\frac{f_l}{f_{co}^{'}} \tag{6.5}$$

$$\frac{\varepsilon_{cu}}{\varepsilon_{co}} = 1.75 + k_2 k_{s2}\frac{f_l}{f_{co}^{'}}\left(\frac{\varepsilon_{h,rup}}{\varepsilon_{co}}\right)^{0.45} \tag{6.6}$$

$$f_l = \frac{2\sigma_j t}{D} = \frac{2E_{frp}\varepsilon_j t}{D} \tag{6.7}$$

$$\varepsilon_{h,rup} = 0.586\varepsilon_{frp} \tag{6.8}$$

$$D = \sqrt{h^2 + b^2} \tag{6.9}$$

$$k_{s1} = (\frac{b}{h})^{\alpha} \frac{A_e}{A_c} \tag{6.10}$$

$$k_{s2} = (\frac{b}{h})^{\beta} \frac{A_e}{A_c} \tag{6.11}$$

$$\frac{A_e}{A_c} = \frac{1-((h/b)(h-2R_c)^2 + (h/b)(b-2R_c)^2)/(3A_g) - \rho_{sc}}{1-\rho_{sc}} \tag{6.12}$$

$$A_g = bh - (4-\pi)R_c^2 \tag{6.13}$$

where σ_c and ε_c are respectively the axial stress and the axial strain of confined concrete; $f_{co}^{'}$ is the compressive strength of unconfined concrete; E_2 is the slope of the straight second portion; ε_t is the axial strain at the transition point; $f_{cc}^{'}$ is the compressive strength of confined concrete; ε_{cu} is the ultimate axial strain of confined concrete; k_1 is the confinement effectiveness coefficient and set to be 3.3; k_2 is the strain enhancement coefficient and set to be 12; k_{s1} and k_{s2} are the shape factors respectively for strength enhancement and strain enhancement; f_l is the confining pressure in an equivalent circular column; ε_j is the nominal hoop rupture strain in the equivalent FRP-confined circular column and assumed to be the actual hoop rupture strain $\varepsilon_{h,rup}$; ε_{frp} is the FRP material ultimate tensile strain and σ_j is the corresponding nominal hoop rupture stress; *t* is the total thickness of FRP; E_{frp} is the elastic modulus of FRP in the hoop direction; D is the diameter of an equivalent column; *h* and *b* are respectively the depth and width of the rectangular column, with h≥b; *α*=2; *β*=0.5; $\frac{A_e}{A_c}$ is the effective confinement area ratio; R_c is the rounded corner radius; ρ_{sc} is the cross sectional area ratio of the longitudinal steel reinforcement; and A_g is the gross area of the column section with rounded corner.

It should be noted that in addition to the web chord, a small square region near each end of the web chord was also considered as a confined region in the analysis, with its side length being equal to the height of the web chord. Taking Specimen F-700×300-N as an example, the height of the web chord is 100 mm, so the confined region is the web chord plus the two small square regions with a side length of 100 mm at the two ends of web chord, as shown in Fig. 6.2.

6.2.3 Numerical schemes

In the present study, six schemes were considered: (1) Scheme-1: BC model with SECANT modulus of concrete; (2) Scheme-2: BC model with INITIAL modulus of concrete; (3) Scheme-3: DP model with damage model ELA; (4) Scheme-4: DP model with damage model PL; (5) Scheme-5: DP model with damage model ELA and the confinement effect of FRP strengthening being considered [referred to as *DP model (Damage model ELA, confined)* for simplicity]; and (6) Scheme-6: DP model with damage model PL and the confinement effect of FRP strengthening being considered [referred to as *DP model (Damage model PL, confined)* for simplicity].

For the control specimens, Schemes-1 and 2 were examined as the DP model has been successfully adopted for the modelling of RC beams in Chen et al. (2011); for specimens with an un-strengthened web opening, Schemes-1 to 4 were examined; for specimens with an FRP-strengthened web opening tested under negative bending, Schemes-1 to 6 were examined; and for specimens tested under positive bending, Schemes-1 to 4 were examined as the web chord with FRP wraps is under tension and the confinement effect of FRP wraps to the concrete in the web chord is insignificant.

6.3 RESULTS AND COMPARISON

Details of the specimens tested by the candidate have been clearly presented in Chapter 5. The FE results of these beams are presented below.

6.3.1 Load-deflection curves

6.3.1.1 Control beams

Two control beams (without a web opening) were tested, with one being a rectangular beam (CB-Rec) and the other one being a T-section beam (CB-T). Only the DP model with different tensile damage models (i.e., ELA and PL) was employed to simulate the two control beams, as they both failed by the crushing of compressive concrete at the mid-span of the beam after the yielding of tension steel bars, which is the typical flexural failure mode of RC beams.

The load-deflection curves obtained from the two schemes (i.e. DP model with damage model PL and DP model with damage model ELA) are compared with the test results in Fig. 6.3. As can be seen from Fig. 6.3, for the rectangular control beam (CB-Rec), the DP model with either tensile damage model provides very close predictions, with the predicted ultimate load from the DP model with damage model ELA being slightly higher than that from the DP model with damage model PL. The predictions agree well with the test results.

For the T-section control specimen (CB-T), the DP model with either tensile damage model gives a very good prediction of the ultimate load, while the cracking load and the stiffness of the second segment of the load-deflection curve from FE analysis are much higher than the test results. The different performance of the FE model in predicting the ultimate load and the cracking load as well as the second-segment stiffness can be contributed to the following reasons: (1) in reality, when the applied load is relatively low, a significant shear lag effect exists in the beam flange, which results in non-uniform distributions of the longitudinal tensile stresses in the concrete and reinforcement of the flange across its width direction. The present 2-D model cannot capture such shear lag effects in the flange and thus the predicted cracking load and the second-segment stiffness are higher than the test results; (2) when the applied load is high enough to make all the longitudinal reinforcement in the flange yield, the tensile stresses in all the longitudinal steel rebars in the flange become uniform, and thus the ultimate load of the beam can be well predicted by the present 2-D model.

6.3.1.2 RC T-section beams with an un-strengthened web opening

A total of 4 RC T-section beams with an un-strengthened web opening were tested, including O-700×300-N, O-800×280-N, O-600×220-N and O-700×200-N. For O-700×300-N and O-800×280-N with a larger web opening (i.e., a smaller height of the top chord), their final failure was controlled by local flexural failure at the end of the web chord closer to the support and the end of the flange chord closer to the loading point (i.e., crushing of compressive concrete of the web and flange chords) and local mixed flexural and shear failure at the end of the web chord closer to the loading point and the end of the flange chord closer to the support. For Specimens O-600×220-N and O-700×200-N with a smaller web opening (i.e., a larger height of the top chord), diagonal cracks (at around 30 to 45 degrees to the horizontal direction) initiated and developed in the span of the web chord and finally controlled the failure of the specimens.

The load-deflection curves obtained from Schemes-1 to 4 are compared with the test results in Fig. 6.4. As can be seen from Figs. 6.4(a) and (b), for RC T-section beams with a larger un-strengthened web opening (i.e. O-700×300-N and O-800×280-N), the BC model with either SECANT modulus or INITIAL modulus heavily overestimate the strength, while the DP model with either tensile damage model provides close predictions of the test results in terms of the ultimate load, with the predicted ultimate load by the DP model with damage model ELA being slightly higher than that by the DP model with damage model PL. The shapes of load-deflection curves predicted by the DP model with either tensile damage model also agree well with the test results, but similar to the situation of the T-section control specimen, the predicted cracking load and the second-segment stiffness are higher than the test results.

As can be seen from Figs. 6.4(c) and (d), for Specimens O-600×220-N and O-700×200-N with a smaller web opening, the DP model with either tensile damage model heavily underestimates the ultimate load of the beams, the BC model with

INITIAL modulus heavily overestimates both the strength and stiffness of the beams, while the BC model with SECANT modulus predicts the ascending portion of the load-deflection curves well but still overestimates the ultimate load. The relatively better performance of the BC model with SECANT modulus for these two specimens is because the two specimens failed in a shear mode, which can be better predicted by the BC model with SECANT modulus as discussed in Chapters 3 and 4.

6.3.1.3 RC T-section beams with an FRP-strengthened web opening

A total of six RC T-section beams with an FRP-strengthened web opening were tested, including F-700×300-N, F-800×280-N, F-600×280-N and F-700×260-N, F-600×220-N and F-700×200-N. Due to the existence of CFRP wraps and CFRP U-jackets, the shear cracks near the ends of the chords were well prevented/mitigated. All these specimens failed by local flexural failure at the two ends of web chord as well as flange chord; the formation of plastic hinges at the ends of the web and flange chords can be clearly seen.

The load-deflection curves obtained from Schemes-1 to 6 are compared with the test results in Fig. 6.5. As can be seen from Fig. 6.5, for all six RC T-section beams with an FRP-strengthened web opening, the BC model with either SECANT or INITIAL modulus of concrete heavily overestimates their strength, while the DP model with either tensile damage model but no consideration of the confinement effect from the FRP strengthening heavily underestimates the ultimate load. With the confinement effect from the FRP strengthening considered, the DP model with tensile damage mode PL gives very close predictions of ultimate loads from the tests for all the six beams, while the DP model with tensile damage mode ELA consistently overestimates the ultimate loads of all the six beams. This indicates that the tensile damage mode PL should be recommended for use in such modelling. The predicted cracking load and second-segment stiffness are again larger than the test results, due to the reason explained earlier.

6.3.1.4 RC T-section beams with an FRP-strengthened web opening tested in positive bending

Two specimens with an FRP-strengthened web opening (i.e., F-700×300-P and F-800×280-P) were tested in positive bending (i.e., the flanges of the beam were in compression). Similar to specimens with an FRP-strengthened web opening tested in negative bending, the two specimens in positive bending also failed in a flexural mode with plastic hinges forming at the two ends of web chord as well as the flange chord.

The load-deflection curves obtained from Schemes-1 to 4 are compared with the test results in Fig. 6.6. As can be seen from Fig. 6.6, for both specimens, all four examined schemes overestimate the strength and stiffness. The gap between the prediction and the test can be possibly attributed to the following reasons: (1) the shear lag effect existing in the beam flange resulted in the non-uniform distribution of longitudinal compressive stresses in the concrete and the reinforcement of the flange across its width, and the current 2-D model with plane stress elements cannot capture such shear leg effects; and (2) the width-to-depth ratio of flange is relatively large (1450/100=14.5). Under compression, therefore, the flange could undergo out-of-plane deformation, which also cannot be reflected by the current 2-D model. The above limitations/simplifications of the present 2-D model can lead to overestimation of the ultimate load of the beam. To resolve this problem, a more advanced 3-D FE model needs to be developed in the future.

6.3.1.5 Comparison of ultimate load

A comparison of the ultimate load between FE predictions and tests for all the specimens tested by the candidate are given in Fig. 6.7 and Table 6.1. It should be noted that in Fig. 6.7 and Table 6.1, for RC T-section beams with an FRP-strengthened web opening tested in negative bending, the term "DP model" means the DP model with the confinement effect from FRP strengthening being considered. As can be seen from Fig. 6.7 and Table 6.1, the DP model with damage model PL gives the closest predictions of the ultimate loads of tests, with an average prediction-to-test ratio of 0.999, a standard deviation (STD) of 0.129, and a coefficient of variation (CoV) of 0.129. The DP model with damage model ELA gives an average prediction-to-test ratio of 1.11, a STD of 0.138, and a CoV of 0.125, and the BC model with SECANT modulus gives an average prediction-to-test ratio of 1.25, a STD of 0.153, and a CoV of 0.122. Although the latter two models give a similar value of CoV to the DP model with damage model PL, both models overestimate the ultimate loads. The BC model with INITIAL modulus significantly overestimates the ultimate loads, with an average prediction-to-test ratio of 1.38, a STD of 0.150, and a CoV of 0.108. The better performance of the DP model with damage model PL is also evidenced by the much smaller scatter in its predictions of test results as shown in Fig. 6.7.

6.3.2 Failure mode

The predicted crack patterns at failure of all the specimens tested by the candidate are plotted in Fig. 6.8, in which the predicted crack patterns of the two beams with a smaller un-strengthened web opening (i.e. O-600×220-N and O-700×200-N) were obtained using the BC model with SECANT modulus and the predicted crack patterns of the other beams were obtained using the DP model with damage model PL. The reason why different models were used for specimens with different failure modes will be explained in the next subsection. The corresponding test crack patterns at failure are also shown in the same figure for the purpose of comparison. As can be seen from Fig. 6.8, the predicted crack patterns agree well with the test observations.

6.3.3 Selection of FE approach

6.3.3.1 General

As concluded in Chapters 3 and 4, for RC beams with an un-strengthened/FRP strengthened web opening (in existing studies) which failed in a shear mode, the BC model with SECANT modulus provides the best prediction. For specimens tested by the candidate and failing in a shear mode, the BC model with SECANT modulus also provides the best prediction. However, for specimens tested by the candidate and failing in a flexural mode, the DP model with damage model PL provides the best prediction while the BC model with SECANT modulus overestimates the ultimate load. The proper selection of the FE approach is therefore dependent on the failure mode of the beam with a web opening, and can be determined using the following steps:

1) Identify the critical chord, which is the chord with a smaller cross-sectional area between the top and bottom chords or the chord with a smaller reinforcement ratio if the cross-sectional areas of the two chords are equal;
2) Calculate the flexural capacities of the critical chord M_{cs} and M_{ch}, respectively in sagging bending and hogging bending;
3) Calculate the shear capacity of the critical chord V_c; and
4) If V_c is smaller than the value of ($M_{cs}+M_{ch}$) divided by the length of the chord, the beam will fail in shear due to the formation of diagonal cracks in the opening region, and the BC model with SECANT modulus should be used; otherwise, the beam will fail in a flexural mode due to the formation of four plastic hinges at the two ends of the two chords, and the DP model with damage model PL should be used.

6.3.3.2 Shear capacity of un-strengthened chord

In the present study, the equations given by the Chinese design code (GB-50011 2010) are used to calculate the shear capacity of the critical chord. Without FRP strengthening, the shear capacity of the critical chord V_c can be calculated using the following equation (GB-50011 2010):

$$V_c = V_{cc} + V_{cs} = 0.7 f_t b_c h_0 + f_{yv} \frac{A_{sv}}{s_s} h_s \tag{6.14}$$

where V_{cc} and V_{cs} are respectively the shear contributions from concrete and steel stirrups, f_t is the tensile strength of concrete, b_c is the width of the chord,

h_0 is the effective height of the chord, f_{yv} is the tensile strength of the steel stirrups, A_{sv} is sum of cross-sectional areas of vertical legs of a stirrup at a certain cross-section of the chord, s_s is the distance between two adjacent stirrups; h_s is the height of the steel stirrup and is assumed to be the actual height of the steel stirrup minus the diameter of the steel stirrup in the present study (the steel stirrups in the chord are cut by the web opening, and the anchorage length of the stirrup is assumed to be equal to the diameter value of the stirrup in the present study). It should be noted that the above assumption was adopted to simplify the problem but there have been no exisitng studies which can support this assumption. Its accuracy/validity, therefore, needs furhter investigations in the future.

6.3.3.3 Shear capacity of FRP-strengthened chord

If the critical chord is strengthened in shear using FRP, the shear capacity of the chord can be calculated using the following equation (GB-50608 2010):

$$V_c = V_{cc} + V_{cs} + V_{cf} \tag{6.15}$$

where V_{cf} is the shear contribution from the FRP and can be calculated as follows.

For FRP complete wraps,

$$V_{cf} = 2\frac{w_f t_f}{(s_f + w_f)} \sigma_{f,vd} h_f (\sin\alpha + \cos\alpha) \tag{6.16}$$

$$\sigma_{f,vd} = \min\{f_{fd}, E_f \varepsilon_{fe,v}\} \tag{6.17}$$

$$\varepsilon_{fe,v} = \frac{8}{\sqrt{\lambda_{Ef}} + 10} \varepsilon_{fd} \tag{6.18}$$

$$\lambda_{Ef} = 2\frac{n_f \omega_f t_f}{b(s_f + \omega_f)} \frac{E_f}{f_t} \tag{6.19}$$

where w_f is the width of FRP sheet, t_f is the thickness of FRP sheet, s_f is the clear distance between two adjacent FRP sheets, $\sigma_{f,vd}$ is the effective tensile stress of FRP sheet, h_f is the height of FRP sheet, α is the angle between the orientation of the FRP and the axis of the beam, f_{fd} is the tensile strength of FRP sheet, E_f is the elastic modulus of FRP, $\varepsilon_{fe,v}$ is the effective strain of FRP sheet, λ_{Ef} is the characteristic value of shear strengthening, ε_{fd} is the maximum tensile strain of FRP, n_f is the layers of FRP sheet.

For FRP U-jackets or side bonded FRP sheets,

$$V_{cf} = K_f \tau_b w_f \frac{h_f^2}{s_f + w_f}(\sin\alpha + \cos\alpha) \tag{6.20}$$

$$K_f = \phi \frac{\sin\alpha\sqrt{E_f t_f}}{\sin\alpha\sqrt{E_f t_f} + 0.3 h_f f_t} \tag{6.21}$$

$$\tau_b = 1.2\beta_w f_t \tag{6.21}$$

$$\beta_w = \sqrt{\frac{2.25 - w_f/(s_f + \omega_f)}{1.25 + w_f/(s_f + \omega_f)}} \tag{6.23}$$

where K_f is the coefficient of FRP debonding; τ_b is the bond strength between FRP and concrete; ϕ is the coefficient of FRP strengthening scheme, ϕ=1 for side bonded FRP sheets and ϕ=1 for FRP U-jackets.

6.3.3.4 Verification

The feasibility of the above method is verified with all the specimens collected in Chapters 3 and 4 and specimens tested by the candidate, as listed in Table 6.2. It can be seen in Table 6.2 that for all specimens that can be well predicted by the BC model with SECANT modulus, the shear capacity of the critical chord is smaller than its flexural capacity, while for all specimens that can be well predicted by the DP model with damage model PL, the shear capacity of the critical chord is larger than its flexural capacity.

It has to be stated that, this method is the best method the candidate can propose at the present stage. It is of course highly desirable to develop a single model which can well predict the behavior of all RC beams with web openings which fail in either a flexural mode or a shear mode. Many options were explored, such as a combination of the DP model and the BC model in different ways. However, a general FE model which applies to all RC beams with a web opening has not been reached. Nevertheless, it may be argued that the use of different models for beams with different failure modes is not unreasonable.

6.4 CONCLUDING REMARKS

A total of six FE schemes were examined in this chapter to simulate the 12 T-section RC beams with an un-strengthened/FRP strengthened web opening. It was found that for the test specimens which exhibited a flexural failure mode, the DP model with damage model PL (also with proper consideration of the confinement effect from the FRP wraps to the web chord) provides the best predictions, while the BC model overestimates the ultimate load significantly; for the test specimens which exhibited a shear failure mode, the BC model with SECANT modulus provides the best predictions. However, it should still be noted that for the two beams with a smaller un-strengthened web opening tested by the candidate (i.e. O-600×220-N and O-700×200-N), the predictions obtained from the BC model with SECANT modulus are only reasonable during the beginning stage but substantially deviate from the test results after the peak load is reached. This may be because that the fall-off of the concrete near the bottom surface of the right end of the top chord cannot be simulated by the FE model (see Figs. 6.8e and f). In conjunction with the findings given in Chapters 3 and 4, it can be concluded that the selection of the FE approach should be based on the possible failure mode for a beam with a web opening: the DP model with damage model PL is recommended for beams with a flexural failure mode, while the BC model with SECANT modulus is recommended for beams with a shear failure mode. A simple method was also proposed in this chapter for the proper selection of the FE approach and verified with the collected existing specimens (in Chapters 3 and 4) as well as the specimens tested by the candidate (in Chapter 5).

6.5 REFERENCES

ABAQUS (2012). *ABAQUS Analysis User's Manual (Version 6.12)*, Dassault Systems SIMULIA Corporation, Providence, Rhode Island, USA.

Abdalla, H.A., Torkey, A.M., Haggag, H.A. and Abu-Amira, A.F. (2003). "Design against cracking at openings in reinforced concrete beams strengthened with composite sheets", *Composite Structures*, 60(2), 197-204.

Allam, S. M. (2005). "Strengthening of RC beams with large openings in the shear zone", *Alexandria Engineering Journal*, 44(1), 59-78.

Chen, G.M., Teng, J.G. and Chen, J.F. (2011). "Finite element modeling of intermediate crack debonding in FRP-plated RC beams", Journal of Composites for Construction, ASCE, 15(3), 399-353.

Chin, S.C., Shafiq, N. and Nuruddin, M.F. (2012). "Strengthening of RC beams with large openings in shear by CFRP laminates: experiment and 2D nonlinear finite element analysis", *Research Journal of Applied Sciences Engineering and Technology*, 4(9), 1172-1180.

Chin, S.C., Shafiq, N. and Nuruddin, M.F. (2016). "Behaviour of RC beams with CFRP-strengthened openings", *Structural Concrete*, 17(1), 32-43.

GB-50010 (2010). *Code for Design of Concrete Structures*, Architectural & Building Press, Beijing, China (in Chinese).

GB-50608 (2010). *Technical Code for Infrastructure Application of FRP Composites*, China Planning Press, Beijing, China (in Chinese).

Lam, L. and Teng, J. G. (2003). "Design-oriented stress-strain model for FRP-confined concrete in rectangular columns", *Journal of Reinforced Plastics and Composites*, 22(13), 1149-1186.

Maaddawy, T. and El-Ariss, B. (2012). "Behavior of concrete beams with short shear span and web opening strengthened in shear with CFRP composites", *Journal of Composites for Construction*, ASCE, 16(1), 47-59.

Maaddawy, T. and Sherif, S. (2009). "FRP composite for shear strengthening of reinforced concrete deep beams with openings", *Composite Structures*, 89(1), 60-69.

Madkour, H. (2009). "Non-linear analysis of strengthened RC beams with web openings", *Proceedings of the Institution of Civil Engineers-Structures and Buildings*, 162(2), 115-128.

Mansur, M.A., Tan K.H. and Wei, W. (1999). "Effects of creating an opening in existing beams", *ACI Structural Journal*, 96(6), 899-906.

Pimanmas, A. (2010). "Strengthening R/C beams with opening by externally installed FRP rods: Behavior and analysis”, *Composite Structures*, 92(8), 1957-1976.

Rots, J. G. (1988). *Computational Modeling of Concrete Fracture*, Ph.D. thesis, Delft University of Technology.

Suresh, J. and Prabhavathy, R. A. (2015). “Behaviour of steel fibre reinforced concrete beams with duct openings strengthened by steel plates”, *International Journal of Advanced Information in Arts, Science & Management*, 4(4), 40-49.

Table 6.1. Test and predicted ultimate loads

Specimen	Test result (kN)	DP model with damage model ELA (kN)		DP model with damage model PL (kN)		BC model with SECANT modulus (kN)		BC model with INITIAL modulus (kN)	
		Prediction	Prediction / test	Prediction	Prediction / test	Prediction	Prediction / test	Prediction	Prediction / test
CB-Rec	340	359.9	1.06	333.5	0.981	-	-	-	-
CB-T	510	520.0	1.02	510.5	1.00	-	-	-	-
O-700×300-N	182	177.2	0.974	165.2	0.91	199.5	1.10	230.1	1.26
O-800×280-N	181	179.3	0.990	158.9	0.878	203.4	1.12	243.0	1.34
O-600×220-N	316	275.9	0.873	243.8	0.772	404.0	1.28	461.6	1.46
O-700×200-N	300	273.0	0.910	236.5	0.788	366.1	1.22	429.6	1.43
F-700×300-N	207	239.7	1.16	216.8	1.05	294.0	1.42	320.8	1.55
F-800×280-N	219	253.7	1.16	221.5	1.01	295.1	1.35	325.6	1.49
F-600×280-N	260	320.4	1.23	279.7	1.08	407.8	1.57	417.8	1.61
F-700×260-N	270	331.1	1.23	296.0	1.10	375.1	1.39	406.7	1.51
F-600×220-N	388	505.9	1.30	407.4	1.05	437.5	1.13	459.6	1.18
F-700×200-N	410	467.9	1.14	406.4	0.991	435.5	1.06	457.6	1.12
F-700×300-p	228	291.2	1.28	277.1	1.22	277.5	1.22	300.7	1.32
F-800×280-P	215	259.7	1.21	249.6	1.16	253.8	1.18	288.2	1.34
Average =			1.11		0.999		1.25		1.38
STD =			0.138		0.129		0.153		0.150
CoV =			0.125		0.129		0.122		0.108

Table 6.2. Comparison of the shear capacity and flexural capacity of the critical chord

Source	Specimen		Shear capacity (kN)		Flexural capacity (kN.m)				$(M_{cs}+M_{cs})/l$[c] (kN)		Mode of failure	
	Un-strengthened (US)	FRP-strengthened (FS)	US	FS	M_{cs}[a]		M_{ch}[b]		US	FS	US	FS
					US	FS	US	FS				
Specimens tested by the candidate	O-700×300-N	F-700×300-N	34.9	95.2	7.0	7.0	14.7	14.7	31.0	31.0	Flexure	Flexure
	O-800×280-N	F-800×280-N	41.1	113.5	7.0	7.0	24.9	24.9	39.8	39.8	Flexure	Flexure
		F-600×280-N	44.1	116.4	6.9	6.9	24.6	24.6	52.6	52.6		Flexure
		F-700×260-N	51.1	135.4	6.9	6.9	32.9	32.9	56.9	56.9		Flexure
	O-600×220-N	F-600×220-N	64.8	172.6	6.6	6.6	48.9	48.9	92.6	92.6	Shear	Flexure
	O-700×200-N	F-700×200-N	71.7	191.4	6.5	6.5	57.0	57.0	90.7	90.7	Shear	Flexure
Teng et al. (2013)	O-500×150		93.1		5.6		82.9		177.1		Shear	
		FRP-500×220	66.7	168.0	5.6	37.6	51.1	52.1	113.5	179.4		Shear
Maaddawy and Ariss (2012)	CN-500×120	S1-500×120	2.1	22.0.	0.3	7.1	9.0	9.0	18.5	32.2	Shear	Shear
		S2-500×120		23.1								
	CN-500×160	S1-500×160	2.1	16.4	0.3	4.8	6.4	6.4	13.5	22.4	Shear	Shear
		S2-500×160		17.0								
Abdalla et al. (2003)	UO8	RO2	11.4	11.4	1.3	>1.3[d]	2.3	>2.3	18.3	>18.3	Shear	Shear
	UO9	RO3	11.6	11.6	1.4	>1.4	2.4	>2.4	12.5	>12.5	Shear	Shear
	E2		4.5		1.0		4.2		8.7		Shear	

Madkour (2009)	E3		4.5		1.0		3.5		7.4		Shear	
	E4		4.5		1.0		2.6		6.0		Shear	
	E5		4.5		1.0		1.7		4.6		Shear	
Allam (2005)	B2	B8	9.7	9.7	1.5	>1.5	7.3	>7.3	19.5	>19.5	Shear	Shear
Suresh and Prabhavathy (2015)	NS250		6.24		0.5		2.9		13.5		Shear	
	NS300		6.24		0.5		2.9		11.3		Shear	
Chin et al. (2012)	B3	B5	5.1	5.1	0.7	>0.7	1.0	>1.0	8.0	>8.0	Shear	Shear

Note:

(a) The flexural capacity of the chord in sagging bending;

(b) The flexural capacity of the chord in hogging bending;

(c) The length of the chord;

(d) The flexural capacity of the chord after FRP-strengthening doesn't need to be further calculated because the shear capacity of the chord after FRP strengthening is still smaller than the flexural capacity of the un-strengthened chord.

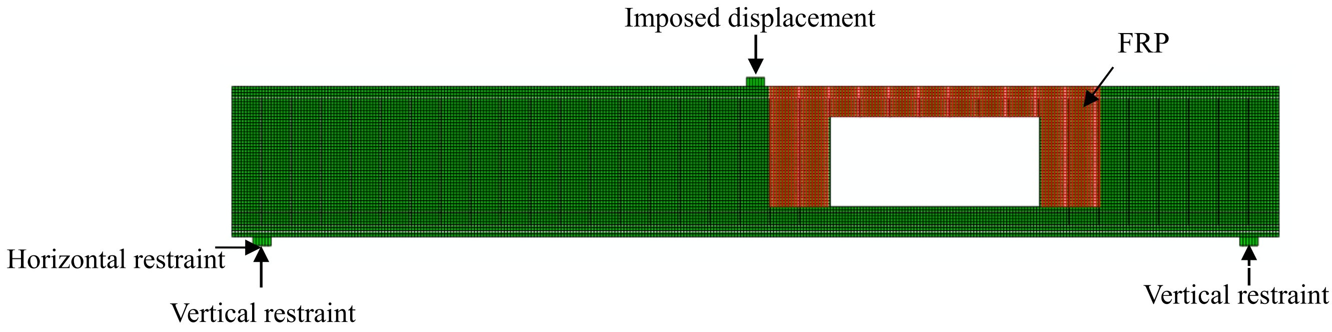

Figure 6.1. Typical FE mesh

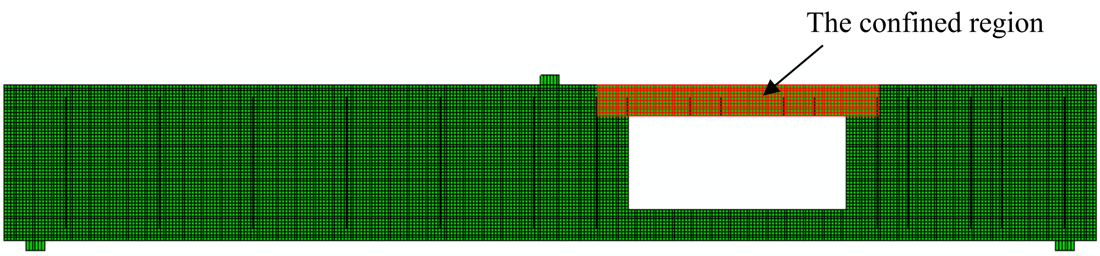

Figure 6.2. The confined region of concrete (F-700×300-N)

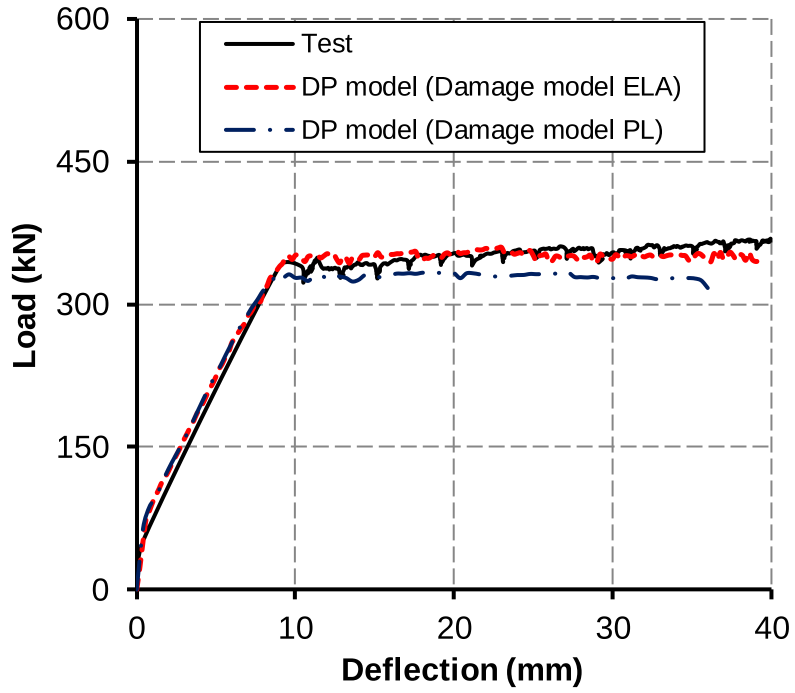

(a) CB-Rec

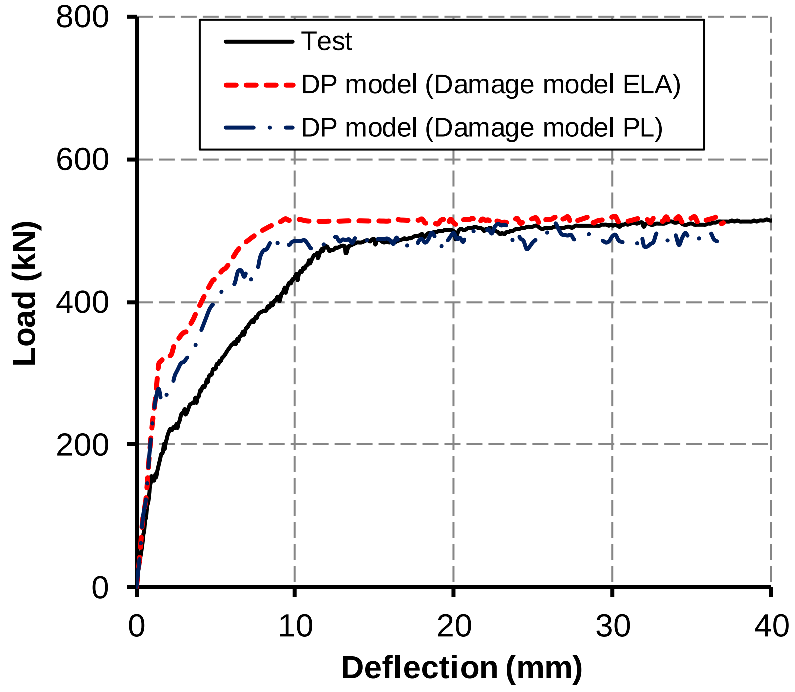

(b) CB-T

Figure 6.3. Comparison of load-deflection curves between FE prediction and test: control beams

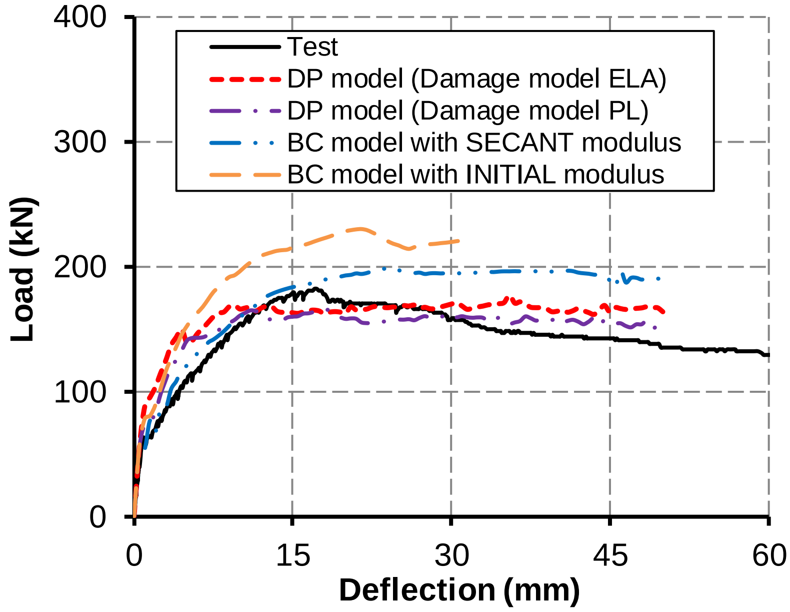

(a) O-700×300-N

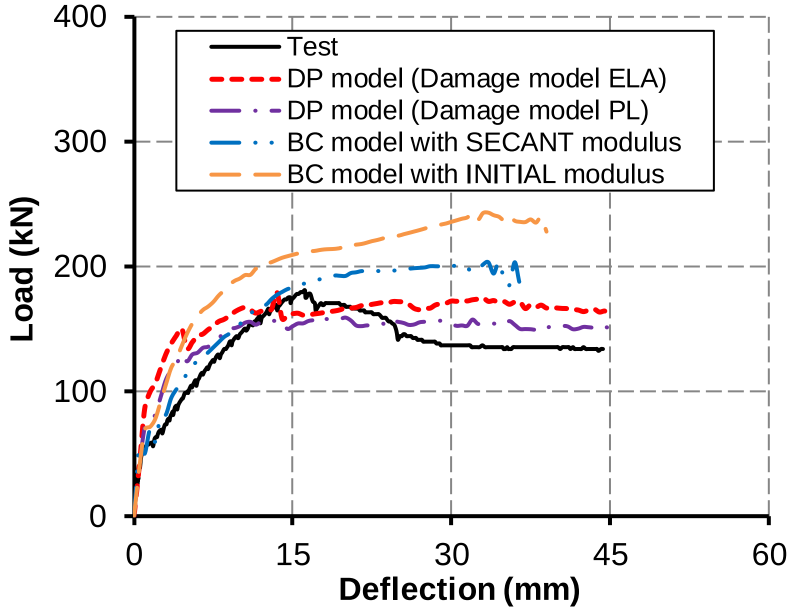

(b) O-800×280-N

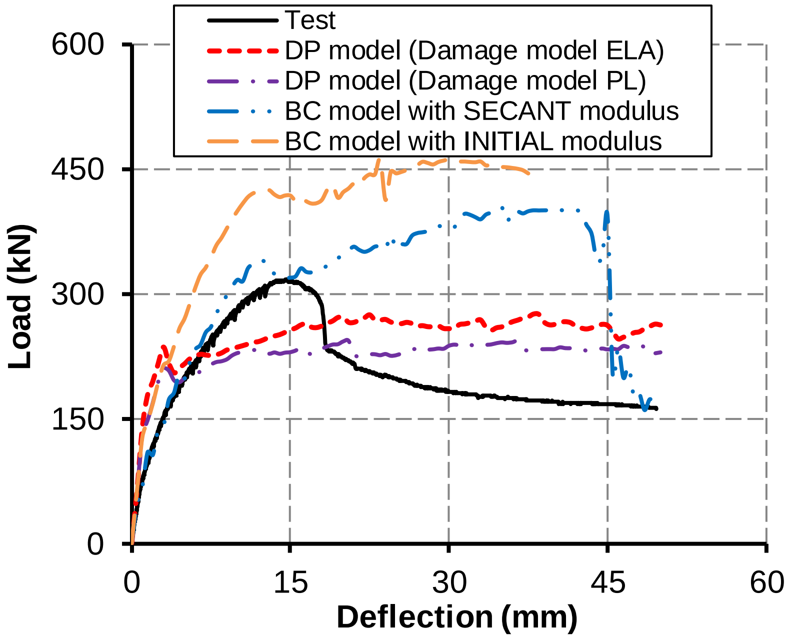

(c) O-600×220-N

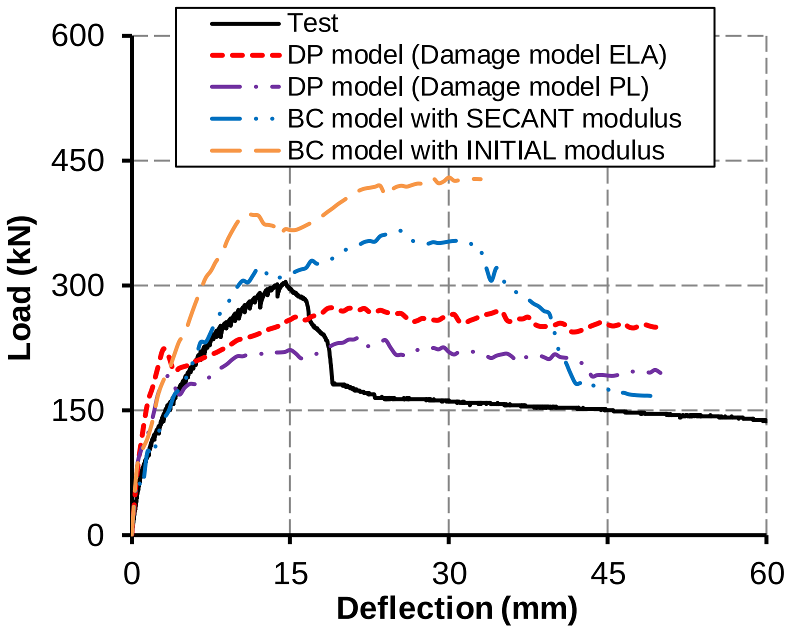

(d) O-700×200-N

Figure 6.4. Comparison of load-deflection curves between FE prediction and test: beams with an un-strengthened web opening

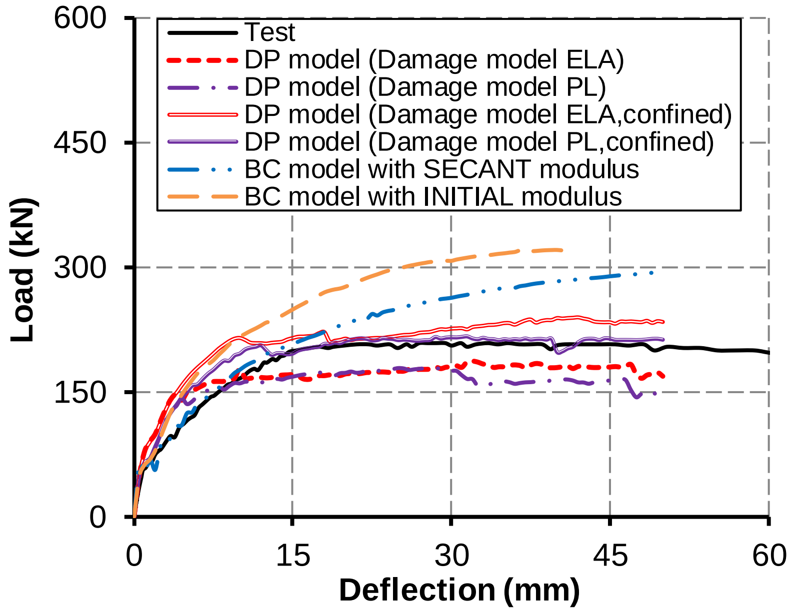

(a) F-700×300-N

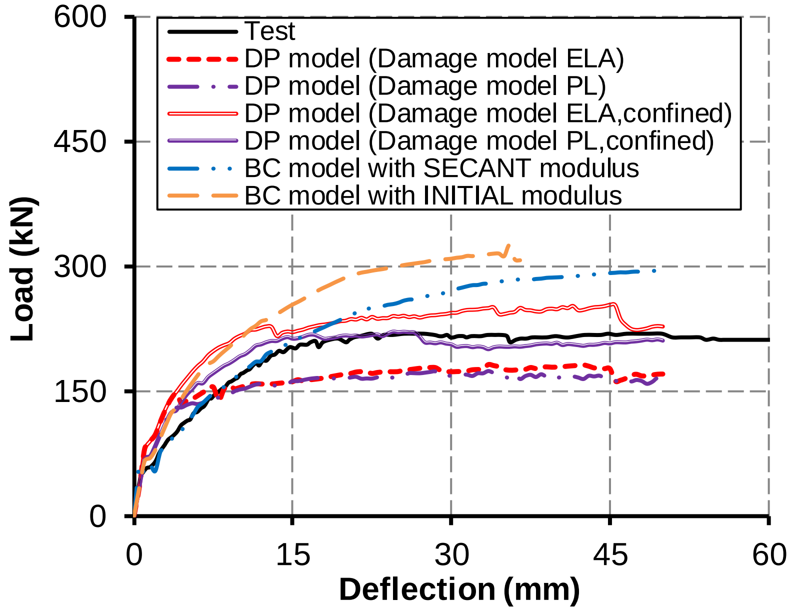

(b) F-800×280-N

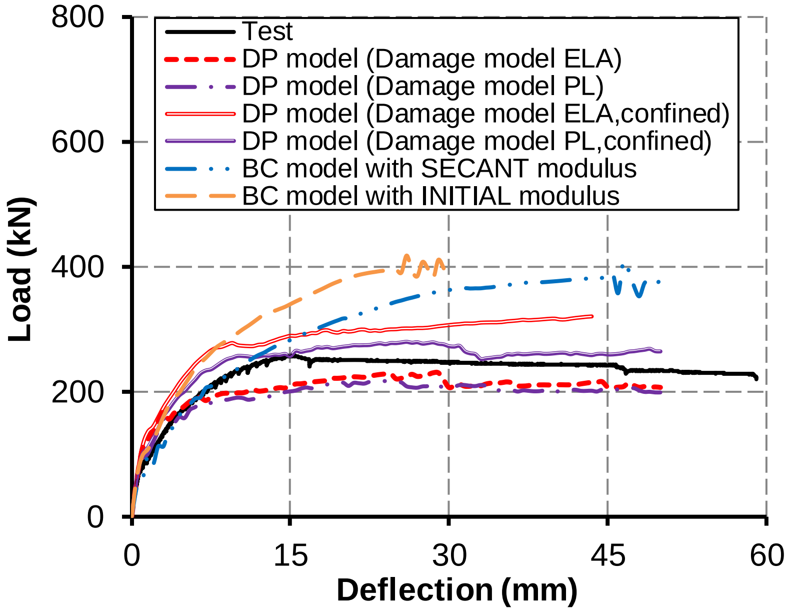

(c) F-600×280-N

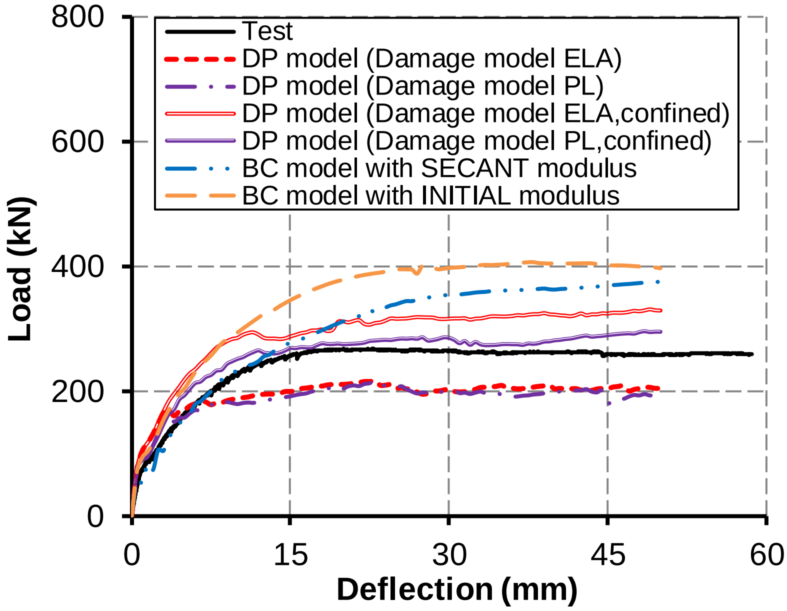

(d) F-700×260-N

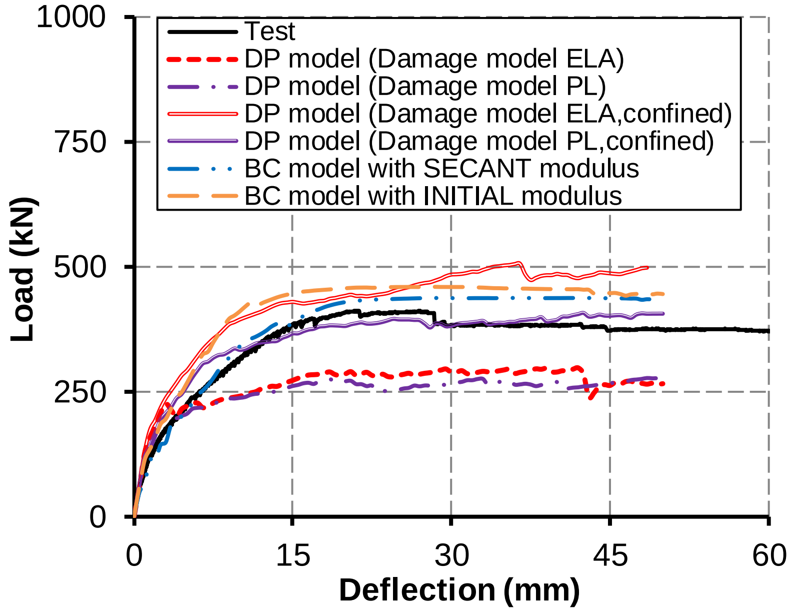

(e) F-600×220-N

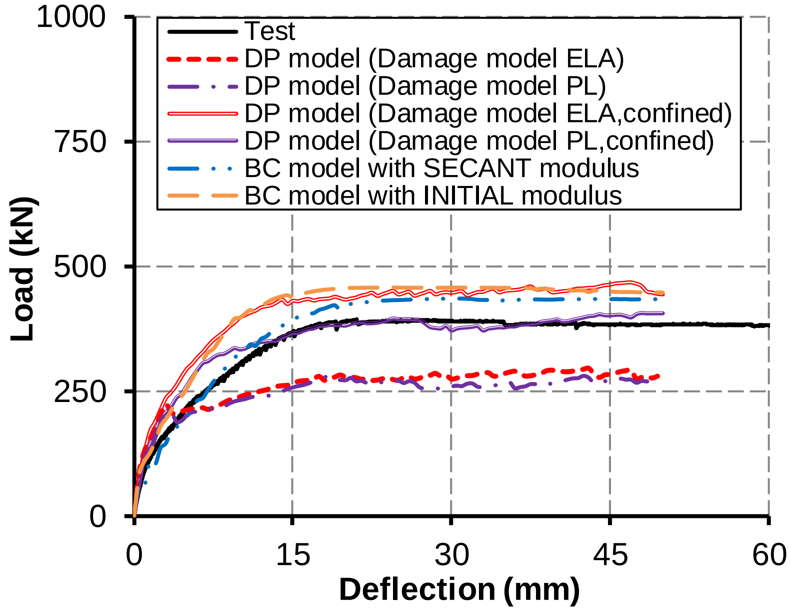

(f) F-700×200-N

Figure 6.5. Comparison of load-deflection curves between FE prediction and test: beams with an FRP-strengthened web opening in negative bending

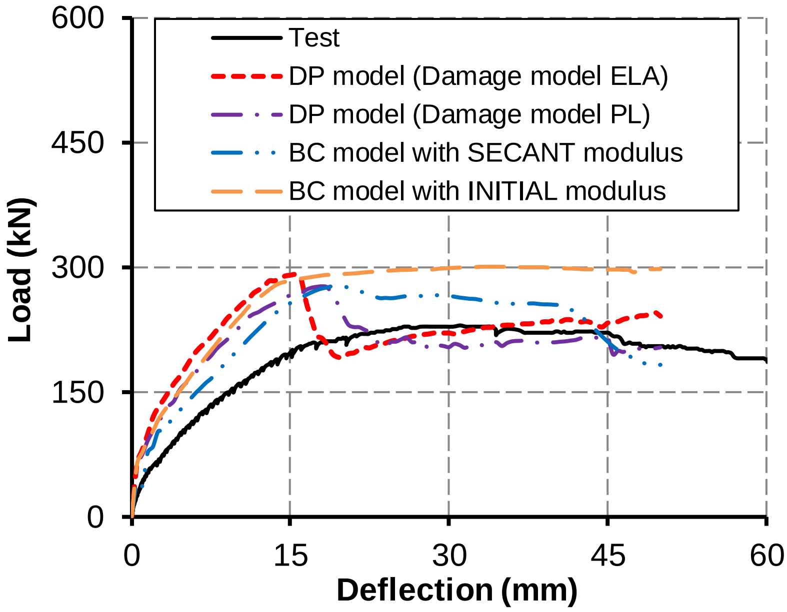

(a) F-700×300-P

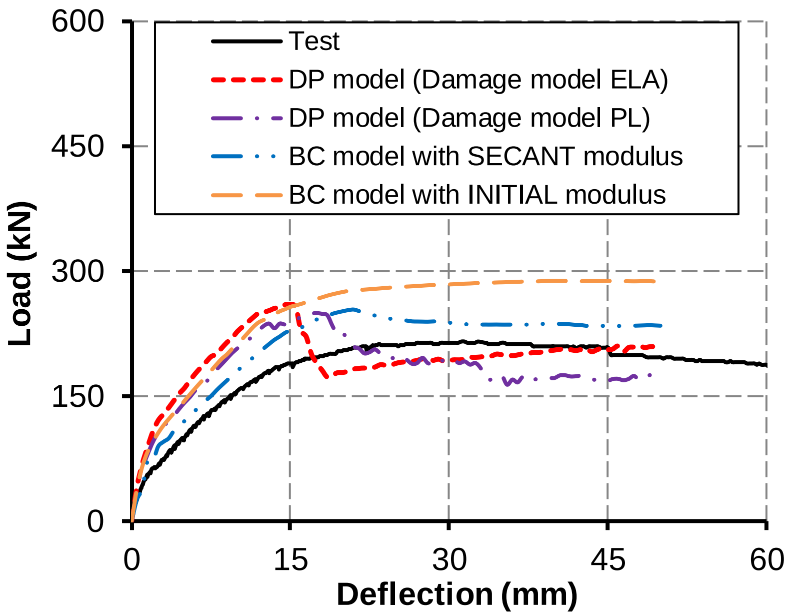

(b) F-800×280-P

Figure 6.6. Comparison of load-deflection curves between FE prediction and test: beams with an FRP-strengthened web opening and tested in positive bending

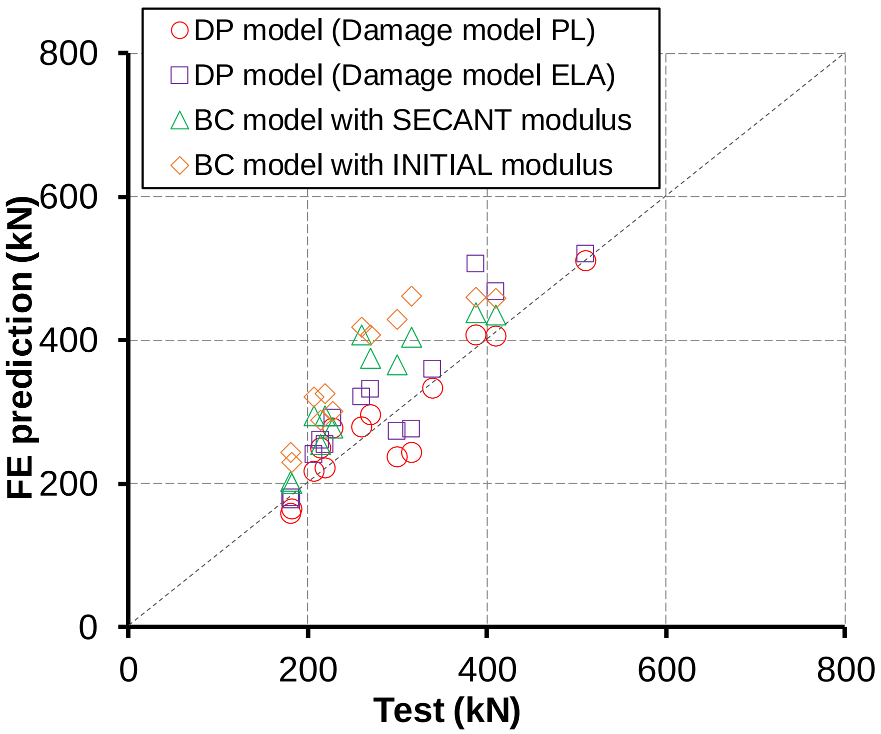

Figure 6.7. Comparison of ultimate loads between FE predictions and tests

(a) CB-Rec

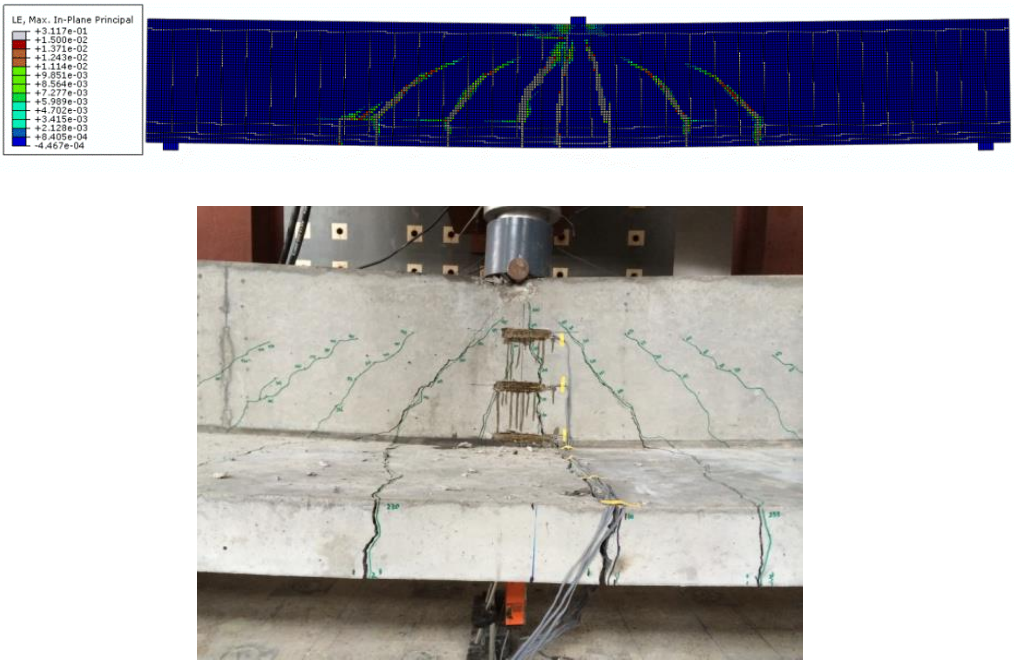

(b) CB-T

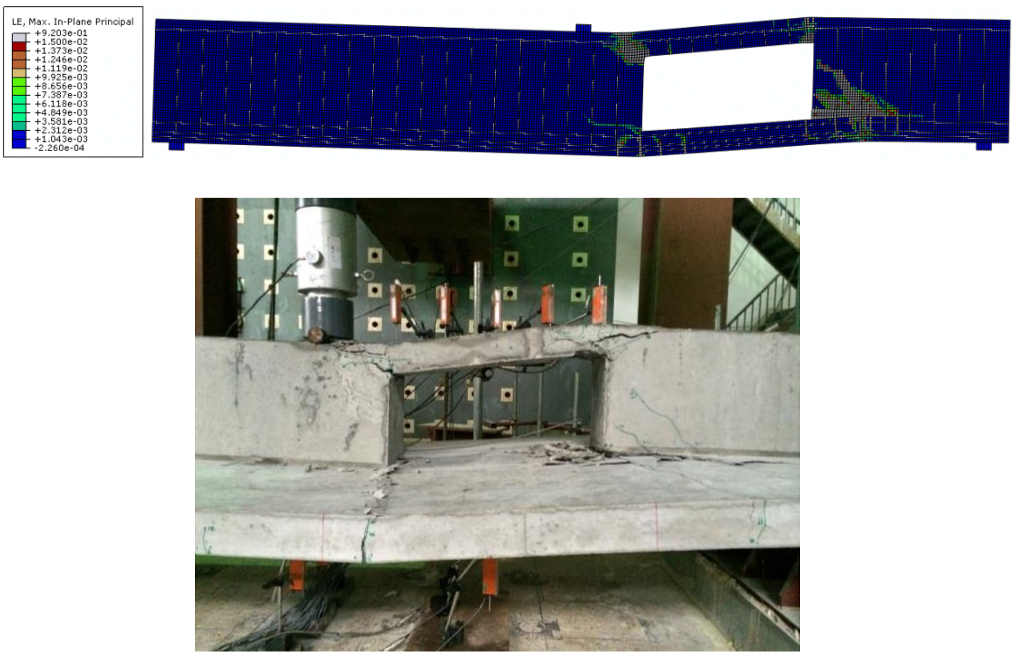

(c) O-700×300-N

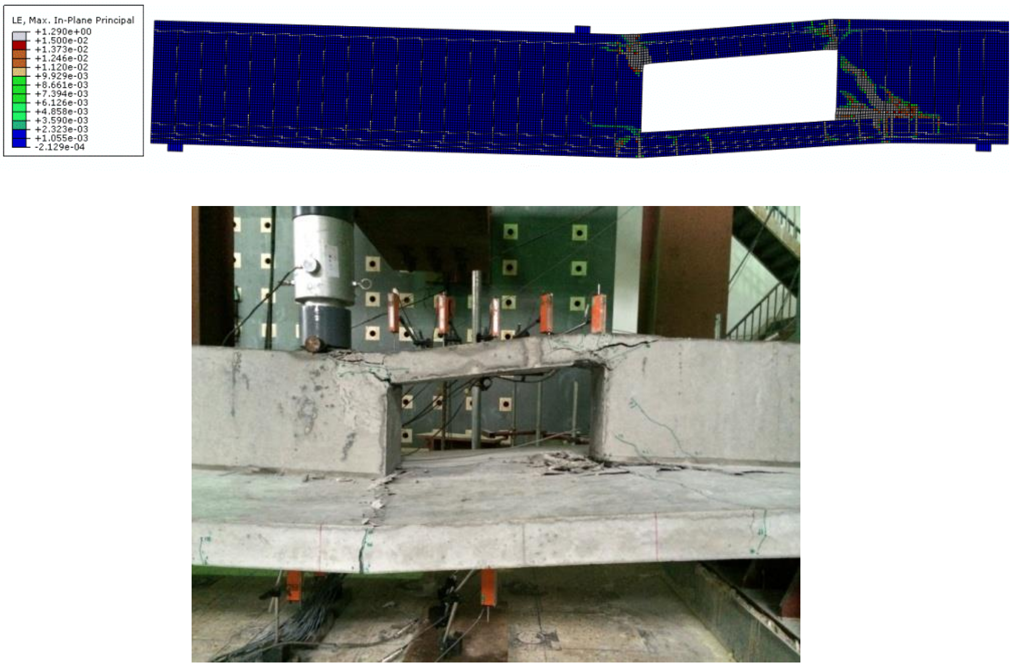

(d) O-800×280-N

(e) O-600×220-N

(f) O-700×200-N

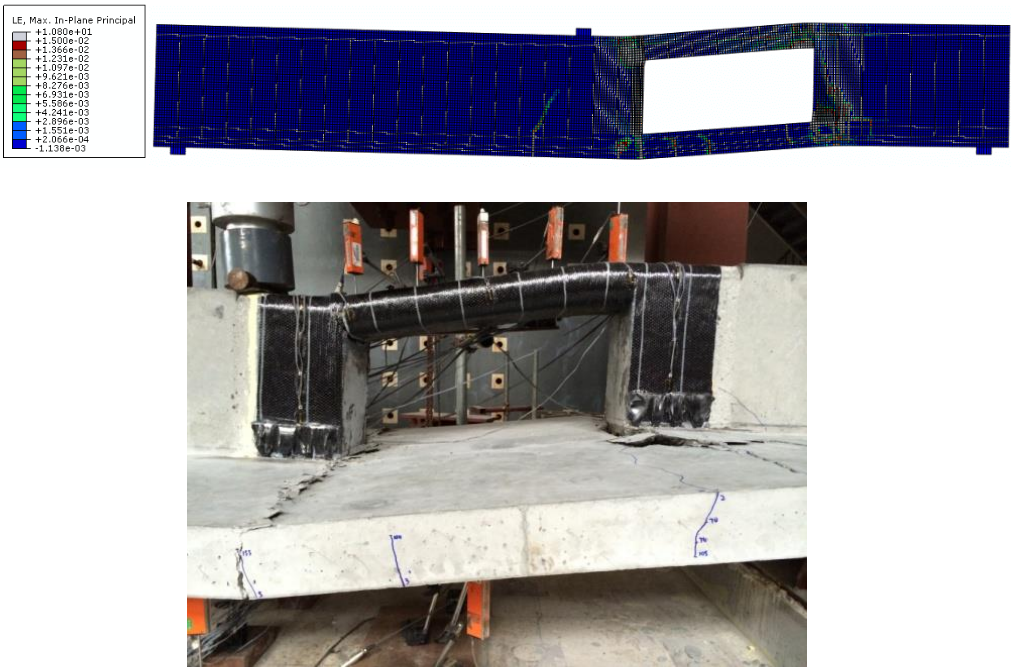

(g) F-700×300-N

(h) F-800×280-N

(i) F-600×280-N

(j) F-700×260-N

(k) F-600×220-N

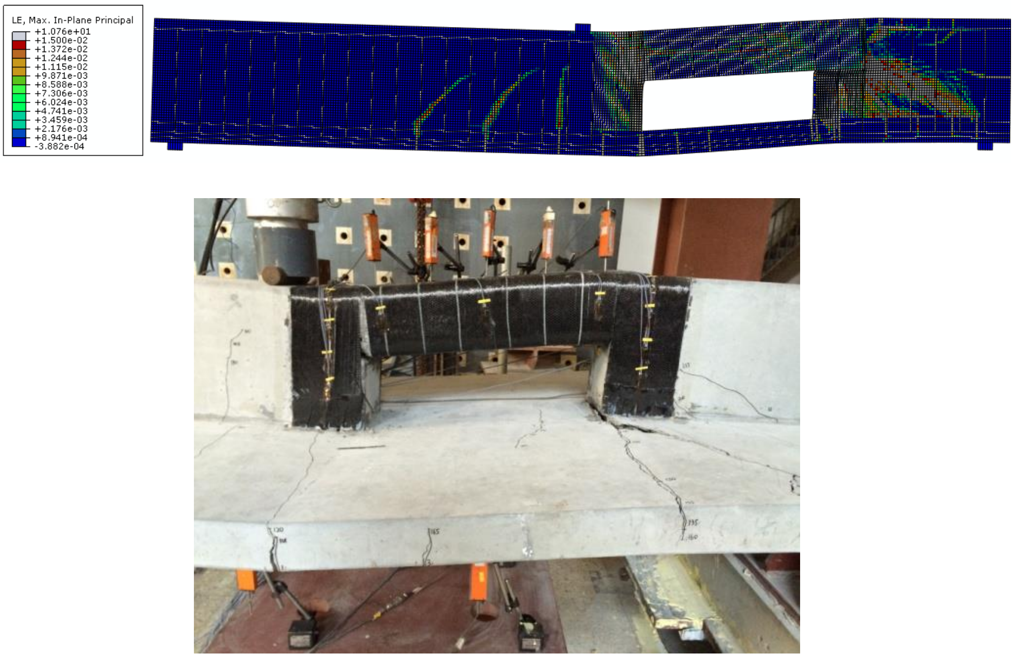

(l) F-700×200-N

(m) F-700×300-P

(n) F-800×280-P

Figure 6.8. Comparison of crack patterns at ultimate state between FE prediction and test

CHAPTER 7

STRENGTH MODEL FOR RC BEAMS WITH A WEB OPENING

7.1 INTRODUCTION

In Chapters 3 to 6, a reliable FE approach for the modelling of RC beams with an un-strengthened/FRP-strengthened web opening has been established. The concrete damaged plasticity model with damage model PL (i.e. power law) was recommended for beams failing in a flexural mode, while the brittle cracking model with SECANT modulus is recommended for beams failing in a shear failure mode. Although the proposed FE models can well predict the behaviour of RC beams with a web opening, the analyses are relatively time-consuming and not easy for use by most engineers. If only the strength of the beam is of concern, it is desirable to develop a simple calculation method for engineering use. For solid RC beams (i.e., RC beams without web openings), the strength can be easily calculated through a conventional section analysis based on the plain cross-section assumption. However, the situation is much more complicated for RC beams with a web opening (especially a large web opening), as the plain cross-section assumption is not applicable any more for cross sections in the opening region. In this chapter, a simple calculation method for predicting the strength of RC beams with a web opening is first proposed, and then a strength model for RC beams with a web opening is established based on the results from the proposed calculation method. The accuracies of the simple calculation method and the strength model are verified with the test results. It should be noted that the present study is only concerned with RC beams with a web opening which exhibit a flexural failure model (i.e., with four plastic hinges forming at the two ends of the top and the bottom chords). The flexural failure mode, which is ductile, is the desired failure mode and should be ensured when the BO technique is implemented, thus the development of the strength model is mainly focused on RC beams with a web opening which exhibit a flexural failure model.

7.2 MANSUR ET AL.'S (1984) MODEL

Mansur's research group from Universiti Teknologi Malaysia has conducted a number of studies on the behavior and design of RC beams with a web opening since 1984 (e.g. Mansur et al. 1984; Mansur et al. 1985; Mansur 1998; Mansur et al. 1999; Mansur 2006). Their studies were mainly concerned with RC beams with a pre-formed web opening and the purpose of making openings in the beams was to provide passages for utility ducts and pipes. In Mansur et al. (1984), a method was developed to predict the strength of RC beams with a large rectangular opening in three-point bending based on the following assumptions:

1) The opening is rectangular in shape; the top and the bottom chords have uniform cross-sections and uniform steel reinforcement throughout the length of the chords;
2) By using a proper reinforcement scheme, the top and the bottom chords have sufficient ductility under combined bending, axial and shear deformations;

3) The top and the bottom chords have sufficient shear resistance, and the corners of the opening are also sufficiently reinforced to prevent premature failure due to stress concentration;
4) The dimensions of the top chord are well designed so that the slenderness effect can be ignored;
5) The top and the bottom chords are assumed to frame into the rigid abutments on the two sides of the opening; and
6) The failure of the beam is controlled by the formation of four plastic hinges, one at each end of the top and the bottom chords.

The calculation method has the following procedure: (1) firstly, the interaction diagrams between axial force (N) and bending moment (M) (referred to as *N-M* curves for simplicity) of the cross sections at the two ends of the top and the bottom chords were evaluated. In order to simplify the analysis, the *N-M* curves were approximated by piecewise linear segments and expressed in a matrix form; (2) based on the above assumptions, the deformed shape of the beam was studied and the conditions of deformation compatibility (i.e. the relationships between the rotations and axial deformations of the two chords) were obtained; and (3) by applying the principle of virtual work, the strength equation of the beam was formulated.

Mansur et al.'s (1984) model adopted the principle of virtual work based on the conditions of deformation compatibility, and the deduction procedure and the obtained expression of the strength model are relatively complicated, which is not desirable for engineering use. In the present study, a simple calculation method was proposed based on conditions of force equilibrium, with both the actual *N-M* curves and the simplified *N-M* curves of the relevant cross sections being examined. More importantly, Mansur et al.'s (1984) model is only concerned with RC beams with a pre-formed web opening which is well reinforced with internal steel bars. For such RC beams, the four plastic hinges at the two ends of the top and the bottom chords usually form due to the yielding of the tension steel bars, and thus the *N-M* curves can be obtained based on the yielding of the tension steel bars. However, for RC beams with a post-formed web opening strengthened with FRP, the tension steel bars in the top chord may not yield at the failure of the beam. Therefore, the calculation of the *N-M* curves of the two cross sections at the two ends of the top chord needs to be studied.

7.3 PROPOSED CALCULATION METHOD

The six assumptions made in Mansur et al.'s (1984) model (as listed in Section 7.2) are followed in the present study. Before introducing the proposed calculation method, the opening region which dominates the strength of the beam is separated from the rest of the beam for force analyses. A free-body diagram of the top and the bottom chords is shown in Fig. 7.1, in which the opening is assumed to be located at the right span of the beam, that is, the left end of the opening is closer to the loading point and the right end of the opening is closer to the right support. As can be seen from Fig. 7.1, both the top chord and the bottom chord are subject to the combined action of bending moment M, shear force V and axial force N. The marked directions of the forces in the figure indicate the positive directions of the forces. M_{tR}, M_{tL}, M_{bR} and M_{bL} are bending moments at the two ends of the chords relative to the midline of the chords; M_{tR} and M_{bR} are respectively bending moments at the right end of the top chord and the bottom chord, and M_{tL} and M_{bL} are respectively bending moments at the left end of the top chord and the bottom chord; V_t and V_b are respectively shear forces in the top chord and the bottom chord; N_t and N_b are respectively axial forces in the top chord and the bottom chord. Based on Fig. 7.1, the equilibrium equations can be obtained as follows.

For the top chord:

$$V_t l = M_{tR} + M_{tL} \tag{7.1}$$

where l is the length of the opening.

For the bottom chord:

$$V_b l = M_{bR} + M_{bL} \tag{7.2}$$

For the right end of the opening:

$$N_t = N_b \tag{7.3}$$

$$M_R = N_t z - M_{tR} - M_{bR} \tag{7.4}$$

$$M_R = V_R L_R \tag{7.5}$$

where M_R is the total moment at the right end of the opening, z is the distance between the midlines of the top and the bottom chords, V_R is the reaction force at the right support calculated from M_R, and L_R is the distance between the right end of the opening and the right support (Fig. 7.1a).

For the left end of the opening:

$$M_L = N_t z + M_{tL} + M_{bL} \tag{7.6}$$

$$M_L = V_L(L_R + l) \tag{7.7}$$

where M_L is the total moment at the left end of the opening, and V_L is the reaction at the right support calculated from M_L.

For the whole beam:

$$V_L = V_R = V_t + V_b \tag{7.8}$$

The proposed calculation method for the strength of an RC beam with a web opening consists of the following steps, which can be operated with the help of Excel:

Step-1: Obtaining the *N-M* curves of cross sections at the two ends of the top and the bottom chords (i.e., N_t - M_{tR} curve, N_t - M_{tL} curve, N_b - M_{bR} curve and N_b - M_{bL} curve) through cross-section analysis. If the chord is confined using FRP complete wraps, the effect of FRP confinement on the concrete should be taken into account. The detailed calculation method of these *N-M* curves will be illustarted in the next section;

Step-2: Assuming a starting value (usually a very small value) of the axial force N_t (or N_b), the corresponding M_{tR}, M_{tL}, M_{bR} and M_{bL} can be determined using the *N-M* curves obtained from Step-1;

Step-3: Substituting the obtained values of M_{tR}, M_{tL}, M_{bR} and M_{bL} and the corresponding value of N_t (or N_b) from Step 2 into Eqs. 7.4-7.7, the corresponding values of V_L and V_R can be obtained; and

Step-4: If the obtained V_L is equal to V_R (i.e., Eq. 7.8 is satisfied), the assumed value of N_t (or N_b) in Step-2 is the correct value, based on which the corresponding moments and forces at the chord ends can be calculated using Eqs. 7.4-7.7 and the ultimate load of the beam can be calculated based on the location of the applied point load. Otherwise, gradually increase the value of N_t (or N_b) with a proper increment and repeat Steps 2-4 until Eq. 7.8 is satisfied.

7.4 VERIFICATION OF THE PROPOSED CALCULATION METHOD

The RC T-section beams with a web opening tested by the candidate are used to verify the accuracy of the proposed calculation method. Specimen F-700×300-N is taken as an example to show the layout of the tested specimens (Fig. 7.2). As presented in Chapter 5, all eight tested RC T-section beams with an FRP-strengthened web opening exhibited a flexural failure mode due to the formation of four plastic hinges at the ends of the chords, as shown in Fig. 7.3. These tested RC T-section beams with an FRP-strengthened web opening satisfy all the assumptions of the proposed calculation method and are thus used to verify the accuracy of the proposed calculation method. Specimen F-700×300-N is taken as an example to illustrate the calculation procedure.

7.4.1 Calculation of the *N-M* curves

The *N-M* curves of cross sections at the ends of the top and the bottom chords are obtained as follows (the locations and directions of the forces are shown in Fig. 7.1). It should be noted that compressive axial forces and hogging bending moments are regarded as positive in plotting the *N-M* curves.

7.4.1.1 N_b-M_{bR} curve (the right end of the bottom chord)

Based on the plain cross-section assumption, strain distributions on the cross section at the right end of bottom chord are shown in Fig. 7.4, in which x represents the height of the compressive zone. This cross section is under a hogging moment; that is, the bottom part of this cross section is under compression while the top part of this cross section is under tension. Two states (i.e. yielding state or ultimate state) of the beam are considered in the calculation of the N_b - M_{bR} curve for comparison purposes: (1) yielding state: the calculation is based on the yielding of the tension steel bars, as shown in Fig. 7.4(a), in which ε_{s2} is the strain of the longitudinal steel bars in the beam web and set to be the yielding strain of the steel bars (0.0024), ε_{s1} and ε_{s3} are respectively the strains of the longitudinal steel bars in the beam flange located closer to the upper surface and the lower surface of the flange, ε_c is the strain of concrete at the bottom surface of the chord; (2) ultimate state: the calculation is based on the crushing of the compressive concrete. The crushing strain of the compressive concrete (ε_{cu}) is set to be 0.0033, following the Chinese design code for concrete structures (GB-50010 2010), as shown in Fig. 7.4(b).

For each assumed axial force N_b, the height of the compressive zone x can be determined, and then the corresponding bending moment M_{bR} can be calculated. It should be noted that M_{bR} is relative to the mid-plane of the chord. By assuming a series of values for N_b, the N_b - M_{bR} curve can be finally obtained for each examined state, as shown in Fig. 7.5. For comparison purposes, the simplified curve ($N_b^{'}$ - $M_{bR}^{'}$ curve) obtained by connecting the intersections between the N_b - M_{bR} curve and the two coordinate axes is also examined in the present study. As shown in Fig. 7.5, the $N_b^{'}$ - $M_{bR}^{'}$ curve is a linear curve. Moreover, as can be seen from Figs. 7.5(a) and (b), the N_b - M_{bR} curves and $N_b^{'}$ - $M_{bR}^{'}$ curves obtained respectively based on the yielding state and ultimate state of the cross section are almost the same, which indicates that the *N-M* curve of this cross section remains nearly unchanged after the yielding of this cross section.

7.4.1.2 N_b-M_{bL} curve (the left end of the bottom chord)

Strain distributions on the cross section at the left end of bottom chord are shown in Fig. 7.6. The two states considered in the calculation of N_b - M_{bR} curve are also considered here (Fig. 7.6). Following a similar procedure as introduced above, the N_b - M_{bL} curve and the $N_b^{'}$ - $M_{bL}^{'}$ curve for each examined state are obtained and shown in Fig. 7.7. The $N_b^{'}$ - $M_{bL}^{'}$ curve is a linear curve (Fig. 7.7). It can also be seen from Fig. 7.7 that the *N-M* curve of this cross section also remains unchanged after the yielding of this cross section.

7.4.1.3 N_t-M_{tR} curve (the right end of the top chord)

Strain distributions on the cross section at the right end of top chord are shown in Fig. 7.8. The bottom part of this cross section is under compression and thus the crushing of concrete happens on the bottom surface of the chord at the failure of chord. As the top chord is confined using FRP wraps, the confinement effect of FRP wraps on the concrete in the top chord should be taken into consideration. In the present study, Lam and Teng's (2003) design-oriented stress-strain model for FRP-confined concrete in rectangular columns was adopted to consider the confinement effect of FRP wraps on the concrete (see Eqs. 6.2-6.13 in Chapter 6). Similar to the calculation of N_b - M_{bR} curve, the two states of the beam cross section (i.e. yielding state or ultimate state) are considered in the calculation of the N_t - M_{tR} curve. It should be noted that, however, unlike the bottom chord, the tension steel bars in the top chord do not yield at the failure of the chord. Instead, the yielding behaviour of the top chord comes from the plastic compressive behaviour of the FRP-confined concrete. According to Lam and Teng (2003), the compressive stress-strain curve of FRP-confined concrete consists of a parabolic first portion and a straight-line second portion with a much smaller slope than the initial slope of the first portion. In the present study, therefore, the transition point between the first and second portions on the stress-strain curve is regarded as the yielding point of the FRP-confined concrete. The two examined states in the calculation of the N_t - M_{tR} curve are therefore as follows: (1) yielding state: the calculation for the state when the compressive strain of concrete reaches the transition point strain on the stress-strain curve for FRP-confined concrete. For the top chord of Specimen F-700×300-N, the compressive strain of concrete at the transition point (ε_{cy}) is equal to 0.0027 [Fig. 7.8(a)], according to Lam and Teng's (2003) model; (2) ultimate state: the calculation for the state when the ultimate compressive strain of FRP-confined concrete is reached. For the top chord of Specimen F-700×300-N, the ultimate compressive strain of the FRP-confined concrete is 0.008 [Fig. 7.8(b)], according to Lam and Teng's (2003) model.

Following a similar procedure as introduced above, the actual N_t - M_{tR} curve and the simplified $N_t^{'}$ - $M_{tR}^{'}$ curve for each examined state were obtained and shown in Fig. 7.9. It should be noted that the *N-M* curve of a cross section under combined compression and bending could have three key points, corresponding to the following three situations, respectively: (1) N_t equals to 0; (2) M_{tR} equals to 0; and (3) when the crushing of concrete and the yielding of tension steel bars occur simultaneously. However, the third situation may not occur, because the steel bars may not yield at the crushing of concrete when the height of the cross section is too small. Therefore, only the first two situations were considered for this cross section in obtaining the simplified curve, leading to a linear simplified curve (dotted line in Fig. 7.9).

7.4.1.4 N_t-M_{tL} curve (the left end of the top chord)

Strain distributions on the cross section at the left end of top chord are shown in Fig. 7.10. The top part of this cross section is under compression and thus the crushing of concrete happens on the top surface of the chord at the failure of chord. The two states considered in the calculation of N_t - M_{tR} curve are also considered here (Fig. 7.10). Following a similar procedure as introduced above, the actual N_t-M_{tL} curve and the simplified $N_t^{'}$-$M_{tL}^{'}$ curve can be obtained, as shown in Fig. 7.11. For this cross section, all the three situations mentioned above occur, therefore, the simplified $N_t^{'}$-$M_{tL}^{'}$ curve is a bi-linear curve.

7.4.1.5 Combined N-M curves

The four *N-M* curves discussed above are combined together and shown in Fig 7.12, with a proper sign convention (i.e., axial forces in compression and hogging bending moments are regarded as positive). Both the actual curve and the simplified curve are included in this figure. The combined *N-M* curves based on the yielding state of the cross sections are shown in Fig. 7.12(a), while those based on the ultimate state of the cross sections are shown in Fig. 7.12(b).

7.4.2 Calculation of the forces

Applying Steps 2 and 3 of the proposed calculation method, the values of V_L and V_R corresponding to a given N_t can be obtained and thus the V_L-N_t curve and V_R-N_t curve can be plotted (Fig. 7.13). In Fig. 7.13, V_L-N_t curve and V_R-N_t curve are obtained from the actual *N-M* curves, while $V_L^{'}$-N_t curve and $V_R^{'}$-N_t curve are obtained from the simplified *N-M* curves. The point of intersection (point V shown in Fig. 7.13) between the V_L-N_t curve and the V_R-N_t curve corresponds to the converged result based on the actual *N-M* curves, while point V' shown in Fig. 7.13 between the $V_L^{'}$ - N_t curve and the $V_R^{'}$ - N_t curve corresponds to the converged result based on the simplified *N-M* curves. The vertical coordinates of points V and V' in Fig. 7.13 are respectively the obtained shear forces from the actual *N-M* curve and the simplified *N-M* curve. Once the shear force in the beam is obtained, the ultimate load of the beam can be calculated based on the location of the applied point load. For specimens in three-point bending, the ultimate load F can be calculated using the following equation:

$$F = \frac{L}{L_{LS}} V_L \tag{7.9}$$

where L is the clear span of the whole beam, L_{LS} is the left shear span of the beam.

The ultimate loads of the eight RC T-section beams with an FRP-strengthened web opening tested by the candidate were calculated using the proposed calculation method and listed in Table 7.1. For each of the two examined states of the cross sections (i.e. yielding state or ultimate state), both the actual and the simplified *N-M* curves were employed to calculate the ultimate load for comparison purposes. As can be seen from Table. 7.1, the ultimate loads of all eight beams calculated based on the actual *N-M* curves are closer to the test results than those calculated based on the simplified *N-M* curves, and the ultimate loads of all eight beams calculated based on the ultimate states of the cross sections are larger than those calculated based on the yielding states of the cross sections. Moreover, as can be seen from Table 7.1, when the actual *N-M* curve is used, the calculation method based on the ultimate state of the cross section slightly overestimates the ultimate load of the beam, with an average prediction-to-test ratio of 1.01, a standard deviation (STD) of 0.038, and a coefficient of variation

(CoV) of 0.038, while the calculation method based on the yielding state of the cross section slightly underestimates the ultimate load of the beam, with an average prediction-to-test ratio of 0.960, a standard deviation (STD) of 0.055, and a coefficient of variation (CoV) of 0.058. When the simplified *N-M* curve is used, the calculation method based on either the ultimate state or the yielding state of the cross section underestimates the ultimate load of the beam, with an average prediction-to-test ratio of 0.945 or 0.885, a standard deviation (STD) of 0.017 or 0.030, and a coefficient of variation (CoV) of 0.018 or 0.034 for the ultimate state and yielding state of the cross section. From the above comparison, it can be seen that: (1) either the actual *N-M* curve or the simplified *N-M* curve corresponding to either the ultimate state or the yielding state of the cross section can lead to acceptable predictions of the test results; and (2) the ultimate load calculated based on the yielding state of the cross section can be treated as the lower bound of the actual ultimate load of the beam, while that calculated based on the ultimate state of the cross section can be treated as the upper bound.

7.5 PROPOSED STRENGTH MODEL

It can be seen from Table 7.1 that, although the calculation method based on the simplified *N-M* curves underestimates the strength of the beams, it still offers quite acceptable predctions. In this section, a strength model based on the simplified *N-M* curves is developed for ease of engineering use.

A simplified global *N-M* curve of the cross-sections at the two ends of top and bottom chords is shown in Fig. 7.14, in which the key points determining the curves are indicated. For example, the Point (M_{10}, 0) represents the point of $N_t^{'}$-$M_{tR}^{'}$ curve where the axial force $N_t^{'}$ equals to 0 and the corresponding bending moment $M_{tR}^{'}$ equals to M_{10}, while the Point ($-M_{22}$, N_{22}) represents the point of $N_t^{'}$ - $M_{tL}^{'}$ curve where the bending moment $M_{tL}^{'}$ reaches its maximum magnitude M_{22}. All these key points can be obtained using the cross-section analysis as presented in the last section. The four curves can be expressed as follows:

$$M_{tR}^{'} = a_{tR} N_t^{'} + b_{tR} \tag{7.10}$$

$$M_{tL}^{'} = a_{tL} N_t^{'} + b_{tL} \tag{7.11}$$

$$M_{bR}^{'} = a_{bR} N_b^{'} + b_{bR} \tag{7.12}$$

$$M_{bL}^{'} = a_{bL} N_b^{'} + b_{bL} \tag{7.13}$$

where

$$a_{tR} = \begin{cases} \dfrac{M_{11} - M_{10}}{N_{11}} & \text{for } N_{tR}^{'} \le N_{11} \\ \dfrac{M_{11}}{N_{11} - N_{10}} & \text{for } N_{tR}^{'} > N_{11} \end{cases} \tag{7.14}$$

$$b_{tR} = \begin{cases} M_{10} & \text{for } N_{tR}^{'} \le N_{11} \\ \dfrac{M_{11} N_{10}}{N_{10} - N_{11}} & \text{for } N_{tR}^{'} > N_{11} \end{cases} \tag{7.15}$$

$$a_{tL} = \begin{cases} \dfrac{M_{22} - M_{20}}{N_{22}} & \text{for } N_{tL}^{'} \le N_{22} \\ \dfrac{M_{22}}{N_{22} - N_{20}} & \text{for } N_{tL}^{'} > N_{22} \end{cases} \tag{7.16}$$

$$b_{tR} = \begin{cases} M_{20} & \text{for } N_{tL}^{'} \le N_{22} \\ \dfrac{M_{22} N_{20}}{N_{20} - N_{22}} & \text{for } N_{tL}^{'} > N_{22} \end{cases} \tag{7.17}$$

$$a_{bR} = -\frac{M_{30}}{N_{30}} \tag{7.18}$$

$$b_{bR} = M_{30} \tag{7.19}$$

$$a_{bL} = -\frac{M_{40}}{N_{40}} \tag{7.20}$$

$$b_{bL} = M_{40} \tag{7.21}$$

According to Eq. 7.3, the following equation should be satisfied:

$$N_t^{'} = N_b^{'} \tag{7.22}$$

Then substituting Eqs. 7.10-7.13 into Eqs. 7.4-7.7 gives

$$V_R L_R = (z - a_{tR} - a_{bR})N_t^{'} - (b_{tR} + b_{bR}) \tag{7.23}$$

$$V_L(L_R + l) = (z - a_{tL} - a_{bL})N_t^{'} - (b_{tL} + b_{bL}) \tag{7.24}$$

According to Eq. 7.8, V_R and V_L should be equal to each other; therefore, combining Eqs. 7.23 and 7.24 gives

$$V_L = V_R = \frac{(b_{tL} + b_{bL})(z - a_{tR} - a_{bR}) + (b_{tR} + b_{bR})(z + a_{tL} + a_{bL})}{(z - a_{tR} - a_{bR})(L_R + l) - (z + a_{tL} + a_{bL})L_R} \tag{7.25}$$

Using Eq. 7.9, the strength of the beam *F* can be finally obtained:

$$F = \frac{L}{L_{LS}} \frac{(b_{tL} + b_{bL})(z - a_{tR} - a_{bR}) + (b_{tR} + b_{bR})(z + a_{tL} + a_{bL})}{(z - a_{tR} - a_{bR})(L_R + l) - (z + a_{tL} + a_{bL})L_R} \tag{7.26}$$

The ultimate loads of the eight RC T-section beams with an FRP-strengthened web opening tested by the candidate were calculated using the proposed strength model and listed in Table 7.2. Both the yielding state and the ultimate state of the cross section are considered for comparison purposes. As can be seen from Table 7.2, for both the yielding state and the ultimate state of the cross section, the ultimate load predicted by the proposed strength model is identical to that predicted by the corresponding calculation method based on the simplified *N-M* curves, which verifies the accuracy of the proposed strength model.

7.6 SUM OF NEGATIVE AND POSITIVE FLEXURAL CAPACITIES OF THE SPECIMENS TESTED BY THE CANDIDATE IN BATCH 2

As explained in Section 5.4, for the T-section RC beams with a web opening of small/medium sizes tested by the candidate (i.e. the specimens tested in Batch 2), there were no specimens tested in positive bending. Therefore, the sums of the negative flexural capacity and the positive flexural capacity (SFCs) of specimens with a small/medium FRP-strengthened web opening are not available from the test, but is examined in this section with the help of the proposed strength model.

The SFCs of the two control specimens (i.e., CB-Rec-2 and CB-T-2) as well as the four T-section beams with a small/medium-size FRP-strengthened web opening (600 mm × 280 mm, 700 mm × 260 mm, 600 mm × 220 mm and 700 mm × 200 mm) are listed in Table 7.3. It should be noted that the negative and positive flexural capacities of the two control specimens were obtained from the FE analyses, as has been explained in Chapter 5; the negative and positive flexural capacities of the four T-section beams with a small/medium-size FRP-strengthened web opening were obtained respectively from the test and the proposed strength model based on the ultimate state of the cross section. As can be seen from Table 7.3, the SFC of Specimen CB-T-2 is 146% of that of the rectangular control beam CB-Rec-2, which indicates that the flange (i.e., the existence of a floor slab in a real structure) has a substantial effect on the SFC. With the presence of a medium-size FRP-strengthened web opening (600 mm × 280 mm or 700 mm × 260 mm), the SFC of the T-section beam can be reduced to around 86% of that of the control beam CB-Rec-2; while with the presence of a small-size FRP-strengthened web opening (600 mm × 220 mm or 700 mm × 200 mm), the SFC of the T-section beam can be reduced to around 112% of that of the control beam CB-Rec-2. All these results indicate that the proposed beam opening (BO) technique is very effective in reducing the SFC, and a web opening between the medium size and small size examined in the experimental study will be able to reduce the flexural capacity of the T-section beam to that of the rectangular beam.

7.7 CONCLUDING REMARKS

In this chapter, based on the strength model developed by Mansur et al. (1984) for RC beams with a pre-formed web opening, an accurate calculation method and a strength model are proposed for predicting the strength of RC beams with an FRP-strengthened web opening. Both the yielding state and the ultimate state of the cross sections at the two ends of top and bottom chords were examined for the proposed calculation method, and it was found that the yielding state leads to a lower bound of the predicted strength of the beam while the ultimate state leads to an upper bound of the predicted strength. In addition to the actual *N*-*M* curve, the simplified *N-M* curve was also examined in applying the proposed calculation method. It was found that the simplified *N-M* curve can lead to slightly conservative but quite acceptable predictions of the strength of the beam. A simple strength model of the beam, therefore, was proposed based on the simplified *N-M* curve for ease of engineering use.

Based on the proposed strength model, the SFCs of the specimens tested by the candidate in Batch 2 were examined. The analysis results indicate that the proposed beam opening technique is very effective in reducing the SFC, and a web opening between the medium size and small size examined in the experimental study is capable of reducing the flexural capacity of the T-section beam to the desired value (i.e., the flexural capacity of the rectangular beam). It should be noted that, however, more test results are needed to further verify this finding.

7.8 REFERENCES

GB-50010 (2010). *Code for Design of Concrete Structures*, Architectural & Building Press, Beijing, China (in Chinese).

Lam, L. and Teng, J. G. (2003). "Design-oriented stress-strain model for FRP-confined concrete in rectangular columns", *Journal of Reinforced Plastics and Composites*, 22(13), 1149-1186.

Mansur, M.A. (1998). “Effect of opening on the behaviour and strength of R/C beams in shear”, *Cement and Concrete Composites*, 20(6), 477-486.

Mansur, M. A. (2006). “Design of reinforced concrete beams with web openings”, *Proceedings of the 6th Asia-Pacific Structural Engineering and Construction Conference (ASPEC 2006)*, 5-6.

Mansur, M.A., Tan, K.H., and Lee, S.L. (1984). "Collapse loads of R/C beams with large openings", *Journal of Structural Engineering*, ASCE, 110(11), 2602-2610.

Mansur, M.A., Tan, K.H., and Lee, S.L. (1985). "Design method for reinforced concrete beams with large openings", *ACI Journal*, 82(4), 517-524.

Mansur, M.A., Tan K.H. and Wei, W. (1999). "Effects of creating an opening in existing beams", *ACI Structural Journal*, 96(6), 899-906.

Table 7.1. Ultimate loads predicted using the proposed calculation method

Specimen	Test (kN)	Prediction (kN)				Prediction / Test			
		Yielding state		Ultimate state		Yielding state		Ultimate state	
		Simplified *N-M* curve (S)	Actual *N-M* curve (A)	S	A	S	A	S	A
F-700×300-N	207	190	194	200	204	0.918	0.937	0.966	0.986
F-800×280-N	216	192	202	204	208	0.889	0.935	0.944	0.963
F-600×280-N	256	228	240	246	252	0.891	0.938	0.961	0.984
F-700×260-N	265	230	244	252	260	0.868	0.921	0.951	0.981
F-600×220-N	380	322	354	358	382	0.847	0.932	0.942	1.01
F-700×200-N	388	326	358	370	392	0.840	0.923	0.954	1.01
F-700×300-P	228	210	244	210	246	0.921	1.07	0.921	1.08
F-800×280-P	215	194	220	198	224	0.902	1.02	0.921	1.04
Statistical characteristics	**Average =**					0.885	0.960	0.945	1.01
	STD =					0.030	0.055	0.017	0.038
	CoV =					0.034	0.058	0.018	0.038

Table 7.2. Ultimate loads predicted using the proposed strength model

Specimen	Test (kN)	Prediction (kN)				Prediction / Test	
		Yielding state		Ultimate state		Yielding state	Ultimate state
		Proposed strength model	Proposed calculation method[(a)]	Proposed strength model	Proposed calculation method[(a)]		
F-700×300-N	207	190	190	200	200	0.918	0.966
F-800×280-N	216	192	192	204	204	0.889	0.944
F-600×280-N	256	228	228	246	246	0.891	0.961
F-700×260-N	265	230	230	252	252	0.868	0.951
F-600×220-N	380	322	322	358	358	0.847	0.942
F-700×200-N	388	326	326	370	370	0.840	0.954
F-700×300-P	228	210	210	210	210	0.921	0.921
F-800×280-P	215	194	194	198	198	0.902	0.921
Statistical characteristics	**Average =**					0.885	0.945
	STD =					0.030	0.017
	CoV =					0.034	0.018

Note: (a) Calculated based on the simplified *N-M* curves.

Table 7.3. Sum of negative and positive flexural capacities of Batch 2 specimens

Specimen	Negative flexural capacity (kN)	Positive flexural capacity (kN)	Sum of flexural capacities (kN)	Ratio of sum between T-section beam and CB-Rec
CB-Rec-2	320[a]	240[a]	560	100%
CB-T-2	500[a]	320[a]	820	146%
T-section beam with an FRP-strengthened web opening of 600 mm × 280 mm	256	231[b]	487	87.0%
T-section beam with an FRP-strengthened web opening of 700 mm × 260 mm	265	215[b]	480	85.7%
T-section beam with an FRP-strengthened web opening of 600 mm × 220 mm	380	251[b]	631	113%
T-section beam with an FRP-strengthened web opening of 700 mm × 200 mm	388	233[b]	621	111%

Note:

(a) Obtained from the FE model;

(b) Obtained from the proposed strength model.

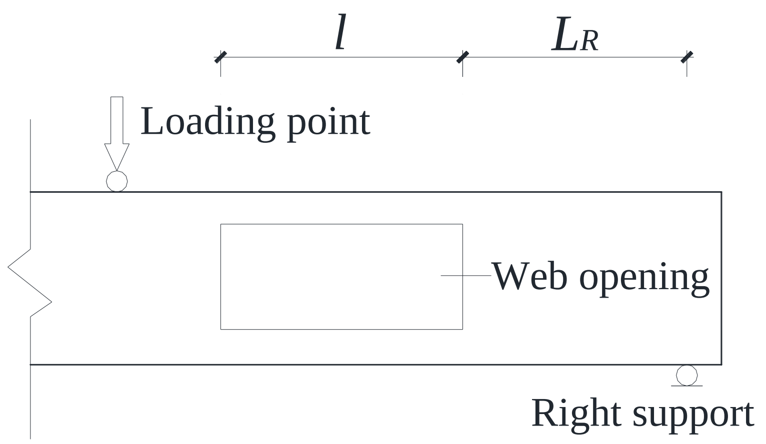

(a) Location of the web opening

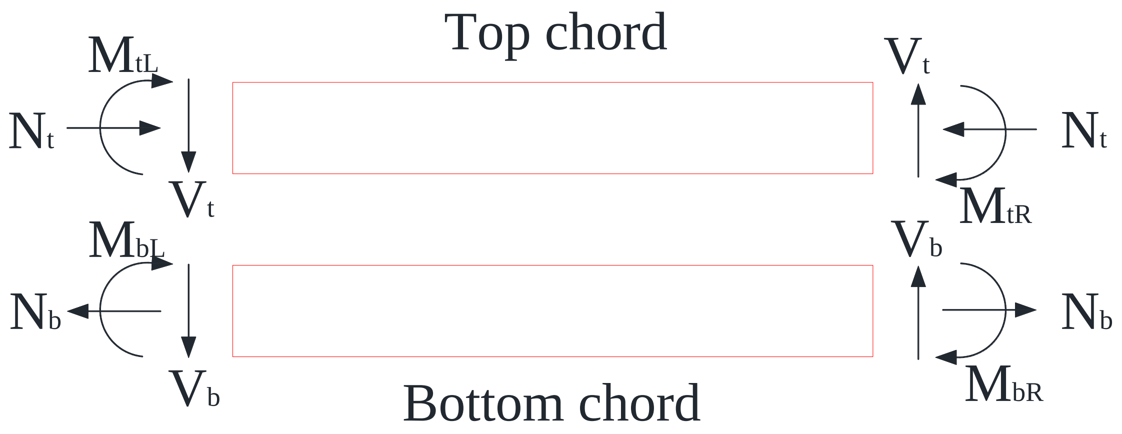

(b) Free-body diagram of the chords

Figure 7.1. Free-body diagram of the chords

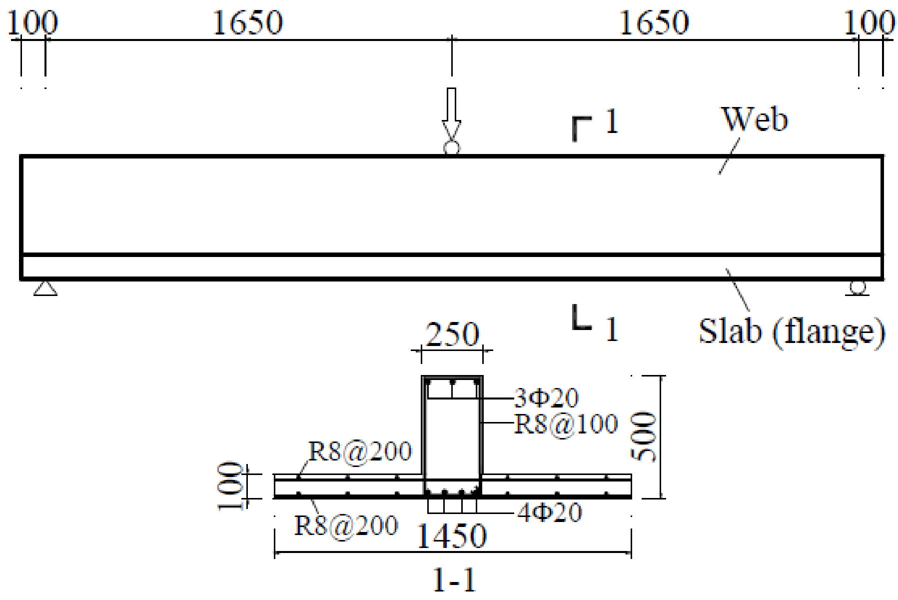

Figure 7.2. Layout of Specimen F-700×300-N (all dimensions in mm)

Figure 7.3. Typical failure mode of RC T-section beams with an FRP-strengthened web opening

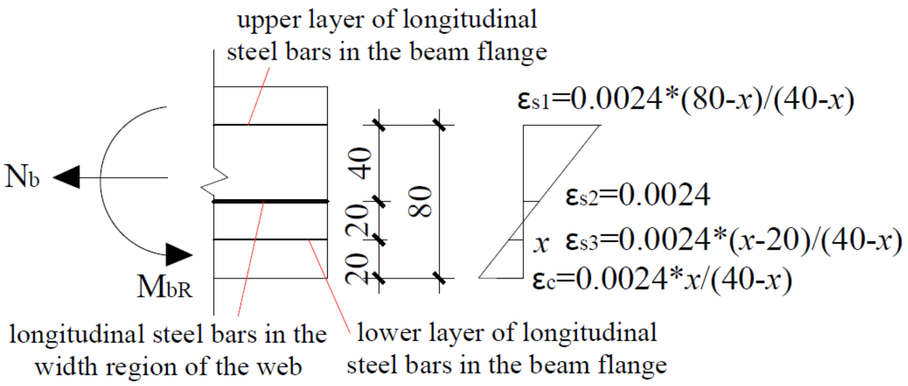

(a) Yielding state

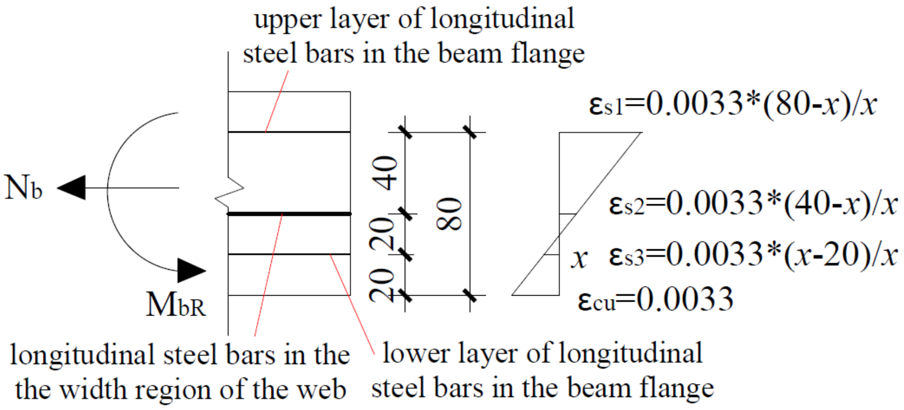

(b) Ultimate state

Figure 7.4. Strain distributions on the cross section at the right end of bottom chord (F-700×300-N)

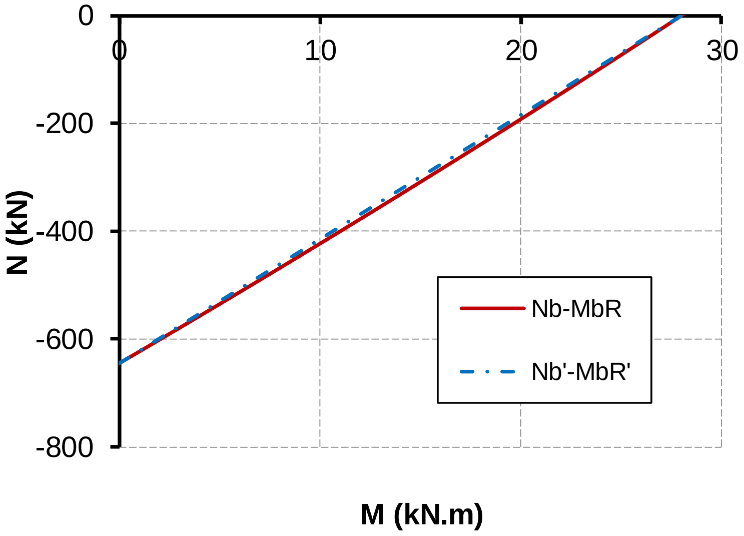

(a) Yielding state

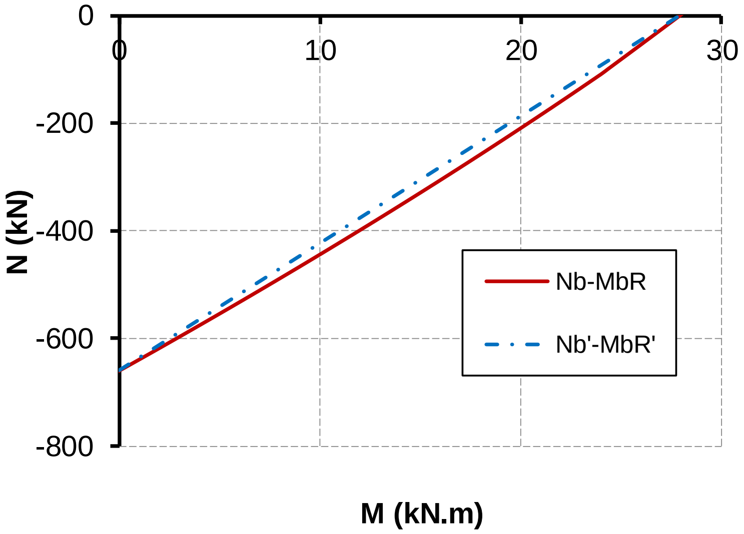

(b) Ultimate state

Figure 7.5. *N*-*M* curves of the cross section at the right end of bottom chord (F-700×300-N)

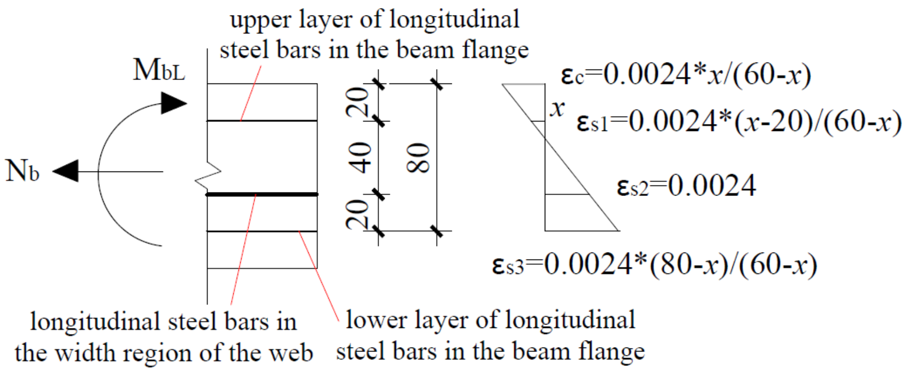

(a) Yielding state

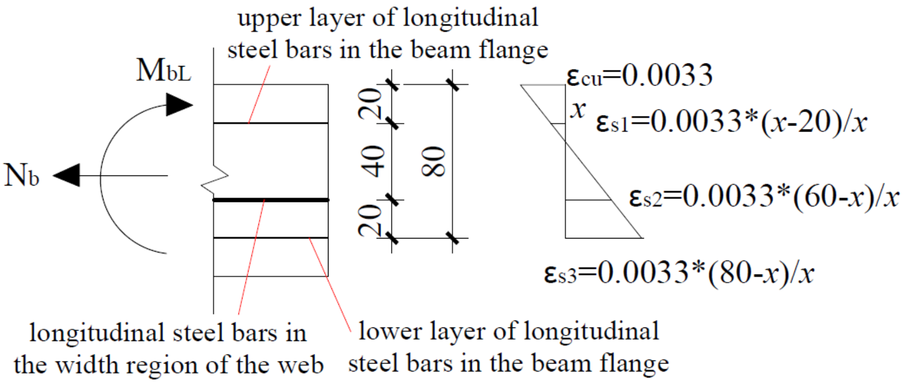

(b) Ultimate state

Figure 7.6. Strain distributions on the cross section at the left end of bottom chord (F-700×300-N)

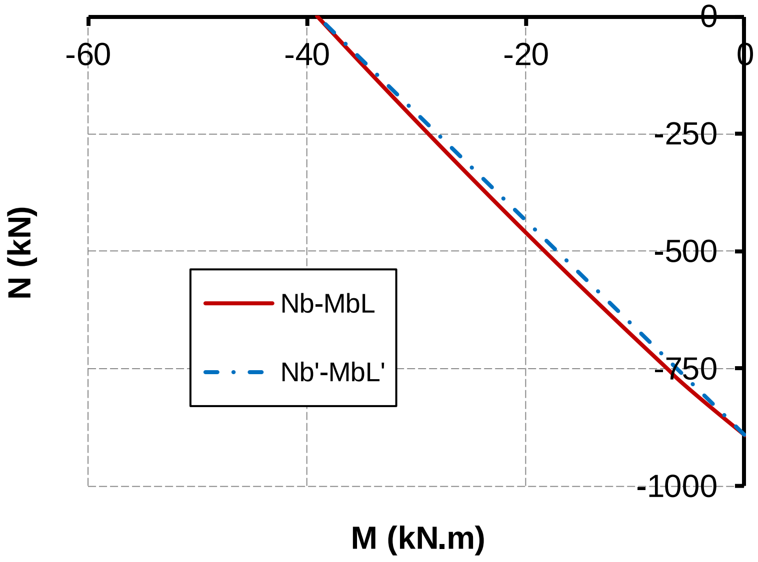

(a) Yielding state

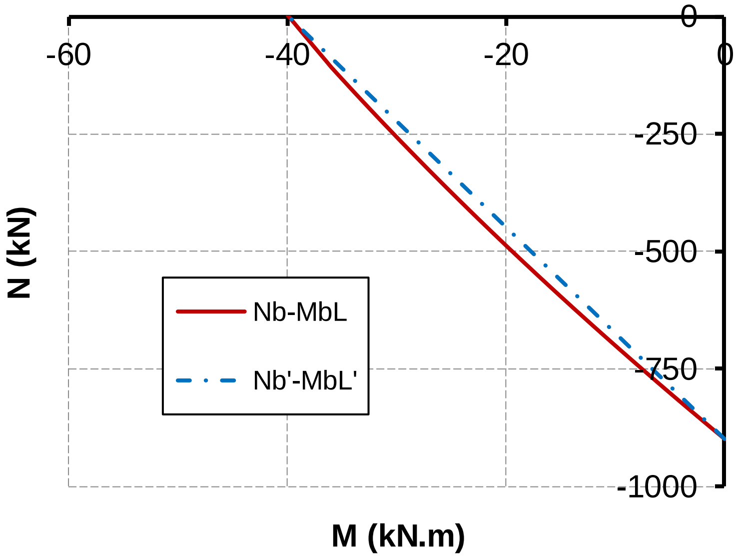

(b) Ultimate state

Figure 7.7. *N-M* curves of the cross section at the left end of bottom chord (F-700×300-N)

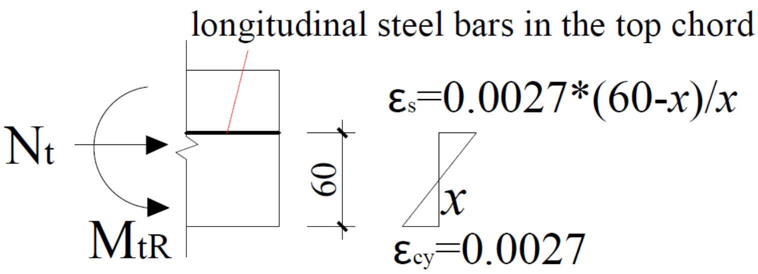

(a) Yielding state

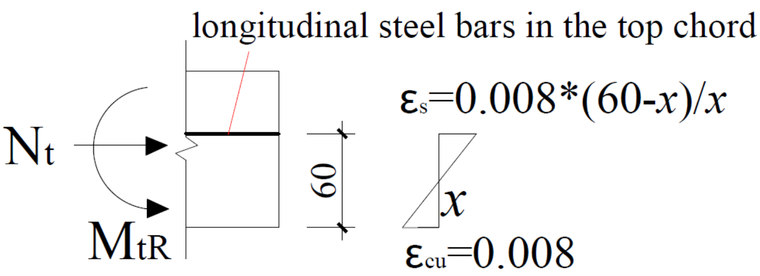

(b) Ultimate state

Figure 7.8. Strain distributions on the cross section at the right end of top chord

(F-700×300-N)

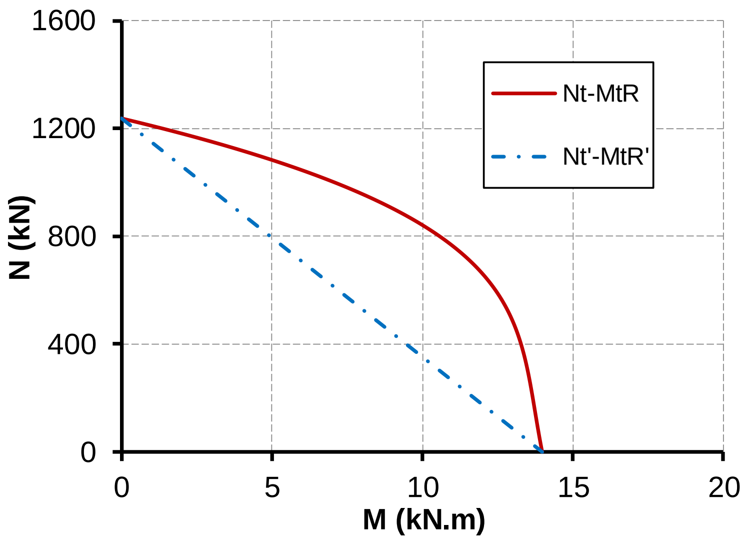

(a) Yielding state

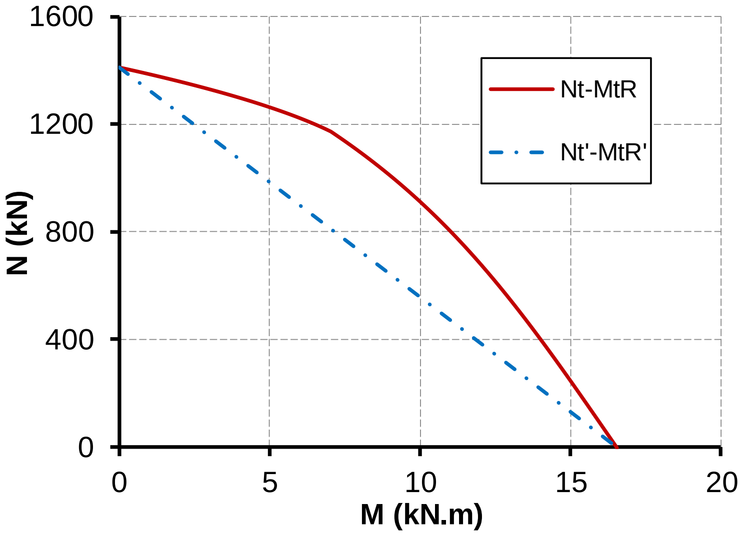

(b) Ultimate state

Figure 7.9. *N*-*M* curves of the cross section at the right end of top chord (F-700×300-N)

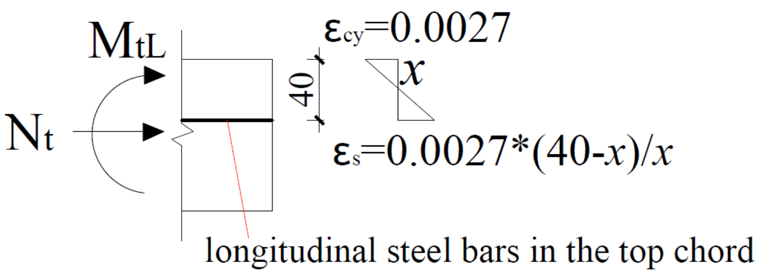

(a) Yielding state

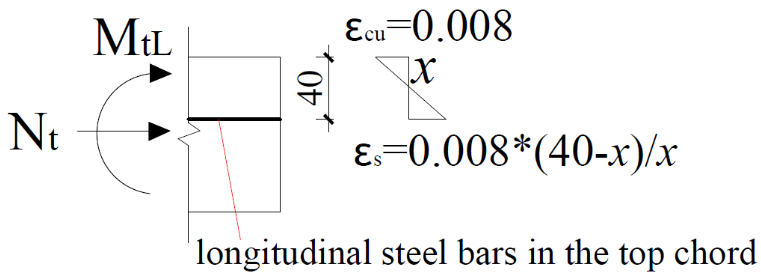

(b) Ultimate state

Figure 7.10. Strain distributions on the cross section at the left end of top chord (F-700×300-N)

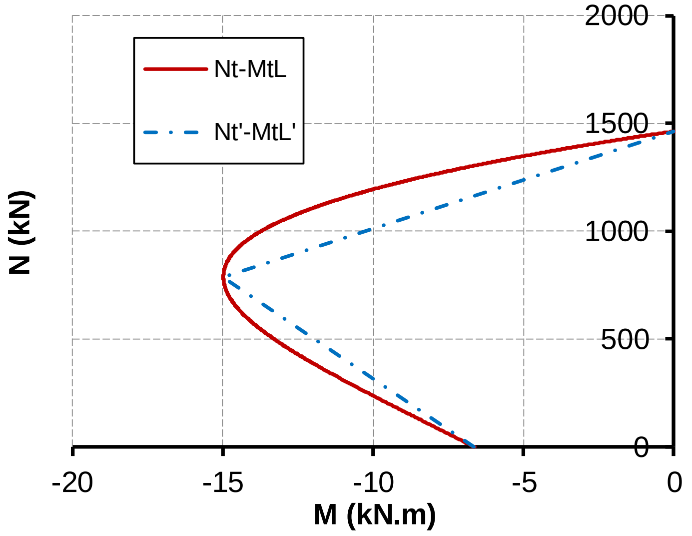

(a) Yielding state

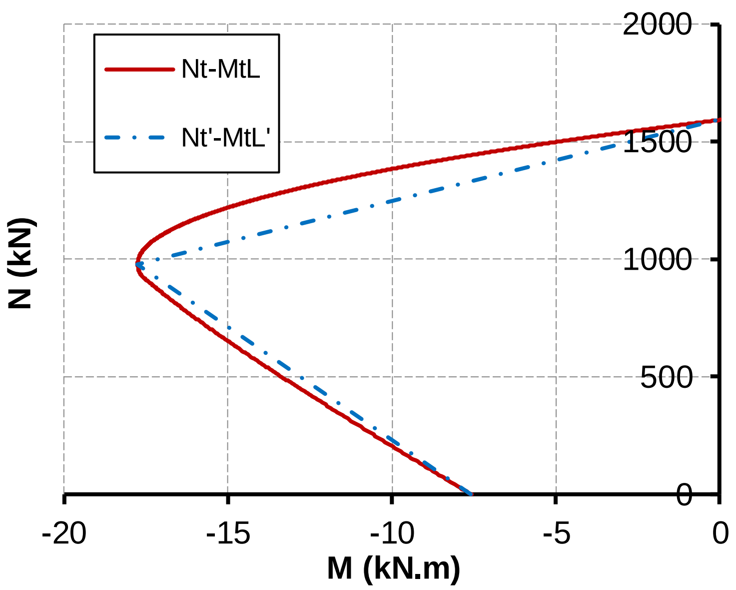

(b) Ultimate state

Figure 7.11. *N*-*M* curves of the cross section at the left end of top chord (F-700×300-N)

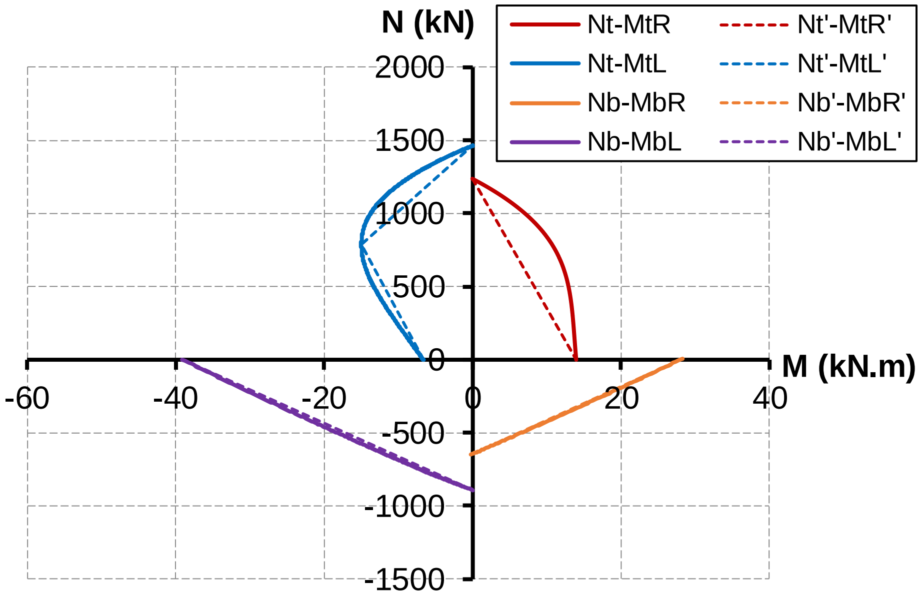

(a) Yielding state

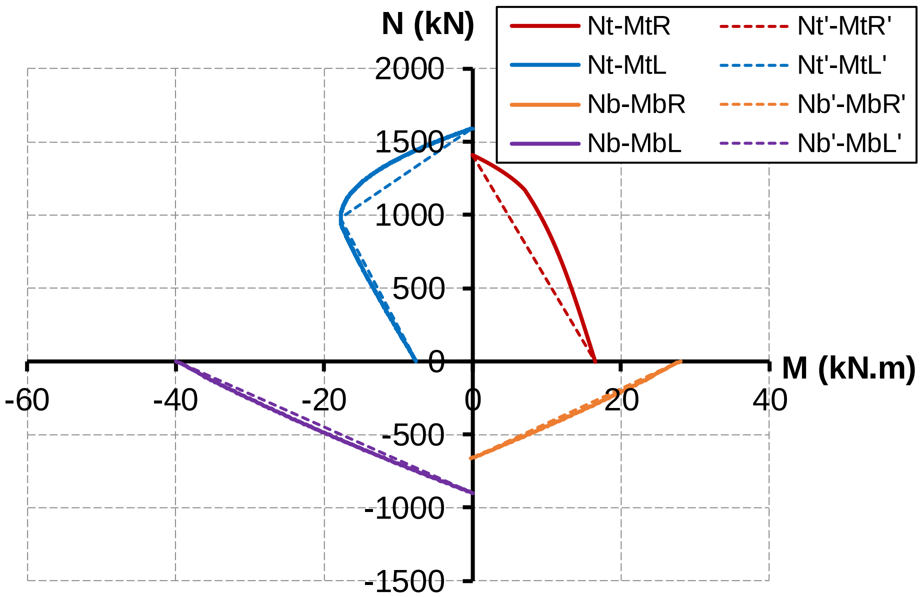

(b) Ultimate state

Figure 7.12. Combined *N*-*M* curves (F-700×300-N)

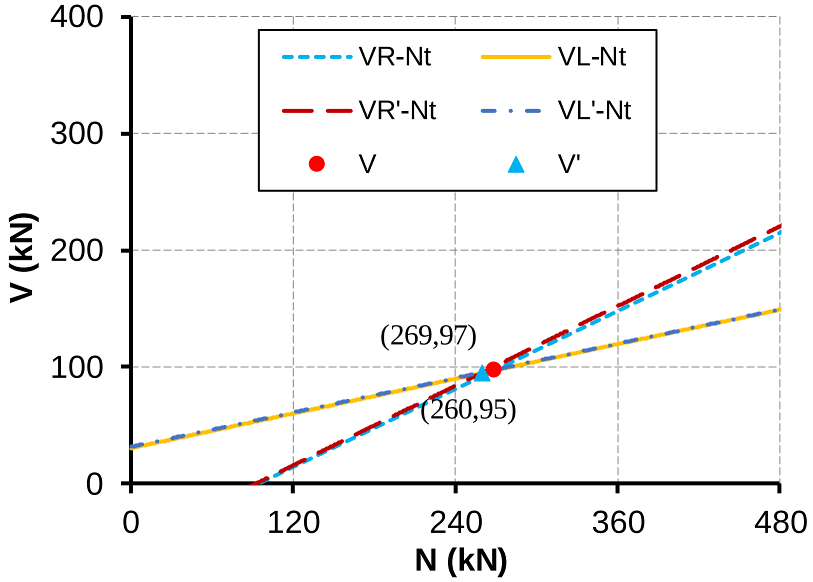

(a) Yielding state

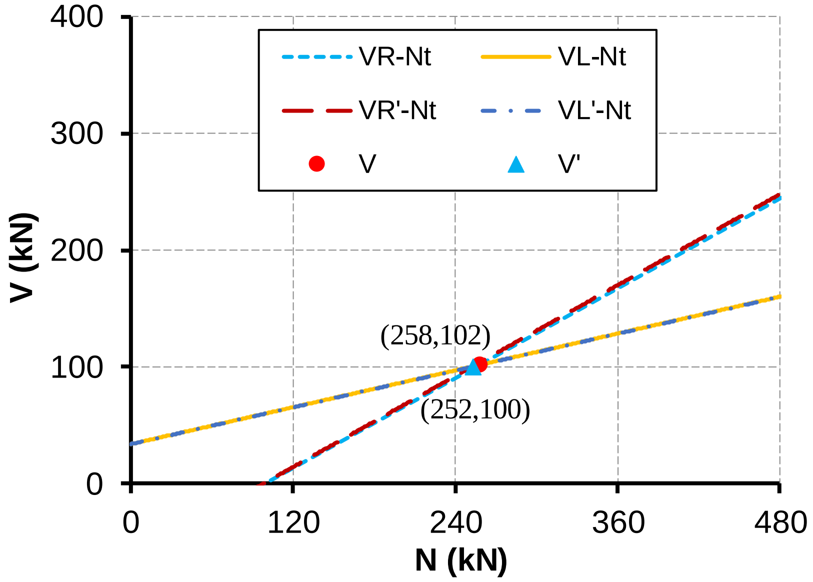

(b) Ultimate state

Figure 7.13. *V-N* curves (F-700×300-N)

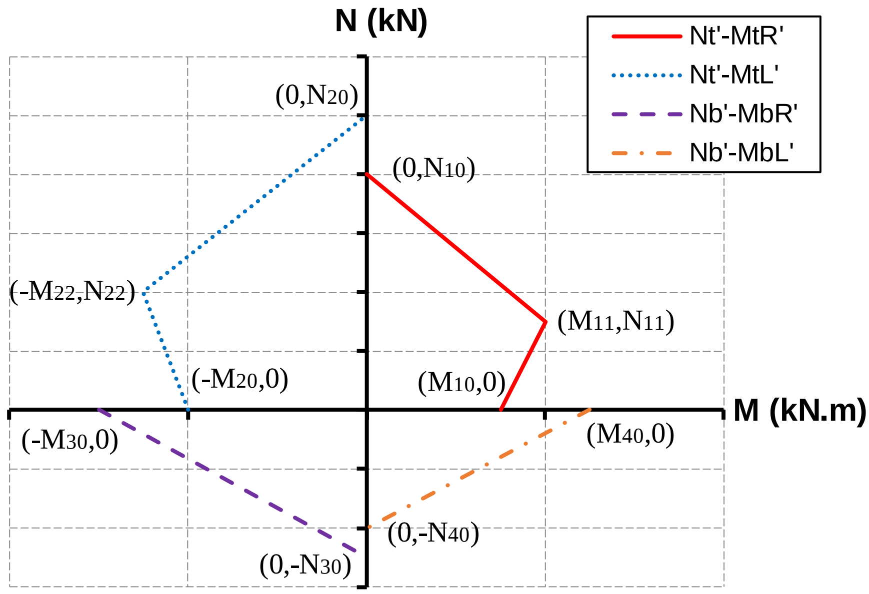

Figure 7.14. Simplified combined *N*-*M* curves

CHAPTER 8

MOMENT-ROTATION RESPONSE OF RC BEAMS WITH A WEB OPENING

8.1 INTRODUCTION

The behaviour of RC beams with a web opening, including their strength, stiffness and crack development during the whole loading process, can be well predicted by the FE models proposed in previous chapters. In addition, the strength of RC beams with a web opening which exhibit a flexural failure mode can be accurately predicted using the calculation method or strength model proposed in Chapter 7. Although the proposed FE models for RC beams have the potential to be extended to model RC frames with beam web openings, it will be very complicated and time-consuming. Instead, it is more common and easier to use beam elements to model RC frames. To do so, the moment (M)-rotation (Θ) relationships (referred to as the M-Θ relationships or the M-Θ models hereafter for simplicity) at the plastic hinges of beams need to be determined first, and then incorporated into beam elements as the property of plastic hinges in the modelling of RC frames.

In this chapter, the M-Θ relationships at the plastic hinges (i.e., at the two ends of the chords) of RC beams with a web opening are extracted from the experimental results. Based on the experimental findings, a simplified M-Θ model is proposed. The proposed M-Θ model is then employed in the FE modelling of RC beams with a web opening using beam elements (OpenSees 2009), and its accuracy is verified with test results.

8.2 *M-θ* RELATIONSHIPS AT THE PLSTIC HINGES OF RC BEAMS WITH A WEB OPENING

The six assumptions made in the proposed calculation method for the strength of RC beams with a web opening in Chapter 7 are followed in the present study. The RC T-section beams with an FRP-strengthened web opening tested by the candidate satisfy all these assumptions and are thus examined. Specimen F-700×300-N is taken as an example to illustrate the details of the test specimens and the arrangement of LVDTs, as shown in Fig. 8.1. The web opening is located in the right shear span of the beam. Five LVDTs (LVDTs 09-13 shown in Fig. 8.1) were placed at equal distance on the web chord to observe the deformation distribution of the web chord. As presented in Chapter 5, all tested RC T-section beams with an FRP-strengthened web opening exhibited a flexural failure mode due to the formation of four plastic hinges at the two ends of top and bottom chords. The left end (i.e. the end closer to the loading point) of the top/bottom chord is under a sagging moment and the right end (i.e. the end closer to the right support) of the top/bottom chord is under a hogging moment, as shown in Fig. 8.2. Based on the observed deformation behaviour and failure mode of these tested RC beams with a web opening and the assumptions that the present study employs, a simplified diagram is proposed to represent such RC beams, as shown in Fig. 8.3. Points A, B, C and D respectively correspond to the left support, the left opening end, the right opening end and the right support. The beam is thus divided into three segments: Segments AB, BC and CD. The top chord and the bottom chord are treated together as a single segment (i.e., Segment BC) plus two plastic hinges at the two ends of the opening (Points B and C). Based on the simplified diagram of the beam, the deformation behaviour of the whole beam is controlled by the *M-Θ* relationships of the two plastic hinges (Points B and C), so the key of the present study is to determine the *M-Θ* relationships of the two plastic hinges: the $M_L - \theta_L$ curve and the $M_R - \theta_R$ curve, where M_L and M_R are bending moments respectively at the left end and right end of the opening, and Θ_L and Θ_R are the corresponding rotations respectively under M_L and M_R.

For the RC T-section beams with an FRP-strengthened web opening tested by the candidate, the vertical deflections of the two ends of the web opening were measured respectively by LVDTs 09 and 13, as shown in Fig. 8.1. Based on the simplified diagram shown in Fig. 8.3, the deflection of point B (i.e., the left end of the opening) measured by LVDT 09 is denoted by y_L, and the deflection of point C (i.e., the right end of the opening) measured by LVDT 13 is denoted by y_R. Once y_L and y_R are obtained, the angles Θ_L and Θ_R can be calculated as:

$$\theta_L = \frac{y_L}{L_L} + \frac{y_O}{l} \tag{8.1}$$

$$\theta_R = -(\frac{y_R}{L_R} + \frac{y_O}{l}) \tag{8.2}$$

where y_O is the relative vertical displacement between the two ends of the opening, $y_O = y_L + y_R$; L_R is the distance between the right end of the opening and the right support; L_L is the distance between the left end of the opening and the left support; l is length of the opening. It should be noted that in this chapter anti-clockwise rotations are regarded as positive while clockwise rotations are regarded as negative; y_L is regarded as positive when Point B goes downward under loading; and y_R is regarded as positive when Point C goes upward under loading.

For each value of y_L (or y_R), the bending moments M_L and M_R can be calculated based on the appied load, and thus the $M_L - \theta_L$ curve and the $M_R - \theta_R$ curve can be determined. The obtained $M_L - \theta_L$ curves and $M_R - \theta_R$ curves of the six RC T-section beams with an FRP-strengthened web opening tested by the candidate are shown in Fig. 8.4. From the *M-Θ* curves ($M_L - \theta_L$ curves and $M_R - \theta_R$ curves) shown in Fig. 8.4, it can be seen that the shapes of all the *M-Θ* curves are similar and can be divided into three nearly linear segments, respectively representing the *M-Θ* relationships before cracking, after cracking and after yielding of the beam. Before the cracking of the beam, *M* increases linearly with the absolute value of *Θ* (|*Θ*|); after the cracking of the beam, *M* still increases with |*Θ*| but at a much smaller slope (i.e. stiffness); after the yielding of the beam, *M* almost remains unchanged with the increase of |*Θ*|.

8.3 PROPOSED *M-Θ* MODEL FOR PLASTIC HINGES OF RC BEAMS WITH A WEB OPENING

Based on the above experimental findings, simplified *M-Θ* models for the two plastic hinges (i.e., at Ponits B and C in Fig. 8.3) of RC beams with a web opening are proposed, as shown in Fig. 8.5. The proposed *M-Θ* models consist of three linear segments, representing the M-Θ relationships respectively before cracking, after cracking and after yielding of the beam. Once the four key Points (M_{Lcr}, Θ_{Lcr}), (M_{Rcr}, Θ_{Rcr}), (M_{Ly}, Θ_{Ly}) and (M_{Ry}, Θ_{Ry}) are obtained, the M-Θ models are determined. M_{Lcr} and M_{Rcr} respectively stand for the bending moments at left end and right end of the opening at the cracking of the beam; Θ_{Lcr} and Θ_{Rcr} respectively stand for the corresponding rotations under M_{Lcr} and M_{Rcr}; M_{Ly} and M_{Ry} respectively stand for the bending moments at left end and right end of the opening at the yielding of the beam (i.e. at the fomation of the plastic hinges); and Θ_{Ly} and Θ_{Ry} respectively stand for the corresponding rotations under M_{Ly} and M_{Ry}. It should be noted that M_{Ly} and M_{Ry} can be obtained using the strength model for RC beams with a web opening proposed in Chapter 7; therefore, the main task of this section is to determine the other six unknowns: M_{Lcr}, M_{Rcr}, Θ_{Lcr}, Θ_{Rcr}, Θ_{Ly} and Θ_{Ry}.

8.3.1 *M-Θ* relationships before the cracking of the beam

The values of M_{Lcr}, M_{Rcr}, Θ_{Lcr} and Θ_{Rcr} can be obtained through a series of theoretical derivations based on the conditions of force equilibrium and deformation compatibility. The specific procedures are detailed as follows. The free-body diagram of the opening region shown in Fig. 7.1 is referred to in the following derivation. However, it should be noted that the four bending moments M_{tR}, M_{tL}, M_{bR} and M_{bL} are with reference to the mid-planes of their corresponding cross sections in Chapter 7, while they are with reference to the centroidal axes of their corresponding cross sections in the present chapter as they will be used in the graph multiplication method for the calculation of chord deforamtions.

8.3.1.1 Equilibrium equations

For the top chord:

$$V_t l = M_{tR} + M_{tL} \tag{8.3}$$

For the bottom chord:

$$V_b l = M_{bR} + M_{bL} \tag{8.4}$$

For the right end of the opening:

$$N_t = N_b \tag{8.5}$$

$$M_R = N_t z_n - M_{tR} - M_{bR} \tag{8.6}$$

$$M_R = VL_R \tag{8.7}$$

where z_n is the distance between the centroids of top and bottom chords, *V* is the reaction at the right support.

For the left end of the opening:

$$M_L = N_t z_n + M_{tL} + M_{bL} \tag{8.8}$$

$$M_L = V(L_R + l) \tag{8.9}$$

8.3.1.2 Equations of deformation compatibility

In addtion to the conditions of force equilibrium, the top and bottom chords also need to meet the conditions of deformation compatibility. Based on the force distribution shown in Fig. 7.1, the relative displacements and rotations between the two ends of the top and the bottom chords can be calculated using the graph multiplication method. It should be noted that the shear deformation in the chords and the second-order effect of the axial force are ignored in the calculation of deformations.

For the top chord:

$$v_t = \frac{(2M_{tL} - M_{tR})l^2}{6EI_t} \tag{8.10}$$

$$\theta_t = \frac{(M_{tL} - M_{tR})l}{2EI_t} \tag{8.11}$$

$$u_t = \frac{N_t l}{EA_t} \tag{8.12}$$

where v_t, u_t and Θ_t are the relative vertical displacement, horizontal displacement and rotation between the two ends of top chord, respectively, E is the elastic modulus of concrete, I_t is the second moment of area of top chord, and A_t is the cross-sectional area of top chord. For the calculation of I_t and A_t, the area of steel bars is converted to an equivalent area of concrete, based on the ratio of elastic modulus.

For the bottom chord:

$$v_{\mathrm{b}} = \frac{(2M_{bL} - M_{bR})l^2}{6EI_b} \tag{8.13}$$

$$\theta_{\mathrm{b}} = \frac{(M_{bL} - M_{bR})l}{2EI_b} \tag{8.14}$$

$$u_b = \frac{N_b l}{EA_b} \tag{8.15}$$

where v_b, u_b and Θ_b are the relative vertical displacement, horizontal displacement and rotation between the two ends of bottom chord, respectively, I_b is the second moment of area of bottom chord, and A_b is the cross-sectional area of bottom chord. The calculation methods of I_b and A_b are the same as those for I_t and A_t, respectively.

According to the conditions of deformation compatibility based on the assumption that the top and the bottom chords are framed into the rigid abutments on the two sides of the opening, the following three equations can be estimated:

$$v_t = v_b \tag{8.16}$$

$$\theta_t = \theta_b \tag{8.17}$$

$$\frac{u_t + u_b}{z_n} = \theta_t = \theta_b \tag{8.18}$$

Substituting Eqs. 8.10 and 8.13 into Eq. 16 and substituting Eqs. 8.11 and 8.14 into Eq. 8.17 give:

$$\frac{2M_{tL} - M_{tR}}{I_t} = \frac{2M_{bL} - M_{bR}}{I_\mathrm{b}} \tag{8.19}$$

$$\frac{M_{tL} - M_{tR}}{I_t} = \frac{M_{bL} - M_{bR}}{I_\mathrm{b}} \tag{8.20}$$

Conbining the above equations of force equilibrium (Eqs. 8.3-8.9) and deformation compatibility (Eqs. 8.18-8.20), all forces in the chords can be found:

$$M_{tR} = [\frac{I_t l}{I_t + I_b} - \frac{2(L_R + l)I_t(A_t + A_b) + \frac{I_t}{I_t + I_b} z_n^2 l A_t A_b}{2(I_t + I_b)(A_t + A_b) + 2z_n^2 A_t A_b}]V \tag{8.21}$$

$$M_{tL}=\frac{2(L_R+l)I_t(A_t+A_b)+\frac{I_t}{I_t+I_b}z_n^2lA_tA_b}{2(I_t+I_b)(A_t+A_b)+2z_n^2A_tA_b}V \quad (8.22)$$

$$M_{bR}=[\frac{I_b l}{I_t+I_b}-\frac{2(L_R+l)I_b(A_t+A_b)+\frac{I_b}{I_t+I_b}z_n^2lA_tA_b}{2(I_t+I_b)(A_t+A_b)+2z_n^2A_tA_b}]V \quad (8.23)$$

$$M_{bL}=\frac{2(L_R+l)I_b(A_t+A_b)+\frac{I_b}{I_t+I_b}z_n^2lA_tA_b}{2(I_t+I_b)(A_t+A_b)+2z_n^2A_tA_b}V \quad (8.24)$$

$$N_t=N_b=\frac{z_nA_tA_b(2M_{tL}-\frac{I_t}{I_t+I_b}lV)}{2I_t(A_t+A_b)} \quad (8.25)$$

As can be seen from Eqs. 8.21-8.25, M_{tR}, M_{tL}, M_{bR}, M_{bL} and N_t (or N_b) are all proportional to *V*. Once M_{tR}, M_{tL}, M_{bR}, M_{bL} and N_t (or N_b) are determined, the relative vertical displacement v_t (v_b) and rotation Θ_t (Θ_b) between the two ends of top/bottom chord can be obtained using Eq. 8.10 (Eq. 8.13) and Eq. 8.11 (Eq. 8.14), respectively. It can be seen from Eqs. 8.10, 8.11, 8.13 and 8.14 that v_t, v_b, Θ_t and Θ_b are all proportional to *V*. Based on the simplified diagram of the beam shown in Fig. 8.3, the following relations can be obtained:

$$\theta_O=\theta_L+\theta_R=\theta_t=\frac{l}{2E}[\frac{2(L_R+l)(A_t+A_b)+\frac{1}{I_t+I_b}z_n^2lA_tA_b}{(I_t+I_b)(A_t+A_b)+z_n^2A_tA_b}-\frac{l}{I_t+I_b}]V \quad (8.26)$$

$$y_O=y_L+y_R=v_t=\frac{l^2}{6E}[\frac{6(L_R+l)(A_t+A_b)+\frac{3}{I_t+I_b}z_n^2lA_tA_b}{2(I_t+I_b)(A_t+A_b)+2z_n^2A_tA_b}-\frac{l}{I_t+I_b}]V \quad (8.27)$$

where θ_O is the relative rotation between the two ends of the opening. It can be seen from Eqs. 8.26 and 8.27 that θ_O and y_O are both proportional to *V*.

In order to verify the accuracy of the above derivation processes, a two-dimensional linear FE model of the opening region in an RC beam was established in ABAQUS (2012), as shown in Fig. 8.6. In the FE model, the chords were modelled using either 4-node plane stress elements CPS4R (as shown in Fig, 8.6a) or 2-node beam element B21 (as shown in Fig, 8.6b). All nodes of right/left end of the top and bottom chords were coupled to a reference point at the middle of left/right end of the opening. All the degrees of freedom of the left reference point were fixed while the vertical load (100 kN, going up) and bending moment (100 kN.m, clockwise) were applied at the right reference point. The material used for the chords was elastic, and its elastic modulus and Poisson's ratio were set to be 30000 N/mm^2 and 0.2, respectively. The width of the beam was set to be 250 mm, while the height of the beam and the height and length of the chords were variables. Geometric nonlinearity was considered in the FE modelling. The comparisons of the relative vertical displacement between the two ends of the opening obtained from the above proposed calculation method and FE modelling are shown in Table 8.1. As can be seen from Table 8.1, the relative vertical displacement obtained from the calculation method is very close to that obtained from FE modelling, with the error being small (around 5%) and consistent. The small error is because the shear deformation in the chords and the second-order effect of the axial force are not considered in the proposed calculation method.

8.3.1.3 The slopes of $M_L - \theta_L$ curve and $M_R - \theta_R$ curve before cracking

Combining Eqs. 8.1, 8.2, 8.26 and 8.27, the following relations can be obtained:

$$y_L = \frac{L_L L_R \theta_O + L_L y_O}{L_L + L_R} \tag{8.28}$$

$$y_R = \frac{L_R y_O - L_L L_R \theta_O}{L_L + L_R} \tag{8.29}$$

$$\theta_L = \frac{L_R \theta_O + y_O}{L_L + L_R} + \frac{y_O}{l} \tag{8.30}$$

$$\theta_R = -(\frac{y_O - L_L \theta_O}{L_L + L_R} + \frac{y_O}{l}) \tag{8.31}$$

It can be seen from Eqs. 8.26, 8.27, 8.30 and 8.31 that θ_R and θ_L are both proportional to *V*. Moreover, it can be seen from Eqs. 8.7 and 8.9 that M_R and M_L are also proportional to *V*. Therefore, dividing Eq. 8.7/Eq. 8.9 by Eq. 8.30/Eq. 8.31 gives the slope of $M_L - \theta_L$ curve/ $M_R - \theta_R$ curve before the cracking of the beam.

8.3.1.4 Determination of M_{Lcr}, M_{Rcr}, θ_{Lcr} and θ_{Rcr}

Once the reaction force at the right end of the beam at the cracking of the beam (V_{cr}) is determined, M_{Lcr} and M_{Rcr} can be obtained, and then Θ_{Lcr} and Θ_{Rcr} can be obtained based on the slopes of the $M_L - \theta_L$ curve and $M_R - \theta_R$ curve before the cracking of the beam obtained in the preceding subsection. As observed in the tests, the first crack appeared at the opening corners for all tested beams with a web opening, therefore, the opening region can be seperated from the beam for analysis. The proposed calculation method for V_{cr} consists of the following steps:

Step-1: Obtain the *N-M* curves of the cross sections at the two ends of top and bottom chords when the cross sections begin to crack.

The calculation method for these *N-M* curves is similar to that used in the proposed strength model for RC beams with a web opening in Chapter 7. For each of the four cross sections at the top and bottom chord ends, the strain of the tensile concrete at the tensile edge of the cross section is set to be the cracking strain of concrete. Assuming a value for the axial force, the height of the compressive zone on the cross section can be determined, and then the corresponding bending moment can be calculated (with reference to the centroidal axis of the cross section). By assuming a series of values for the axial force, the *N-M* curve can be finally obtained. Taking Specimen F-700×300-N as an example, the calculated *N-M* curves of the cross sections at the two ends of top and bottom chords corresponding to cracking of the cross sections are shown in Fig. 8.7.

Step-2: Calculate the reaction forces at the right support corresponding to the cracking of the cross sections at the two ends of top and bottom chords.

As have been shown in Subsection 8.3.1.2, the bending moments and axial forces at the two ends of the chords can be expressed in Eqs. (8.21)-(8.25). It can be seen from Eqs. (8.21)-(8.25) that M_{tR}, M_{tL}, M_{bR}, M_{bL} and N_t (or N_b) are all proportional to *V*. Taking the right end of top chord as an example, M_{tR} and N_t can be expressed as: $M_{tR}=a_{tR}V$, $N_t = a_t V$, where

$$a_{tR}=\frac{I_t l}{I_t+I_b}-\frac{2(L_R+l)I_t(A_t+A_b)+\dfrac{I_t}{I_t+I_b}z_n^2 l A_t A_b}{2(I_t+I_b)(A_t+A_b)+2z_n^2 A_t A_b} \tag{8.32}$$

$$a_t = \frac{z_n A_t A_b}{2I_t(A_t + A_b)}\left[\frac{2(L_R + l)I_t(A_t + A_b) + \frac{I_t}{I_t + I_b} z_n^2 l A_t A_b}{(I_t + I_b)(A_t + A_b) + z_n^2 A_t A_b} - \frac{I_t l}{I_t + I_b}\right] \quad (8.33)$$

Dividing pairs of M_{tR} and N_t on the M_{tR} - N_t curve obtained in Step-1 (as shown in Fig. 8.7) respectively by a_{tR} and a_t gives a series of pairs of M_{tR} / a_{tR} and N_t / a_t. The solution is obtained when $M_{tR} / a_{tR} = N_t / a_t (= b_{tR})$, and the reaction force at the right support corresponding to the cracking of the right end of top chord (V_{crtR}) is determined (i.e. $V_{crtR} = b_{tR}$).

Step-3: Determine V_{cr}.

Following Step-2, the reaction force at the right end of the beam corresponding to the cracking of the right end of top chord (V_{crtR}), the left end of top chord (V_{crtL}), the right end of bottom chord (V_{crbR}) and the left end of bottom chord (V_{crbL}) can be obtained, and the smallest one among them is the actual reaction force at the right end of the beam at the cracking of the beam (V_{cr}). The reaction forces V_{crtR}, V_{crtL}, V_{crbL} and V_{crbR} of the six tested beams are listed in Table 8.2. As can be seen from Table 8.2, the predicted V_{cr} values are very close to those from the tests for all six beams, which verifies the accuracy of the proposed calculation method for V_{cr} of the beam. Moreover, the calculated results show that for all six beams, the first crack appears at the left end of bottom chord, which also coincides with the experimental findings. Once V_{cr} is determined, M_{Lcr} and M_{Rcr} and their corresponding rotations θ_{Lcr} and θ_{Rcr} can be obtained accordingly.

Following the above steps, the $M_L - \theta_L$ curve and $M_R - \theta_R$ curve before the cracking of the beam can be obtained.

8.3.2 *M-Θ* relationships after the cracking of the beam

After the cracking of the beam, cracks further develop at the four opening corners. As a result, the second moments of area of cross sections near the chord ends decrease, and the second moments of area of the cross sections are no longer identical along the chord length. The calculation method for the *M-Θ* curve before the cracking of the beam, therefore, is no longer applicable in the calculation of the *M-Θ* curve after the cracking of the beam. Referring to Fig. 8.5, once the values of M_{Ly}, Θ_{Ly}, M_{Ry} and Θ_{Ry} are determined, the *M-Θ* relationships after the cracking of the beam are determined. The value of M_{Ly} and M_{Ry} can be obtained using the strength model proposed in Chapter 7, thus the target of this subsection is to find the values of Θ_{Ly} and Θ_{Ry}.

8.3.2.1 Equilibrium equations

A simplified free-body diagram of the opening region after cracking is proposed and shown in Fig. 8.8, in which l_{tR}, l_{tL}, l_{bR} and l_{bL} are the lengths of cracking regions respectively at the right end of top chord, the left end of top chord, the right end of bottom chord and the left end of bottom chord; I_{tR}, I_{tL}, I_{bR} and I_{bL} are the second moments of area of the cross sections after cracking respectively at the right end of top chord, the left end of top chord, the right end of bottom chord and the left end of bottom chord. As analyzed above, after cracking, the second moment of area of cross section in the cracking region decreases with the increase of the height of the crack. However, in order to simplify the calculation, the second moments of area of cross sections in the cracking region are assumed to be identical, as shown in Fig. 8.8. For instance, the second moment of area of the cross sections after cracking at the right end of top chord is assumed to be I_{tR} (Fig. 8.8). Moreover, it should be noted that M_{tR}, M_{tL}, M_{bR} and M_{bL} are with reference to the centroidal axes of the corresponding cross sections. Based on Fig. 8.8, the following equilibrium equations can be obtained for the top and bottom chords.

For the top chord:

$$V_t l = M_{tR} + M_{tL} + N_t x_t \tag{8.34}$$

where x_t is the distance between the centroids of the cross sections at the left end and right end of top chord after cracking.

For the bottom chord:

$$V_b l = M_{bR} + M_{bL} + N_b x_b \tag{8.35}$$

where x_b is the distance between the centroids of the cross sections at the left end and right end of bottom chord after cracking.

For the right end of the opening:

$$N_t = N_b \tag{8.36}$$

$$M_R = VL_R = -M_{tR} - M_{bR} + N_t z_R \tag{8.37}$$

where z_R is the distance between the centroids of the top and bottom chords at the right end of the opening after cracking.

For the left end of the opening:

$$M_L = V(L_R + l) = M_{tL} + M_{bL} + N_t z_L \tag{8.38}$$

where z_L is the distance between the centroids of the top and bottom chords at the left end of the opening after cracking.

8.3.2.2 Equations of deformation compatibility

The top and bottom chords also need to meet the conditions of deformation compatibility. Based on the force distribution shown in Fig. 8.8, the relative displacements and rotations between the two ends of the top and the bottom chord can be calculated respectively using the graph multiplication method.

For the top chord:

$$\begin{aligned} v_{tc} &= \frac{(2l - l_{tL})l_{tL}}{2EI_{tL}}\left(\frac{l - l_{s1}}{l}M_{tL} - \frac{l_{s1}}{l}M_{tR}\right) \\ &+ \frac{(l - l_{tL} + l_{tR})(l - l_{tL} - l_{tR})}{2EI_t}\left(\frac{l - l_{tL} - l_{s2}}{l}M_{tL} - \frac{l_{tL} + l_{s2}}{l}M_{tR}\right) \\ &- \frac{l_{tR}{}^2}{2EI_{tR}}\left(\frac{3l - 2l_{tR}}{3l}M_{tR} - \frac{2l_{tR}}{3l}M_{tL}\right) \\ &= a_{v2}M_{tL} - a_{v1}M_{tR} \end{aligned} \tag{8.39}$$

$$\begin{aligned} \theta_{tc} &= \frac{l_{tL}}{2EI_{tL}}\left[2M_{tL} - \frac{l_{tL}}{l}(M_{tR} + M_{tL})\right] \\ &+ \frac{(l - l_{tL} - l_{tR})}{2EI_t}\left(-\frac{l + l_{tL} - l_{tR}}{l}M_{tR} + \frac{l - l_{tL} + l_{tR}}{l}M_{tL}\right) \\ &- \frac{l_{tR}}{2EI_{tR}}\left[2M_{tR} - \frac{l_{tR}}{l}(M_{tR} + M_{tL})\right] \\ &= a_{\theta 2}M_{tL} - a_{\theta 1}M_{tR} \end{aligned} \tag{8.40}$$

$$u_{tc} = \frac{N_t l_{tL}}{EA_{tL}} + \frac{N_t(l - l_{tL} - l_{tR})}{EA_t} + \frac{N_t l_{tR}}{EA_{tR}} \\ = a_{ut} N_t \tag{8.41}$$

where

$$l_{s1} = \frac{(3l - 2l_{tL})l_{tL}}{3(2l - l_{tL})} \tag{8.42}$$

$$l_{s2} = \frac{(l - l_{tL} - l_{tR})(2l_{tR} + l - l_{tL})}{3(l - l_{tL} + l_{tR})} \tag{8.43}$$

$$a_{v1} = \frac{(2l - l_{tL})l_{s1}l_{tL}}{2EI_{tL}l} - \frac{(l - l_{tL} + l_{tR})(l - l_{tL} - l_{tR})(l_{tL} + l_{s2})}{2EI_t l} - \frac{(3l - 2l_{tR})l_{tR}{}^2}{6EI_{tR}l} \\ = \frac{1}{6El}\left(\frac{3l_{tL}^2 l - 2l_{tL}^3}{I_{tL}} + \frac{-l^3 + 4l_{tL}l^2 + 2l_{tR}l^2 - 9l_{tL}^2 l + 3l_{tR}^2 l + 4l_{tL}^3 - 6l_{tL}l_{tR}^2 - 2l_{tR}^3}{I_t} + \frac{3l_{tR}^2 l - 2l_{tR}^3}{I_{tR}}\right) \tag{8.44}$$

$$a_{v2} = \frac{(2l - l_{tL})(l - l_{s1})l_{tL}}{2EI_{tL}l} + \frac{(l - l_{tL} + l_{tR})(l - l_{tL} - l_{tR})(l - l_{tL} - l_{s2})}{2EI_t l} + \frac{l_{tR}{}^3}{3EI_{tR}l} \\ = \frac{1}{3El}\left(\frac{3l_{tL}l^2 - 2l_{tL}^2 l + l_{tL}^3}{I_{tL}} + \frac{l^3 - 4l_{tL}l^2 + l_{tR}l^2 + 3l_{tL}^2 l - l_{tL}^3 - l_{tR}^3}{I_t} + \frac{l_{tR}^3}{I_{tR}}\right) \tag{8.45}$$

$$a_{\theta 1} = \frac{l_{tL}{}^2}{2EI_{tL}l} + \frac{(l + l_{tL} - l_{tR})(l - l_{tL} - l_{tR})}{2EI_t l} + \frac{(2l - l_{tR})l_{tR}}{2EI_{tR}l} \tag{8.46}$$

$$a_{\theta 2} = \frac{(2l - l_{tL})l_{tL}}{2EI_{tL}l} + \frac{(l - l_{tL} + l_{tR})(l - l_{tL} - l_{tR})}{2EI_t l} + \frac{l_{tR}^2}{2EI_{tR}l} \tag{8.47}$$

$$a_{ut} = \frac{l_{tL}}{EA_{tL}} + \frac{l - l_{tL} - l_{tR}}{EA_t} + \frac{l_{tR}}{EA_{tR}} \tag{8.48}$$

where v_{tc}, u_{tc} and Θ_{tc} are the relative vertical displacement, horizontal displacement and rotation between the two ends of top chord after cracking, respectively; A_{tR} and A_{tL} are the cross-sectional areas of respectively the right end and left end of top chord after cracking, with the area of steel bars being converted to that of concrete based on the ratio of elastic modulus.

For the bottom chord:

$$\begin{aligned}
v_{bc} &= \frac{(2l-l_{bL})l_{bL}}{2EI_{bL}}\left(\frac{l-l_{s3}}{l}M_{bL}-\frac{l_{s3}}{l}M_{bR}\right) \\
&+\frac{(l-l_{bL}+l_{bR})(l-l_{bL}-l_{bR})}{2EI_b}\left(\frac{l-l_{bL}-l_{s4}}{l}M_{bL}-\frac{l_{bL}+l_{s4}}{l}M_{bR}\right) \\
&-\frac{{l_{bR}}^2}{2EI_{bR}}\left(\frac{3l-2l_{bR}}{3l}M_{bL}-\frac{2l_{bR}}{3l}M_{bR}\right) \\
&= a_{v4}M_{bL}-a_{v3}M_{bR}
\end{aligned} \tag{8.49}$$

$$\begin{aligned}
\theta_{bc} &= \frac{l_{bL}}{2EI_{bL}}[2M_{bL}-\frac{l_{bL}}{L}(M_{bR}+M_{bL})] \\
&+\frac{(l-l_{bL}-l_{bR})}{2EI_b}\left(\frac{l-l_{bL}+l_{bR}}{l}M_{bL}-\frac{l+l_{bL}-l_{bR}}{l}M_{bR}\right) \\
&-\frac{l_{bR}}{2EI_{bR}}[2M_{bR}-\frac{l_{bR}}{l}(M_{bR}+M_{bL})] \\
&= a_{\theta 4}M_{bL}-a_{\theta 3}M_{bR}
\end{aligned} \tag{8.50}$$

$$\begin{aligned}
u_{bc} &= \frac{N_b l_{bL}}{EA_{bL}}+\frac{N_b(l-l_{tL}-l_{tR})}{EA_b}+\frac{N_b l_{bR}}{EA_{bR}} \\
&= a_{ub}N_b
\end{aligned} \tag{8.51}$$

where

$$l_{s3}=\frac{(3l-2l_{bL})l_{bL}}{3(2l-l_{bL})} \tag{8.52}$$

$$l_{s4}=\frac{(l-l_{bL}-l_{bR})(2l_{bR}+l-l_{bL})}{3(l-l_{bL}+l_{bR})} \tag{8.53}$$

$$a_{v3} = \frac{(2l-l_{bL})l_{s3}l_{bL}}{2EI_{bL}l} + \frac{(l-l_{bL}+l_{bR})(l-l_{bL}-l_{bR})(l_{bL}+l_{s4})}{2EI_{b}l} + \frac{(3l-2l_{bR})l_{bR}^{\ 2}}{6EI_{bR}l}$$
$$= \frac{1}{6El}\left(\frac{3l_{bL}^2 l-2l_{bL}^3}{I_{bL}} + \frac{-l^3+4l_{bL}l^2+2l_{bR}l^2-9l_{bL}^2 l+3l_{bR}^2 l+4l_{bL}^3-6l_{bL}l_{bR}^2-2l_{bR}^3}{I_b} + \frac{3l_{bR}^2 l-2l_{bR}^3}{I_{bR}}\right)$$

(8.54)

$$a_{v4} = \frac{(2l-l_{bL})(l-l_{s3})l_{bL}}{2EI_{bL}l} + \frac{(l-l_{bL}+l_{bR})(l-l_{bL}-l_{bR})(l-l_{bL}-l_{s4})}{2EI_{b}L} + \frac{l_{bR}^{\ 3}}{3EI_{bR}l}$$
$$= \frac{1}{3El}\left(\frac{3l_{bL}l^2-2l_{bL}^2 l+l_{bL}^3}{I_{bL}} + \frac{l^3-4l_{bL}l^2+l_{bR}l^2+3l_{bL}^2 l-l_{bL}^3-l_{bR}^3}{I_b} + \frac{l_{bR}^3}{I_{bR}}\right) \quad (8.55)$$

$$a_{\theta 3} = \frac{l_{bL}^{\ 2}}{2EI_{bL}l} + \frac{(l+l_{bL}-l_{bR})(l-l_{bL}-l_{bR})}{2EI_{b}l} + \frac{(2l-l_{bR})l_{bR}}{2EI_{bR}l} \quad (8.56)$$

$$a_{\theta 4} = \frac{(2l-l_{bL})l_{bL}}{2EI_{bL}l} + \frac{(l-l_{bL}+l_{bR})(l-l_{bL}-l_{bR})}{2EI_{b}l} + \frac{l_{bR}^2}{2EI_{bR}l} \quad (8.57)$$

$$a_{ub} = \frac{l_{bL}}{EA_{bL}} + \frac{l-l_{bL}-l_{bR}}{EA_{b}} + \frac{l_{bR}}{EA_{bR}} \quad (8.58)$$

where v_{bc}, u_{bc} and Θ_{bc} are the relative vertical displacement, horizontal displacement and rotation between the two ends of bottom chord after cracking, respectively; A_{bR} and A_{bL} are the cross-sectional areas of respectively the right end and left end of bottom chord after cracking.

According to the conditions of deformation compatibility based on the assumption that the top and the bottom chords are framed into the rigid abutments on the two sides of the opening, the following three equations should be satisfied:

$$v_{tc} = v_{bc} \quad (8.59)$$

$$\theta_{tc} = \theta_{bc} \quad (8.60)$$

$$\frac{u_{tc}+u_{bc}}{z_R}=\theta_{tc}=\theta_{bc} \tag{8.61}$$

8.3.2.3 Determination of the lengths of cracking regions l_{tR}, l_{tL}, l_{bR} and l_{bL}

The top chord is selected as an example to illustrate the calculation of the cracking lengths. As shown in Fig. 8.9, M_{tRcr} and M_{tLcr} are cracking moments of the cross sections respectively close to the right end and left end of top chord (similarly, M_{bRcr} and M_{bLcr} are cracking moments of the cross sections respectively close to the right end and left end of bottom chord). According to the diagram shown in Fig. 8.9, the lengths of cracking regions l_{tR}, l_{tL}, l_{bR} and l_{bL} can all be obtained as follows:

$$l_{tR}=\frac{M_{tR}-M_{tRcr}}{M_{tL}+M_{tR}}l \tag{8.62}$$

$$l_{tL}=\frac{M_{tL}-M_{tLcr}}{M_{tL}+M_{tR}}l \tag{8.63}$$

$$l_{bR}=\frac{M_{bR}-M_{bRcr}}{M_{bL}+M_{bR}}l \tag{8.64}$$

$$l_{bL}=\frac{M_{bL}-M_{bLcr}}{M_{bL}+M_{bR}}l \tag{8.65}$$

The bending moments at the chord ends (M_{tR}, M_{tL}, M_{bR}, M_{bL}) at the yielding of the beam can be obtained using the strength model proposed in Chapter 7. It should be noted here, however, in the calculation the ultimate state of the beam was used due to the following reasons: (1) it has been observed in the tests that when the beam yielded, the applied load kept almost unchanged till the final failure of the beam; therefore, it is not unreasonable to use the strength of the beam at ultimate state to represent that at the yielding of the beam; and (2) In Chapter 7, although the yielding state of the beam can also be considered in the proposed strength model, it is based on the assumption that all the four chord ends yield at the same time, which is in fact not true for most cases. This is why in Chapter 7, the proposed strength model can provide more accurate predictions to the strength of the beam if the ultimate state is adopted.

In the calculation of M_{tR}, M_{tL}, M_{bR} and M_{bL}, the axial force in the top/bottom chord (N_t or N_b) can also be obtained. By adopting the obtained N_t or N_b and using the *N-M* curves corresponding to the cracking of the cross sections of the top and bottom chords obtained in Subsection 8.3.1.4 (as shown in in Fig. 8.7), the cracking moments of the cross sections of the chords (M_{tRcr}, M_{tLcr}, M_{bRcr} and M_{bLcr}) at the yielding of the beam can also be obtained. However, it should be noted that the bending moments of *N-M* curves shown in Fig. 8.7 are with reference to the centroidal axes of the corresponding cross sections, thus the obtained M_{tRcr}, M_{tLcr}, M_{bRcr} and M_{bLcr} from Fig. 8.7 should be transformed to be with reference to the mid-planes of the corresponding cross sections.

8.3.2.4 Determination of θ_{Ly} and θ_{Ry}

The internal forces at the two ends of top and bottom chords (i.e. M_{tR}, M_{tL}, M_{bR}, M_{bL}, N_t, N_b, V_t and V_b) and the lengths of cracking regions (l_{tR}, l_{tL}, l_{bR} and l_{bL}) at the yielding of the beam have all been obtained in the last subsection. As can be seen from Fig. 8.8 and Eqs. 8.39-8.41, 8.49-8.51, however, to obtain the relative displacements and rotations between the two ends of the chords when the beam yields, there are still twelve remaining unknowns: M_{tR}, M_{tL}, M_{bR}, M_{bL}, I_{tR}, I_{tL}, I_{bR}, I_{bL}, A_{tR}, A_{tL}, A_{bR} and A_{bL}. The twelve remaining unknowns are all related to four independent unknowns, i.e., the locations of the centroidal axes of the cross sections in the four cracking regions. Therefore, the key to obtain Θ_{Ly} and Θ_{Ry}, which can be calculated using Eqs. 8.30 and 8.31, is to determine the locations of the centroidal axes of the cross sections in the four cracking regions.

As has been stated in Chapter 7, the yielding of the two cross sections at the two ends of bottom chord is due to the yielding of the tension steel bars, while the yielding of the two cross sections at the two ends of top chord is due to the strain of the concrete reaches the strain corresponding to the transition point between the first and second portions on the stress-strain curve for FRP-confined concrete (Lam and Teng 2003). The locations of the centroidal axes of the four cross sections at the two ends of top and bottom chords corresponding to the yielding of these cross sections can then be obtained through cross-sectional analyses. However, these four cross sections usually do not yield at the same time, and instead, they yield one by one, and the beam yields only when all the four cross sections yield. After the yielding of the cross section, the location of the centroidal axis changes. Therefore, at the yielding of the beam, the location of the centroidal axis of the cross section which is the final of the four cross sections to yield is that corresponding to the yielding of the cross section, while the locations of the centroidal axes of the other three cross sections which yield earlier have changed according to the corresponding internal forces at these cross sections. Therefore, the locations of the centroidal axes of the other three cross sections are three unknowns and need to be determined through a trial and error process, using the following steps:

Step-1: Assume one of the four cross sections is the cross section which is the last to yield, and calculate the location of the centroidal axis of this cross section corresponding to the yielding of this cross section through a section analysis. With the obtained position of the centroidal axis, the bending moment about the centroidal axes of this cross section, the second moment of area and the equivalent cross-sectional area of this cross section can be obtained.

Step-2: Determine the centroidal axes of the other three cross sections which have yielded earlier. With the bending moment, second moment of area and the equivalent cross-sectional area of the cross section in Step-1 obtained, the unknowns in Eqs. 8.39-8.41, 8.49-8.51 (M_{tR}, M_{tL}, M_{bR}, M_{bL}, I_{tR}, I_{tL}, I_{bR}, I_{bL}, A_{tR}, A_{tL}, A_{bR} and A_{bL}) are reduced from twelve to nine. These nine unknowns are functions of the locations of the centroidal axes of the three cross sections which have yielded earlier, which means that the number of independent unknowns is three. If the three equations of deformation compatibility (Eqs. 8.59-8.61) can be solved (i.e., the solution exists), the assumed cross section is indeed the one which is the last to yield and the three independent unknowns (centroidal axes of the three cross sections which have yielded earlier) can be determined using Eqs. 8.59-8.61.

Step-3: If the three equations of deformation compatibility (Eqs. 8.59-8.61) cannot be solved (i.e., the solution does not exist), select one of the other three cross sections to be the last cross section to yield and repeat Steps 1 and 2. Repeat the above steps until the solution of Eqs. 8.59-8.61 can be found.

Step-4: Once the three independent unknowns (centroidal axes of the three cross sections which have yielded earlier) are determined, the relative vertical displacement and rotation between the two ends of the opening at yielding of the beam can be calculated respectively using Eqs. 8.39 and 8.40. Then θ_{Ly} and θ_{Ry} can be calculated respectively using Eqs. 8.30 and 8.31.

The calculation results show that for all six RC T-section beams with an FRP-strengthened web opening tested by the candidate, the cross section at the right end of bottom chord is the last cross section to yield.

8.3.3 Comparisons of *M-θ* curves between prediction and test

Using the calculation methods proposed in Subsections 8.3.1 and 8.3.2, the $M_L - \theta_L$ curve and $M_R - \theta_R$ curve can be predicted (i.e. M_{Lcr}, M_{Rcr}, θ_{Lcr}, θ_{Rcr}, θ_{Ly} and θ_{Ry} can be determiend). The rotations (θ_{Lcr}, θ_{Rcr}, θ_{Ly} and θ_{Ry}) obtained respectively from the calculation methods and tests for the six RC T-section beams with an FRP-strengthened web opening tested by the candidate are listed in Table. 8.3. As can be seen from Table. 8.3, the predicted rotations are all a little smaller than the corresponding test results, which may be because that the shear deformation and the second-order effect of axial force when calculating the deflections of the chords are not considered in the proposed calculation methods.

Based on the comparison of rotations between prediction and test, an amplification factor of 1.2 is suggested for the rotations (i.e., θ_{Lcr}, θ_{Rcr}, θ_{Ly} and θ_{Ry}) predicted by the proposed calculation methods. By applying the suggested amplification factor, the comparison of the *M-θ* curves (the $M_L - \theta_L$ curve and the $M_R - \theta_R$ curve) between prediction and test is plotted in Fig. 8.10. It can be seen from Fig. 8.10 that the predicted *M-θ* curves agree well with test results.

8.4 FURTHER VERIFICATION OF THE PROPOSED M-Θ MODEL

In this section, simulations of the tested specimens were conducted using OpenSees (2009), with the proposed *M-θ* model being adopted in the FE models, to further verify the accuracy of the proposed *M-θ* model. OpenSees (2009) is commonly adopted in the simulation of seismic performance of RC frames and was therefore also chosen for the simulation of RC beams with a web opening to assess its feasibility.

8.4.1 FE model in OpenSees

The schematic of the FE model of an RC beam with a web opening established in OpenSees (2009) is shown in Fig. 8.11, in which, the numbering of nodes is given by numbers in circles and the numbering of elements is given by numbers without circles. The developed FE model has a total of 7 nodes and 6 elements. Node 1 and Node 7 are located at the two ends (i.e., supports) of the beam; Node 2 is located at the midspan of the beam (i.e., the location of the loading point);

the locations of Node 3 and Node 4 coincide with each other and are at left end of the web opening (i.e, the end close to the loading point); the locations of Node 5 and Node 6 also coincide with each other and are at the eight end of the web opening (i.e., the end close to the right support). Element 4 which is formed by Node 4 and Node 5 represents the opening region, which is treated as a rigid body and thus defined as an Elastic Beam Column Element (OpenSees 2009) with a very large elastic modulus. The use of two nodes at the same location was to build a ZeroLength element (OpenSees 2009); therefore, Element 3 connecting Node 3 and Node 4 and Element 5 connecting Node 5 and Node 6 are two ZeroLength Elements respectively representing the two plastic hinges at the two ends of the web opening. The ElasticMultiLinear Material available in OpenSees (2009) was used to define the properties of Elements 3 and 4, i.e., the moment-rotation relationships ($M_L - \theta_L$ curve and $M_R - \theta_R$ curve) at the two plastic hinges. The remaining three elements (Elements 1, 2 and 6) are used to model the solid parts of the beam (i.e., the part without a web opening). These three elements are Force-Based Beam-Column Elements (OpenSees 2009) and the solid sections were defined as a Fiber Section (OpenSees 2009). The steel was defined as an elastic-perfectly plastic material and the concrete was modelled using the Concrete02 Material model (OpenSees 2009). The horizontal and vertical displacements of Node 1 and the vertical displacement of Node 7 are fixed. The point load is applied at Node 2 using a displacement-controlled mode.

8.4.2 FE results

For comparison purposes, two schemes are examined in the present study: (1)

Scheme-1: the model as presented above (referred to as "***normal***" in Fig. 8.12); and (2) Scheme-2: the solid parts of the beam (Elements 1, 2 and 6) are assumed to be elastic (referred to as "***elastic***" in Fig. 8.12).

The load-deflection curves obtained from the above two schemes are compared with the test results in Fig. 8.12. As can be seen from Fig. 8.12, for all six RC T-section beams with an FRP-strengthened web opening tested by the candidate, the ***normal*** model provides better predictions than the ***elastic*** model. The predicted load-deflection curves from the ***normal*** model agree well with the test results. As can be seen from Fig. 8.12, the predicted load-deflection curves from the ***elastic*** model are stiffer than those from the ***normal*** model, and the difference between them increases with the decrease of opening size. This can be explained by the crack patterns at the failure of these beams, as shown in Fig. 8.13. For the two beams with a large web opening (F-700x300-N and F-800x280-N), cracks mainly appeared in the opening region (as shown in Figs. 8.13a and b), so it is not unreasonable to treat the solid parts of the beam as elastic. For the two beams with a medium web opening (F-600x280-N and F-700x260-N), some cracks also appeared in the solid parts of the beam (as shown in Figs. 8.13c and d), so the elastic assumption for the solid parts of the beam causes larger difference of predictions between the ***normal*** model and the ***elastic*** model (as shown in Figs. 8.12c and d). And for the two beams with a small web opening (F-600x220-N and F-700x200-N), more cracks appeared in the solid parts of the beam (as shown in Figs. 8.13e and f), so the difference of predictions between the ***normal*** model and the ***elastic*** model induced by the elastic assumption for the solid parts of the beam further increases (as shown in Figs. 8.12e and f).

8.5 *M-Θ* MODEL FOR RC BEAMS WITH WEB OPENINGS IN AN RC FRAME

It should be noted that Eqs. 8.1, 8.2, 8.30 and 8.31 are based on the test set-up adopted by the candidate (Fig. 8.3). For RC frame beams with one web opening at each end of the beam, the schematic of the beam is shown in Fig. 8.14, in which only one end of the beam is considered (the other end of the beam can be treated in a similar way). Points A, B, C and D in Fig. 8.14 respectively correspond to the edge of the frame column, the left end of the web opening, the right end of the web opening and the inflection point closer to the left end of the beam.

For such a situation, the proposed calculation methods for the relative displacements and rotations between the two ends of top and bottom chords (Eqs. 8.10-8.15, 8.39-8.41, 8.49-8.51) are still appliable, but the calculation of Θ_L and Θ_R (Eqs. 8.1, 8.2, 8.30 and 8.31) needs to be adjusted. As the web opening is located very close to the edge of the column, the vertical displacement between Points A and B is very small and can be ignored. Based on Fig. 8.14, the angles Θ_L and Θ_R can be calculated as:

$$\theta_L = \frac{y_O}{l} \tag{8.66}$$

$$\theta_R = -(\frac{y_R}{L_R} + \frac{y_O}{l}) \tag{8.67}$$

Combining Eqs. 8.66 and 8.26 gives:

$$\theta_R = \theta_O - \frac{y_O}{l} \tag{8.68}$$

8.6 CONCLUDING REMARKS

This chapter has presented a study on the moment-rotation (*M-Θ*) response of RC beams with a web opening which exhibit a flexural failure model. Based on the simplified diagram for the beam, an *M-Θ* model for the two plastic hinges (i.e., $M_L - \theta_L$ curve and $M_R - \theta_R$ curve) at the two ends of the web opening is proposed. The predicted *M-Θ* curves agree well with those obtained from the tests.

To further verify the accuracy of the proposed *M-Θ* model, FE modelling of RC beams with a web opening was conducted using OpenSees (2009), with the *M-Θ* model appropriately incorporated. The predicted load-deflection curves agree well with the test results.

Although the *M-Θ* model is based on the test set-up adopted by the candidate (Fig. 8.3), the proposed calculation method is general and can be adapted to other situations with slight modifications, such as RC frame beams with a web opening at each end of the beam (Fig. 8.14).

8.7 REFERENCES

ABAQUS (2012). *ABAQUS Analysis User's Manual (Version 6.12)*, Dassault Systems SIMULIA Corporation, Providence, Rhode Island, USA.

OpenSees (2009). *Open System for Earthquake Engineering Simulation*, Pacific Earthquake Engineering Research Center, University of California at

Berkeley, http://opensees.berkeley.edu.

Table 8.1. Relative vertical displacements between the two ends of the opening

Beam height (mm)	Opening size		Chord height		Calculed result (mm)	FE result (mm)		Calculed result/FE result	
	Length (mm)	Height (mm)	Top chord (mm)	Bottom chord (mm)		Solid element	Beam element	Solid element	Beam element
500	700	350	50	100	4.79	5.05	5.00	0.949	0.958
		300	100		2.83	2.98	2.96	0.950	0.956
		250	150		1.55	1.67	1.66	0.928	0.934
500	900	300	100	100	5.82	5.90	5.98	0.986	0.973
	800				4.14	4.27	4.29	0.970	0.965
	700				2.83	2.98	2.96	0.950	0.956
	600				1.82	1.97	1.93	0.924	0.943
600	700	400	100	100	2.63	2.78	2.76	0.946	0.953
550		350			2.72	2.86	2.84	0.951	0.958
500		300			2.83	2.98	2.96	0.950	0.956
Mean value								0.950	0.955
STD =								0.018	0.011
CoV =								0.019	0.012

Table 8.2. Reaction forces at the right end of the beam at cracking of the beam (V_{cr})

Specimen	V_{crtR} (kN)	V_{crtL} (kN)	V_{crbR} (kN)	V_{crbL} (kN)	Predicted V_{cr} using the proposed calculation method (kN)	V_{cr} from test (kN)	Prediction/Test
F-700×300-N	146	72	50	31	31	30	1.033
F-800×280-N	64	43	49	30	30	28	1.071
F-600×280-N	195	73	59	38	38	38	1.000
F-700×260-N	83	48	58	38	38	38	1.000
F-600×220-N	146	60	78	53	53	55	0.964
F-700×200-N	99	55	80	54	54	55	0.982
Mean value							1.008
STD =							0.039
CoV =							0.038

Table 8.3. Comparisons of rotations obtained from the calculation method and tests

Specimen	Θ_{Lcr}			Θ_{Rcr}			Θ_{Ly}			Θ_{Ry}		
	Prediction	Test	Prediction /Test	Prediction	Test	Prediction /Test	Prediction	Test	Prediction /Test	Prediction	Test	Prediction /Test
F-700×300-N	0.00107	0.00111	0.964	0.00071	0.00081	0.877	0.02134	0.02869	0.744	0.01969	0.02584	0.762
F-800×280-N	0.00119	0.00125	0.952	0.00084	0.00098	0.857	0.02530	0.03004	0.842	0.02351	0.02603	0.903
F-600×280-N	0.00091	0.00103	0.883	0.00054	0.00072	0.750	0.01930	0.02408	0.801	0.01778	0.02036	0.873
F-700×260-N	0.00106	0.00113	0.938	0.00068	0.00083	0.819	0.02404	0.02891	0.832	0.02218	0.02377	0.933
F-600×220-N	0.00091	0.00092	0.989	0.00047	0.00070	0.671	0.02107	0.02388	0.882	0.01955	0.01733	1.128
F-700×200-N	0.00105	0.00111	0.946	0.00056	0.00081	0.691	0.01742	0.02138	0.815	0.01566	0.01471	1.065
Mean value			0.945			0.778			0.819			0.944
STD =			0.035			0.086			0.046			0.133
CoV =			0.037			0.111			0.056			0.141

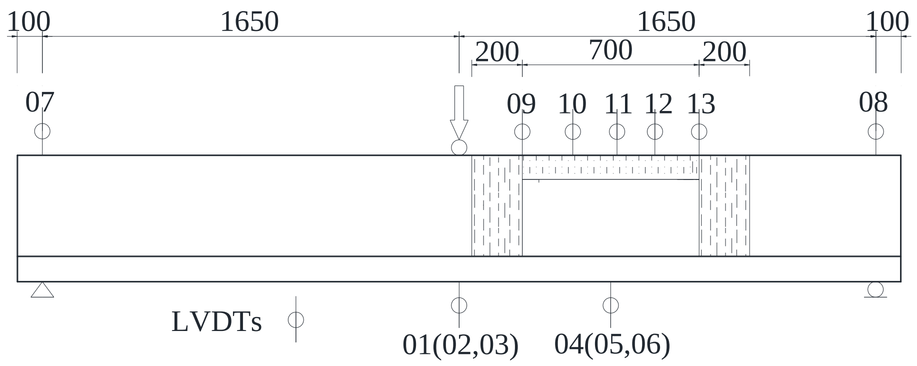

Figure 8.1. Details of F-700×300-N and arrangement of LVDTs (dimensions in mm)

(a) The whole beam

(b) The opening region

Figure 8.2. Typical failure mode of RC T-section beams with an FRP-strengthened web opening

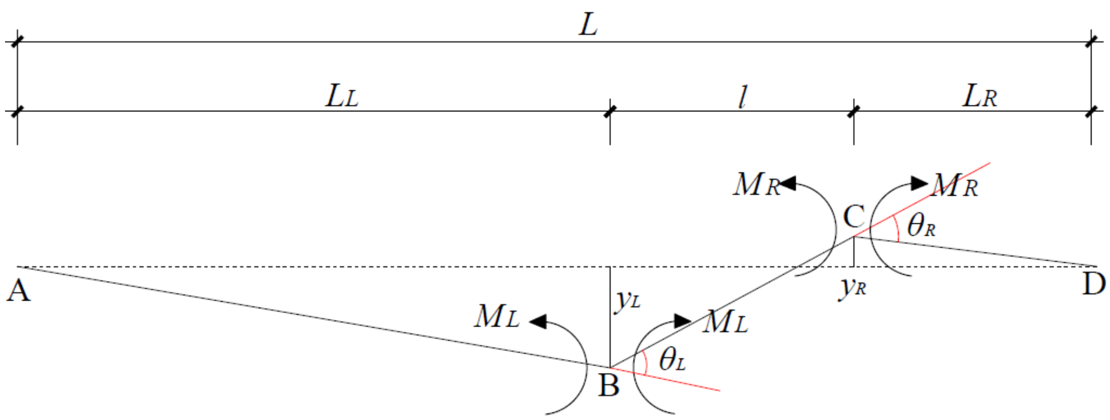

Figure 8.3. Simplified representation of an RC beam with a web opening

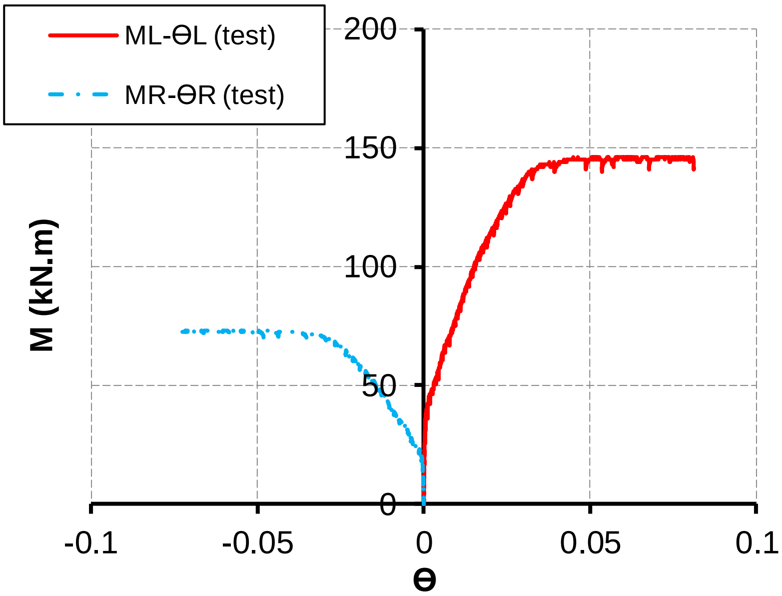

(a) F-700×300-N

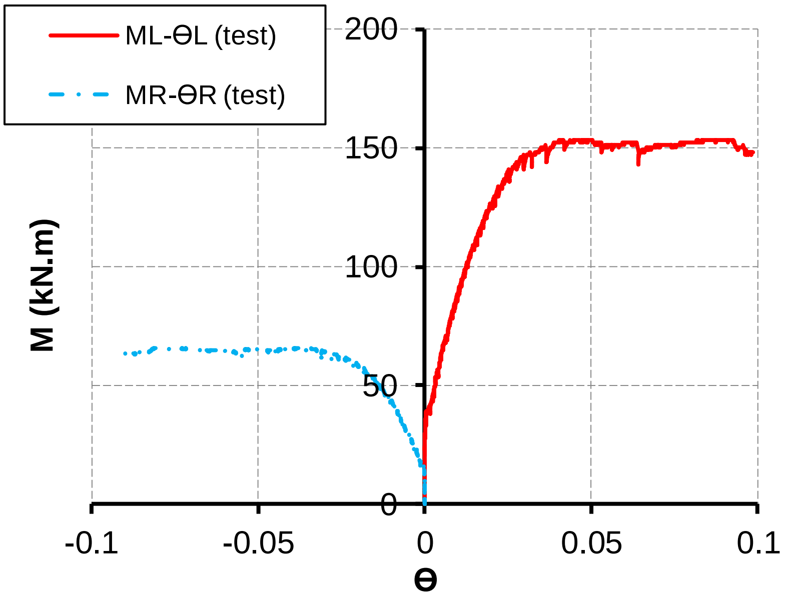

(b) F-800×280-N

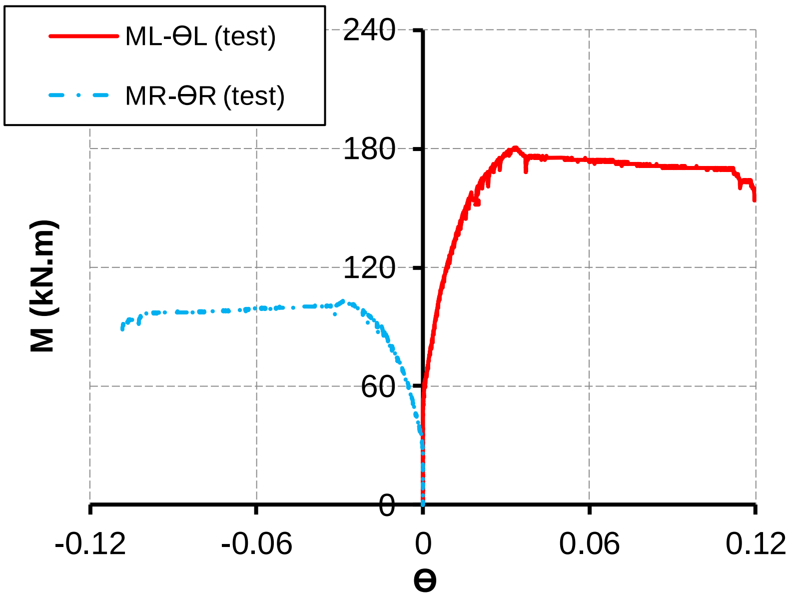

(c) F-600×280-N

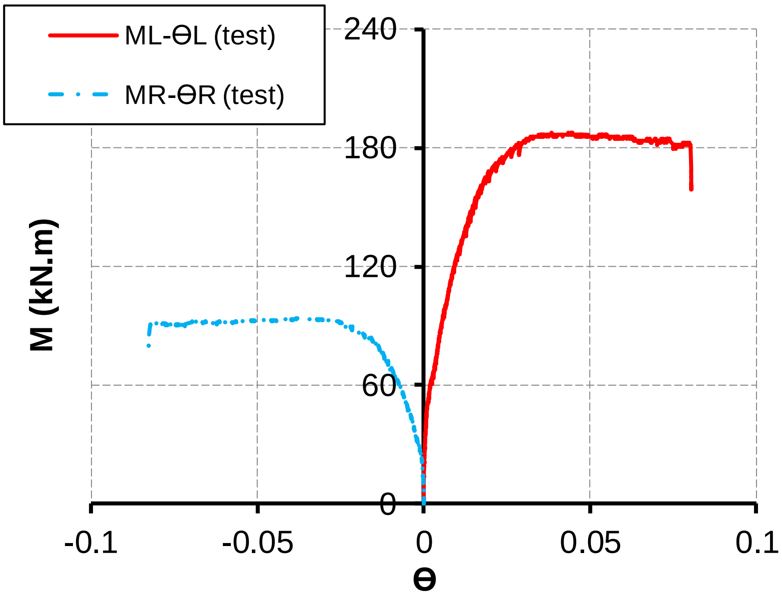

(d) F-700×260-N

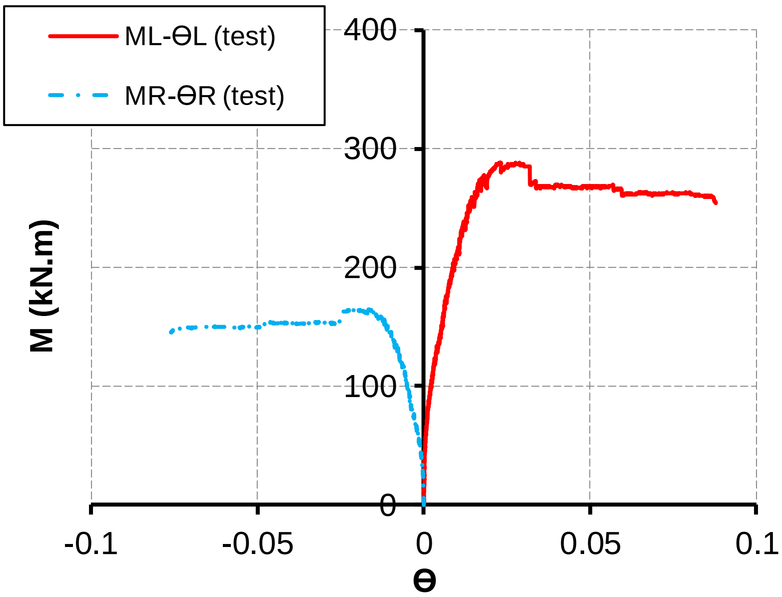

(e) F-600×220-N

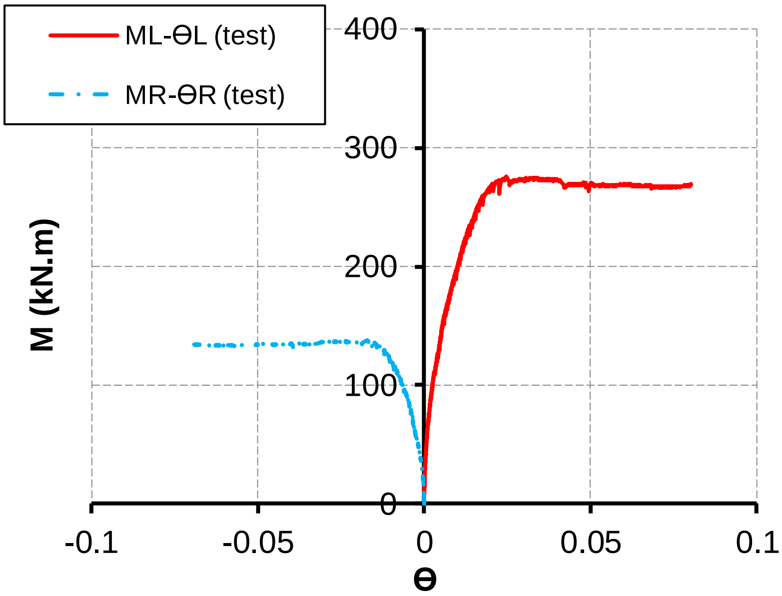

(f) F-700×200-N

Figure 8.4. $M_L-\theta_L$ curves and $M_R-\theta_R$ curves of the tested RC T-section beams with an FRP-strengthened web opening

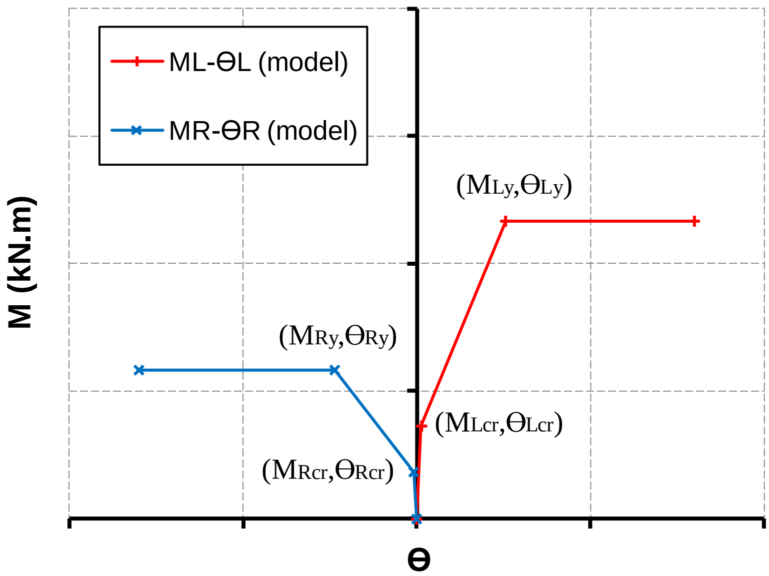

Figure 8.5. Proposed *M-Θ* model for the plastic hinge at each end of the web opening

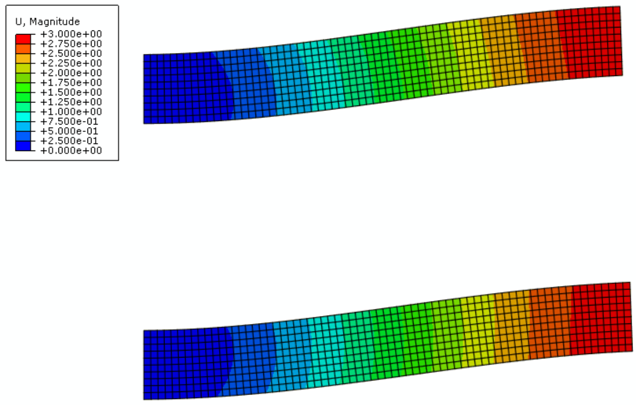

(a) Solid element

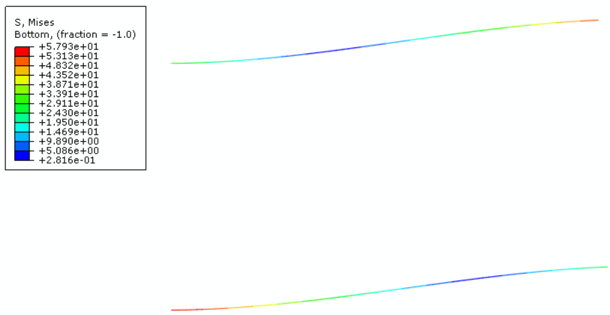

(b) Beam element

Figure 8.6. FE modelling of the opening region

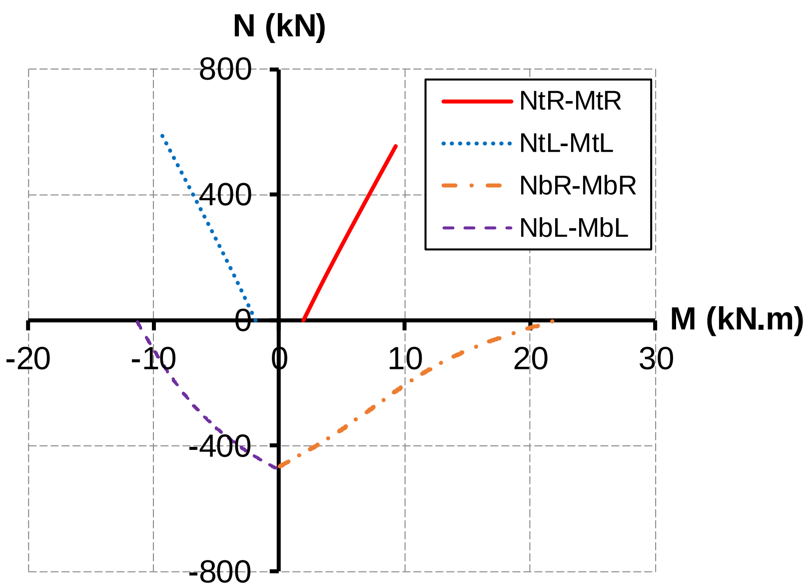

Figure 8.7. N-M curves of cross sections at the two ends of top and bottom chords at cracking (F-700×300-N)

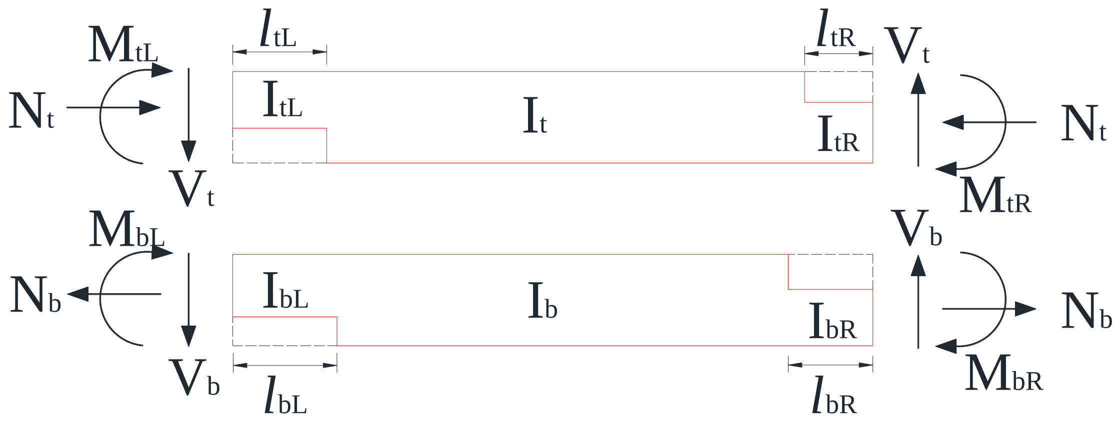

Figure 8.8. Free-body diagram of the opening region after cracking

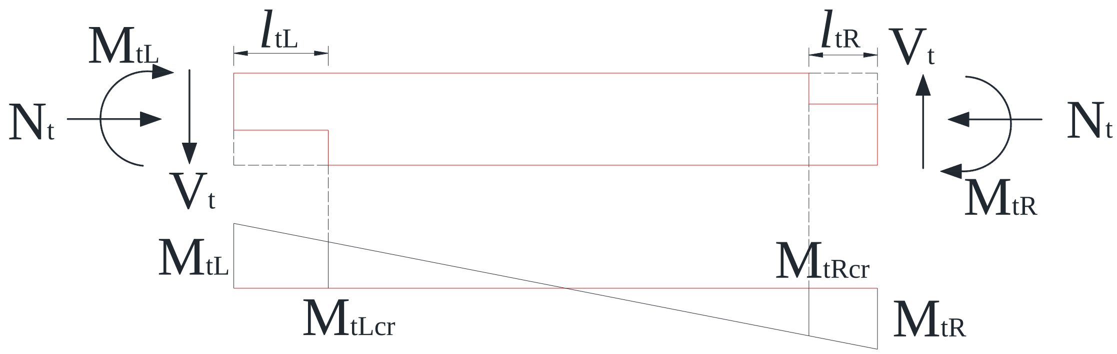

Figure 8.9. Calculation of the length of cracking region

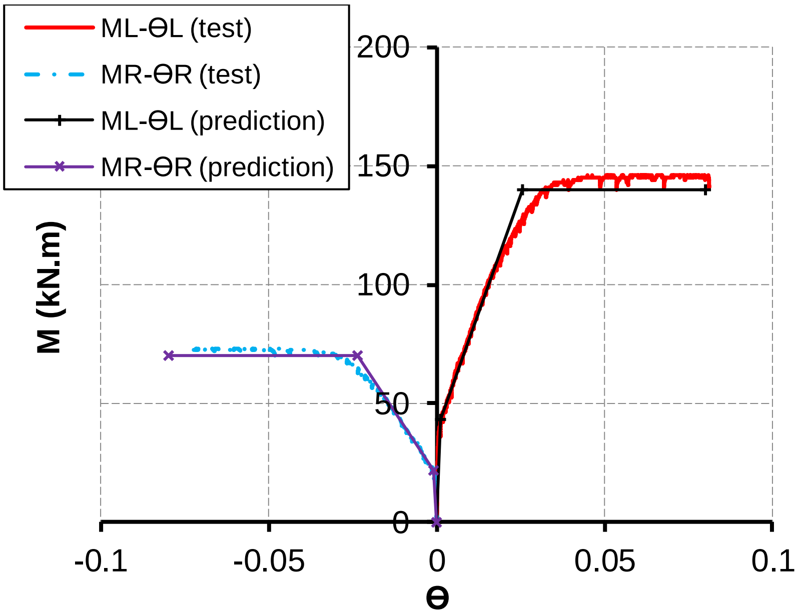

(a) F-700×300-N

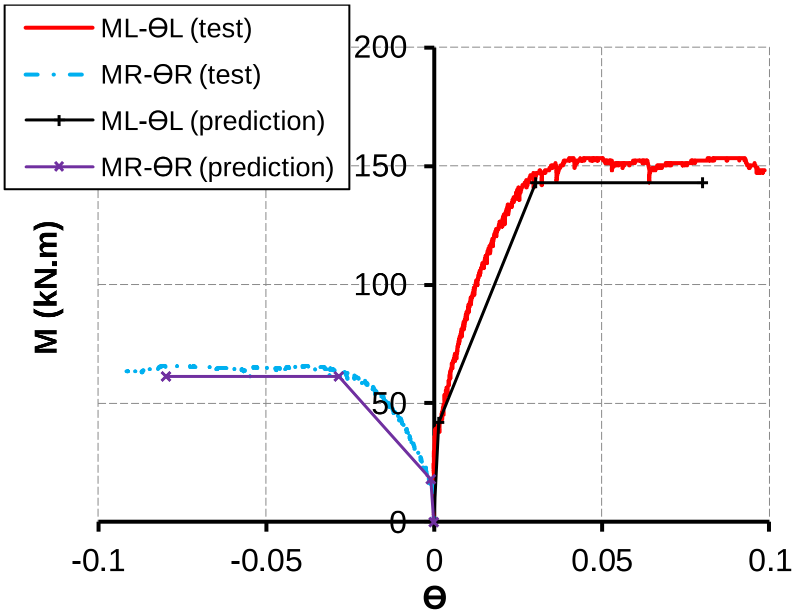

(b) F-800×280-N

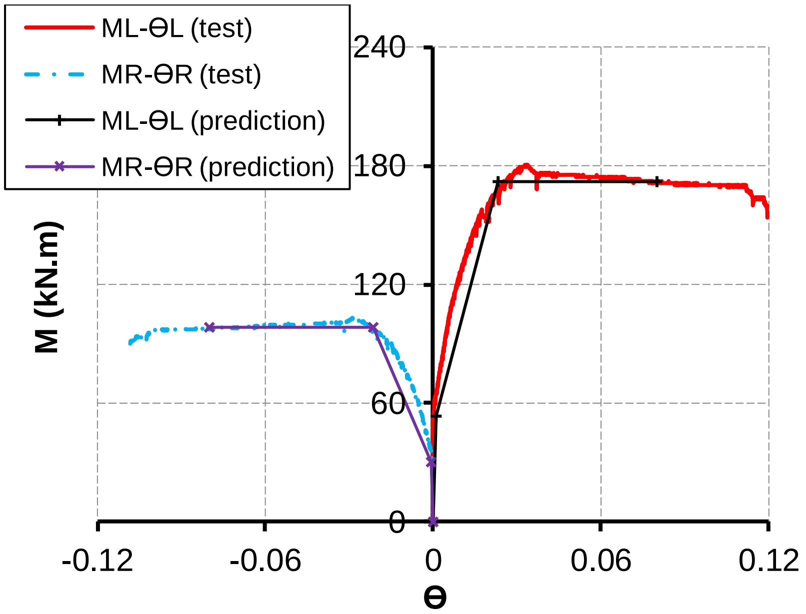

(c) F-600×280-N

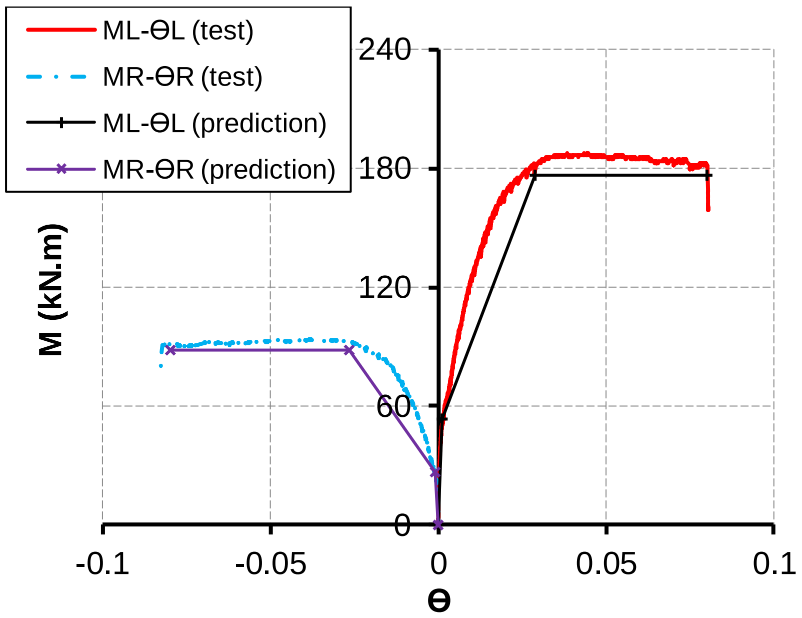

(d) F-700×260-N

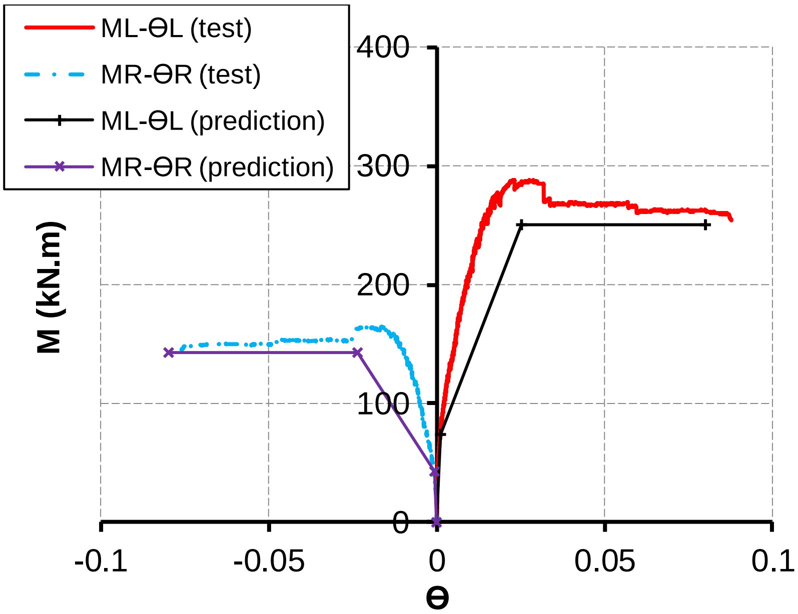

(e) F-600×220-N

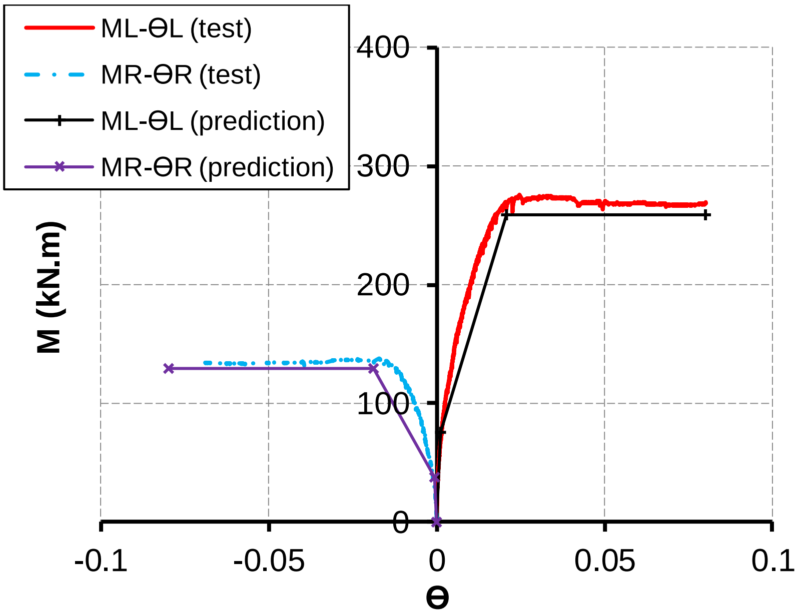

(f) F-700×200-N

Figure 8.10. Comparison of *M-Θ* curves between prediction and test

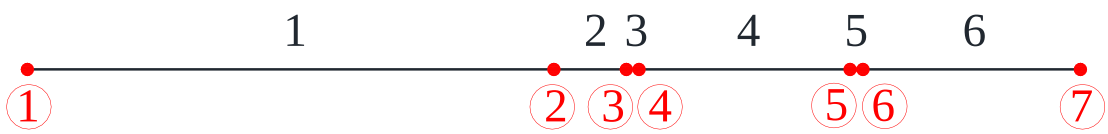

Figure 8.11. FE model of an RC beam with a web opening in OpenSees (2009)

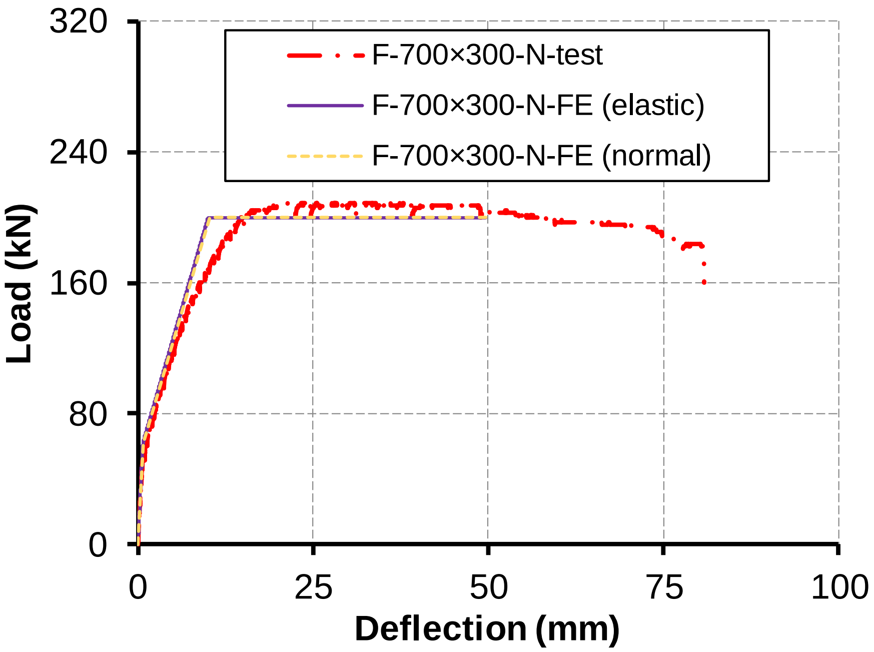

(a) F-700×300-N

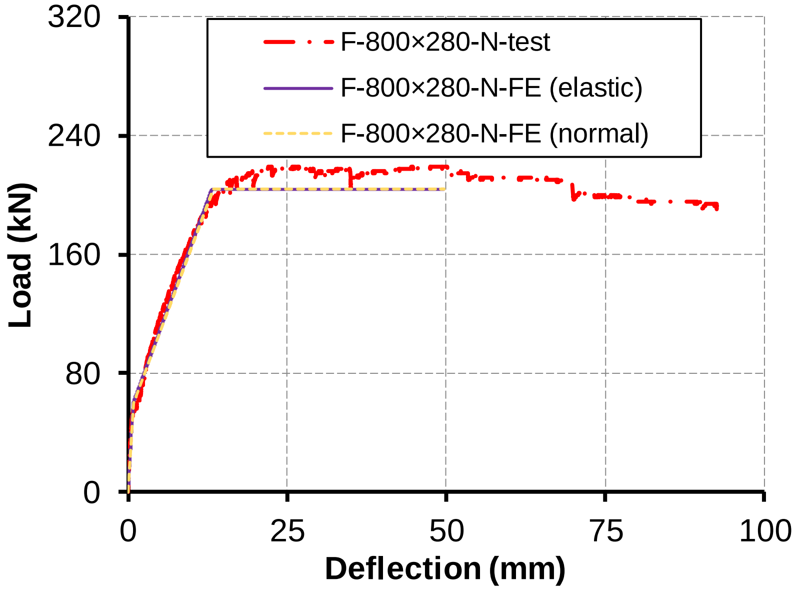

(b) F-800×280-N

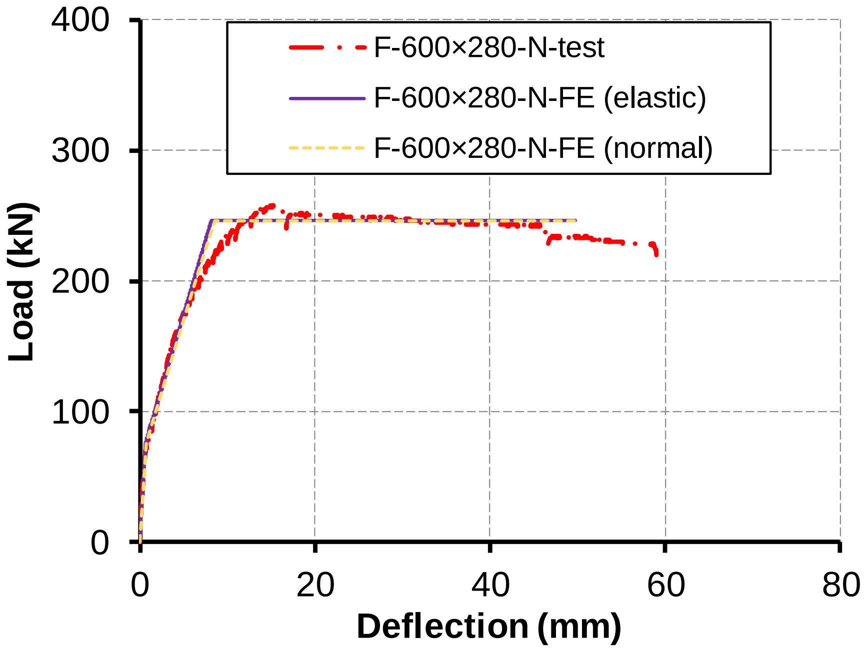

(c) F-600×280-N

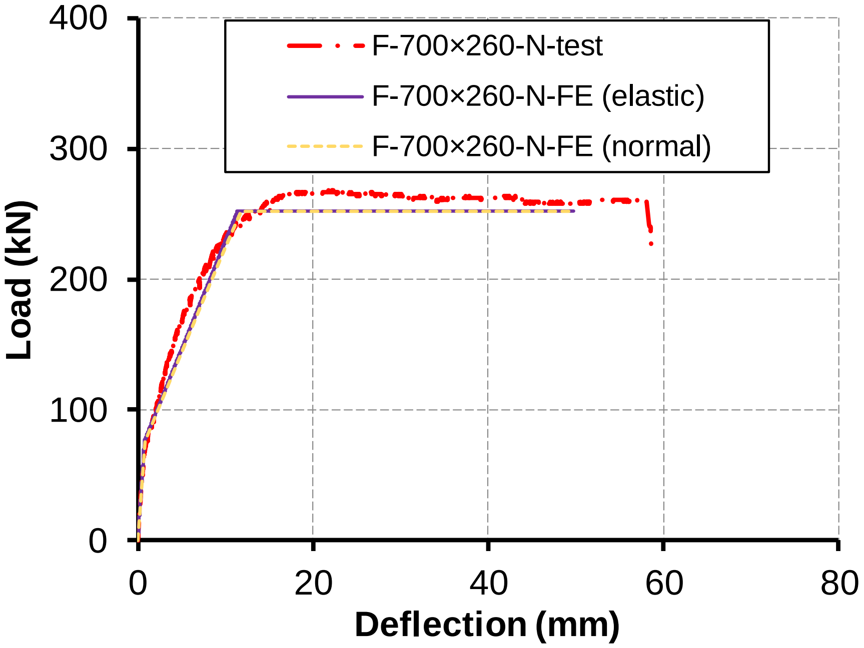

(d) F-700×260-N

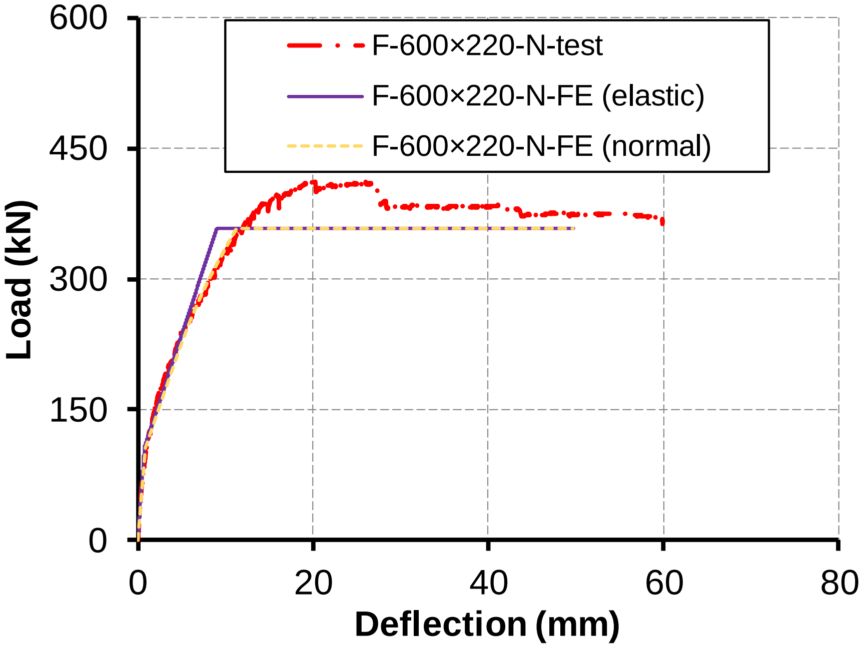

(e) F-600×220-N

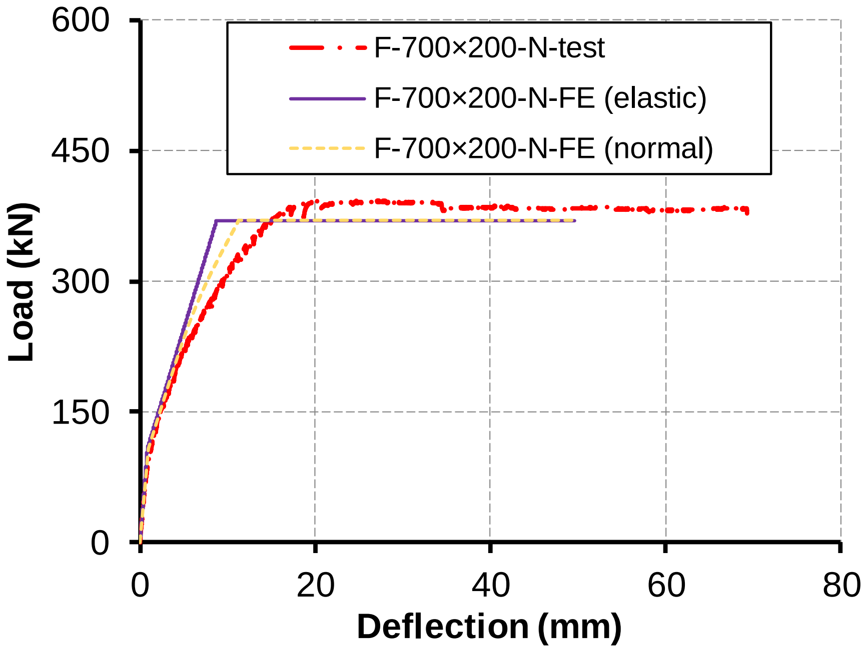

(f) F-700×200-N

Figure 8.12. FE results versus test results

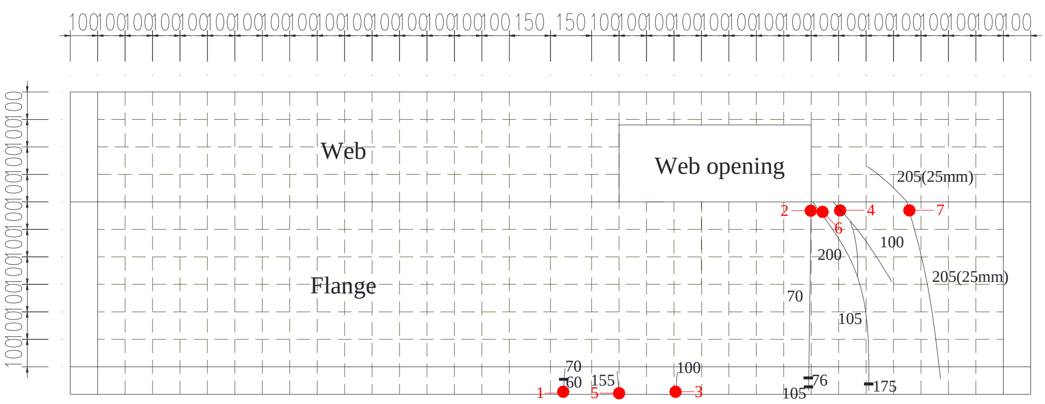

(a) F-700x300-N

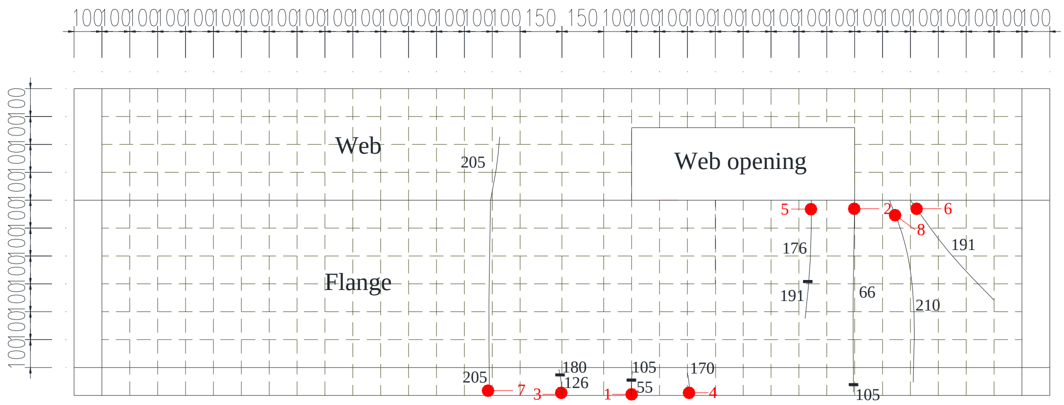

(b) F-800x280-N

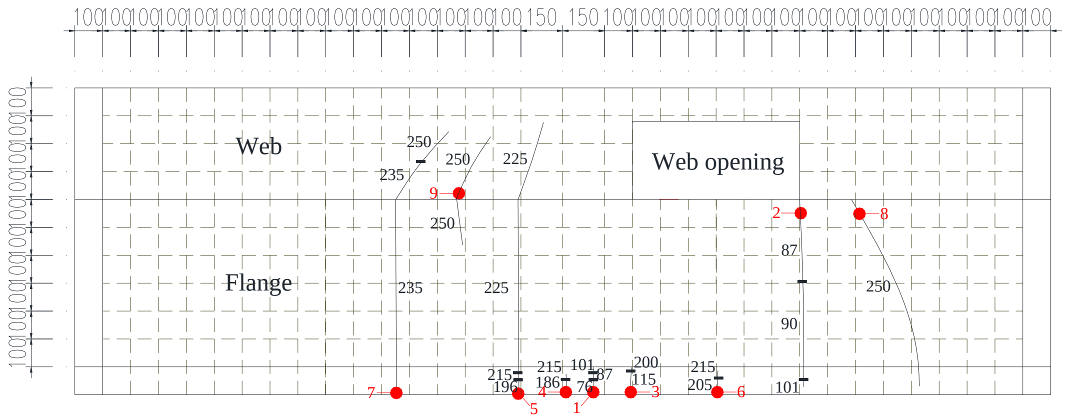

(c) F-600x280-N

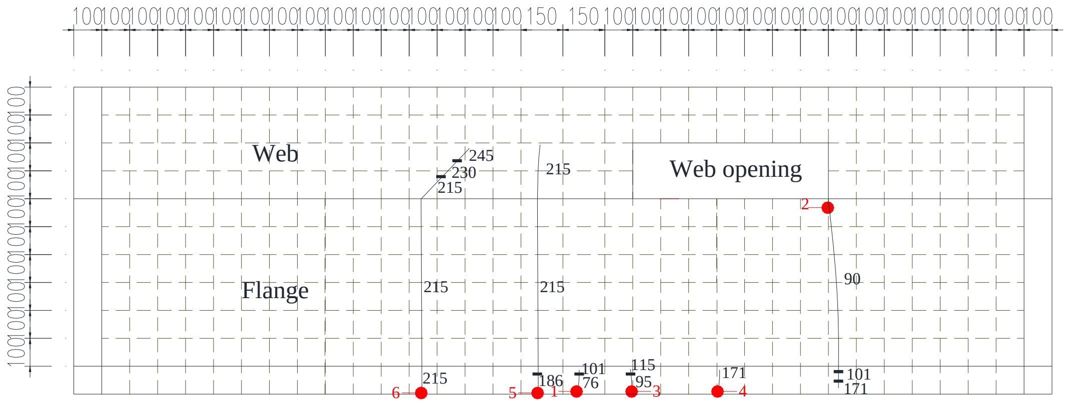

(d) F-700x260-N

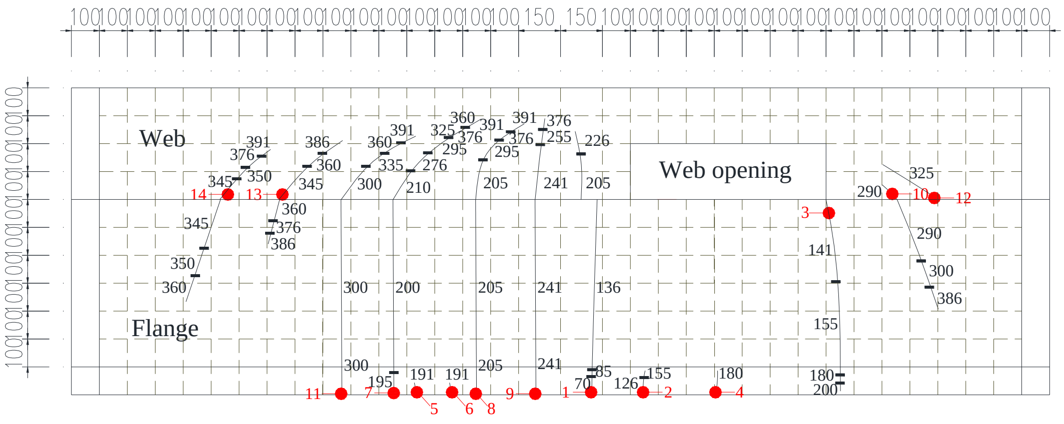

(e) F-600x220-N

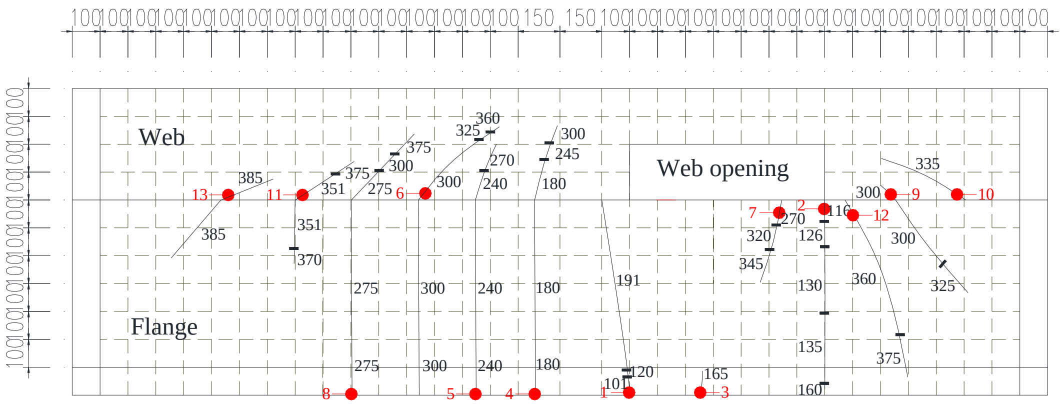

(f) F-700x200-N

Figure 8.13. Crack patterns at failure of RC beams with an FRP-strengthened web opening

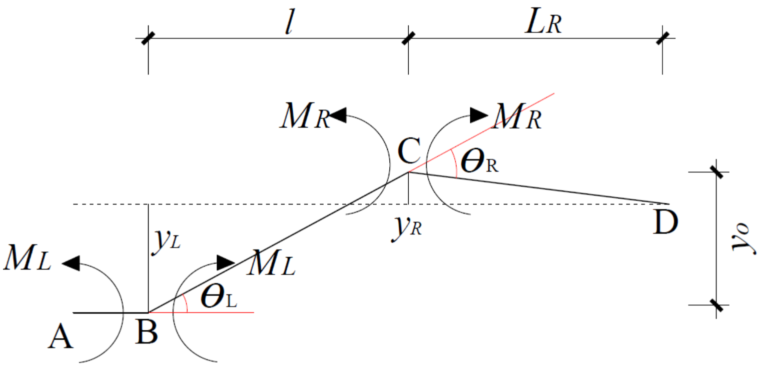

(a) Under sagging bending

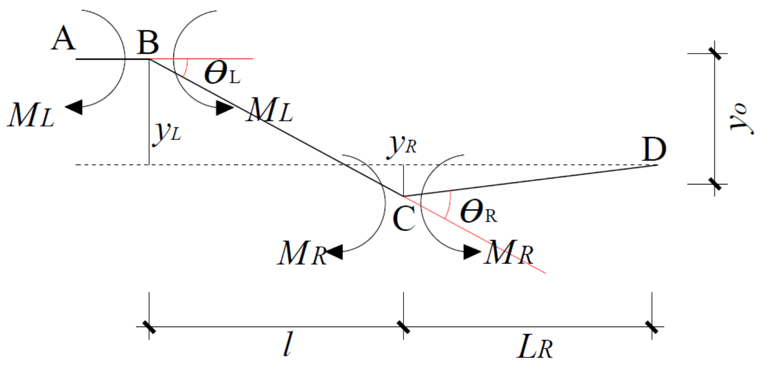

(b) Under hogging bending

Figure 8.14. Simplified representation for one end of an RC frame beam with one web opening at each end of the beam

CHAPTER 9

CONCLUSIONS

9.1 INTRODUCTION

As has been discussed in Chapter 1, three seismic retrofit techniques based on the method of beam-end weakening in combination with FRP strengthening (the BWFS method) to enforce the strong column-weak beam hierarchy where necessary and/or appropriate have been proposed by Prof. Teng's group (Teng et al. 2013), including the beam opening (BO) technique, the section reduction (SR) technique and the slab slit (SS) technique. Of these three techniques, the beam flexural capacity reduction caused by the SR and the SS techniques can be estimated relatively easily, but the same is not true about the BO technique. Moreover, the BO technique can be employed to meet the functional requirement of passages for utility ducts/pipes. Therefore, the present thesis has been mainly focused on the effect of the BO technique on the flexural capacity of the beam, with the objectives being to assess its feasibility and to develop appropriate analysis/design methods. The thesis has presented a systematic study on the behaviour of RC beams with a web opening, covering in-depth experimental, numerical and theoretical studies.

A large number of existing experimental studies (Mansur et al. 1999; Abdalla et al. 2003; Allam 2005; Maaddawy and Sherif 2009; Pimanmas 2010; Chin et al. 2012; Maaddawy and Ariss 2012; Suresh and Prabhavathy 2015; Chin et al. 2016) have addressed the effect of drilling an opening in an existing beam and the design of the associated strengthening measure, and most of these studies proposed the use of bonded FRP reinforcement for the strengthening intervention. These studies were motivated by the need to create openings in an existing structure for the passage of utility ducts and pipes, and were thus focused on restoring the strength of the beam through FRP strengthening. These studies confirmed the significant strength reduction due to the creation of an opening in the beam and the feasibility of FRP strengthening to compensate for the weakening effect of the opening. However, most existing experimental studies were focused on rectangular beams, with only the study of Mansur et al. (1999) being concerned with T-section beams, so more experimental studies were obviously needed to investigate the effect of drilling a web opening in T-section beams. Thus, an experimental study on full-scale RC T-section beams with a web opening was conducted and the test results were presented and interpreted in Chapter 5. A total of 14 full-scale RC beams, including one rectangular beam and 13 T-section beams, were designed and tested under static loading to assess the effect of the BO technique on the behaviour of T-section RC beams. The studied parameters covered the dimensions of web opening and the effect of FRP strengthening (including CFRP wraps on the concrete web chord and CFRP U-jackets on the beam web). The experimental study also provided detailed tests for the calibration and verification of the numerical and theoretical studies conducted by the candidate.

Although the experimental studies conducted by other researchers and the candidate provided useful information on the behaviour of RC beams with a web opening, a reliable method for predicting the performance of such RC beams was not available. While experimental studies are essential in understanding the structural behaviour of RC beams with a web opening, many behavioural aspects can be better or more efficiently examined using a finite element (FE) model. Indeed, FE modelling can serve as a powerful and economical alternative to laboratory testing in understanding the structural behaviour of and in the development of a design method for RC beams with a web opening. However, most of the existing studies on the behavior of RC beams with a web opening were experimentally based, with only a very limited amount of research being based on the numerical modeling of beams with a web opening using the FE method. The limited number of existing numerical studies on RC beams with a web opening had not been able to provide a reliable FE model for predicting the behaviour of such RC beams. Thus, studies were conducted with the aim of developing such a reliable FE approach with the general purpose package ABAQUS (2012), and these studies were presented in Chapters 3, 4 and 6. Three alterative FE approaches were proposed, and their predictions were compared with results of existing tests on RC beams with an un-strengthened web opening collected from the published literature, results of existing tests on RC beams with an FRP-strengthened web opening collected from the published literature, and results of tests on RC T-section beams with a web opening conducted by the candidate respectively in Chapters 3, 4 and 6 to identify the most reliable approach. The proposed FE approaches employed the dynamic analysis approach (i.e., the explicit central difference method available in ABAQUS) instead of the static analysis approach (e.g. the Newton-Raphson method and the arc-length method), in order to overcome the severe numerical convergence difficulties commonly encountered in the modelling of cracked concrete using static analysis approaches. The modelling of concrete, especially the cracked concrete, the bond behaviour between the concrete and the internal steel reinforcement, and the bond behaviour between the concrete and the externally bonded FRP reinforcement, as well as the determination of the dynamic parameters, were carefully considered in the FE studies.

Although the proposed FE approaches can well predict the behaviour of RC beams with a web opening, the analyses are relatively time-consuming and are not suitable for use by most practicing engineers. If only the ultimate strength of the beam is of concern, therefore, it is worth developing a simple calculation method for engineering use. In Chapter 7, a simple calculation method for predicting the strength of RC beams with a web opening which exhibit a flexural failure model was first proposed, and then a strength model for RC beams with a web opening which exhibit a flexural failure model was established based on the results from the proposed calculation method. The accuracies of the simple calculation method and the strength model were verified with the test results.

Moreover, although the proposed FE approaches for RC beams have the potential to be extended to model RC frames with beam web openings, such approaches will be very complicated and time-consuming. Instead, it is more common and much more desirable to use beam elements to model RC frames. To do so, the moment (M)-rotation (Θ) relationship (referred to as the M-Θ relationship or M-Θ model for simplicity) for the plastic hinges of the beam needs to be established first, which can then be incorporated into beam elements as a property of the plastic hinges in the modelling of RC frames with beam web openings. In Chapter 8, the M-Θ relationships for the idealized plastic hinges at the two ends of a web opening in RC beams were extracted from the experimental results. Based on the experimental findings, a simplified M-Θ model was proposed. The proposed M-Θ model was then employed in the FE modelling of RC beams with a web opening using beam elements (OpenSees 2009), and its accuracy was verified with the test results.

It should be noted that the work presented in this thesis has been limited to the BO technique. Research needed on the other two proposed techniques (i.e. the SR technique and the SS technique) is highlighted towards the end of this chapter.

9.2 EXPERIMENTAL STUDIES ON RC BEAMS WITH A WEB OPENING

To demonstrate the effectiveness of the proposed BO technique, a total of 14 full-scale RC beams, including one rectangular beam and 13 T-section beams, were tested, and the test results were presented in Chapter 5. Two specimens (CB-Rec and CB-T) did not have a web opening and were treated as control specimens. CB-Rec was a rectangular beam, which was used to simulate the situation where the contribution from the cast-in-place slab is ignored in design, while CB-T was a T-section beam, which was used to represent the real situation in the structure where the slab makes a significant contribution to the flexural capacity of the beam. The remaining 12 specimens were T-section RC beams which had the same dimensions as CB-T but a web opening in the right shear span. The studied parameters covered the dimensions of the web opening (i.e., length × height) and the effect of FRP strengthening. A total of six different web opening sizes (length × height being 700 mm × 300 mm, 800 mm × 280 mm, 600 mm × 280 mm, 700 mm × 260 mm, 600 mm × 220 mm and 700 mm × 200 mm, respectively) were examined, which can be divided into three groups: large web openings (700 mm × 300 mm and 800 mm × 280 mm), medium web openings (600 mm × 280 mm and 700 mm × 260 mm) and small web openings (600 mm × 220 mm and 700 mm × 200 mm). The proposed FRP strengthening system included CFRP wraps on the concrete web chord and CFRP U-jackets on the beam web within 200 mm from each vertical edges of the web opening. To avoid premature debonding of the bonded CFRP U-jackets, CFRP spike anchors were used to anchor the CFRP U-jackets to the flange of the beam. Based on the test results, the following conclusions can be drawn:

1) The proposed BO technique can effectively reduce both the negative flexural capacity (i.e., with the beam flange in tension) and the positive flexural capacity (i.e., with the beam flange in compression) of T-section RC beams;
2) The two control specimens (i.e., CB-Rec and CB-T) failed by crushing of compressive concrete at the mid-span of the beam after the yielding of tension steel bars, which is the typical flexural failure mode of RC beams. For the two RC T-section beams with a large un-strengthened web opening, the final failure was controlled by local flexural failure at the right end of the web chord and the left end of the flange chord (i.e., crushing of compressive concrete of the web and flange chords) and local mixed flexural and shear failure at the left end of the web chord and the right end of the flange chord;

for the two RC T-section beams with a small un-strengthened web opening, diagonal cracks (at around 30 to 45 degrees to the horizontal direction) initiated and developed in the web chord and finally governed the failure of the specimens. For the eight RC T-section beams with a CFRP-strengthened web opening tested in either negative bending or positive bending, due to the existence of CFRP wraps and CFRP U-jackets, the shear cracks near the ends of the web chord were well prevented/mitigated. All these eight specimens failed by local flexural failure at the two ends of web chord as well as flange chord; the formation of plastic hinges at the ends of the web and flange chords were observed;

3) Increasing either the length or the height of web opening reduced the load-carrying capacity of the beam. However, increasing the height of web opening was found to be more efficient in reducing the load-carry capacity than increasing the length, as evidenced by the result that the reduction in the load-carrying capacity of the beam caused by an increase of 20 mm in the height of web opening is comparable to that caused by an increase of 100 mm in the length of web opening; and

4) The proposed FRP strengthening system, including a CFRP wrap on the web chord and two properly anchored CFRP U-jackets on the beam web, significantly improved the deformation capacity as well as ductility of the beam; it also enhanced the load-carrying capacity and stiffness of the beam, which was however not the purpose of strengthening. The performance improvement due to the bonded FRP reinforcement can be attributed to the following reasons: (1) the CFRP wrap on the web chord enhances its shear resistance and provides confinement to the chord when it is in compression,

thus enhancing the compressive strength and ductility of the web chord; and (2) the FRP U-jackets with spike anchors restrain the development of cracks at the two ends of the web chord and the horizontal crack between the web and the flange of the beam, thus mitigating the brittle failure of the beam induced by these cracks.

9.3 NUMERICAL STUDIES ON RC BEAMS WITH A WEB OPENING

Chapters 3, 4 and 6 respectively presented FE studies of existing RC beams with an un-strengthened web opening collected from the published literature, RC beams with an FRP-strengthened web opening collected from the published literature, and RC T-section beams with a web opening tested by the candidate. Three alterative FE approaches employing the explicit central difference method available in ABAQUS (2012) as the solution method were proposed: (1) the brittle cracking model, with the secant modulus of concrete recommended by Ye (2005) and Pimanmas (2010) being used, was employed to simulate the cracked concrete (referred to as the ***BC model with SECANT modulus***); (2) the brittle cracking model, with the initial elastic modulus of concrete given by ACI-318 (2014) being used, was employed to simulate the cracked concrete (referred to as the ***BC model with INITIAL modulus***); and (3) the concrete damaged plasticity model was adopted to simulate the behaviour of cracked concrete (referred to as the ***DP model***). The proposed FE approaches were two-dimensional (2-D), with the concrete being modelled using plane stress elements. The shear bond behaviour between steel bars and concrete was represented using the bond-slip model proposed by CEB-FIP (1993). For RC beams with an FRP-strengthened web opening, the bond-slip model for externally bonded FRP proposed by Lu et al. (2005) was adopted to simulate the bond behaviour between FRP and concrete; and to consider the confinement effect from FRP wraps on the web chord concrete, the design-oriented stress-strain model developed by Lam and Teng (2003) for FRP-confined concrete in rectangular columns was employed. Parametric studies were conducted to achieve a proper choice of parameter values for the dynamic solution method as well as a proper shear-retention factor model for concrete, in order to obtain accurate predictions of the quasi-static behaviour of RC beams with a web opening under monotonic loading. Based on the numerical results presented in these three chapters, the following conclusions can be drawn:

1) Based on the parametric studies, the damping factor β was chosen to be 1×10^{-5}, and the loading time was chosen to be $50T_1$ where T_1 is the period of the fundamental vibration mode of the beam. The dynamic method with these parametric values was found to be efficient for obtaining the static structural response of the RC beams with a web opening;
2) For existing RC beams with an un-strengthened web opening collected from the published literature, which all exhibited a shear failure mode due to the formation of a diagonal crack that started as small inclined cracks in the corners of the opening, the ***BC model with SECANT modulus*** gives the best predictions of load-deflection curves and is thus recommended for use in the modelling of such RC beams; the ***BC model with INITIAL modulus*** overestimates the ultimate load as well as the stiffness, indicating that the use of secant elastic modulus of concrete is more suitable for such modelling

owing to the intrinsic nonlinear behavior of concrete in tension; the ***DP model*** was found to overestimate the elastic stiffness and underestimate or overestimate the ultimate load, although this model has shown good performance in the modelling of RC beams strengthened in flexure with FRP plates, which indicates that the ***DP model*** might not be suitable for the modelling of RC structures whose failure is dominated by the tensile and significant shear behavior of concrete;

3) For existing RC beams with an FRP-strengthened web opening collected from the published literature, which all failed by shear in the opening region after the debonding/rupture of FRP, the ***BC model with SECANT modulus*** gives the most accurate predictions of the load-deflection curve in terms of both the predicted ultimate load and the predicted stiffness, the ***BC model with INITIAL modulus*** consistently overestimates the ultimate load as well as the stiffness of the beam, and the ***DP model*** usually significantly underestimates the ultimate load but overestimates the stiffness. The ***BC model with SECANT modulus*** is thus again recommended for use in the modelling of such RC beams;

4) For the specimens tested by the candidate which exhibited a flexural failure mode, the ***DP model*** (with proper consideration of the confinement effect from the FRP wraps to the web chord when such FRP wraps exist) provides the best predictions, while the ***BC model*** overestimates the ultimate load significantly; for the specimens tested by the candidate which exhibited a shear failure mode, the ***BC model with SECANT modulus*** provides the best predictions;

5) The findings summarized above indicate that the selection of the FE approach

for RC beams with a web opening should be based on the possible failure mode of the beam: the ***DP model*** is recommended for beams with a flexural failure mode, while the ***BC model with SECANT modulus*** is recommended for beams with a shear failure mode. A simple method was proposed for the proper selection of the FE approach by comparing the shear capacity with the flexural capacity of the critical chord. If the shear capacity is smaller than the flexural capacity of the critical chord, the ***BC model with SECANT modulus*** should be used; otherwise, the ***DP model*** should be used. This proposed method was verified with the collected existing beam specimens as well as the beam specimens tested by the candidate;

6) The adopted dynamic analysis approach not only overcomes the severe numerical convergence difficulties commonly encountered in the modelling of cracked concrete using static analysis approaches, but also captures the local dynamic responses caused by the sudden releases of energy, due to phenomena such as the initiation and development of FRP debonding. Therefore, the development history of the kinetic energy during the whole loading process of the specimen was examined to identify the initiation of FRP debonding. By using this method, the predicted and test points of initiation of FRP debonding on the load-deflection curves were shown to be very close to each other for all the specimens considered in the comparison;
7) The predicted failure process and crack pattern using the proper FE approach also agree well with the test observations for all the existing specimens as well as the specimens tested by the candidate, which further proves the accuracy of the proposed FE approaches; and
8) It should be noted that although the numerical studies presented in this thesis

were conducted on RC beams with a rectangular web opening, the conclusions are also believed to be largely applicable to RC beams with a web opening of other shapes (e.g. a circular web opening).

9.4 THEORETICAL STUDIES ON RC BEAMS WITH A WEB OPENING

In Chapter 7, a calculation method and a strength model were proposed for predicting the strength of RC beams with a web opening which exhibit a flexural failure model (i.e., with four plastic hinges forming at the two ends of top and bottom chords). Both the yielding state and the ultimate state of the cross sections at the two ends of top and bottom chords were examined for the proposed calculation method, and it was found that the yielding state leads to a lower bound of the predicted strength of the beam while the ultimate state leads to an upper bound prediction of the strength. In addition to the actual *N-M* curves, the simplified *N-M* curves were also examined for use in the proposed calculation method. It was found that the simplified *N-M* curves can lead to slightly conservative but quite acceptable predictions of the strength of the beam. A simple strength model of the beam, therefore, was proposed based on the simplified *N-M* curves for ease of engineering use.

Based on the proposed strength model, the sums of the negative flexural capacity and the positive flexural capacity (SFCs) of the specimens tested by the candidate in Batch 2 were examined. The analysis results indicated that the proposed BO technique is very effective in reducing the SFC, and a web opening size between the medium one and small one examined in the experimental study is able to reduce the flexural capacity of the T-section beam to the desired value (i.e., the flexural capacity of the rectangular beam).

Moreover, in Chapter 8, a study on the moment-rotation (*M-Θ*) response of RC beams with a web opening which exhibit a flexural failure model was presented. Based on the simplified idealization for the beam, an *M-Θ* model for the two plastic hinges (i.e., $M_L - \theta_L$ curve and $M_R - \theta_R$ curve) at the two ends of the web opening was proposed. The predicted *M-Θ* curves agreed well with those obtained from the tests.

To further verify the accuracy of the proposed *M-Θ* model, FE modelling of RC beams with a web opening was conducted using OpenSees (2009), with the *M-Θ* model appropriately incorporated. The predicted load-deflection curves from FE modelling agree well with the test results.

Although the *M-Θ* model was based on the test set-up adopted by the candidate, the proposed calculation method is general and can be easily adapted for use in other situations with slight modifications, such as beams with a web opening at each end of the beam in RC frames.

9.5 FUTURE STUDIES

Firstly, the experimental study on RC T-section beams with a web opening presented in Chapter 5 was mainly focused on the influence of a web opening on the negative flexural capacity of T-section beams, while the results of two specimens with an FRP-strengthened web opening tested in positive bending showed that a web opening can also reduce the positive flexural capacity of T-section beams. To more clearly clarify the influence of a web opening on the positive flexural capacity of T-section beams, further experimental studies are needed.

Moreover, as presented in Chapter 6, for the two specimens with an FRP-strengthened web opening tested in positive bending by the candidate (i.e., F-700×300-P and F-800×280-P), all the proposed FE approaches overestimate the strength and stiffness. The gap between the prediction and the test value can be possibly attributed to the following reasons: (1) the shear lag effect existing in the beam flange resulted in the non-uniform distribution of the longitudinal compressive stresses in the concrete and the reinforcement of the flange in the width direction, and the current 2-D model which adopted plane stress elements cannot capture such shear leg effects but simply assumed that the compressive stresses are uniform across the width of the flange; and (2) the width-to-depth ratio of flange is relatively large. Under compression, therefore, the flange could undergo out-of-plane deformation, which also cannot be reflected by the current 2-D model. The above limitations/simplifications of the present 2-D model can lead to overestimation of the ultimate load of the beam. To resolve this problem, a more advanced 3-D FE model needs to be developed in a future study.

While the studies on RC beams with a web opening presented in the present thesis is the first step to assess the performance of the proposed BO technique in achieving the strong column-weak beam hierarchy in RC frames, studies on beam-column assemblies are an inevitable next step. Therefore, experimental and numerical studies on beam-column assemblies with beam web openings need to be conducted in the future to further assess the effectiveness of the proposed BO technique in achieving the strong column-weak beam hierarchy in RC frames.

Of the proposed three seismic retrofit techniques (the BO technique, the SR technique and the SS technique), the work presented in this thesis has been limited to the BO technique. Although the flexural capacity reduction caused by the SR and the SS techniques can be estimated relatively easily, studies on the effectiveness of the SR and the SS techniques are still needed. To the best of the candidate's knowledge, the SR technique is new and no research is available on its effectiveness and the relevant design method; only a few studies on the effectiveness of the SS technique have been conducted. Therefore, further research needs to be conducted on effectiveness of the SR technique and the SS technique.

Recently, Feng et al. (2017) proposed a novel method using kinked rebars in the beams for improving the seismic performance and progressive collapse resistance of RC frame structures. The kinked rebar has locally curved regions (usually near the inflection points in beams) which can be gradually straightened under tension. Due to the lower initial yielding flexural capacity compared with that of a cross section reinforced with traditional straight bars, the beam section reinforced with kinked rebars will yield first when the RC frame is subjected to seismic loading, and thus the strong column-weak beam hierarchy can be realized. Although this method was originally proposed for new construction, the concept has the potential to be adopted in the BWFS method for existing structures. The feasibility and effectiveness of kinked rebars in reducing the flexural capacity of the beam is worth further investigations, and thus relevant studies will be conducted in the future.

Considering a plane RC frame as a simple common case subject to seismic loading, the two beams framing into an internal beam-column joint are bent in opposite directions at their ends respectively: one of the two beams is in positive bending while the other one is in negative bending. In the experimental study presented in this thesis, both T-section beams in negative bending and T-section beams in positive bending were tested. It was found from the tests that the proposed BO technique can effectively reduce both the negative flexural capacity and the positive flexural capacity of T-section beams, and the behaviour of T-section beams in negative bending and that of T-section beams in positive bending are similar. Moreover, the developed strength model and moment-rotation model in this thesis apply to both RC beams in negative bending and RC beams in positive bending. However, the behaviour of RC beams with a web opening in an RC frame subjected to seismic loading differs to some extent from the behaviour of individual RC beams with a web opening under negative bending or positive bending. The findings for RC beams with a web opening need to be further verified/improved for application to RC frames with beam web openings. Therefore, based on the findings of the present thesis, studies on the behaviour of RC frames with beam web openings need to be conducted to further demonstrate the effectiveness of the BO technique.

In the present study, FE models and a strength model were developed for RC beams with a web opening, and their accuracies have been verified with experimental results. One can design the location and size of the web opening in an RC beam by using the FE models or the strength model. It should be noted that as the behavior of individual RC beams with web openings and RC beams in RC frames with beam web openings may be slightly different, the FE models and strength model need to be further verified/improved when they are used for RC frames with beam web openings against seismic actions. Therefore, the detailed design of beam web openings in RC frames subjected to seismic loading is still a task for future study.

Lastly, in the future, the reliable FE models established in this thesis for the modelling of RC beams with a web opening will be employed in parametric studies to generate extensive data to further verify the accuracies of the strength model and M-Θ model for RC beams with a web opening proposed in this thesis. These FE models will also be employed in parametric studies to investigate other parameters that were mot investigated in the experimental study presented in this thesis. Furthermore, in the future studies, the FE models will be extended for the modelling of RC beam-columns joints with web openings in beams.

9.6 REFERENCES

ABAQUS (2012). *ABAQUS Analysis User's Manual (Version 6.12)*, Dassault Systems SIMULIA Corporation, Providence, Rhode Island, USA.

Abdalla, H.A., Torkey, A.M., Haggag, H.A. and Abu-Amira, A.F. (2003). "Design against cracking at openings in reinforced concrete beams strengthened with composite sheets", *Composite Structures*, 60(2), 197-204.

ACI 318 (2014). *Building Code Requirements for Structural Concrete and Commentary* (*ACI 318-14)*, ACI Committee 318, American Concrete Institute, Farmington Hills, MI.

Allam, S. M. (2005). "Strengthening of RC beams with large openings in the shear zone", *Alexandria Engineering Journal*, *44*(1), 59-78.

CEB-FIP. (1993). *CEB-FIP Model Code 90*, Thomas Telford, London.

Chin, S.C., Shafiq, N. and Nuruddin, M.F. (2012). "Strengthening of RC beams with large openings in shear by CFRP laminates: experiment and 2D nonlinear finite element analysis", *Research Journal of Applied Sciences Engineering and Technology*, 4(9), 1172-1180.

Chin, S.C., Shafiq, N. and Nuruddin, M.F. (2016). "Behaviour of RC beams with CFRP-strengthened openings", *Structural Concrete*, 17(1), 32-43.

Feng, P., Qiang, H., Qin, W. and Gao, M. (2017). "A novel kinked rebar configuration for simultaneously improving the seismic performance and progressive collapse resistance of RC frame structures", *Engineering Structures*, 147, 752-767.

Lam, L. and Teng, J. G. (2003). "Design-oriented stress-strain model for FRP-confined concrete in rectangular columns", *Journal of Reinforced Plastics and Composites*, 22(13), 1149-1186.

Lu, X.Z., J.G. Teng, Ye, L.P. and Jiang, J.J. (2005). "Bond-slip models for FRP sheets /plates bonded to concrete", *Engineering Structures*, 27(6), 920-937.

Maaddawy, T. and Sherif, S. (2009). “FRP composite for shear strengthening of reinforced concrete deep beams with openings”, *Composite Structures*, 89(1), 60-69.

Maaddawy, T. and El-Ariss, B. (2012). “Behavior of concrete beams with short shear span and web opening strengthened in shear with CFRP composites”, *Journal of Composites for Construction*, ASCE, 16(1), 47–59.

Mansur, M.A., Tan, K.H., and Lee, S.L. (1984). “Collapse loads of R/C beams with large openings”, *Journal of Structural Engineering*, ASCE, 110(11), 2602-2610.

Mansur, M.A., Tan K.H. and Wei, W. (1999). “Effects of creating an opening in existing beams”, *ACI Structural Journal*, 96(6), 899-906.

OpenSees (2009). *Open System for Earthquake Engineering Simulation*, Pacific Earthquake Engineering Research Center, University of California at Berkeley, http://opensees.berkeley.edu.

Pimanmas, A. (2010). “Strengthening R/C beams with opening by externally installed FRP rods: Behavior and analysis”, *Composite Structures*, 92(8), 1957-1976.

Suresh, J. and Prabhavathy, R. A. (2015). “Behaviour of steel fibre reinforced concrete beams with duct openings strengthened by steel plates”, *International Journal of Advanced Information in Arts, Science & Management*, 4(4).

Teng, J.G., Zhang, S.S., Jing, D.H., Nie, X.F. and Chen, G.M. (2013). “Seismic retrofit of RC frames through beam-end weakening in conjunction with FRP strengthening”, *Proceedings of the 4th Asia-Pacific Conference on FRP in Structures (APFIS 2013)*, 1-8.

Ye, L.P. (2005). *Concrete Structures (Second Edition)*, Tsinghua University Press, Beijing, China (in Chinese).